Sheffield Hallam University

A Sheffield Hallam University thesis

The Synthesis and Development of Novel, Easily Processable *Poly*(N-Isopropylacrylamide)- Based Hydrogels

Victoria Boyes

A thesis submitted in partial fulfilment of the requirements of

Sheffield Hallam University

for the degree of Doctor of Philosophy

September 2012

Collaborating Organisation: Smith & Nephew Extruded Films
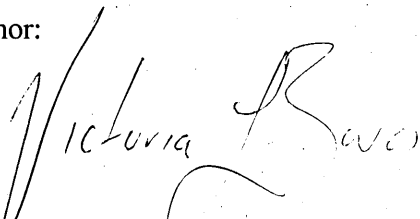
Declaration

The work described in this thesis was carried out by the author in the Materials and Engineering Research Institute at Sheffield Hallam University, between October 2008 and August 2012. The author declares that this work has not been submitted for any other degree. The work is original except where acknowledged by reference.

Author:

(Victoria Boyes)

Director of Studies:

(Dr. Christopher Sammon)

Acknowledgements

Abstract

This work describes the invention of a synthetic method which allows a fully-reacted PNIPAM/ clay nanocomposite system to remain a watery liquid until it is cooled to a predetermined temperature. Beyond this temperature, the polymer/ clay precursor hydrogel liquid (PCPH) spontaneously forms a cross-linked hydrogel that does not re-liquefy upon re-heating, but instead, possesses all of the highly utilisable stimuli-responsive properties typical of PNIPAM-based nanocomposite hydrogels synthesised *in situ*.

This novel methodology simultaneously addresses issues including cytotoxicity, processability, injectability, cross-linking and mechanical stability. In addition, PCPH synthesis requires no specialist equipment, inexpensive and basic components typical of cross-linked hydrogels (water, monomer, clay and initiator), requires no purification steps and can be maintained as a fully-reacted liquid at evaluated temperatures for up to several weeks with no apparent loss of eventual functionality. The ability to create a fully polymerised hydrogel polymer with a liquid intermediate state has allowed the incorporation of biologically active dopants which can be dispersed and distributed homogeneously throughout the matrix prior to "phase transition triggered nanoparticle anchored gelation" (or PTTNAG) of the hydrogel. Human mesenchymal stem cells (MSCs), have been incorporated into the gel by i) placing them on the assembled gel surface - the cells responded by migrating and proliferating throughout the matrix of the gel, and more interestingly, ii) combining the MSCs with the PCPH in the liquid phase and allowing PTTNAG of the polymer matrix to occur around the cells. In both cases, cell viability was excellent throughout a series of 14 -28 day experiments.

The work was expanded by the exploration of PTTNAG temperature tailorability. This was achieved with the incorporation of the relatively polar comonomer dimethylacrylamide (DMAc), and non-polar comonomer glycedyl methacrylate (GMAc) which respectively increased and decreased the PTTNAG and lower-critical solution temperature (LCST) of the resulting gels. Crucially, it was found that the PTTNAG temperature can be tailored precisely and incorporation of DMAc did not affect cell viability.

The process also opened several novel avenues for gel processing possibilities, including facile casting, extruding and electrospinning. Well defined and uniform electrospun fibres with diameters ~300nm are presented. The production of continuous, uniform flat PNIPAM/ clay sheets of 300µm -1000µm achieved using an industrial film extrusion line is detailed. This work represents an innovation in the way in which such hydrogels can be manufactured and produced safely and cleanly, with no additives, no energy input and no toxic by- products.

Interactions between polymer and water are examined by monitoring the dehydration of 3 separate hydrogel formulations using ATR-FTIR. The pseudo diffusion coefficient (in this instance, the diffusion of water *out* of the polymer matrix) was not affected by dopant composition, but instead, the intercept of the slope was altered markedly.

Cross-link type, cross-link density, initiation method and addition of dopants have a strong influence on the swelling/ deswelling behaviour of the hydrogels under study. PNIPAM/ clay gels exhibit much larger volume changes than those prepared with chemical cross-linking agent methylenebisacrylamide (BIS). Deswelling magnitude increases with decreasing cross-linker content for all gel types examined. Thermal deswelling is hindered in dopant-incorporated networks. The aqueous dilution of the nanocomposite in the liquid phase affects gel deswelling behaviour when clay concentration is low. De/reswelling of PNIPAM/ clay, PNIPAM/ BIS and gelatine-doped PNIPAM/ clay gels can be induced by adjusting the alcohol volume fraction of the media. BIS cross-linked gels exert restricted swelling/ deswelling behaviours compared to those cross-linked with clay. Cross-link density within systems does not have a significant impact on cononsolvency behaviour, although the incorporation of gelatine imposes some restriction on it, directly relative to gelatine concentration.

X-ray diffraction (XRD) data proved the exfoliation of clay in the nanocomposite system post- PTTNAG. DMA data revealed that the viscoelasticity of the gels can be tailored with varying the nature and quantity of dopant materials. Gels doped with hyaluronic acid (HA) most closely resemble the mechanical properties of bovine NP tissue.

Table of Contents

Chapter 2 - Experimental   48

Chapter 3 - The Development of a PNIPAM/ Clay Nanocomposite Liquid Gel Precursor   77

Chapter 6 – The Influence of Alcoholic Solutions and Dopants on the Phase Behaviour of PNIPAM   183

Chapter 7- PCPH as an Injectable, Functional Therapy for Degenerative Disc Disease   215

List of Abbreviations

~	Approximately
°	Degree
°C	Degrees Celsius
°Cmin^{-1}	Degrees Celsius per minute
μm	Micrometer
AF	Annulus Fibrosus
AIBN	Azobisisobutyronitrile
APS	Ammonium Persulfate
ATR-FTIR	Attenuated Total Reflection – Fourier Transform Infrared Spectroscopy
ATRP	Atom Transfer Radical Polymerisation
BHT	Butylated Hydroxytoluene
BIS	N, N'methylenebisacrylamide
cm	Centimetre
cm^{-1}	Wavenumber
D	Diffusion Coefficient
D$_H$	Z- Average Hydrodynamic Diameter
DLS	Dynamic Light Scattering
DMA	Dynamic Mechanical Analysis
DMAc	N,N-Dimethylacrylamide
DMF	Dimethylformamide
DNA	Deoxyribonucleic Acid
DSC	Differential Scanning Calorimetry

EBSD	Electron Backscatter Diffraction Detector
EDS	Energy Dispersive X-ray Spectrometry
ESEM	Environmental Scanning Electron Microscopy
EWC	Equilibrium Water Constant
FTIR	Fourier Transform Infrared Spectroscopy
G'	Storage Modulus (elastic properties)
G"	Loss Modulus (viscous properties)
GMAc	Glycedyl Methacrylate
GPC	Gel Permeation Chromatography
HA	Hyaluronic Acid
HEMA	Hydroxyethyl Methacrylate
HF	Hydrofluoric Acid
Hz	Hertz
IPN	Interpenetrating Polymer Network
IVD	Intervertebral Discs
Kg	Kilogram
KPS	Potassium Persulfate
LCST	Lower- Critical Solution Temperature
LVSEM	Low-Voltage Scanning Electron Microscopy
m	Metre
MALDI-TOF-MS	Matrix-Assisted Laser Desorption/ Ionisation Time-of-Flight Mass Spectrometry
MCR	Multivariate Curve Resolution
mg	Milligram
mm	Millimetre

M_n	Number Average Molecular Weight
MPa	Megapascal
MSC	Mesenchymal Stem Cells
M_w	Molecular Weight
MWD	Molecular Weight Distribution
n	Number of experiments
nm	Nanometre
NP	Nucleus Pulposus
Pa	Pascal
PCPH	Polymer/ Clay Precursor Hydrogel
PDMAc	*Poly*(N,N'-Dimethylacrylamide)
PTTNAG	Phase Transition-Triggered Nanoparticle Anchored Gelation
PNIPAM	*Poly*(N-isopropylacrylamide)
RAFT	Reversible Addition–Fragmentation Chain Transfer Polymerisation
R_h	Hydrodynamic Radius
rpm	Revolutions per minute
SAXS	Small Angle X-ray Scattering
SD	Standard deviation
SEC	Size Exclusion Chromatography
SEM	Scanning Electron Microscopy
SNEF	Smith & Nephew Extruded Films
SRP	Stimuli Responsive Polymer
Tan δ	Tan Delta (loss tangent (G"/ G')
TEM	Transmission Electron Microscopy

TEMED	N' N'tetramethylethylenediamine
TGA	Thermogravimetric Analysis
THF	Tetrahydrofuran
UV	Ultraviolet
w/v	Weight in volume
w/w	Weight in weight
XRD	X-ray Diffraction
ZPD	Point of Zero Path Difference
Δ	Change
δ	Bending vibration
ν	Stretching vibration

1

Introduction

Chapter 1 – Introduction

1.1   Polymers overview

Polymers are long- chain molecules composed of a large number of repeating units and have very high molecular weights. They can be synthetically produced and also occur very commonly in nature. Naturally occurring polymers are often water-based and include proteins, glycogen, DNA, silk, wool, cellulose, starches and latex. Synthetic polymers such as polyethylene, polyester, nylon, Teflon, and epoxy are synthesised and produced commercially and have a wide range of behavioural properties and uses. Polymers are synthesised by the process of polymerisation – a chemical process by which a large number of molecular units or "monomers" are joined sequentially, forming a long chain of repeating monomer units. In some polymers, only one monomer type is used. In others, up to several different monomers may be combined in ordered or random conformations. In addition, polymers can be linear, branched, "combed", cross-linked or have a star-like architecture.

1.1.1   Homopolymeric systems

A polymer prepared using a single monomeric species is a called a homopolymer. The polymer on which the majority of this study is based, *poly*(N-isopropylacrylamide) (PNIPAM), lies within this category.

1.1.2   .   Copolymeric systems

A copolymer is formed when two different species of monomer are joined within a single polymer chain, and the term copolymerisation refers to a method employed to chemically synthesise such a material. The classification of copolymeric materials is based upon how the monomers are arranged, for example:

<div align="center">

-A-B-A-B-A-B-A-B-A-B-A-B-A-B-A-

Alternating copolymer

</div>

An alternating copolymer has regular repeating single units arranged in an alternating fashion.

<div align="center">

-A-A-A-B-A-B-B-A-A-B-B-B-A-B-A-A-B-

Random copolymer

</div>

In a random copolymer, the units may be arranged in any order. Also referred to as statistical copolymers, a truly random copolymer is obtained if the mole fraction of a monomer species equals that of the probability of finding a particular monomer at a particular location along the chain [1].

-A-A-A-A-A-A-A-B-B-B-B-B-B-B-

Block copolymer

Block copolymers can be thought of as two covalently linked homopolymer units, with monomeric subunits of each type grouped together. Occasionally, an intermediate, non-repeating unit called a junction block is required to link the two subunit types. Polymers consisting of two distinct blocks are termed diblock copolymers, and those with 3 are known as triblock copolymers.

The polymer structure can also exist in a branched state, whereby a single principal polymer chain has one or more tethered side-chains. Specialist branched polymers can also be synthesised in the form of starts, brushes and combs. The given examples are those of dipolymers, i.e. those composed of 2 types of structural unit. A copolymer comprising three separate monomeric species is termed a "terpolymer".

1.1.3   Interpenetrating polymer networks (IPNs)

An interpenetrating polymer network (IPN) is a polymer system consisting of two or more partially or fully- interlaced independent networks which are not chemically or physically bonded to each other, as shown schematically in fig 1.2. Many IPNs exhibit dual-phase continuity, i.e., at least two polymers in the system are continuous on a macroscopic scale.

● Cross-linked junction

Polymers A and B, respectively
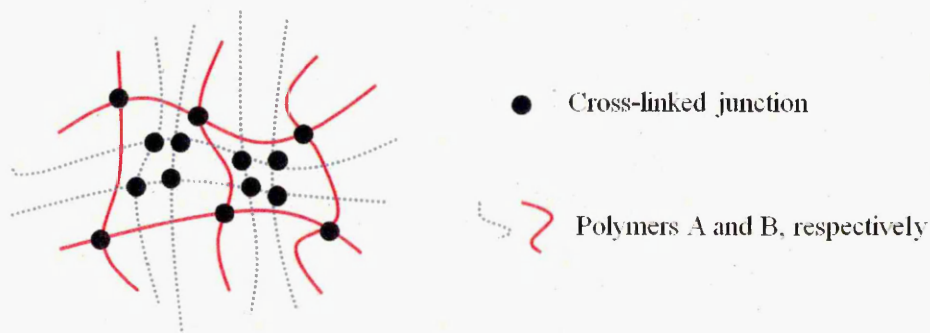
Figure 1.2. Schematic representation of an interpenetrating polymer network.

1.1.4 Multipolymeric systems

Multipolymeric polymers are synthesised by polymerising three or more types of monomer together in tailored quantities to form a unique behavioural profile.

1.1.5 Amphiphilic polymers

An amphiphile is a chemical compound possessing both hydrophilic (water-loving) and hydrophobic (water-hating) properties. Amphiphilic copolymer networks incorporate hydrophilic and hydrophobic monomer species, and it is common for amphiphilic species to spontaneously self-assemble into a diverse range of morphologies. Their phase separation behaviour arises from the interactions between hydrophilic and hydrophobic domains of the polymer, and those between polymer and solvent [2-3]. Fatty acids, detergents and hydrocarbon-based surfactants are examples of amphiphilic molecules.

1.2 Hydrogels and Stimuli responsive polymers

The term "hydrogel" encompasses a class of highly water-swollen polymers (10-1000 times their dry mass) which are cross-linked to maintain a stable 3D network [4]. Generally speaking, the extraordinarily hydrophilic nature of these materials is attributed to amide, hydroxyl, carboxyl, sulfide or other covalently bound polar groups on the polymer carbon backbone. When a hydrogel contains its maximum capacity of water, it is said to have reached its equilibrium water constant (EWC).

Published items containing the word "hydrogel".
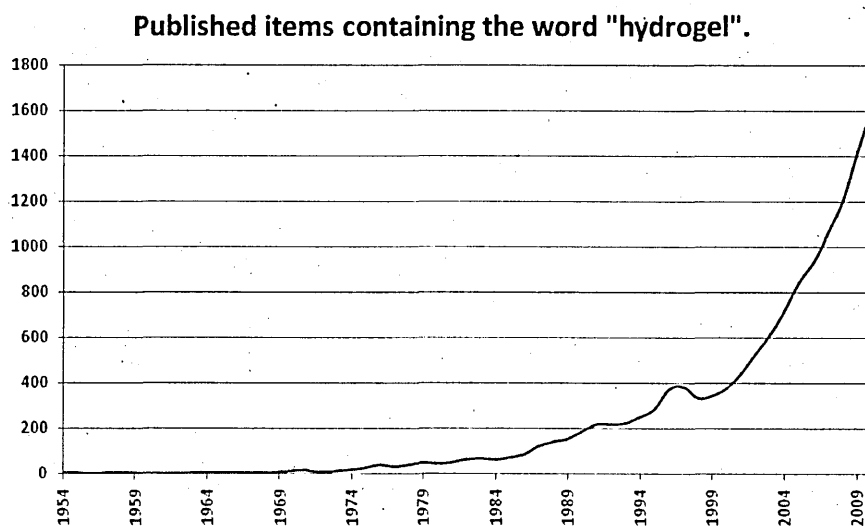
Figure 1.1 The number of *Web of Knowledge* search results for "Hydrogel".

Some polymers exhibit sensitivity to external stimuli such as temperature or pH, and are therefore referred to as "stimuli responsive polymers", or SRPs. Stimuli responsive properties have been observed in natural, synthetic and several biopolymers involved in biochemical processes [5-6]. One such natural biopolymer is pH-sensitive Chitosan, a linear polysaccharide commercially derived from chitin, is an integral part of the structure of the crustacean exoskeleton and also found in the cell walls of certain fungi. Polypeptides (long amino acid chains with which proteins are constructed) are a family of thermo responsive materials, and the thermodynamic driving forces of their α-helix to coil transition were first examined 1950's by Schellman [7-8], who observed thermally-triggered structural and conformational changes in chain structure.

The pioneering studies of SRPs in the 1950s was very heavily geared around biological applications; it was found that when cross-linked, their swellability, flexibility and potential adaptability could be tailored to resemble those of natural living tissue and were viable candidates for cell support and tissue scaffolding [9]. Fig 1.1. Shows how markedly interest in hydrogel materials increased during the 1990s, followed by an even more earnest expansion of interest during the 2000s. As the technology progressed, potential applications for synthetic SRPs began to include intelligent textiles [10-11] artificial muscles and robotics [12-13], and actuators and sensors [12, 14-15].

Much effort has been invested in the development of macromolecules which are environmentally sensitive and respond to specific triggers. Common triggers include changes in electrolyte concentration [16-18], temperature [19-25] and changes in pH [17, 24, 26]. Systems that change in physical conformation in response to magnetic field, light [27], electricity [28] and specific biological molecules such as enzymes, glucose and antigens [29] have also been considered. Among the most extensively documented are SRPs that respond to temperature.

1.2.1   Hydrogel classification

Hydrogels can be categorised in several ways, the most basic classification being the distinction between natural and synthetic materials. Further to this, they can be distinguished in three more specific ways; by their physical structural features, ionic charge and preparation method.

Based on structural features, hydrogels can be classed as having semi-crystalline, amorphous, or hydrogen-bonded structures. Accounting for ionic charge, hydrogels can

be classified as anionic, cationic, neutral or ampholytic. Based on the preparation method, four further groups can be distinguished; homopolymeric hydrogels, copolymeric hydrogels, multipolymeric hydrogels and interpenetrating polymeric hydrogels, and can be distinguished further to this by method of cross- linking.

1.3. Background of *Poly*(N-isopropyl) acrylamide (PNIPAM)

Poly(N-isopropyl) acrylamide (PNIPAM), the polymer at the heart of this research, is an amphiphilic polymer which is water soluble at room temperature. It has been studied extensively because of its amphiphilic properties. As a homopolymer, PNIPAM has a sharp lower- critical solution temperature (LCST) between 30°C [30] and 35°C [31] (where the discrepancy can be influenced by macromolecular structure, chain length [32], polydispersity [33] and/ or cross-linking factors [34]). It transforms from a hydrophilic and swollen (coil) conformation below this temperature to a compact, relatively dehydrated hydrophobic (globule) conformation above it [35]. Linear PNIPAM is also highly soluble in organic solvents such as acetone and chloroform, as well as simple alcohols including ethanol and methanol. Upon warming beyond ~33°C, an aqueous PNIPAM solution instantaneously switches from a transparent solution into a turbid, white-coloured suspension. This phase transition is reversible, and a warm turbid suspension will immediately fully recover its optical clarity upon cooling. When PNIPAM chains are cross-linked, the resulting self-supporting hydrogel collapses and shrinks at temperatures above its LCST, and expands and swells at temperatures below its LCST.

Over the last two decades, the frequency of PNIPAM-based publications has increased markedly year-on-year, reaching a plateau around 2008. As illustrated by Fig. 1.3., interest in PNIPAM has increased dramatically, and it has become by far the most extensively studied of all thermally-responsive aqueous hydrogels. [23, 36].

The first publications focussing on PNIPAM appeared in 1956, where the process of formulation and polymerisation of N-isopropylacrylamide (NIPAM) monomer (Fig 1.4.) were rationally discussed [37-38]. A focus on the novel, counter-intuitive thermal phase-separation behaviour which it exhibited in aqueous media appeared later, as discussed in section 1.3.2.

Published Items each Year
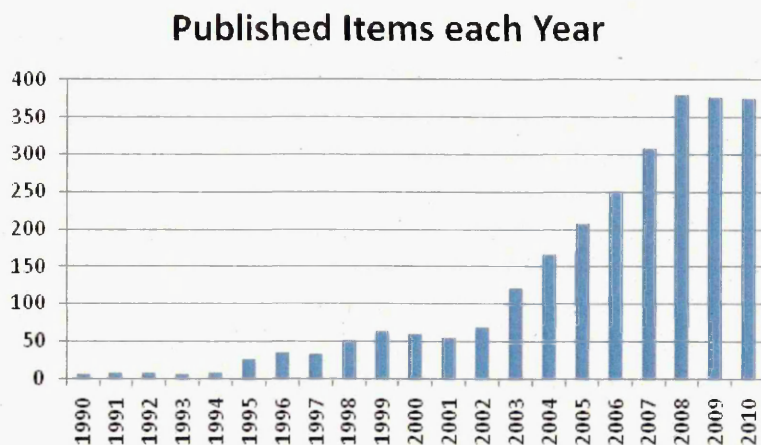
Figure 1.3. The number of *Web of Knowledge* search results for "PNIPAM".
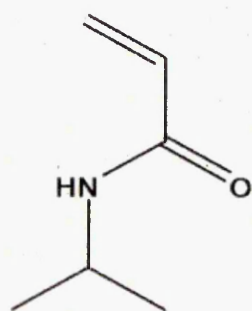
Figure 1.4. The structure of N-isopropylacrylamide (NIPAM) monomer.

Complex nanostructures consisting of organic and inorganic components have been researched extensively as functional nanocomposite materials. Particularly in the last 20 years, polymeric hydrogels composed of PNIPAM have been of considerable interest to researchers due to these precise and modifiable stimuli-responsive properties, and as such, the potential uses of PNIPAM have been explored in the fields of biology [39-46], chemistry, [47-52] physics [53-58] and medicine [43, 59-62]. To illustrate, a particularly attractive application of PNIPAM is molecular gating. Several research groups have designed and produced devices which incorporate temperature sensitive components which isolate, separate and detect analytes from samples of very low volume and/ or concentration [63-65]. Ebara *et al* discovered that PNIPAM-based polymers (*poly*(*N*-isopropylacrylamide-*co*-2-carboxyisopropylacrylamide)) could either show or hide arginine/glycine/aspartic acid recognition sequences for human cell binding and detaching [19].

PNIPAM has been successfully synthesised *in situ* in forms such as macroscopic gels [66-67], microgels [68-70], films [42, 44, 71], fibres [72-74] and coatings [75-77]. The sharp and dramatic switch in hydrophobic-hydrophilic character PNIPAM exhibits around its LCST (and therefore substantial variation in colloidal properties- primarily size, and colloidal stability and electrophoretic mobility of the particles) at temperatures close to that of the human body allows for significant potential as an intelligent material for use in the biomedicine. Until relatively recently, however, PNIPAM polymers and their derivatives were thought to have extremely poor biocompatibility, based mainly on the assumption that, considering the high toxicity of acrylic monomers, NIPAM would be toxic, teratogenic and carcinogenic [78]. These assumptions were largely based on toxicity evaluations of acrylamide monomers, which induced developmental, neural and reproductive retardation in various species [79-81]. In spite of this, subcutaneous and orally administrative testing of the potential toxicity of PNIPAM and its copolymers were carried out in mice [82]. The results definitively conclude that the polymer exerted no toxic effects as well as absence of cumulative toxicity, although the authors expressed the mandatory requirement for further cytological study.

The adverse effects attributed to acrylamide monomer exposure may be attributed to its size, namely its ability to cross cell membranes. In addition, the involvement of its conjugated double bond (which can partake in nucleophilic reactions with functional groups containing active hydrogen), in chemical activity with integral cell processes has been shown to interrupt cell division, affect cell osmotic stability and inhibit nucleic acid synthesis [83-85]. The removal of this double bond during free radical polymerisation and subsequent removal of reactive groups, as well as a substantial increase in size preventing the crossing of cell membranes may go some way toward explaining the recent success in live cell proliferation on highly purified PNIPAM gels [41, 43, 46, 60, 86].

1.3.1 Lower Critical Solution Temperature (LCST) Theory

When a polymer becomes miscible in its solvent upon an increase in temperature, it exhibits an upper critical solution temperature (UCST). One that becomes insoluble with increase in temperature exhibits a lower critical solution temperature (LCST). The LCST is defined as the temperature at which coil-to-globule transition of the polymer network occurs due to sufficient disruption of hydrogen bonding between the amide groups of the polymer and the water molecules, allowing hydrophobic interactions to

form between the non-polar domains of the system. In other words, the solvent changes from "good" to "poor" [33, 87-88]. For free PNIPAM chains in solution, the net observable result of this phenomenon is PNIPAM precipitation and subsequent increase in solution turbidity, and for swollen 3-dimensional cross-linked PNIPAM, collapse of the structure, expulsion of water from the network and decrease in gel size. The extent and speed of this collapse depends heavily on type of cross-linking agent present and crosslink density (both points to be addressed in more detail in section 1.4).
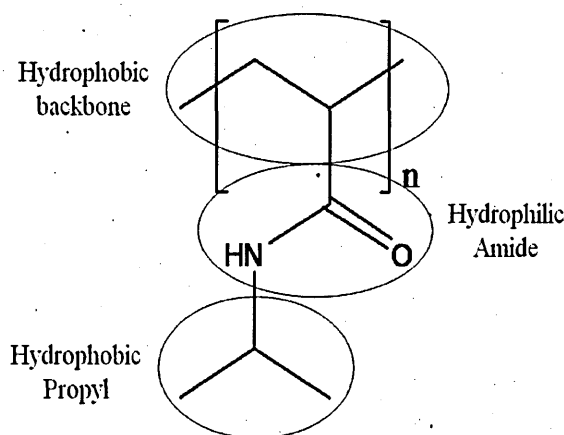
Figure 1.5. The structure of Poly(*N*-isopropylacrylamide) with functional groups indicated.

Although water desorption often occurs as a result of many complex mechanisms, it is generally accepted that precipitation/ reabsorption is observed as a net result of the quest for thermodynamic stability. When the temperature is below the LCST, there are sufficient hydrogen bonding interactions between water molecules and the polymer's amide N-H and C=O groups, shown in fig 1.5, and a favourable contribution is made to the free energy of mixing ($\Delta H_M < 0$). For cross-linked systems, as schematically represented in fig 1.6., the hydrophilic regime is dominant, and large volumes of water occupy the polymer chains and interstitial spaces and the gel exists in a hydrated, highly swollen state. Conversely, at temperatures above the LCST, hydrogen bonds are disrupted and the ordering of water molecules becomes entropically unfavourable in the presence of hydrophobic moieties. In order to limit the entropic loss, their water solubility is heavily compromised [33, 89] the isopropyl groups are pulled together by
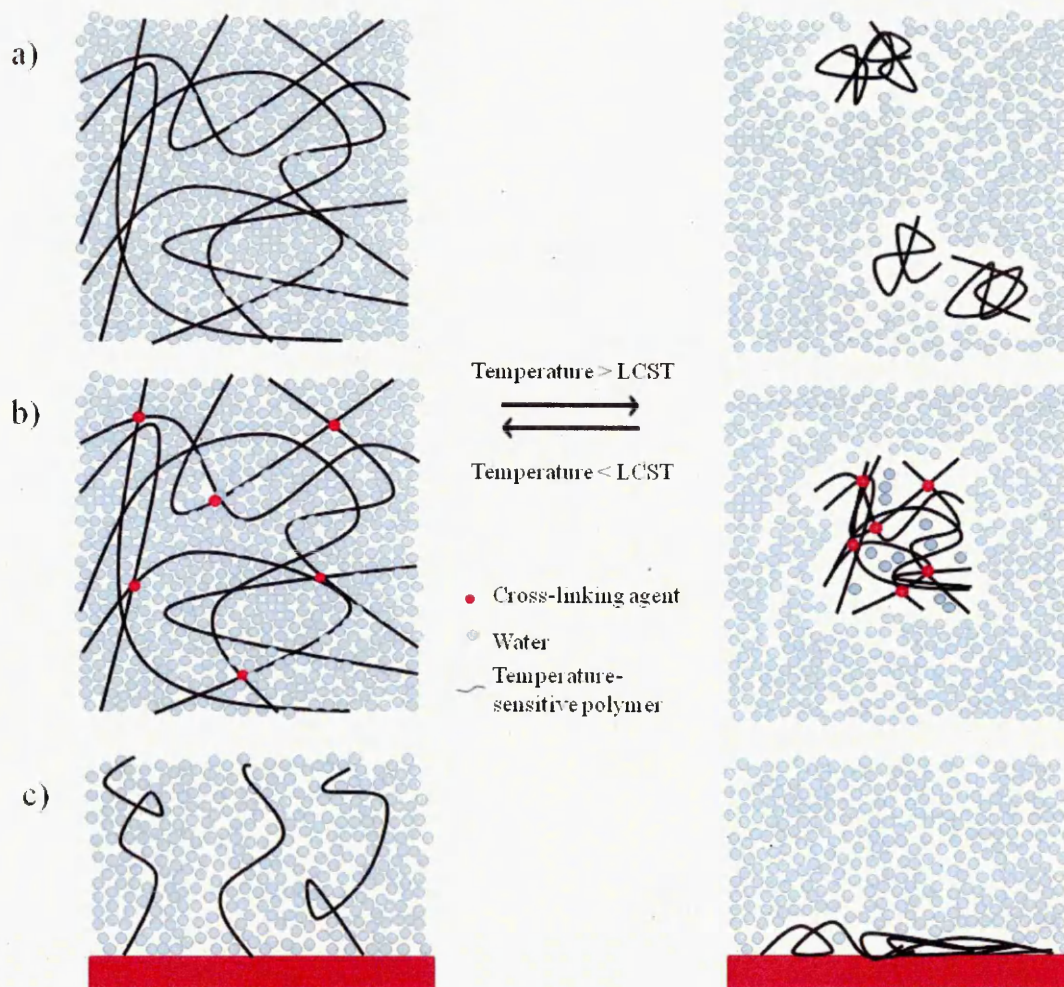
Figure 1.6. The macroscopic transition of PNIPAM above and below its lower critical solution temperature as a) free chains in aqueous media b) a cross-linked gel system, and C) tethered at one end to a surface.

hydrophobic interaction, and the polymer physically collapses. A further increase in temperature enhances the unfavourable contribution of entropy to the system, and the relative magnitude of this "hydrophobic effect" is directly proportional to thermal input [32-33, 49, 64]. Details further to this regarding the precise LCST mechanism are subject to a degree of ambiguity. For example, Winnik suggested that the clouding of a polymer solution occurs in two distinctive stages, the first being the folding of individual polymer chains, and the second involving the aggregation of the folded polymer globules [90]. Winnik fails to precisely detail the mechanism by which the singular polymer chains transform to precipitated globules, however. Chi Wu [91] published a review containing results of the mechanism of collapse of linear PNIPAM chains between 33.02°C and 30.02°C. Fig 1.6. schematically summarises their conclusion.
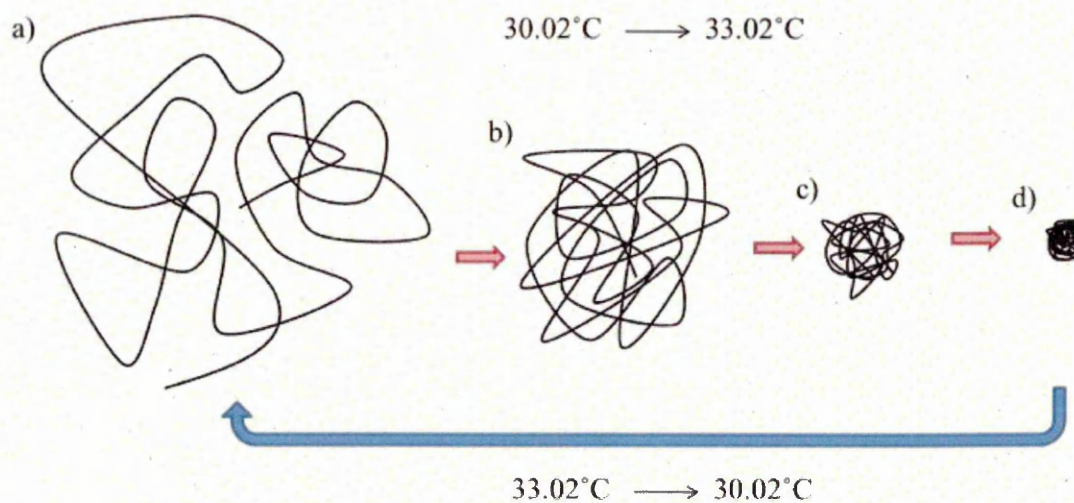
Figure 1.7. Schematic representation of the four states of a collapsing PNIPAM chain in aqueous media according to Chi Wu; a) Random coil, b) crumpet coil, c) molten globule and d) collapsed globule [91]. A hysteresis loop exists between warming above the LCST and cooling below it.

It was concluded using dissolving kinetics models (as a function of hydrodynamic radius R_h) that when the water/ PNIPAM compatibility was decreased (solubility changed from "good" to "poor"), chain collapse occurs in 4 distinct stable phases, as shown in fig 1.7. The coiled NIPAM chain is thought to initially shrink into a loosely-packed "crumpet" state before passing through a knotted "molten globule" state before reaching its final fully collapsed globule state. Interestingly, the group concluded that the reswelling of the chains did not follow the same route, and therefore a hysteresis exists between the two processes.

1.3.2 Lower- Critical Solution Temperature (LCST) of PNIPAM

The observation of an LCST was first documented for free PNIPAM in water by Scarpa et al in 1967 [92]. The article describes a precipitation and resolvation from the solution as an "inverse temperature coefficient of solubility". Shortly afterward in 1968, with inspiration gathered from sparing reports made during the previous decade of an apparent precipitation of specific polar polymers upon heating [93-94], a more detailed examination of the phenomenon was published by Heskins and Guillet [95]. They used a phase diagram to conclude that phase separation was a manifestation of greater entropy existing in two phases compared to an inhomogeneous solution. Surprisingly, the rapid, predictable and sharp volume transition of PNIPAM was not observed nor

11

recorded by Heskins and Guillet during their investigations of its thermodynamic properties.

The first fully comprehensive analysis of the thermodynamics of the LCST phenomenon came from two publications by Tanaka et al in 1978 [96-97], following their observation of the large volume changes in crosslinked polyacrylamide gels the previous year [98]. Thus began the general acceptance of acrylamide-based gels as intelligent, stimuli-responsive networks which were capable of large transparency and volume change responses upon a relatively small change in temperature over a certain temperature range. The group followed their observations with the first study of the discontinuous phase transition of non-ionic PNIPAM gel, and drew its distinctions from a regular non-ionic acrylamide gel with a continuous volume change. They deduced that whether the volume change of a gel was continuous or discontinuous depends on a parameter given by equation 1.1:

$$S = (b/a)^4 (2f + 1)^4$$

Equation 1.1

Where *b/a* represents the ratio of persistence length of the chain *b* and its effective radius *a*, and is indicative of the "stiffness" of the polymer. Parameter *f* represents the total number ionisable groups per chain [99]. According to this theory, an S value smaller than 290 is indicative of a continuously changing gel, where as those above 290 have sufficient ionised functional groups and/ or stiffness undergo discontinuous change [26]. The group's observations showed PNIPAM volume change to be in the order of eight times, making S = 800 and subsequent *b/a* = 5.3 [26]. The preliminary understanding of the phenomenon was followed by a further article in 1986 detailing the LCST behaviour of PNIPAM in mixed alcoholic solvents [100]. This was the initial appearance of the phenomenon of cononsolvency re-entrant swelling behaviour, which will be examined more closely in chapter 6 of this thesis.

Commonly, PNIPAM hydrogels are prepared at ambient temperature from an aqueous solution of NIPAM monomer, initiator, accelerator and chemical cross-linking agent. Since the LCST of PNIPAM is somewhere in the region of 30 -35°C, propagation at room temperature proceeds in a hydrophilic, homogeneous solution which yields continuous gels. Alternatively, PNIPAM hydrogels can be prepared by beginning the polymerisation process below the LCST and gradually increasing the temperature to one

that is above it, resulting in macroporous gel with a large pore size and volume, an elevated specific surface area and a faster expansion and contraction rate [101-102].

1.3.3 Tailoring the LCST of PNIPAM

A linear polymeric species which displays LCST behaviour can be cross-linked to give a thermally-triggered phase-switching gel network. Organically cross-linked gels exert low volume change and slower deswelling rate than their inorganically cross-linked counterparts. Cross-link density (and therefore inter-cross-link space) also heavily dictates the gels volume change capacity [103-104]. This is due to the Gibbs free energy of mixing the solvent and polymer is subject to two contributions: the first for mixing the solvent with the polymer network, the second being a manifestation of the elasticity of the network [105]. More densely cross-linked gels take longer to deswell and reach equilibrium than those with a more loosely cross-linked matrix [106].

In addition, several basic additive approaches exist to alter the temperature at which phase separation occurs to some degree. For example, the use of salts can decrease the LCST [107-109], whereby the relative increase of insolubility and decrease in LCST in aqueous/ salt systems follows the Hofmeister series [107]. It is thought that ions exhibiting a large charge to volume ratio (such as sulphates) dehydrate the polymer chains thus preventing effective network hydration and decreasing solubility of the system [87]. Conversely, anionic surfactants such as dodecylsulfate increase the LCST of PNIPAM by interacting with chain segments, subsequently inducing polymer-polymer repulsion [110].

The precise temperature at which phase change occurs can be also be tailored by introducing hydrophobic or hydrophilic moieties during polymerisation (non-polar moieties reduce the phase-change temperature; polar moieties increase it, a phenomenon examined in detail in section 7.4). Further to this, the copolymerisation of NIPAM monomer with hydrophobic comonomers containing increasing lengths of alkyl side groups exert lower LCST in comparison to pure PNIPAM gel, and a linear correlation between the transition temperature and length of the hydrophobic alkyl side group has been demonstrated [111].

13

1.3.3.1   Tailoring the LCST of PNIPAM-based copolymer hydrogel systems

As previously discussed, hydrogels swell on contact with aqueous media as water enters their interstitial spaces. The manner and degree in which the solvent/ polymer interaction occurs is heavily dependent on factors such the polymer-solvent thermodynamic compatibility and physical mobility restrictions as a result of cross-linking density.

The hydrophilic nature of a given hydrogel network is generally owed to the presence of functional groups such as carboxyl (-COOH) hydroxyl (-OH), primary amidic (-CONH$_2$), amidic (-CONH-), and sulphonic (-SO$_3$H), as well as others located within the polymer backbone or within side chains. It is also possible, however, to design hydrogels which contain specific proportions of hydrophobic polymers via the copolymerisation or interpenetration (see section 1.2.4.4) of hydrophilic and hydrophobic polymers.

A tuneable LCST is a property highly utilisable for countless engineering and biomedical applications. Of the latter, much interest surrounds the release of a drug in the solution phase at a pre-programmed "trigger" temperature, for example, infected/ inflamed tissue and cancerous growths emit more heat than their surrounding tissues [112]. An LCST tuned to be that of the aforementioned tissues may allow medication to be released preferentially at those sites, perhaps even with a view to increasing a drug dose at specific loci and therefore preventing damage or poisoning to healthy tissue. Also, an identical LCST can be achieved when a) a small fraction of a highly insoluble monomeric component is incorporated, and b) on the incorporation of larger fraction of relatively highly soluble monomer. This potentially allows additional control of solute-polymer interaction in the system.

A fundamental issue in the proposed utilisation of PNIPAM for human biomedical purposes is that it undergoes phase change at temperatures below the human homeostatic temperature of 37°C. The copolymerisation of NIPAM with hydrophilic or hydrophobic species has been shown to directly influence the temperature at which phase transition occurs. To illustrate, NIPAM has been successfully copolymerised with hydrophilic acrylic acid [113] (this formulation incorporates additional functionality, as the hydrophilic carboxylic groups also give rise to pH sensitivity of the PNIPAAm-co-AAc gels) [114-115], acrylamide [116], alginate [117], N,N-dimethylacrylamide (DMAc) [118-119] and hydroxyethyl methacrylate (HEMA) [120-121], which increase

the LCST of PNIPAM-based polymers, and with hydrophobic monomers such as, glycedyl methacrylate (GMAc) [122] which decrease it.

1.3.4 PNIPAM Synthesis

A number of methods have been adopted to synthesise PNIPAM, the most common approaches being redox initiation in aqueous solution [54, 123-128], Reversible addition–fragmentation chain transfer polymerisation (RAFT) [129-136], atom transfer radical polymerisation (ATRP) [137-143] and radiation initiated [144-147], although this list is by no means exhaustive. A brief overview of each of the aforementioned methods is given below.

1.3.4.1 Free-radical initiation in aqueous / organic media

A free radical is a molecular or elemental species with an unpaired electron associated with its structure. The unpaired electrons are profoundly reactive, and their addition to the double bond of a monomer generates another unpaired electron, and subsequent monomers are linked together in rapid succession. Therefore the reactive radical is continuously relocated at the end of the propagating polymer chain until the reaction is terminated:

a) Initiation:

$$R\text{-}R \longrightarrow 2R\bullet$$

$$R^{I} \quad CH_2{=}CH_2 \longrightarrow R{-}CH_2CH_2\bullet$$

b) Propagation:

$$R{-}CH_2CH_2\bullet \quad CH_2{=}CH_2 \longrightarrow R{-}CH_2CH_2CH_2CH_2\bullet$$

$$R{-}CH_2CH_2CH_2CH_2\bullet \quad CH_2{=}CH_2 \longrightarrow R{-}CH_2CH_2CH_2CH_2CH_2CH_2\bullet$$

c) Termination:

$$2 \; R\text{-}(CH_2CH_2)_nCH_2CH_2\bullet \longrightarrow R\text{—}(CH_2CH_2)_nCH_2CH_2\text{—}CH_2CH_2(CH_2CH_2)_nR$$

$$2 \; R\text{-}(CH_2CH_2)_nCH_2CH_2\bullet \longrightarrow R\text{-}(CH_2CH_2)_nCH=CH_2 \; + \; R\text{-}(CH_2CH_2)_nCH_2CH_3$$
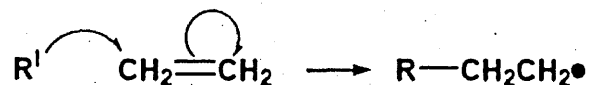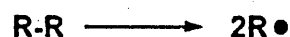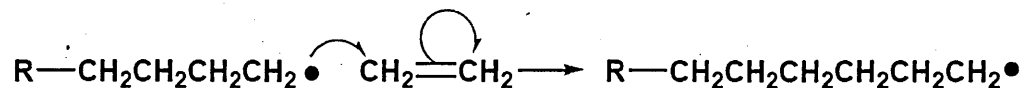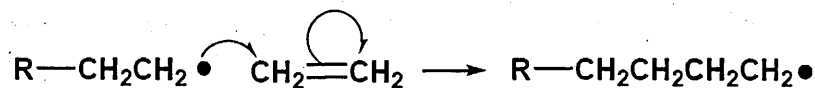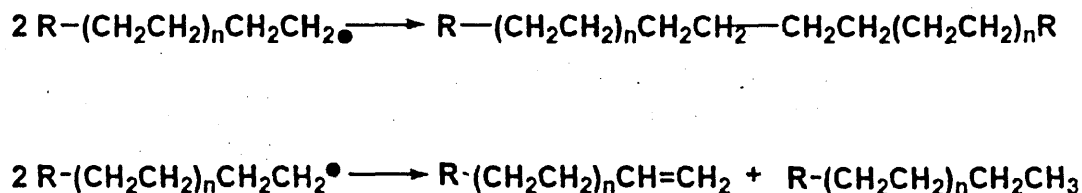
Figure 1.8

The initiator (R•) is typically an organic compound which can easily be dissociated by heat or light to produce free radical species, and the radical must be stable for enough time to allow reaction with a monomer and generation of an active centre.

Azo compounds (organic compounds containing the azo -N=N- group) undergo thermal decomposition upon heating. For example, figure 1.9. shows how azobisisobutyronitrile (AIBN) cleaves symmetrically to form two 2-cyanoprop-2-yl radicals, eliminating a molecule of nitrogen gas:
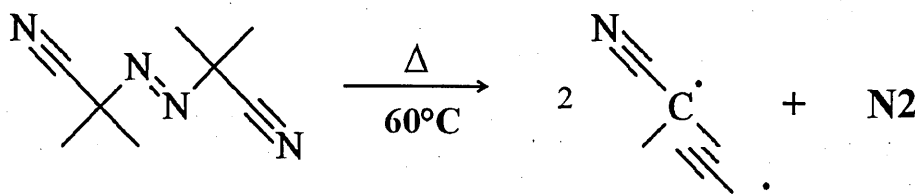
Figure 1.9. Azobisisobutyronitrile (AIBN) cleaving symmetrically to form two 2-cyanoprop-2-yl radicals.

AIBN can also be subject to photolysis (the chemical process by which molecules are broken into its constituent units through the absorption of light), and is decomposed by an identical scheme as that depicted above. The decomposition is induced by UV radiation at a wavelength of ~360nm. A more detailed explanation of this type of initiation can be found in section 1.3.4.4.

Theoretically, propagation of the polymer chain could terminate when all of the monomer in the system is consumed. In practise, the high reactivity of free radical species readily results in the formation of inactive covalent bonds wherever possible. Propagation ceases when the radical is deactivated by the destruction of the active centre, which occurs readily upon contact with another radical species [148] (figure 1.8c). Thus, if the radical concentration is high, the probability of radical interaction is increased and short polymer chains result. Conversely, if long chains are required, small initiator concentrations are used.

Chain-end termination can have several causes; interaction with residual or dissolved oxygen, interaction with an inhibitor, a transfer of the active center to another monomer or to the solvent, meeting of two active centres of propagating polymer chains, or the interaction of an active centre and an initiating radical.

Different approaches can be taken to tailor the molecular weight (M_w) of the resulting polymers. For example, as previously mentioned, increasing the number of initiating radicals increases the number of propagating chains, reducing their overall M_w [149], an increase in temperature encourages faster propagation reactions and a lower M_w [136], and an increase in pressure encourages faster propagation yet inhibits radical deactivation, increasing the overall M_w [136].

Not all monomers successfully propagate in response to all types of initiators. Radical initiation is most effective in the presence of vinyl monomers (and a carbon-carbon double bond) and aldehydes and ketones (in the presence of a carbon-oxygen double bond) [150]. The selection of a suitable initiator for these types of polymerisations depends heavily on two factors – the solubility of the initiator and its dissociation/ decomposition temperature. If the polymerisation is to be performed in an aqueous or organic solvent, it is imperative that the initiator dissolves in the solvent and that its dissociation temperature does not exceed the boiling temperature of that solvent.

PNIPAM gels can be produced in the form of microgels, macrogels, films, rods and fibres. PNIPAM micro/ nanospheres are produced by fee radical polymerisation at temperatures exceeding the LCST (also sometimes referred to as dispersion polymerisation). This can be performed with or without a surfactant and/ or crosslinking agent. Until now, solution polymerisation was required to produce larger-sized and structured gels. This involves a redox initiated free radical polymerisation at temperatures below that of the LCST, and requires NIPAM monomer, a cross-linking agent, an initiator, and an accelerating agent. The most typical free radical method for NIPAM solution polymerisation is that which uses a combination of either potassium persulfate or ammonium persulfate as an initiator, together with an accelerator - N,N,N',N' tetramethylethylenediamine (TEMED) or sodium metabisulphate [35, 127, 151-152].

1.3.4.2   Reversible Addition-Fragmentation chain Transfer (RAFT)

One of several kinds of controlled radical polymerisation, RAFT polymerisation is a highly utilised method for PNIPAM synthesis [129], and allows the design of polymers

with complex architectures, such as linear block copolymers [153], comb-like [154-155], star [156], brush polymers [157] and dendrimers [158]. It is a method of "living" free-radical polymerisation, in other words, the ability for the propagating chain to terminate is removed. The specific details of this technique are not relevant in this thesis; however the reader is directed to a comprehensive review detailing the scope and applications of the RAFT process, published by its inventors, Rizzardo *et al* [159].

1.3.4.3   Atom Transfer Radical Polymerisation (ATRP)

Another example of a living free-radical polymerisation technique is atom transfer radical polymerisation (ATRP), which was independently discovered by Mitsuo Sawamoto *et al* and Jin-Shan Wang and Krzysztof Matyjaszewski in 1995. This technique affords the production of PNIPAM brushes [160], stars [161], combs [162], and copolymers of various architectures [163-166], and unlike RAFT techniques, it allows controlled evolution of molecular weight and polydispersity. As a full explanation of this technique beyond the scope of this thesis, and the reader is referred to an excellent review of this technique by Braunecker *et al* [167].

1.3.4.4   Radiation polymerisation

Another technique that has been utilised in PNIPAM synthesis is radiation polymerisation, and types of radiation with can be used are ionising radiation (using linear accelerator electrons [168] or cobalt- 60 gamma rays [169-170]), or UV radiation of a particular wavelength.

Radiation can initiate the polymerisation and cross-link the resulting chains. As reported by Nagaoka et al [171], the formation of the monomer radical occurs via 1) the direct effect of radiation and 2) an indirect effect whereby products of water radiolysis react with the monomer. They detail the formation of radical on the isopropyl group of the monomer (which is stable, and therefore unlikely to contribute to the polymerisation or cross-linking) along with the formation of carboxyl alkyl radical [171]. Although it had been thought that most monomers required a small amount of chemical cross-linking agent and/ or relatively high doses of radiation in order for cross-linking to occur [172], Nagaoka et al concluded that no additive was necessary to obtain a PNIPAM hydrogel with good mechanical properties using relatively low doses of radiation. As such, this straightforward and additive-free process is potentially advantageous for the preparation of hydrogels intended for biological applications, providing simultaneous

polymerisation, cross-linking and sterilisation without concern for biological response to toxic initiator or cross-linking agent.

Radiation can also facilitate the grafting of PNIPAM onto substrates, giving rise to thermal hydrophilic/ hydrophobic control of surfaces. For example, As early as 1988, Uenoyama and Hoffman endeavoured to be able to inhibit a biological response to model implants by grafting PNIPAM onto silicone rubber substrates [173]. Munoz-Munoz et al synthesised and grafted PNIPAM onto polypropylene films utilising gamma radiation with a view to developing "switching" medicated coatings on medical devices.[174].

1.4.   Cross-linked *poly*(N-isopropylacrylamide) (PNIPAM)

Hydrogels can be classed a) chemically cross-linked, whereby polymer chain functional groups are irreversibly anchored to one another via the use of radiation or cross-linking agent to form insoluble 3-dimensional networks, or b) physically cross-linked, whereby polymer chains are tethered through intermolecular forces such as hydrophobic association or van der Walls forces. The key points of interest of both of these class of polymer is summarised below.

1.4.1   Chemical crosslinks

Prior to 2002, most conventional PNIPAM hydrogels were synthesised using an organic cross-linking agent. PNIPAM gels cross-linked using BIS as chemical cross-linker, were introduced by Pelton and Chibante in 1986 [175]. These gels, however, were shown to result in significant limitations with regards to their optical, structural and mechanical properties, due to their rigid and inhomogeneous cross-linked networks. The cross-linking reaction occurs at irregular points along the polymer chain; therefore chain lengths between cross-links have a broad distribution (refer to fig 1.11).

Rigid chemical bridges between neighbouring polymer chains
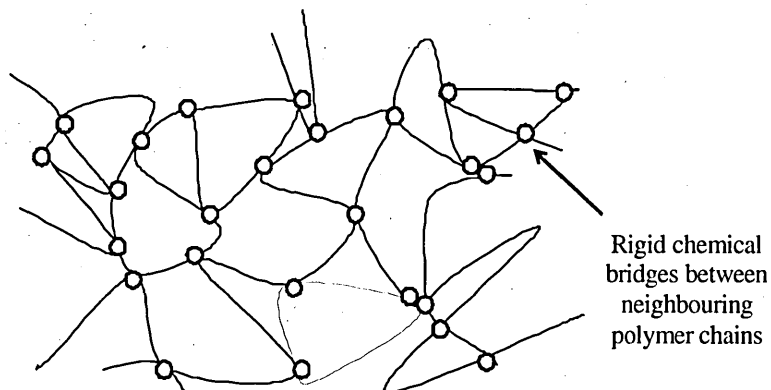
Figure 1.11. Conventional chemically cross-linked gel structure model.

19

This heterogeneous aggregation of cross-linking points has also been shown to get worse as cross-linker concentration increases [34, 67, 103], severely limiting the potential of the PNIPAM to effectively respond to temperature change, as in addition to their inferior mechanical properties, chemically cross-linked networks demonstrate poor functional properties such as retarded deswelling rate, low swelling capacity and erratic solute release [21, 104, 125]. Several attempts have been made to address the aforementioned issues, such as the incorporation of additional inorganic components, such as silica [104], inorganic clay [21], and organically modified clays [176]. In all these cases, however, mechanical and absorption properties were not significantly improved. It would appear that the inorganic components did not behave as reinforcing agents as expected, but the role played by the chemical cross-links in the gel's fragility remained dominant.

Several other new types of network structures have been attempted to address the mechanical and swellability issues of hydrogel matrices, with varying degrees of success. For example, the synthesis of interpenetrating (or double) hydrogel networks [177-179], the addition of macromolecular microspheres [180] the incorporation of starch-based nanospheres as cross-linking agents [181], the use of silk fibroin [182], the development of networks with linear chains and figure-of-eight sliding cross-links [183-185] and the use of exfoliated clay as an inorganic cross-linking agent, forming a polymer/ clay nanocomposite [186-188]. Of these approaches, it is the polymer/ clay nanocomposite systems which provide the most improved mechanical, optical and swelling/ deswelling properties.

1.4.2 Physical crosslinks

In 2002, Kazutoshi Haraguchi found that the mechanical, optical, structural and absorption properties of PNIPAM were dramatically improved with the use of exfoliated inorganic clay platelets in place of conventional organic chemical cross-links. This revolutionary nanocomposite hydrogel, which was polymerised in the presence of clay *in situ* using free-radical polymerisation, was shown to exhibit excellent mechanical properties, such as 1000% improvement on elongation at break, fracture energy up to 3300 times that of its predecessors, and a strength, modulus and swelling/ deswelling capacity which could be modified and controlled by adjusting clay concentration [188]. These properties were credited to the fact that the clay acts as a multifunctional cross-linking agent through non-covalent interactions, and the polymer

chains attached to the clay sheets are free and flexible, taking an almost random conformation between the relatively large distances between clay platelets (fig 1.12.).

Recovery
Elongation
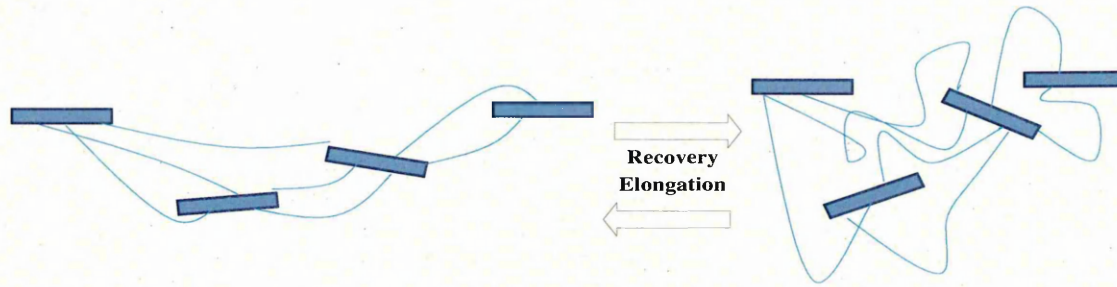
Figure 1.12. A schematic representation of flexible polymer chains grafted onto neighbouring clay platelets. A, during elongation, and B, recovery.

The restrictions placed on chemically cross-linked gels due to large numbers of cross-links down the length of the chain are no longer applicable, and rather than the brittle and fragile gels achievable previously, the gel itself exhibited flexible, rubber-like behaviour.

1.5   Clays

Clays occur naturally as constituents of geological material, mainly as fine particles (with diameters ranging from a few μm to hundredths of a μm) with a sheet structure and a very large surface area. They have been the object of considerable interest to academics and industry because they often have a high capacity for cation exchange, useful swelling properties, and high adsorption capacities. Common clay minerals include smectite, vermiculite, mica, kaolinite, montmorillonite, and chlorite, each with a unique behavioural profile.

1.5.1   Structure, Properties and Types of Clays

Clays exist as layered structures. On a molecular level, they are crystalline in structure, and composition is determined by the atomic arrangement and combination within each clay layer (or platelet). The simple building blocks of a clay platelet consist of silica tetrahedra sheets and octahedral sheets. In silica tetrahedra, four oxygen atoms surround a central silicon atom (forming a silica-tetrahedral sheet) as shown in fig 1.13.
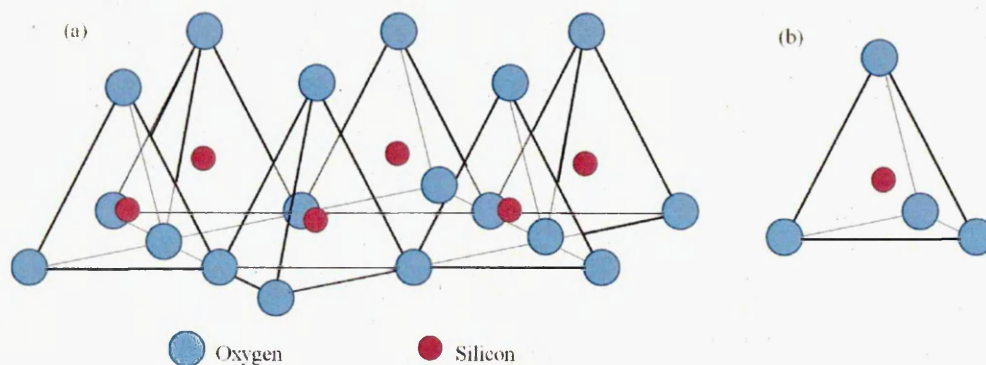
Figure 1.13. Diagrammatic representation of (a) the sheet arrangement of silica tetrahedra and (b) an individual silica tetrahedron.

The silica tetrahedral structure forms a pseudo-hexagonal arrangement, and a hexagonal void appears in the centre of each arrangement, referred to as the ditrigonal cavity. The oxygen atoms either become external (such as Hydroxyl) groups, or form bonds to an octahedral sheet.
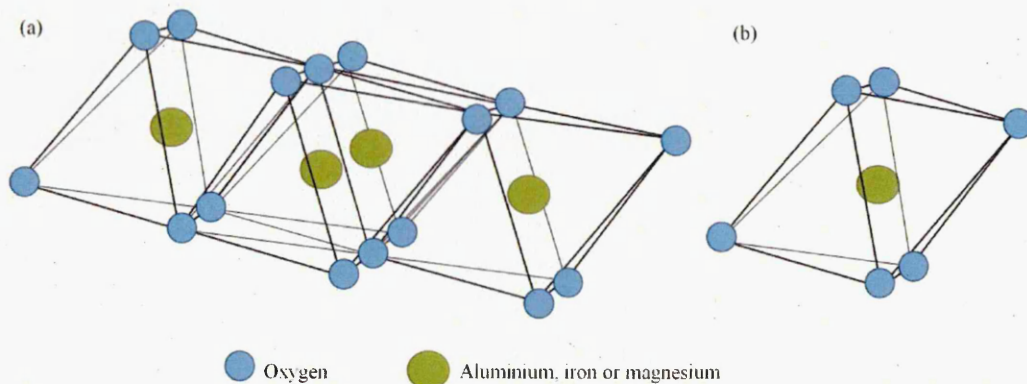
Figure 1.14. Diagrammatic representation of (a) the structure of an octahedral sheet, and (b) an individual octahedron.

Octahedral sheets consist of six hydroxyl anions or oxygen atoms surrounding a central aluminium, iron or magnesium atom. Adjacent octahedral groups share these anions and a planar network is formed (fig 1.14). The tetrahedral and octahedral sheets are superimposed on one another and fused by the sharing of oxygen atoms, and the fused sheets collectively constitute a clay layer. The layers form regular stacks, with a large surface area and a high aspect ratio.

22

Tetrahedral sheet

Octahedral sheet

(a)   (b)
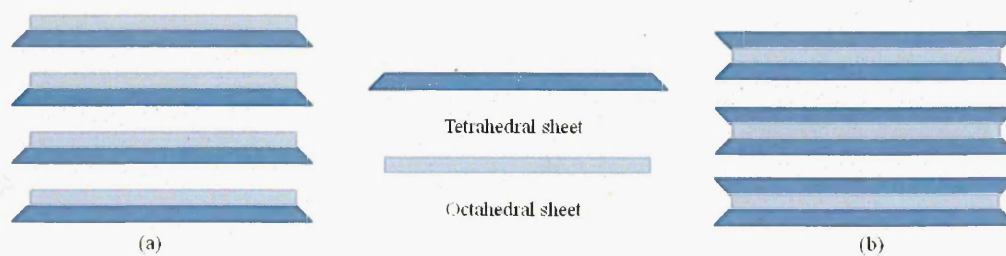
Figure 1.15. The arrangement of clay layers

The basis for classification of these minerals is the molecular arrangement of the platelets; for example, a Kaolin group consists of one octahedral layer fused to tetrahedral layer (in a 1:1 conformation, (Fig 1.15a)), and has the general formula $Al_2Si_2O_5(OH)_5$. Smectites, vermiculites, mica and talc are composed of a single octahedral sheet fused to two tetrahedral sheets in a sandwich-style 2:1 conformation (Fig 1.15b). Of these, Smectites are of the most utilised in nanocomposite technology because of their ability to swell in solvent and undergo cation exchange (also called isomorphous substitution). In very simplistic terms, this process involves the replacement of inter-layer ions with ions of a similar size and lower charge (for example, Al^{3+} is replaced by Mg^{2+} in an octahedral sheet, and Si^{4+} is replaced by Al^{3+} in a tetrahedral sheet), resulting in an excess of electrons. The net negative charge is counteracted by the adsorption of species such as K^+, Ca^{2+}, Na^+ or Mg^{2+}, which provides a charged aqueous environment within the inter-layer space (or gallery). These cations are shared between clay layers and results in the layers being bound to one another. The distance between similar atomic planes in clay (the interatomic spacing, and therefore distance between the clay platelets) is referred to as the d- spacing, and is measured in angstroms.

Increasing hydration

Increasing dehydration e.g. Oven drying
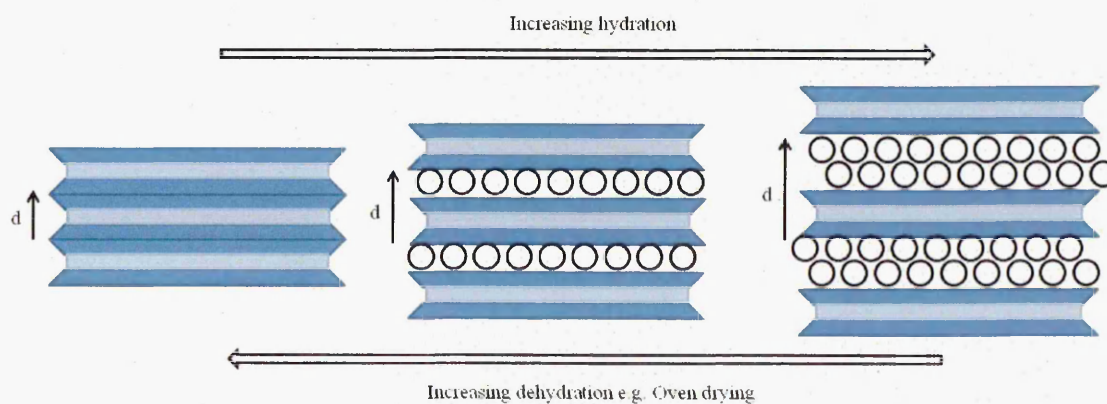
Figure 1.16. The swelling of clay platelets and resulting increase in d-spacing.

23

The d-spacing increases when water is absorbed into the inter-layer gallery. The net result is a swelling of the clay, as represented in fig 1.16. The swellability of the clay depends largely on the strength of this electrostatic bonding between the cations and the clay layer, the weaker the interaction, the more easily water and polar molecules can be absorbed into the clay gallery.

1.5.2 Laponite

Laponite is a synthetic smectite clay which appears in several personal, household paper and polymer products, and is manufactured at the Rockwood site in Widnes, UK [189]. It has Mg^{2+} and Li^+ cations in the octahedral sites, with Na^+ cations within the interlayer space. The idealised formula for Laponite is $Na_{0.7}[Mg_{5.5}Li_{0.4} Si_8O_{20}(OH)_4]$, and the platelets are typically ~30nm in diameter with a thickness of 0.92nm [190]. As a completely synthetic mineral, it has a well defined structural and chemical composition and is devoid of some inorganic components found in natural layered silicates, such as iron oxides.

In the field of polymer science, Laponite has proven commercially useful for several applications. Amongst these are its dispersion within polymers; as Laponite is hydrophilic and swells readily in aqueous media, the clay particles can be dispersed amongst hydrophilic polymers (poly(vinyl alcohol), for example) without further replacement of interlayer Na^+ cations. In the case of hydrophobic polymers (such as polyethylene), an improvement in compatibility of the clay and polymer is required. For this, interlayer Na^+ ions are exchanged for alkylammonium cations and aid the dispersion of the inorganic clay particles in the polymeric matrix [191].

1.6 Nanocomposite Materials

As a loose definition, a nanocomposite is a material which incorporates two or more individual components, one of which has dimensions on the nanometre scale (< 100nm) that are combined to obtain the optimal properties of each component and a unique property profile. The extraordinarily high aspect ratio of the nanoscale phase and its exceptionally high surface to volume ratio makes nanocomposites differ from conventional composite materials. The nanoscale component can be made up of sheets (such as exfoliated layered silicates), particles (such as minerals), or nanofibres (such as carbon nanotubes). In the presence of the nanoscale component, the properties of the matrix material are affected drastically. The design and development of composite

materials, as well as the optimisation of the manufacturing process for optimal performance is therefore integral to the engineering of specialist materials.

Nanocomposites are abundantly evident in nature, with naturally-occurring and biologically formed reagents and polymers (sugars, carbohydrates, proteins and lipids) forming amazingly adept composites which comprise bone, shell, exoskeleton and wood.

1.6.1 Polymer-matrix nanocomposites

Nanoparticles such as metals, carbon nanotubes or clays have been incorporated into a polymer matrix to enhance mechanical [192-197], barrier [198-203], fire resistance [204-206], transparency [187, 193, 197, 207-214], permeability [201, 203, 215-220], stiffness [195, 221-226], electrical [227-235] and thermal stability [194, 206, 221, 236-238], as well as allow improvements in tensile strength [193, 195-197, 199] and elongation at break [195-197, 199, 239] when compared to that of the pristine polymer.

1.6.2 Polymer/ clay nanocomposites

The true beginning of polymer nanocomposite innovation was in 1989 with the development of clay/Nylon-6 nanocomposites by Toyota, to produce tough, heat resistant timing belt covers which exhibited substantial improvements on the physical properties of the pristine Nylon 6 polymer [240-241]. Significant effort was thus applied to the understanding and utility of these materials by research groups the world over.

Figure 1.17 shows a diagrammatic representation of the three main types of composite morphologies found in clay/ polymer composites. The type of composite obtained usually depends on the preparation method and the type of clay used.

When the clay layers are not sufficiently separated in order for the polymer to intercalate between them, the composite obtained is distinctly phase-separated, and the properties of the material is generally not much changed from that of regular microcomposite materials [186]. In addition, a poorly dispersed composite material has, in some cases, been shown to exert worsened mechanical properties when compared those to the polymer alone [186]. When the structure is intercalated, platelet separation has occurred to a degree which allows little more than a few single polymer chains to extend between the layers.
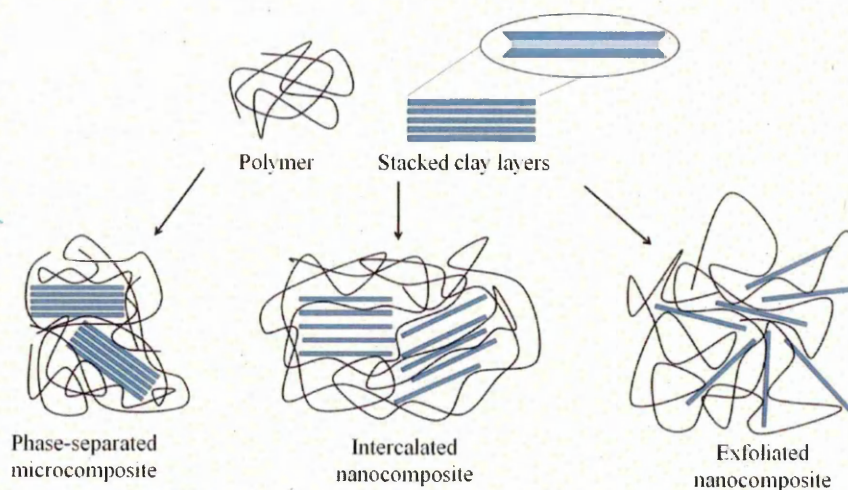
Figure 1.17. Schematic of the types of clay layer orientation in a polymer nanocomposite matrix.

Ordered, stacked platelet morphology is still apparent and high interference interactions are detectable from X-ray diffraction (XRD) patterns, however. When a complete uniform dispersion of clay layers is obtained within a continuous polymer phase, the system is considered to be delaminated, or "exfoliated" [242] (fig 1.17.). This conformation provides the highest possible aspect ratio, and the large number of polymer/ clay surface interactions is responsible for the significant improvement in the nanomaterial properties. When these types of structures are achieved, no diffraction pattern is visible in x-ray diffractograms.

Owing to their availability, low cost and ability to provide dramatic improvements at very low loadings, considerable interest has grown addressing the formulation and properties of polymer/ clay nanomaterials. Although the intercalation of polymers with layered silicates has been known to science for almost fifty years [243], the art of polymer/ clay intercalation has gained rapid momentum in both industry and academia in the last 2 decades.

1.6.3   PNIPAM/ Clay Nanocomposites

As previously discussed, the mechanical and swelling properties of PNIPAM has been extensively examined [244-246]. It has been observed that at the high concentrations of cross-linker required for mechanical stability, most cross-linkers hinder the swelling/ deswelling capabilities of the gels and shift as well as broaden the volume transition temperature [247]. It is well documented in recent years that the properties of PNIPAM are enhanced significantly by the incorporation of inorganic layered silicates into the

26

gels [21, 104, 186, 197, 245, 248-249]. The addition of clay minerals to PNIPAM has improved the properties of the resulting hydrogel whilst retaining (even enhancing) the intrinsic hydrophilic/ hydrophobic phase transition of the polymer.

The development of PNIPAM/ clay nanocomposites was pioneered by Haraguchi et al, who in 2002, proposed a model for the polymer/ clay network structure, basing it on analytical data from FTIR, DSC, XRD, TEM and TGA measurements [193], and reported its compatibility with their mechanical, swelling and optical observations [196-197, 250]. They proved the multifunctionality of the clay platelets by calculating that the number of cross-linking points per clay platelet were in the order of ~50 to ~120, depending on clay concentration [250]. A substantially increased degree of equilibrium swelling is reported when compared to chemically cross-linked PNIPAM gels [34, 251], and this is attributed to a relatively low effective cross-link density value.

They also report a consistent elongation at break of the nanocomposite gels to be more than 1000%, regardless of the respective polymer or clay content [196], along with extremely high time-dependent recovery following large strain applications [197]. Also demonstrated are improvements in modulus and strength as a function of clay content and polymer density [196]. The swelling and mechanical phenomena are attributed to the dynamic polymer/ clay interaction, and therefore adaptive continuous rearrangement of polymer chains and clay platelets during elongation, compression, swelling and deswelling.

When compared with chemically cross-linked PNIPAM systems, Haraguchi et al report a precise and sharp LCST of PNIPAM/ clay gels which is shifted upwards to a small degree with increasing clay loading [250]. The manifestation of retractive tensile forces at the LCST have also been observed [248] by applying stress to the gel in a temperature-controlled aqueous environment. The force profiles of the gels showed excellent correlation to volume-change data during temperature-cycling.

Another key observation by the group was the significant improvement in optical transparency when chemical cross-links are replaced with clay. The opacity of chemically cross-linked systems has been attributed to the inhomogeneous distribution of cross-link points [250], and excellent optical clarity of clay networks, regardless of clay content or polymer density, indicates a uniform clay/ polymer network. These conclusions were supported by dynamic light scattering (DLS), small angle neutron scattering (SANS) and small angle x-ray scattering (SAXS) data [252].

27

A crucial series of investigations by the group were those surround the biocompatibility of their clay/ PNIPAM systems [86]. They show that clay/ PNIPAM gels are capable of absorbing water, blood plasma and saline to their interstitial spaces, and even exhibit good blood and tissue compatibility during short-term cavity implantation. The gels are capable of withstanding sterilisation by γ radiation or with an autoclave without their thermal stability being compromised. Cytocompatibility was shown to be good, showing that the presence of PNIPAM or clay did not affect or disturb the culturing cells, although the samples were subject to significant purification beforehand (they were washed and immersed in regularly- replaced water above the LCST for 10 days), in order to remove potentially toxic residual monomer and initiator. They present a thermo-sensitive Clay/ PNIPAM substratum which is capable of cell adhesion and release without the intervention of trypsin treatment, as a reduction in temperature to 20°C enabled spontaneous cell detachment from the surface in the form of a cell sheet. They also found that cell culture development was not possible in chemically cross-linked PNIPAM systems regardless of cross-link concentration [86], despite all parameters other than cross-link type being identical.

1.7   Aims and Objectives of This Study

The aim of the presented research was to explore the possibility of applying existing nanotechnology to address technical challenges in the development of new PNIPAM-based stimuli-responsive materials with a number of high value applications. Particularly appropriate uses for these types of materials include targeted drug delivery, would management, and biological tissue scaffolding.

One major technical challenge in the production of these materials is that which addresses the adjustment of the LCST and response mechanism, and use was made of existing synthetic methodologies to innovatively build on the capabilities of existing materials. Four main approaches were adopted to achieve this; (i) by examining and comparing the effect of the initiation method (UV radiation vs. thermal) and cross-link type (chemical vs. physical) on the deswelling mechanism and phase transition temperature of the PNIPAM gels, (ii) the examination of how biologically-compatible interstitial dopants affect temperature response of PNIPAM gels of various cross-link densities, (iii) the study of alcohol- induced cononsolvency behaviour of PNIPAM gels as a function of cross-link type, cross-link concentration, initiation method and dopant

species, and (iiii), the relative response change of PNIPAM as a function of ratio of hydrophilic/ hydrophobic comonomer.

Diffusion behaviour of small molecules through thin films of cross-linked PNIPAM was examined by attenuated total reflection – Fourier transform infrared spectroscopy (ATR-FTIR) to acquire information on solvent/ polymer interactions and diffusion kinetics of the system.

Another major technical issue for these materials is their processability, more specifically, overcoming issues which currently pose serious limitations to their use as biological substrates and scaffolds. Current technologies include; (i) the prior polymerisation of PNIPAM based gels which are subsequently dried and powdered prior to injection into the vicinity of a vertebral fracture or other cavity prior to cross-linking *in situ* [253], (ii) the injection of a polymerised gel/ photoinitiator/ cross-linking agent solution under the skin, and subsequent permanent cross-linking via exposure to UV radiation [254], and (iii), the formation of a copolymeric hydrogel which is injected into damaged inter-vertebral spinal discs followed by a di- or multi-functional aldehyde cross-linking agent which forms a stable polymer matrix over a period of 2 days [255]. Most existing technologies of this type requires the cross-linking of the preformed polymers *in situ* posing biocompatibility issues, requiring that reactive biohazardous and potentially cytotoxic cross-linking agents and /or initiators are injected into body cavities, or potentially harmful doses of radiation are required to penetrate the skin. In addition, excessive curing times (such as that outlined in example (iii), involve substantial impracticalities such as the immobilisation of the patient for several days. Existing methods also require several operational steps and specialist equipment, therefore requiring significant financial cost, expertise and processing time. PNIPAM sheets have also been produced by pouring a monomer/ initiator/ accelerator solution into a mould at a temperature above which the initiator dissociates, and allowing polymerisation to proceed *in situ*. This method requires encapsulation of the entire apparatus under an oxygen-free, nitrogen atmosphere and extensive post- synthesis purification. [86]

Here is presented the development of a novel PNIPAM/ clay precursor which addresses all of the aforementioned issues. Polymerised fully at a high temperature as a low viscosity, opaque liquid, it solidifies to spontaneously form a clear PNIPAM/ clay gel. Investigations undertaken to examine the tolerance of biologically active species to the

gel in its precursor and post- PTTNAG state, as well as the ability to form such a polymer/ clay liquid precursor which encompasses other hydrophilic/ hydrophobic moieties in order to tailor the LCST and setting temperature are also presented. This invention allows the development of new and exciting technologies which can be tailored to specific medical and industrial uses.

1.8 References

1.   Painter P. C., Fundamentals of Polymer Science. 2 ed. 1997: CRC Press.

2.   Dougan, L., et al., Molecular self-assembly in a model amphiphile system. Physical Chemistry Chemical Physics, 2010. 12(35): p. 10221-10229.

3.   Li, X., et al., Rich Self-Assembly Behavior from a Simple Amphiphile. Chemphyschem, 2010. 11(14): p. 3074-3077.

4.   Hoffman, A.S., Hydrogels for biomedical applications. Advanced Drug Delivery Reviews, 2002. 54(1): p. 3-12.

5.   Jeong, B., Gutowska, A., Lessons from nature: stimuli-responsive polymers and their biomedical applications (vol 20, pg 305, 2002). Trends in Biotechnology, 2002. 20(8): p. 360-360.

6.   Jeong, B., Kim, S., Bae, Y., Thermosensitive sol-gel reversible hydrogels. Advanced Drug Delivery Reviews, 2002. 54(1): p. 37-51.

7.   Schellman, J.A., The Factors Affecting the Stability of Hydrogen-bonded Polypeptide Structures in Solution. The Journal of Physical Chemistry, 1958. 62(12): p. 1485-1494.

8.   Schellman, J.A., The stability of hydrogen-bonded peptide structures in aqueous solution. Comptes rendus des travaux du Laboratoire Carlsberg. Serie chimique, 1955. 29(14-15): p. 230-59.

9.   Byrne, M.E., Park, K., Peppas,N., Molecular imprinting within hydrogels. Advanced Drug Delivery Reviews, 2002. 54(1): p. 149-161.

10.   Chen, S., et al., Effect of molecular weight on shape memory behavior in polyurethane films. Polymer International, 2007. 56(9): p. 1128-1134.

11.   De Rossi, D., Della Santa, A., Mazzoldi, A., Dressware: wearable hardware. Materials Science & Engineering C-Biomimetic and Supramolecular Systems, 1999. 7(1): p. 31-35.

12.   Shahinpoor, M., et al., Ionic polymer-metal composites (IPMCs) as biomimetic sensors, actuators and artificial muscles - a review. Smart Materials & Structures, 1998. 7(6): p. R15-R30.

13.   Shahinpoor, M., Mojarrad, M., Salehpoor, M., Electrically induced large amplitude vibration and resonance characteristics of ionic polymeric membrane-metal composites artificial muscles. Smart Structures and Integrated Systems - Smart Structures and Materials 1997, ed. M.E. Regelbrugge. Vol. 3041. 1997. 829-838.

14.   Leng, J.S., et al., Significantly reducing electrical resistivity by forming conductive Ni chains in a polyurethane shape-memory polymer/carbon-black composite. Applied Physics Letters, 2008. 92(20), Article Number: 204101.

15.   Bar-Cohen, Y., Zhang, Q., Electroactive polymer actuators and sensors. Mrs Bulletin, 2008. 33(3): p. 173-181.

16.   Schmidt, D.J., et al., Electrochemically Controlled Swelling and Mechanical Properties of a Polymer Nanocomposite. Acs Nano, 2009. 3(8): p. 2207-2216.

17.   Ahn, S., Monge, E., Song, S., Ion and pH Effect on the Lower Critical Solution Temperature Phase Behavior in Neutral and Acidic Poly(organophosphazene) Counterparts. Langmuir, 2009. 25(4): p. 2407-2418.

18.   Li, D., He, Q., Li, J., Smart core/shell nanocomposites: Intelligent polymers modified gold nanoparticles. Advances in Colloid and Interface Science, 2009. 149(1-2): p. 28-38.

19.   Ebara, M., et al., Temperature-responsive cell culture surfaces enable "on-off" affinity control between cell integrins and RGDS ligands. Biomacromolecules, 2004. 5(2): p. 505-510.

20.   Hernandez, E., Orozco-Avila, I., Temperature-Sensitive Hydrogels: A Gentle Way of Concentrating Cellulase Enzymes. Macromolecular Symposia, 2009. 283(84): p. 139-143.

21.   Liang, L., Liu, J., Gong, X., Thermosensitive poly(N-isopropylacrylamide)-clay nanocomposites with enhanced temperature response. Langmuir, 2000. 16(25): p. 9895-9899.

22.   Lin, S.C., et al., Enhanced protein renaturation by temperature-responsive polymers. Biotechnology and Bioengineering, 2000. 67(5): p. 505-512.

23.   Pelton, R., Temperature-sensitive aqueous microgels. Advances in Colloid and Interface Science, 2000. 85(1): p. 1-33.

24.   Yang, J., et al., pH/temperature dual stimuli responsive microgels based on interpenetrating polymer network structure. Acta Polymerica Sinica, 2009(7): p. 638-644.

25.   Muller, S.J., Stoeber, B., Liepmann, D., Microflow control strategies based on thermally-responsive triblock copolymers. Abstracts of Papers of the American Chemical Society, 2007: p. 233- 340.

26.   Tanaka, T., et al., PHASE-TRANSITIONS IN IONIC GELS. Physical Review Letters, 1980. 45(20): p. 1636-1639.

27.   Qiu, Y., Park, K., Environment-sensitive hydrogels for drug delivery. Advanced Drug Delivery Reviews, 2001. 53(3): p. 321-339.

28.   Fujiwara, N., et al., Preparation of gold-solid polymer electrolyte composites as electric stimuli-responsive materials. Chemistry of Materials, 2000. 12(6): p. 1750-1754.

29.   Miyata, T., Uragami, T., Nakamae, K., Biomolecule-sensitive hydrogels. Advanced Drug Delivery Reviews, 2002. 54(1): p. 79-98.

30.   Yim, H., et al., Temperature-dependent conformational change of PNIPAM grafted chains at high surface density in water. Macromolecules, 2004. 37(5): p. 1994-1997.

31.   Huber, D.L., et al., Programmed adsorption and release of proteins in a microfluidic device. Science, 2003. 301(5631): p. 352-354.

32.   Plunkett, K.N., et al., PNIPAM chain collapse depends on the molecular weight and grafting density. Langmuir, 2006. 22(9): p. 4259-4266.

33.   Okada, Y., Tanaka, F., Cooperative hydration, chain collapse, and flat LCST behavior in aqueous poly(N-isopropylacrylamide) solutions. Macromolecules, 2005. 38(10): p. 4465-4471.

34.   Haraguchi, K., Synthesis and properties of soft nanocomposite materials with novel organic/inorganic network structures. Polymer Journal, 2011. 43(3): p. 223-241.

35.   Xu, Y., Li, G., Haraguchi, K., Gel Formation and Molecular Characteristics of Poly(N-isopropylacrylamide) Prepared by Free-Radical Redox Polymerization in Aqueous Solution. Macromolecular Chemistry and Physics, 2010. 211(9): p. 977-987.

36.   Saunders, B.R., Vincent, B., Microgel particles as model colloids: theory, properties and applications. Advances in Colloid and Interface Science, 1999. 80(1): p. 1-25.

37.   E.H. Sprecht., H.T. Neher. [online] Assigned to Rohm & Haas. United States patent 2,773,063. 1956. Patent from USPTO last accessed 2 January 2013 at: http://patft.uspto.gov.

38.   E.H. Sprecht., H.T. Neher. [online], Assigned to Rohm & Haas. Great Britain patent 722,196. 1956. Patent from USPTO last accessed 2 January 2013 at: http://patft.uspto.gov.

39.   Deka, S.R., et al., Magnetic nanobeads decorated by thermo-responsive PNIPAM shell as medical platforms for the efficient delivery of doxorubicin to tumour cells. Nanoscale, 2011. 3(2): p. 619-629.

40.   Gan, T., Guan, Y., Zhang, Y., Thermogelable PNIPAM microgel dispersion as 3D cell scaffold: effect of syneresis. Journal of Materials Chemistry, 2010. 20(28): p. 5937-5944.

41.   Naha, P.C., et al., Intracellular localisation, geno- and cytotoxic response of polyN-isopropylacrylamide (PNIPAM) nanoparticles to human keratinocyte (HaCaT) and colon cells (SW 480). Toxicology Letters, 2010. 198(2): p. 134-143.

42.   Nash, M.E., et al., Straightforward, One-Step Fabrication of Ultrathin Thermoresponsive Films from Commercially Available pNIPAm for Cell Culture and Recovery. ACS Applied Materials & Interfaces, 2011. 3(6): p. 1980-1990.

43.   Ohya, S., Matsuda, T., Poly(N-isopropylacrylamide) (PNIPAM)-grafted gelatin as thermoresponsive three-dimensional artificial extracellular matrix: molecular and formulation parameters vs. cell proliferation potential. Journal of Biomaterials Science-Polymer Edition, 2005. 16(7): p. 809-827.

44.   Schmidt, S., et al., Adhesion and Mechanical Properties of PNIPAM Microgel Films and Their Potential Use as Switchable Cell Culture Substrates. Advanced Functional Materials, 2010. 20(19): p. 3235-3243.

45.   Trongsatitkul, T., Budhlall, B., Multicore-Shell PNIPAm-co-PEGMa Microcapsules for Cell Encapsulation. Langmuir, 2011. 27(22): p. 13468-13480.

46. Wang, T., et al., Rapid cell sheet detachment from alginate semi-interpenetrating nanocomposite hydrogels of PNIPAm and hectorite clay. Reactive & Functional Polymers, 2011. 71(4): p. 447-454.

47. Tang, F., et al., Hybrid conjugated polymer-Ag@PNIPAM fluorescent nanoparticles with metal-enhanced fluorescence. Journal of Materials Chemistry, 2011. 21(42): p. 16943-16948.

48. Jiang, C., Qian, W., Composites of Intelligent PNIPAM Hydrogels and Au Nanoparticles. Progress in Chemistry, 2010. 22(8): p. 1626-1632.

49. Mijalis, A.J., et al., Effects of LCST phenomena on the protonation state of constituents of amine-containing PNIPAM copolymers. Abstracts of Papers of the American Chemical Society, 2011: p. 241-248.

50. Salcher, A., et al., CdSe/CdS nanoparticles immobilized on pNIPAm-based microspheres. Journal of Materials Chemistry, 2010. 20(7): p. 1367-1374.

51. Sanchez-Iglesias, A., et al., Synthesis of Multifunctional Composite Microgels via In Situ Ni Growth on pNIPAM-Coated Au Nanoparticles. Acs Nano, 2009. 3(10): p. 3184-3190.

52. Wang, Z., Wu, P., Spectral Insights into Gelation Microdynamics of PNIPAM in an Ionic Liquid. Journal of Physical Chemistry B, 2011. 115(36): p. 10604-10614.

53. Tagit, O., et al., Influence of the length and grafting density of PNIPAM chains on the colloidal and optical properties of quantum dot/PNIPAM assemblies. Nanotechnology, 2011. 22(26): Article Number: 265701

54. Riskin, M., Tel-Vered, R., Willner, I., Thermo-Switchable Charge Transport and Electrocatalysis Using Metal-Ion-Modified pNIPAM-Functionalized Electrodes. Advanced Functional Materials, 2009. 19(15): p. 2474-2480.

55. Budhlall, B.M., Marquez, M., Velev, O., Microwave, Photo- and Thermally Responsive PNIPAm-Gold Nanoparticle Microgels. Langmuir, 2008. 24(20): p. 11959-11966.

56. Heinz, P., et al., Phase transition of pNIPAM grafted on plasma-activated PEO monitored in-situ by quartz crystal microbalance, in Proceedings of the 17th International Vacuum Congress/13th International Conference on Surface Science/International Conference on Nanoscience and Technology, L. Johansson and E. Rubel, Editors. 2008.

57. Rubio-Retama, J., et al., Synthesis and characterization of thermosensitive PNIPAM microgels covered with superparamagnetic gamma-Fe_2O_3 nanoparticles. Langmuir, 2007. 23(20): p. 10280-10285.

58. Shen, J., et al., Ternary phase diagram for the Belousov-Zhabotinsky reaction-induced mechanical oscillation of intelligent PNIPAM colloids. Journal of Physical Chemistry A, 2007. 111(48): p. 12081-12085.

59. Zintchenko, A., Ogris, M., Wagner, E., Temperature dependent gene expression induced by PNIPAM-based copolymers: Potential of hyperthermia in gene transfer. Bioconjugate Chemistry, 2006. 17(3): p. 766-772.

60.   Song, M., et al., Application of the Blending of PNIPAM-co-PS Nanofibers with Functionalized Au Nanoparticles for the High-Sensitive Diagnosis of Cancer Cells. Journal of Nanoscience and Nanotechnology, 2009. 9(2): p. 876-879.

61.   Ohya, S., Nakayama, Y., Matsuda, T., In vivo evaluation of poly(N-isopropylacrylamide) (PNIPAM)-grafted gelatin as an in situ-formable scaffold. Journal of artificial organs : the official journal of the Japanese Society for Artificial Organs, 2004. 7(4): p. 181-186.

62.   Ohya, S., et al., The potential of poly(N-isopropylacrylamide) (PNIPAM)-grafted hyaluronan and PNIPAM-grafted gelatin in the control of post-surgical tissue adhesions. Biomaterials, 2005. 26(6): p. 655-659.

63.   Roy, I., Gupta, M.N., Smart polymeric materials: Emerging biochemical applications. Chemistry & Biology, 2003. 10(12): p. 1161-1171.

64.   Lokuge, I., Wang, X., Bohn, P., Temperature-Controlled Flow Switching in Nanocapillary Array Membranes Mediated by Poly(N-isopropylacrylamide) Polymer Brushes Grafted by Atom Transfer Radical Polymerization†. Langmuir, 2006. 23(1): p. 305-311.

65.   Bohn, P.W., Nanoscale Control and Manipulation of Molecular Transport in Chemical Analysis. Annual Review of Analytical Chemistry, 2009. 2(1): p. 279-296.

66.   Haraguchi, K., Takehisa, T., Novel manufacturing process of nanocomposite hydrogel for bio-applications. Manufacturing Engineering and Materials Handling, 2005 Pts A and B. Vol. 16. 2005: p. 119-126.

67.   Miyazaki, S., et al., Gelation mechanism of poly(N-isopropylacrylamide)-clay nanocomposite gels. Macromolecules, 2007. 40(12): p. 4287-4295.

68.   Guan, Y., Zhang, Y., PNIPAM microgels for biomedical applications: from dispersed particles to 3D assemblies. Soft Matter, 2011. 7(14): p. 6375-6384.

69.   Lu, M., et al., Preparation and Properties of Thermosensitive P(St-NIPAM)/PNIPAM-Ag Composite Microgels. Acta Chimica Sinica, 2011. 69(20): p. 2385-2392.

70.   Parasuraman, D., Serpe, M., Poly (N-Isopropylacrylamide) Microgels for Organic Dye Removal from Water. Acs Applied Materials & Interfaces, 2011. 3(7): p. 2732-2737.

71.   Zhou, Y.M., et al., Nanocomposite hydrogels: a novel Wound dressings. 2010 3rd International Conference on Biomedical Engineering and Informatics, ed. W.Z.M.W.L.S.Y. Yu. 2010: p. 432-434.

72.   Song, F., Wang, X., Wang, Y., Poly (N-isopropylacrylamide)/poly (ethylene oxide) blend nanofibrous scaffolds: Thermo-responsive carrier for controlled drug release. Colloids and Surfaces B-Biointerfaces, 2011. 88(2): p. 749-754.

73.   Feng, X., et al., Poly 196-PNIPAm/PVA thermo-sensitive fibers. Abstracts of Papers of the American Chemical Society, 2009. 6423: p. 238-245.

74.   Feng, X., et al., Temperature-sensitive Properties of PNIPAm/PVA Hydrogel Fibers Used for Artificial Muscles. 2010 International Forum on Biomedical Textile Materials, Proceedings. 2010: p. 18-22.

75.   Wang, P., et al., Poly (N-Isopropylacrylamide)-Coated Multifunctional Nanoparticles for Cell Tracking. Photomedicine and Laser Surgery, 2010. 28(2): p. 201-205.

76.   Liu, R., et al., Thermally-responsive surfaces comprising grafted poly(N-isopropylacrylamide) chains: Surface characterisation and reversible capture of dispersed polymer particles. Journal of Colloid and Interface Science, 2009. 340(2): p. 166-175.

77.   Liu, Y., Tu, W., Cao, D., Synthesis of Gold Nanoparticles Coated with Polystyrene-block-poly(N-isopropylacrylamide) and Their Thermoresponsive Ultraviolet-Visible Absorbance. Industrial & Engineering Chemistry Research, 2010. 49(6): p. 2707-2715.

78.   Tanii, H., Hashimoto, K., Invitro neurotoxicity study with dorsal-root ganglia for acrylamide and its derivatives. Toxicology Letters, 1991. 58(2): p. 209-213.

79.   Shipp, A., et al., Acrylamide: Review of toxicity data and dose-response analyses for cancer and noncancer effects. Critical Reviews in Toxicology, 2006. 36(6-7): p. 481-608.

80.   Chapin, R.E., et al., The reproductive and neural toxicities of acrylamide and 3 analogues in Swiss mice, evaluated using the continuous breeding protocol. Fundamental and Applied Toxicology, 1995. 27(1): p. 9-24.

81.   Tyl, R.W., et al., Rat two-generation reproduction and dominant lethal study of acrylamide in drinking water. Reproductive Toxicology, 2000. 14(5): p. 385-401.

82.   Malonne, H., et al., Preparation of poly (N-isopropylacrylamide) copolymers and preliminary assessment of their acute and subacute toxicity in mice. European Journal of Pharmaceutics and Biopharmaceutics, 2005. 61(3): p. 188-194.

83.   Starostina, N.G., et al., Morphological and physiological changes in bacterial cells treated eith acrylamide. European Journal of Applied Microbiology and Biotechnology, 1983. 18(5): p. 264-270.

84.   McCollister, D. E., et al., (1965). Toxicologic investigations of polyacrylamides. Toxic. appl. Pharmac. 7, 639. Food and Cosmetics Toxicology, 1966. 4(0): p. 459.

85.   McCollister, D.D., et al., Toxicologic investigations of polyacrylamides. Toxicology and Applied Pharmacology, 1965. 7(5): p. 639-651.

87.   Baltes, T., Garret-Flaudy, F., Freitag, R., Investigation of the LCST of polyacrylamides as a function of molecular parameters and the solvent composition. Journal of Polymer Science Part a-Polymer Chemistry, 1999. 37(15): p. 2977-2989.

88.   Schild, H.G., Muthukumar, M., Tirrell, D., Cononsolvency in mixed aqueous solutions of poly(N-isopropylacrylamide). Macromolecules, 1991. 24(4): p. 948-952.

89.   Lutz, J.F., Akdemir, Ö., Hoth, A., Point by Point Comparison of Two Thermosensitive Polymers Exhibiting a Similar LCST: Is the Age of Poly(NIPAM) Over? Journal of the American Chemical Society, 2006. 128(40): p. 13046-13047.

90.   Winnik, F.M., Phase transition of aqueous poly(N-isopropylacrylamide) solutions - a study bu nonradiative energy transfer. Polymer, 1990. 31(11): p. 2125-2134.

91.   Chi Wu, G.Z., Folding and Formation of Mesoglobules in Dilute Copolymer Solutions. Adv Polym Sci, 2005. 195(1): p. 101-176.

92.   Scarpa, J.S., et al., Slow hydrogen-deuterium exchange in a non-.alpha.-helical polyamide. Journal of the American Chemical Society, 1967. 89(24): p. 6024-6030.

93.   Malcolm, G.N., Rowlinson, J.S., The thermodynamic properties of aqueous solutions of polyethylene glycol, polypropylene glycol and dioxane. Trans. Faraday Soc., 1957. 53: p. 921-931.

94.   Meyerhoff, K.U., Hydrodynamic properties of methyl cellulose in solution. Die Makromolekulare Chemie, 1961. 47: p. 168–184. .

95.   Heskins, M., Guillet, J.E., Solution Properties of Poly(N-isopropylacrylamide). Journal of Macromolecular Science: Part A - Chemistry, 1968. 2(8): p. 1441-1455.

96.   Tanaka, T., Collapse of gels and critical endpoint. Physical Review Letters, 1978. 40(12): p. 820-823.

97.   Tanaka, T., Dynamics of critical concentration fluctuations in gels. Physical Review A, 1978. 17(2): p. 763-766.

98.   Tanaka, T., Ishiwata,S., Ishimoto, C., Critical behaviour of density fluctuations in gels. Physical Review Letters, 1977. 38(14): p. 771-774.

99.   Hirokawa, Y., Tanaka, Y.,Volume phase transition in a nonioniv gel. Journal of Chemical Physics, 1984. 81(12): p. 6379-6380.

100.   Amiya, T., et al., Re-entrant phase-transition of N-isopropylacrylamide gels in mixed solvents. Journal of Chemical Physics, 1987. 86(4): p. 2375-2379.

101.   Kabra, B.G., Gehrke, S.H., Synthesis of fast response, temperature sensitive poly(N-isopropylacrylamide) gel. Polymer Communications, 1991. 32(11): p. 322-323.

102.   Wu, X.S., Hoffman, A.S., Yager, P., Synthesis and characterisation of thermally reversible macroporous poly(N-isopropylacrylamide) hydrogels. Journal of Polymer Science. Part a-Polymer Chemistry, 1992. 30(10): p. 2121-2129.

103.   Haraguchi, K., Song, L., Microstructures formed in co-cross-linked networks and their relationships to the optical and mechanical properties of PNIPA/clay nanocomposite gels. Macromolecules, 2007. 40(15): p. 5526-5536.

104.   Xiang, Y., et al., A new polymer/clay nano-composite hydrogel with improved response rate and tensile mechanical properties. European Polymer Journal, 2006. 42(9): p. 2125-2132.

105.   Zhou, L., et al., Demixing of amphiphile-polymer mixtures investigated using density functional theory. Physica a-Statistical Mechanics and Its Applications, 2009. 388(15-16): p. 3093-3099.

106.   Haraguchi, K., Nanocomposite Gels -Fundamental Significance and New Functions. Kobunshi Ronbunshu, 2008. 65(10): p. 619-633.

107.   Zhang, Y.J., et al., Specific ion effects on the water solubility of macromolecules: PNIPAM and the Hofmeister series. Journal of the American Chemical Society, 2005. 127(41): p. 14505-14510.

108.   Hirotsu, S., Critical points of the volume phase transition in N-isopropylacrylamide gels. Journal of Chemical Physics, 1988. 88(1): p. 427-431.

109.   Freitag, R., et al., Salt effects on the thermoprecipitation of poly-(N-isopropylacrylamide) oligomers from aqueous solution. Langmuir, 2002. 18(9): p. 3434-3440.

110.   Loh, W., Teixeira, L., Lee, L., Isothermal calorimetric investigation of the interaction of poly(N-isopropylacrylamide) and ionic surfactants. Journal of Physical Chemistry B, 2004. 108(10): p. 3196-3201.

111.   Badiger, M.V., et al., Molecular tailoring of thermoreversible copolymer gels: Some new mechanistic insights. Journal of Chemical Physics, 1998. 109(3): p. 1175-1184.

112.   Lue, S.J., et al., Tuning of Lower Critical Solution Temperature (LCST) of Poly(N-Isopropylacrylamide-co-Acrylic acid) Hydrogels. Journal of Macromolecular Science Part B-Physics, 2011. 50(3): p. 563-579.

113.   Adem, E., et al., Characterization of interpenetrating networks of acrylic acid (AAc) and N-isopropylacrylamide (NIPAAm) synthesized by ionizing radiation. Radiation Physics and Chemistry, 2009. 78(7-8): p. 549-552.

114.   Pei, Y., et al., The effect of pH on the LCST of poly(N-isopropylacrylamide) and poly(N-isopropylacrylamide-co-acrylic acid). Journal of Biomaterials Science-Polymer Edition, 2004. 15(5): p. 585-594.

115.   Zhang, J., et al., Dual thermo- and pH-sensitive poly(N-isopropylacrylamide-co-acrylic acid) hydrogels with rapid response behaviors. Polymer, 2007. 48(6): p. 1718-1728.

116.   Chen, J., et al., Synthesis and properties of poly(N-isopropylacrylamide-co-acrylamide) hydrogels. Macromolecular Symposia, 2005. 225: p. 103-111.

117.   de Moura, M.R., et al., Release of BSA from porous matrices constituted of alginate-Ca$^{(2+)}$ and PNIPAAm-interpenetrated networks. Materials Science & Engineering C-Materials for Biological Applications, 2009. 29(8): p. 2319-2325.

118.   Liu, X., et al., Photochemical synthesis and characterization of poly(N, N-dimethylacrylamide-co-N-isopropylacrylamide) hydrogels with fast responsibility. Acta Polymerica Sinica, 2007(9): p. 850-856.

119.   Vogt, A.P., Sumerlin, B., Tuning the Temperature Response of Branched Poly(N-isopropylacrylamide) Prepared by RAFT Polymerization. Macromolecules, 2008. 41(20): p. 7368-7373.

120.   Lee, W.F., Huang, Y., Thermoreversible hydrogels XIV. Synthesis and swelling behavior of the (N-isopropylacrylamide-co-2-hydroxyethyl methacrylate) copolymeric hydrogels. Journal of Applied Polymer Science, 2000. 77(8): p. 1769-1781.

121.   Verestiuc, L., et al., Functionalized chitosan/NIPAM (HEMA) hybrid polymer networks as inserts for ocular drug delivery: Synthesis, in vitro assessment, and in vivo evaluation. Journal of Biomedical Materials Research Part A, 2006. 77(4): p. 726-735.

122.   Choudhary, V., et al., Studies on the copolymerisation of N-isopropyl-acrylamide with glycidyl methacrylate. Macromolecular Symposia, 2004. 210: p. 49-57.

123. Bokias, G., Durand, A., Hourdet, D., Molar mass control of poly(N-isopropylacrylamide) and poly(acrylic acid) in aqueous polymerizations initiated by redox initiators based on persulfates. Macromolecular Chemistry and Physics, 1998. 199(7): p. 1387-1392.

124. Arica, M.Y., et al., Immobilization of catalase in poly(isopropylacrylamide-co-hydroxyethylmethacrylate) thermally reversible hydrogels. Polymer International, 1999. 48(9): p. 879-884.

125. Cao, Z., et al., Fabrication and properties of thermosensitive organic/inorganic hybrid hydrogel thin films. Langmuir, 2008. 24(10): p. 5543-5551.

126. Yang, D., et al., Preparation of water-soluble multi-walled carbon nanotubes by Ce(IV)-induced redox radical polymerization. Progress in Natural Science, 2009. 19(8): p. 991-996.

127. Haraguchi, K., Stimuli-responsive nanocomposite gels. Colloid and Polymer Science, 2011. 289(5-6): p. 455-473.

128. Wang, Y.P., et al., Preparation and characterization of poly(N-isopropylacrylamide) films on a modified glass surface via surface initiated redox polymerization. Materials Letters, 2005. 59(14–15): p. 1736-1740.

129. Convertine, A.J., et al., Facile, controlled, room-temperature RAFT polymerization of N-isopropylacrylamide. Biomacromolecules, 2004. 5(4): p. 1177-1180.

130. Feng, X.S. et al., Synthesis of amphiphilic miktoarm ABC star copolymers by RAFT mechanism using maleic anhydride as linking agent. Macromolecules, 2002. 35(13): p. 4888-4893.

131. Kujawa, P., et al., Amphiphilic telechelic poly(N-isopropylacrylamide) in water: From micelles to gels. European Physical Journal E, 2005. 17(2): p. 129-137.

132. Xia, Y., et al., Thermal response of narrow-disperse poly(N-isopropylacrylamide) prepared by atom transfer radical polymerization. Macromolecules, 2005. 38(14): p. 5937-5943.

133. Biswas, C.S., et al., Effects of Tacticity and Molecular Weight of Poly(N-isopropylacrylamide) on Its Glass Transition Temperature. Macromolecules, 2011. 44(14): p. 5822-5824.

134. Isoda, K., et al., RAFT-generated poly(N-isopropylacrylamide)-DNA block copolymers for temperature-responsive formation of polymer micelles. Reactive & Functional Polymers, 2011. 71(3): p. 367-371.

135. Licea-Claverie, A., et al., Tailoring the temperature sensitivity of poly(N-isopropylacrylamide) by RAFT-copolymerization: Linear random, linear block, and star copolymers. Abstracts of Papers of the American Chemical Society, 2009. 238.

136. Ganachaud, F., et al., Molecular weight characterization of poly(N-isopropylacrylamide) prepared by living free-radical polymerization. Macromolecules, 2000. 33(18): p. 6738-6745.

137.　Kurz, V., et al., In Situ Characterization of Thermo-Responsive Poly(N-Isopropylacrylamide) Films with Sum-Frequency Generation Spectroscopy. Chemphyschem, 2010. 11(7): p. 1425-1429.

138.　Turan, E., et al., Synthesis of thermoresponsive poly(N-isopropylacrylamide) brush on silicon wafer surface via atom transfer radical polymerization. Thin Solid Films, 2010. 518(21): p. 5950-5954.

139.　Bontempo, D., et al., One-step synthesis of low polydispersity, biotinylated poly(N-isopropylacrylamide) by ATRP. Chemical Communications, 2005(37): p. 4702-4704.

140.　Duan, Q., et al., Synthesis and thermoresponsive property of end-functionalized poly(N-isopropylacrylamide) with pyrenyl group. Journal of Polymer Science Part a-Polymer Chemistry, 2006. 44(3): p. 1117-1124.

141.　Masci, G., et al., Atom transfer radical polymerization of N-isopropylacrylamide. Macromolecular Rapid Communications, 2004. 25(4): p. 559-564.

142.　Xia, Y., et al., End group effect on the thermal response of narrow-disperse poly(N-isopropylacrylamide) prepared by atom transfer radical polymerization. Macromolecules, 2006. 39(6): p. 2275-2283.

143.　Yim, H., et al., Effects of grafting density and molecular weight on the temperature-dependent conformational change of poly(N-isopropylacrylamide) grafted chains in water. Macromolecules, 2006. 39(9): p. 3420-3426.

144.　Burillo, G., et al., IPN's of acrylic acid and N-isopropylacrylamide by gamma and electron beam irradiation. Nuclear Instruments & Methods in Physics Research Section B-Beam Interactions with Materials and Atoms, 2007. 265(1): p. 104-108.

145.　El-Mohdy, et al., Preparation of fast response superabsorbent hydrogels by radiation polymerization and crosslinking of N-isopropylacrylamide in solution. Radiation Physics and Chemistry, 2008. 77(3): p. 273-279.

146.　Kumar, V., et al., Radiation induced synthesis and swelling characterization of thermo-responsive N-isopropylacrylamide-co-ionic hydrogels. European Polymer Journal, 2006. 42(2): p. 235-246.

147.　Ortega, A., et al., Radiation polymerization and crosslinking of (N-isopropylacrylamide) in solution and in solid state. Polymer Bulletin, 2007. 58(3): p. 565-573.

148.　Carrington, A., A free radical. Annual Review of Physical Chemistry, 2001. 52: p. 1-12.

149.　Clay, P.A., Gilbert, A., Molecular weight distributions in free-radical polymerizations .2. Low-conversion bulk polymerization. Macromolecules, 1997. 30(7): p. 1935-1946.

150.　Odian, G., Principles of Polymerization 4th ed. 1994, New York: Wiley-Interscience.

151.　Morones, J., Frey, W., Room temperature synthesis of an optically and thermally responsive hybrid PNIPAM–gold nanoparticle. Journal of Nanoparticle Research, 2010. 12(4): p. 1401-1414.

152.   Ju, X.-J., et al., Effects of internal microstructures of poly(N-isopropylacrylamide) hydrogels on thermo-responsive volume phase-transition and controlled-release characteristics. Smart Materials & Structures, 2006. 15(6): p. 1767-1774.

153.   Nuopponen, M., et al., Aggregation behaviour of well-defined amphiphilic diblock copolymers with poly (N-isopropylacrylamide) and hydrophobic blocks. Polymer, 2004. 45(11): p. 3643-3650.

154.   Han, D.H. Pan, C., A novel strategy to synthesize double comb-shaped water soluble copolymer by RAFT polymerization. Macromolecular Chemistry and Physics, 2006. 207(9): p. 836-843.

155.   Liu, Q.F., P. et al., Synthesis and swelling behavior of comb-type grafted hydrogels by reversible addition-fragmentation chain transfer polymerization. Journal of Polymer Science Part a-Polymer Chemistry, 2005. 43(12): p. 2615-2624.

156.   Plummer, R., et al., Solution properties of star and linear poly(N-isopropylacrylamide). Macromolecules, 2006. 39(24): p. 8379-8388.

157.   Hu, T.J., et al., The coil-to-globule-to-brush transition of linear thermally sensitive poly(N-isopropylacrylamide) chains grafted on a spherical microgel. Journal of Physical Chemistry B, 2002. 106(26): p. 6659-6662.

158.   Ge, Z.S., Luo, S., Liu, S., Syntheses and self-assembly of poly(benzyl ether)-b-poly(N-isopropylacrylamide) dendritic-linear diblock copolymers. Journal of Polymer Science Part a-Polymer Chemistry, 2006. 44(4): p. 1357-1371.

159.   . Moad, G., E. et al., Living radical polymerization by the RAFT process. Australian Journal of Chemistry, 2005. 58(6): p. 379-410.

160.   Kizhakkedathu, J.N., Norris-Jones, R., Brooks, D., Synthesis of well-defined environmentally responsive polymer brushes by aqueous ATRP. Macromolecules, 2004. 37(3): p. 734-743.

161.   Liu, Y., et al., Star Polymers with Both Temperature Sensitivity and Inclusion Functionalities. Macromolecules, 2010. 43(24): p. 10221-10230.

162.   Wan, L.-S., et al., Construction of comb-like poly(N-isopropylacrylamide) layers on microporous polypropylene membrane by surface-initiated atom transfer radical polymerization. Journal of Membrane Science, 2009. 327(1-2): p. 174-181.

163.   Cui, Y., et al., Synthesis of thermosensitive PNIPAM-co-MBAA nanotubes by atom transfer radical polymerization within a porous membrane. Macromolecular Rapid Communications, 2005. 26(19): p. 1552-1556.

164.   Kizhakkedathu, J.N., et al., Synthesis and characterization of well-defined hydrophilic block copolymer brushes by aqueous ATRP. Polymer, 2004. 45(22): p. 7471-7489.

165.   Li, C., et al., Synthesis of Amphiphilic and Thermo responsive ABC Miktoarm Star Terpolymer via a Combination of Consecutive Click Reactions and Atom Transfer Radical Polymerization. Journal of Polymer Science Part a-Polymer Chemistry, 2009. 47(16): p. 4001-4013.

166.   Li, G., et al., Double-responsive core-shell-corona micelles from self-assembly of diblock copolymer of poly(t-butyl acrylate-co-acrylic acid)-b-poly (N-isopropylacrylamide). Polymer, 2006. 47(13): p. 4581-4587.

167.   Braunecker, W.A., Matyjaszewski, J., Controlled/living radical polymerization: Features, developments, and perspectives. Progress in Polymer Science, 2007. 32(1): p. 93-146.

168.   Yamada, N., et al., Thermoresponsive polymeric surfaces - control of attachment and detachment of cultured cells. Makromolekulare Chemie-Rapid Communications, 1990. 11(11): p. 571-576.

169.   Biazar, E., et al., Cell engineering: nanometric grafting of poly-N-isopropylacrylamide onto polystyrene film by different doses of gamma radiation. International Journal of Nanomedicine, 2010. 5: p. 549-556.

170.   Friedrich, T., Tieke,B., Intelligent Hydrogels Via Gamma-Ray Induced Polymerization of Micellar Monomer Solutions and Microemulsions. Macromolecular Symposia, 2010. 287: p. 16-21.

171.   Nagaoka, N., et al., Synthesis of N-isopropylacrylamide hydrogels by radiation polymerization and cross-inking. Macromolecules, 1993. 26(26): p. 7386-7388.

172.   Guven, O., Sen, M., Preparation and characterisation of poly(N-vinyl 2-pyrrolidine) hydrogels. Polymer, 1991. 32(13): p. 2491-2495.

173.   Uenoyama, S., Hoffman, A., Synthesis and characterisation of acrylamide-N-isopropylacrylamide copolymer grafts on silicone rubber substrates. Radiation Physics and Chemistry, 1988. 32(4): p. 605-608.

174.   Munoz-Munoz, F., et al., Novel interpenetrating smart polymer networks grafted onto polypropylene by gamma radiation for loading and delivery of vancomycin. European Polymer Journal, 2009. 45(7): p. 1859-1867.

175.   Pelton, R.H. and P. Chibante, Preparation of aqueous latices with N-isopropylacrylamide. Colloids and Surfaces, 1986. 20(3): p. 247-256.

176.   Ha, M., A. Atallah, and R. Krishnamoorti, Effect of organically modified layered silicates on the morphology of symmetrical blends of polystyrene and poly(methyl methacrylate). Polymer, 2011. 52(25): p. 5890-5896.

177.   Na, Y.H., et al., Structural characteristics of double network gels with extremely high mechanical strength. Macromolecules, 2004. 37(14): p. 5370-5374.

178.   Saito, J., J.P. Gong, and Y. Osada, Hydrogels with extremely high mechanical strength. Membrane, 2006. 31(6): p. 302-306.

179.   Furukawa, H. and J.P. Gong, Tough Hydrogel - Learn from Nature, in Artificial Muscle Actuators Using Electroactive Polymers, P.B.Y.C.F. Vincenzini, Editor. 2009. p. 40-45.

180.   Huang, T., et al., A novel hydrogel with high mechanical strength: A macromolecular microsphere composite hydrogel. Advanced Materials, 2007. 19(12): p. 1622-1626.

181. Tan, Y., et al., Designing Starch-Based Nanospheres to Make Hydrogels with High Mechanical Strength. Macromolecular Materials and Engineering, 2009. 294(12): p. 855-859.

182. Kim, U.J., et al., Structure and properties of silk hydrogels. Biomacromolecules, 2004. 5(3): p. 786-792.

183. Iro, K., New Developments of Polymer Cross-Linking: Slide-Ring Polymeric Materials. Kobunshi Ronbunshu, 2008. 65(7): p. 445-457.

184. Ito, K., Slide-ring materials using topological supramolecular architecture. Current Opinion in Solid State & Materials Science, 2010. 14(2): p. 28-34.

185. Okumura, Y., Topological gel: a third kind of gel consisting of linear polymer chains and figure-of-eight cross-links. Kobunshi Ronbunshu, 2005. 62(8): p. 380-389.

186. Alexandre, M., Dubois, P., Polymer-layered silicate nanocomposites: preparation, properties and uses of a new class of materials. Materials Science & Engineering R-Reports, 2000. 28(1-2): p. 1-63.

187. Caseri, W.R., Nanocomposites of polymers and inorganic particles: preparation, structure and properties. Materials Science and Technology, 2006. 22(7): p. 807-817.

188. Haraguchi, K., et al., Mechanism of forming organic/inorganic network structures during in-situ free-radical polymerization in PNIPA-clay nanocomposite hydrogels. Macromolecules, 2005. 38(8): p. 3482-3490.

189. Rockwood, A. Laponite Technical Brochure. Available from: http://www.scprod.com/pdfs/LaponiteBrochureE.pdf.

190. Haraguchi, K., M. Ebato, and T. Takehisa, Polymer-clay nanocomposites exhibiting abnormal necking phenomena accompanied by extremely large reversible elongations and excellent transparency. Advanced Materials, 2006. 18(17): p. 2250-2260.

191. Liu, Q., et al., Foams stabilized by Laponite nanoparticles and alkylammonium bromides with different alkyl chain lengths. Colloids and Surfaces a-Physicochemical and Engineering Aspects, 2010. 355(1-3): p. 151-157.

192. Liu, L.M., et al., Studies on nylon 6 clay nanocomposites by melt-intercalation process. Journal of Applied Polymer Science, 1999. 71(7): p. 1133-1138.

193. Haraguchi, K., Takehisa, K., Nanocomposite hydrogels: A unique organic-inorganic network structure with extraordinary mechanical, optical, and swelling/de-swelling properties. Advanced Materials, 2002. 14(16): p. 1120-1124.

194. Wang, S.J., et al., Synthesis and properties of silicone rubber organomontmorillonite hybrid nanocomposites. Journal of Applied Polymer Science, 1998. 69(8): p. 1557-1561.

195. Tien, Y.I. et al., High-tensile-property layered silicates/polyurethane nanocomposites by using reactive silicates as pseudo chain extenders. Macromolecules, 2001. 34(26): p. 9045-9052.

196.   Haraguchi, K., et al., Compositional effects on mechanical properties of nanocomposite hydrogels composed of poly(N,N-dimethylacrylamide) and clay. Macromolecules, 2003. 36(15): p. 5732-5741.

197.   Haraguchi, K., Li, H., Mechanical properties and structure of polymer-clay nanocomposite gels with high clay content. Macromolecules, 2006. 39(5): p. 1898-1905.

198.   Messersmith, P.B., Giannelis, P., Synthesis and barrier properties of poly(epsilon-caprolactone)-layered silicane nanocomposites. Journal of Polymer Science Part a-Polymer Chemistry, 1995. 33(7): p. 1047-1057.

199.   Ray, S.S., et al., New polylactide-layered silicate nanocomposites. 2. Concurrent improvements of material properties, biodegradability and melt rheology. Polymer, 2003. 44(3): p. 857-866.

200.   Maiti, P., et al., New polylactide/layered silicate nanocomposites: Role of organoclays. Chemistry of Materials, 2002. 14(11): p. 4654-4661.

201.   Osman, M.A., et al., Polyurethane adhesive nanocomposites as gas permeation barrier. Macromolecules, 2003. 36(26): p. 9851-9858.

202.   Park, H.M., et al., Environmentally friendly polymer hybrids - Part I - Mechanical, thermal, and barrier properties of thermoplastic starch/clay nanocomposites. Journal of Materials Science, 2003. 38(5): p. 909-915.

203.   Frounchi, M., et al., Gas barrier properties of PP/EPDM blend nanocomposites. Journal of Membrane Science, 2006. 282(1-2): p. 142-148.

204.   Kashiwagi, T., et al., Nanoparticle networks reduce the flammability of polymer nanocomposites. Nature Materials, 2005. 4(12): p. 928-933.

205.   Porter, D., et al., Nanocomposite fire retardants - A review. Fire and Materials, 2000. 24(1): p. 45-52.

206.   Leroux, F., Besse, J., Polymer interleaved layered double hydroxide: A new emerging class of nanocomposites. Chemistry of Materials, 2001. 13(10): p. 3507-3515.

207.   Hsiue, G.H., et al., Microstructural and morphological characteristics of PS-SiO$_2$ nanocomposites. Polymer, 2000. 41(8): p. 2813-2825.

208.   Lee, S., et al., Refractive index engineering of transparent ZrO$_2$-polydimethylsiloxane nanocomposites. Journal of Materials Chemistry, 2008. 18(15): p. 1751-1755.

209.   Lu, C.L., et al., Preparation and characterization of ZnS-polymer nanocomposite films with high refractive index. Journal of Materials Chemistry, 2003. 13(9): p. 2189-2195.

210.   Majumdar, D., et al., Clay-polymer nanocomposite coatings for imaging application. Applied Clay Science, 2003. 23(5-6): p. 265-273.

211.   Saujanya, C., Radhakrishnan,S., Structure development and crystallization behaviour of PP/nanoparticulate composite. Polymer, 2001. 42(16): p. 6723-6731.

212.   Strange, M., et al., Biodegradable polymer solar cells. Solar Energy Materials and Solar Cells, 2008. 92(7): p. 805-813.

213.   Sun, J., et al., Electrical and optical properties of ceramic-polymer nanocomposite coatings. Journal of Polymer Science Part B-Polymer Physics, 2003. 41(14): p. 1744-1761.

214.   Wang, T., et al., Waterborne, nanocomposite pressure-sensitive adhesives with high tack energy, optical transparency, and electrical conductivity. Advanced Materials, 2006. 18(20): p. 2730-+.

215.   Bharadwaj, R.K., et al., Structure-property relationships in cross-linked polyester-clay nanocomposites. Polymer, 2002. 43(13): p. 3699-3705.

216.   Choudalakis, G. et al., Permeability of polymer/clay nanocomposites: A review. European Polymer Journal, 2009. 45(4): p. 967-984.

217.   Merkel, T.C., et al., Ultrapermeable, reverse-selective nanocomposite membranes. Science, 2002. 296(5567): p. 519-522.

218.   Merkel, T.C., et al., Effect of nanoparticles on gas sorption and transport in poly(1-trimethylsilyl-1-propyne). Macromolecules, 2003. 36(18): p. 6844-6855.

219.   Ng, C.B., et al., A study of the mechanical and permeability properties of nano- and micron titanium dioxide filled epoxy composites. Advanced Composites Letters, 2001. 10(3): p. 101-111.

220.   Xu, B., et al., Calculating barrier properties of polymer/clay nanocomposites: Effects of clay layers. Polymer, 2006. 47(8): p. 2904-2910.

221.   Luo, J.J., Daniel, I., Characterization and modeling of mechanical behavior of polymer/clay nanocomposites. Composites Science and Technology, 2003. 63(11): p. 1607-1616.

222.   Liu, X.H., Wu, Q., PP/clay nanocomposites prepared by grafting-melt intercalation. Polymer, 2001. 42(25): p. 10013-10019.

223.   Podsiadlo, P., et al., Ultrastrong and stiff layered polymer nanocomposites. Science, 2007. 318(5847): p. 80-83.

224.   Shah, D., et al., Dramatic enhancements in toughness of polyvinylidene fluoride nanocomposites via nanoclay-directed crystal structure and morphology. Advanced Materials, 2004. 16(14): p. 1173-1181.

225.   Wetzel, B., et al., Epoxy nanocomposites with high mechanical and tribological performance. Composites Science and Technology, 2003. 63(14): p. 2055-2067.

226.   Zilg, C., et al., Morphology and toughness/stiffness balance of nanocomposites based upon anhydride-cured epoxy resins and layered silicates. Macromolecular Chemistry and Physics, 1999. 200(3): p. 661-670.

227.   Croce, F., et al., Nanocomposite polymer electrolytes for lithium batteries. Nature, 1998. 394(6692): p. 456-458.

228.   Lau, K.T., Hui, D., The revolutionary creation of new advanced materials - carbon nanotube composites. Composites Part B-Engineering, 2002. 33(4): p. 263-277.

229.   Chen, G.H., et al., Preparation of polymer/graphite conducting nanocomposite by intercalation polymerization. Journal of Applied Polymer Science, 2001. 82(10): p. 2506-2513.

230.   Cho, M.S., et al., Synthesis and electrical properties of polymer composites with polyaniline nanoparticles. Materials Science & Engineering C-Biomimetic and Supramolecular Systems, 2004. 24(1-2): p. 15-18.

231.   Du, F.M., et al., Nanotube networks in polymer nanocomposites: Rheology and electrical conductivity. Macromolecules, 2004. 37(24): p. 9048-9055.

232.   Gangopadhyay, R. and A. De, Conducting polymer nanocomposites: A brief overview. Chemistry of Materials, 2000. 12(3): p. 608-622.

233.   Gojny, F.H., et al., Evaluation and identification of electrical and thermal conduction mechanisms in carbon nanotube/epoxy composites. Polymer, 2006. 47(6): p. 2036-2045.

234.   Roy, M., et al., Polymer nanocomposite dielectrics - The role of the interface. Ieee Transactions on Dielectrics and Electrical Insulation, 2005. 12(4): p. 629-643.

235.   Tanaka, T., et al., Proposal of a multi-core model for polymer nanocomposite dielectrics. Ieee Transactions on Dielectrics and Electrical Insulation, 2005. 12(4): p. 669-681.

236.   Kashiwagi, T., et al., Thermal and flammability properties of polypropylene/carbon nanotube nanocomposites. Polymer, 2004. 45(12): p. 4227-4239.

237.   Zanetti, M., et al., Thermal behaviour of poly(propylene) layered silicate nanocomposites. Macromolecular Rapid Communications, 2001. 22(3): p. 176-180.

238.   Zhu, J., et al., Studies on the mechanism by which the formation of nanocomposites enhances thermal stability. Chemistry of Materials, 2001. 13(12): p. 4649-4654.

239.   Ou, Y.C., Yang, F., Yu, Z., New conception on the toughness of nylon 6/silica nanocomposite prepared via in situ polymerization. Journal of Polymer Science Part B-Polymer Physics, 1998. 36(5): p. 789-795.

240.   Kojima, Y., et al., Mechanical properties of Nylon 6-clay hybrid. Journal of Materials Research, 1993. 8(5): p. 1185-1189.

241.   Usuki, A., et al., Synthesis of Nylon 6-clay hybrid. Journal of Materials Research, 1993. 8(5): p. 1179-1184.

242.   Schmidt, D., et al., New advances in polymer/layered silicate nanocomposites. Current Opinion in Solid State & Materials Science, 2002. 6(3): p. 205-212.

243.   Blumstein, A., Polymerisation of adsorbed monolayers: II. Thermal degradation of the inserted polymers. J. Polym Sci 1965. 3: p. 2665 - 2673.

244.   Zhang, X., et al., Using mixed solvent to synthesize temperature sensitive poly(N-isopropylacrylamide) gel with rapid dynamics properties. Biomaterials, 2002. 23(5): p. 1313-1318.

245.   Haraguchi, K., et al., Tuneable optical and swelling/deswelling properties associated with control of the coil-to-globule transition of poly(N-isopropylacrylamide) in polymer-clay nanocomposite gels. Macromolecules, 2007. 40(19): p. 6973-6980.

246.   Shinde, V.S., et al., Core–Shell Morphology in Poly(N-isopropyl acrylamide) Copolymer Gels Induced by Restricted Diffusion of Surfactant. Langmuir, 2001. 17(9): p. 2585-2588.

247.   Xue, W., Champ, S., Huglin, B., Network and swelling parameters of chemically crosslinked thermoreversible hydrogels. Polymer, 2001. 42(8): p. 3665-3669.

248.   Haraguchi, K., Taniguchi, S., Takehisa, T., Reversible Force Generation in a Temperature-Responsive Nanocomposite Hydrogel Consisting of Poly(N-isopropylacrylamide) and Clay. Chemphyschem, 2005. 6(2): p. 238-241.

249.   Shibayama, M., et al., Structure and dynamics of poly(N-isopropylacrylamide)-clay nanocomposite gel. Macromolecules, 2004. 37(25): p. 9606-9612.

250.   Haraguchi, K., et al., Effects of clay content on the properties of nanocomposite hydrogels composed of poly(N-isopropylacrylamide) and clay. Macromolecules, 2002. 35(27): p. 10162-10171.

251.   Haraguchi, K., et al., The unique optical and physical properties of soft, transparent, stimulus-sensitive nanocomposite gels - art. no. 665400, in Liquid Crystals XI, I.C. Khoo, Editor. 2007. p. O6540-O6540.

252.   Shibayama, M., et al., Structure and Dynamics of Poly(N-isopropylacrylamide)–Clay Nanocomposite Gels. Macromolecules, 2004. 37(25): p. 9606-9612.

253.   Marcolongo, M., et al., Bioactive thermogelling polymer systems and methods of their use. (2006) [online] United States patent 8110212. Patent from USPTO last accessed 2 January 2013 at: http://patft.uspto.gov.

254.   David, N., Fluidic Tissue Augmentation Compositions and Methods. (2007) [online] United States patent application number 11/685,094. Patent from USPTO last accessed 2 January 2013 at: http://patft.uspto.gov.

255.   Gordon, N., Method to repair a damaged intervertebral disc through the use of a bioadhesive, thermogelling hydrogel. (2008) [online] United States patent 0076852. Patent from Espacenet last accessed 2 January 2013 at: http://worldwide.espacenet.com

2

Experimental

Chapter 2 - Experimental

2.1.   Analytical techniques

2.1.1   Infrared (IR) Spectroscopy

Widely used as an instrumental characterisation technique for organic and inorganic analysis, infrared (IR) spectroscopy is a popular tool in identifying compound structure. The technique relies on the absorption of IR light at frequencies which correspond to characteristic vibrational energy levels of chemical functional groups within a sample.

The wavelength of infrared radiation lies within the range of 0.78 and 1000 $\square$m in the electromagnetic spectrum. For IR spectroscopy, the wavelength of IR radiation is presented as "wavenumbers" in the units cm^{-1}. The wavenumber is equal to $1/\lambda$ (cm^{-1}). The infrared region can be subdivided into "near IR" (0.78- 2.5 μm or 12800-4000cm^{-1}), "mid-IR" (2.5 – 50μm or 4000-400cm^{-1}), and "far-IR" (50-1000 μm or 400-20cm^{-1}) [1]. Electromagnetic radiation is absorbed by molecules, but at only very specific wavelengths.

The Plank- Einstein equation (Equation 2.1) demonstrates the relationship between Plank's constant (h) (6.625 x 10^{-34} m^2 kg s^{-1} or J s), the energy of a photon (E), and the frequency of the associated electromagnetic wave (v):

$$E = hv$$

Equation 2.1

The frequency of the vibration is directly proportional to the square root of the ratio of the vibrational force which is in turn proportional to the masses of the corresponding atoms. A lower atomic mass or a stronger chemical bond will result in a higher vibrational frequency and vice- versa. For example, C≡N and C≡C bond stretches occur at higher frequencies than those of C=O, C=C, and C=N. Conversely, C-H, O-H , C-C, C-N, and N-H stretches occur at the lowest frequencies. In addition, a C-H stretch occurs at a higher frequency than a C-C stretch, and a C-O stretch occurs at a frequency lower than them both.

Only specific vibrational energies for a given system are possible and therefore only IR photons with specific energies will be absorbed. Therefore vibrational frequencies are

quantised, and a change in molecular vibration occurs when the photon frequency matches the vibrational frequency of the molecule. A change in net dipole moment during vibration is also required for absorption to occur [2]. This is known as the selection rule.

2.1.1.2 Attenuated Total Reflectance - Fourier Transform Infrared Spectroscopy (ATR -FTIR)

When light propagates through a material with a high refractive index (n_1) at an angle (θ) greater than the critical angle, it will be totally internally reflected at the interface of a material with a lower refractive index (n_2). At the point of reflection, a standing wave is formed (the evanescent wave) which has components in all directions and decays exponentially. It is a surface characterisation technique and appropriate when samples are difficult to analyse by transmission, if they are for example, thick or strongly absorbing. Crucially, the refractive index of the crystal must be greater than that of the sample to ensure the beam is internally reflected rather than transmitted. A schematic of the ATR setup is shown in figure 2.1.
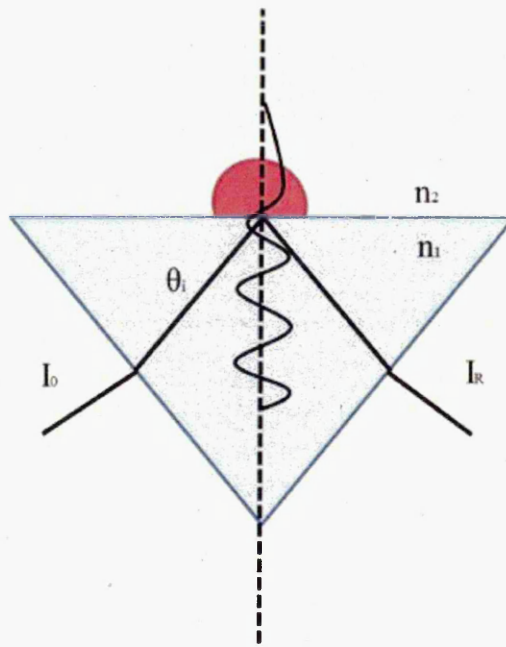
Figure 2.1. Schematic representation of ATR apparatus.

The region of total reflection begins at an angle higher than a critical angle using Snell's Law (equation 2.2):

$$\sin \theta_c = \frac{n_2}{n_1}$$

Equation 2.2

50

Where: θc is the critical angle, n_2 is the refractive index of the sample and n_1 is the refractive index of the ATR crystal.

The depth of penetration (which is ~ 3x d_p) of the evanescent wave and subsequent sampling depth of the resulting spectrum can be calculated using equation 2.3:

$$d_p = \frac{\lambda_1}{2\pi n_1 \sqrt{\sin^2 \theta - (n_2 / n_1)^2}}$$

Equation 2.3

It is therefore possible to alter the d_p by using crystals of varying refractive indices and the angle of incidence.

In practise, the d_p usually in the order of a few micrometers, so very close contact between sample and crystal is integral. The evanescent field extending into the sample decays exponentially with distance from the interface. Each peak in an ATR-FTIR spectrum is attributed to a specific quantity of energy absorbed by a specific functional group present in the evanescent field.

To analyse solid samples, a sapphire plate is used to firmly press the sample onto the diamond crystal surface. For liquid samples, it is sufficient to pour a small amount directly onto the crystal. The infrared analysis in this study was performed using a Thermo Nicolet Nexus FTIR spectrometer which consists of three major components: a radiation source, an interferometer, and a detector. The interferometer used was a Michelson interferometer, which is comprised of a fixed mirror, a moving mirror and a beam splitter, as shown in figure 2.2:
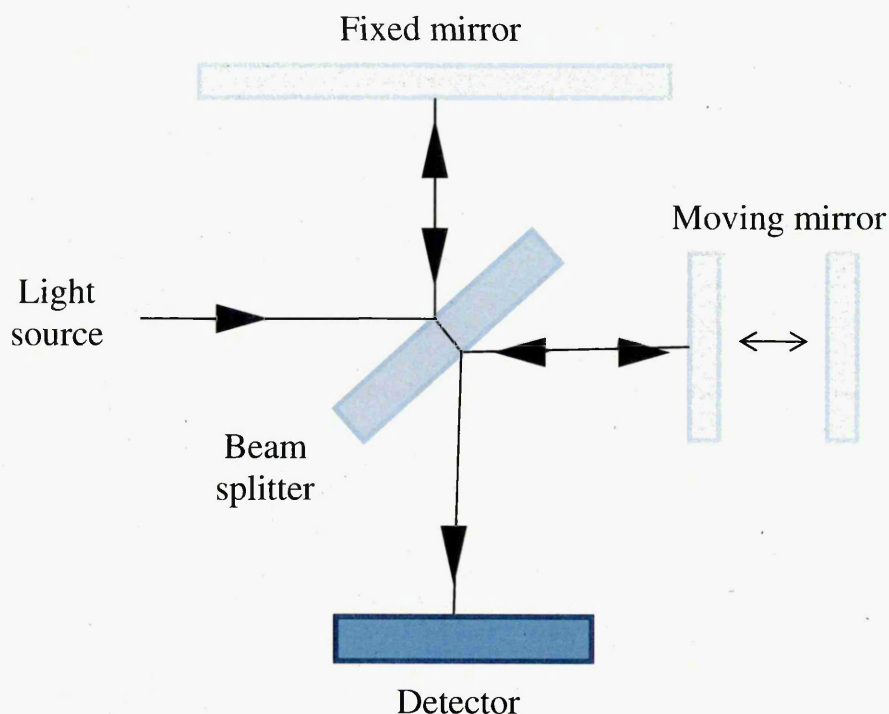
Figure 2.2. Schematic representation of a Michelson Interferometer.

An infrared beam is passed into the interferometer and onto the beam splitter, where half is reflected to a moving mirror whilst half is transmitted to a fixed mirror. The two beams are subsequently recombined at the beam splitter and changes in the relative position of the two mirrors causes the generation of an interference pattern. If the two mirrors are of precisely equal distance from the beam splitter, the two beams are exactly in phase with one another. This is referred to as the point of zero path difference, or ZPD, and results in maximum constructive interference. When the moving mirror travels in either direction, the two beams become out of phase and at 180°, maximum deconstructive interference occurs. In the case of ATR, after recombination the beam is passed through the crystal and collected by a detector. There is a proportional relationship between the square root of the number of scans performed and the signal to noise ratio of the resulting spectrum; the more scans performed, the more improved the signal to noise ratio becomes.

A graph of intensity of the path-length difference over the recombined beam after the application of a Fourier Transform mathematical operation (an interferogram) contains information about the frequencies present in the beam.

2.1.1.3   ATR-FTIR experimental parameters

Infrared analysis was performed at the Materials and Engineering Research Institute at Sheffield Hallam University using a variable temperature Graseby Specac Single Reflection Golden Gate ATR sampling accessory, attached to a Thermo Nicolet Nexus Spectrometer with a thermocouple accessory set to at 27°C, unless otherwise stated. The spectra were collected using 64 scans at a resolution of 4cm^{-1}, unless otherwise stated.

2.1.2   ATR FT-IR imaging

FTIR imaging using ATR mode is patented by Varian [3], and like conventional FTIR spectroscopic instrumentation, ATR-FTIR imaging is effectively a surface technique, capable of providing chemical information with a sample penetration depth of ~1-2 microns. Unlike conventional ATR-FTIR, which utilises a single detection element, FTIR imaging utilises a combination of a focal plane array detector and an infrared spectrometer, allowing spatial as well as spectroscopic data to be collected simultaneously over a specified "field of view". The technique is based on a 64 x 64 element infrared array detector which allows simultaneous measurements of 4096 spectra from specified locations in a sample. The result is a 1096-pixel chemical image and the technique has been employed to provide chemical "maps" of a wide range of materials, from polymers [4-8] to pharmaceutics [9-11], biological systems [12] and forensic science [13]. The technique provides information as to analyte location within a sample by the depiction of different materials as different colours with the straightforward relation of the chemical properties of a material to a certain colour. To allow this, a characteristic spectroscopic signature within the chemical properties of a material must be located within the spectra. It is important to note that the colours on a final ATR-FTIR image have no absolute physical or chemical meaning. Rather, they allow comparisons of relative analyte compositions at different loci of the sample.

2.1.2.1   ATR FT-IR imaging experimental parameters

FTIR spectra were collected using a variable temperature Graseby Specac single reflection diamond ATR attached to a Thermo Nicolet Nexus bench equipped with a Mercury-Cadmium-Telluride detector. 128 scans were performed for each measurement

at a resolution of 4 cm^{-1}. Single- beam background spectra of the blank ATR crystal were collected before each experiment and ratioed against the final spectra.

2.1.3 Dynamic Light Scattering (DLS)

Dynamic Light Scattering (also known as Photon Correlation Spectroscopy) is a popular and effective technique used to determine the size of particles in dispersion. It involves projecting monochromatic light onto a dispersion containing particles undergoing Brownian motion (particle movement owed to bombardment from solvent molecules which are themselves in motion). Light is scattered from particles in dispersion, and Brownian motion of the particles causes intensity fluctuations in the scattered light. The correlation function is used to analyse these fluctuations and give the diffusion coefficient, hydrodynamic radius (or z-average particle size), particle size distribution and describe the particle's motion in solution using the Stokes- Einstein equation. Small molecules move more quickly in solution than larger particles and therefore produce a faster decay in the correlation function. In addition, the technique allows the quantification of molecular weight, translational diffusion constant and radius of gyration.
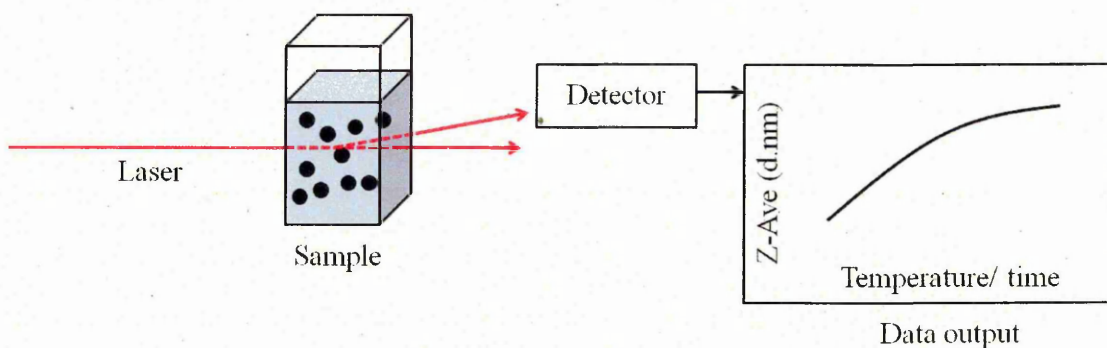
Figure 2.3. Schematic representation of a Dynamic Light Scattering setup.

It is important to note that the z-average diameter obtained from Dynamic Light Scattering is hydrodynamic diameter and is presumed to be that of a sphere. The calculated translational diffusion coefficient will be inclusive of any surface structure in addition to the particle core, and will also depend on the particle concentration in the dispersion.

2.1.3.1   DLS Experimental Parameters

DLS was performed under the supervision of Lee Fielding (Department of Chemistry, University of Sheffield) at the University of Sheffield, with kind thanks to Professor Steven Armes. The Malvern Zetasizer Nano ZS instrument equipped with a 4 mW He-Ne solid-state laser operating at 633 nm. The angle of the back-scattered light detector was at 173°.

2.1.4   Gel Permeation Chromatography (GPC)

Gel Permeation Chromatography (or Size Exclusion chromatography - SEC) is one of the most utilised, versatile and convenient analytical techniques for the characterisation of the total molecular weight and molecular weight distribution of a polymer. It is based on the ability to separate molecules according to their "effective size" in solution as polymer chains dissolved in an appropriate solvent (the mobile phase) move through a column of porous, rigid particles (the stationary phase). Smaller molecules readily enter the pores of the stationary phase, thus causing a delay in their elution from the column, whilst larger molecules do not enter the pores but pass quickly through the column. Upon elution, the sample passes through a detector (or series of detectors) which provides information on the quantity of material eluting from the column at any given time. The data is processed by analytical software, which references the information against a calibration curve of molecular weight vs. retention time. If the reference standards are chemically identical to the sample, accurate data are obtained. Often, reference standards are only of a similar chemistry to the analysed sample, and in such circumstances, results are comparative.

The width of individual chromatographic peaks is indicative of the size distribution of the molecules be it "narrow" or "broad", and the size distribution curve is referred to as the molecular weight distribution (MWD) curve.
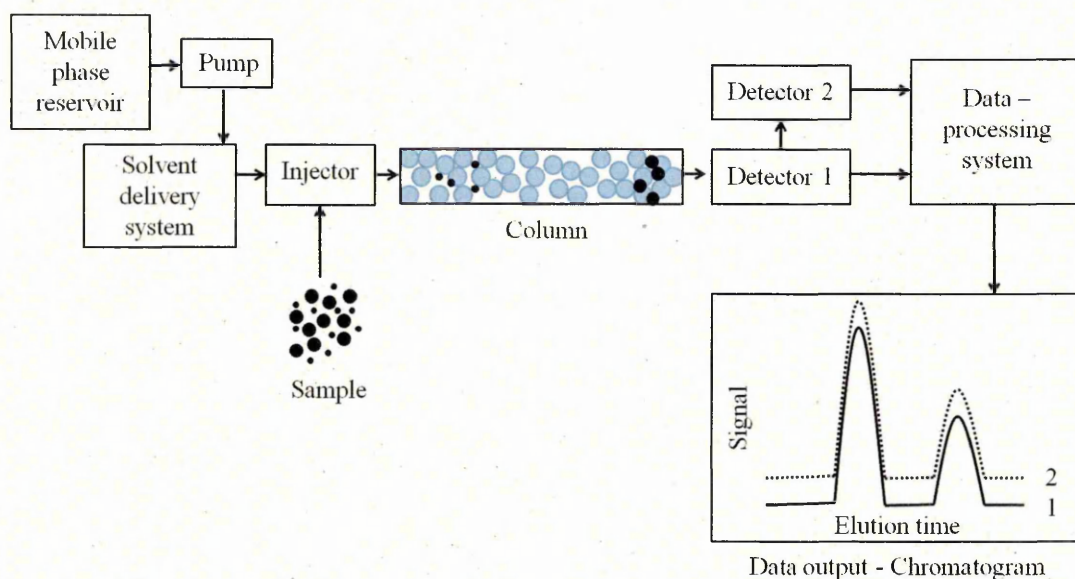
Figure 2.4. Schematic representation of Gel Permeation Chromatography apparatus.

2.1.4.1   GPC Experimental Parameters

GPC was performed under the supervision of Melanie Hannah (Department of Chemistry, University of Sheffield) at the University of Sheffield, with kind thanks to Professor Steven Rimmer.

Molecular weights of the linear polymers were determined using a Polymer Laboratories gel 10 micron mixed-B LS column and an ERMA refractive index detector ERC-7512 at room temperature with GPC grade tetrahydrofuran (THF) (Fisher scientific) stabilised with 250ppm butylated hydroxytoluene (BHT) (Aldrich) as the flow phase. The flow rate was 1ml/min with a sample concentration of 10mg/ ml. The calibration curve was produced with narrowly distributed anionic polystyrene standards (polymer laboratories).

2.1.5   Thermogravimetric Analysis (TGA)

Thermogravimetric data assesses the thermostability of a sample and relies on excellent precision in the measurement of weight, temperature, and temperature change. It allows changes in the weight of a sample to be observed as a function of temperature. Points of relatively significant weight loss associated with sample degradation can be indicative of sample composition, namely water content, solvent residues and levels of organic and inorganic components, whereas weight gain might indicate a chemical process such as oxidation. The prevention of oxidation reactions can be prevented by continuously purging the system with an inert gas.

A TGA instrument typically consists of a high precision balance on which a crucible, loaded with approximately 15mg of sample is placed. The crucible is heated in a temperature-controlled furnace under a controlled atmosphere. During analysis, the sample is heated by what is typically a linear temperature gradient, which can exceed 1000°C if required. The sample weight is plotted against temperature in real time using specialised (STAR E) software.

The shape of the resulting weight loss curve is influenced by several factors:

- A suitable crucible must be chosen so that it is a) able to withstand the highest temperature used in the analysis without degrading or undergoing oxidation, and b) not chemically interact with the sample.
- The heating rate – generally speaking, a slower heating rate is preferred as to reveal a more detailed weight loss curve and ensure that the temperature of the sample is closer to that which is recorded for the furnace, although this can result in a reduction of the signal to noise ratio.
- Larger samples may harbour temperature gradients and "trap" volatile components, leading to poorly resolved weight-loss peaks [14].
- A large particle size distribution of powders sometimes leads to poor data reproducibility [14].
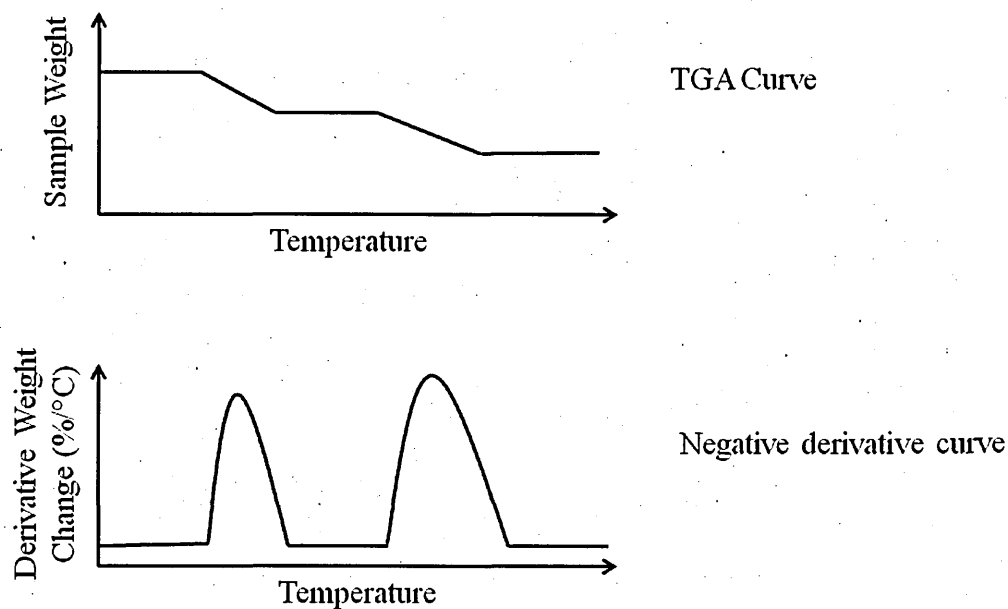
Figure 2.5. Diagrammatic representation of TGA thermogram and derivative thermogram (dTG) curves.

A thermogram, shown in figure 2.5, gives the weight change as a function of temperature. Often, weight loss curves look similar and transformation is required before results can be interpreted clearly. A negative derivative weight loss curve (dTG) (figure 2.5) can be created to distinguish points of significant events.

2.1.5.1   TGA Experimental Parameters

Thermogravimetric analysis was performed at the Materials and Engineering Research Institute at Sheffield Hallam University using a Mettler TG50 with 15-25ml min^{-1} N$_2$ purge. Samples were placed into a clean dry alumina crucible before the temperature was increased from 20°C to 800°C at the rate if 1°C/min^{-1}.

2.1.6   X-Ray Diffraction (XRD)

XRD is a non-destructive characterisation technique which is used to identify crystalline phases and crystal orientation within a sample.

X-rays are electromagnetic radiation with energies of ~100 eV to 100 keV. Only short wavelength X-rays are used in diffraction instrumentation (1keV – 120 keV), and these are ideally suited for the examination of atomic structural arrangements. In a laboratory x-ray instrument, a high- voltage electron beam bombards a solid target, and the electron deceleration on impact generates a continuous stream of parallel monochromatic X-rays. The X-rays penetrate the sample bulk and provide information about its structure.

The atoms in a crystalline material are arranged into atomic planes that are spaced a fixed distance apart (d), and can be resolved into many atomic planes, each with a different d-spacing. Some waves will leave the sample "in phase" and will result in defined X-ray beams with high energies leaving the sample at various angles. These angles and intensity of the diffracted beam are used to calculate interplanar atomic spacings. This phenomenon is called X-ray diffraction.
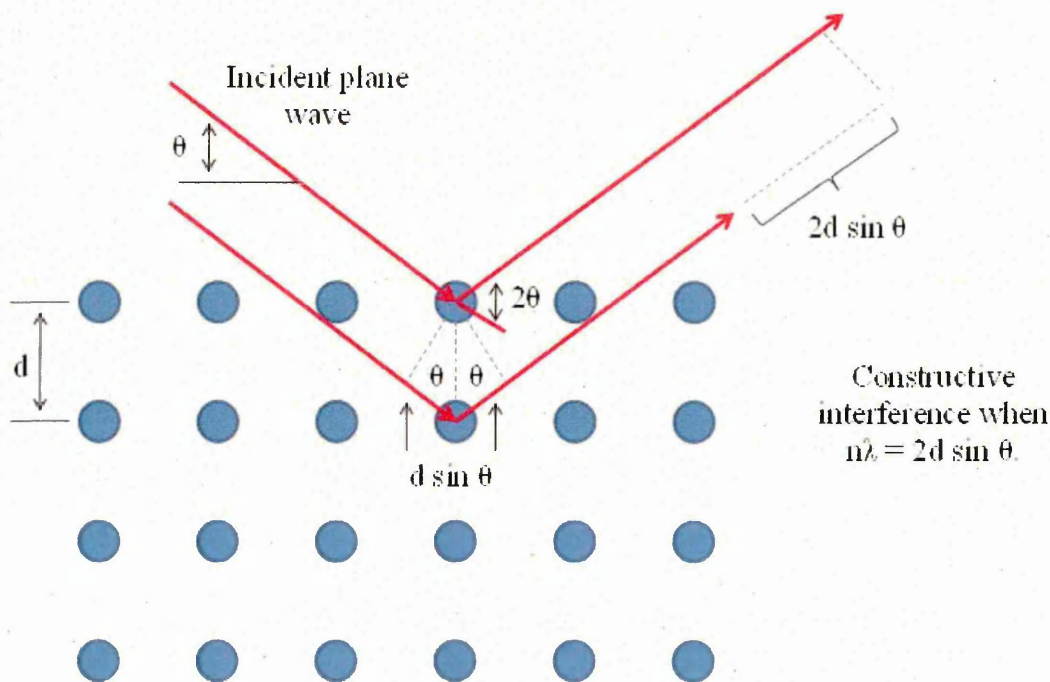
Figure 2.6. A schematic representation of Bragg's diffraction.

These diffracted beams are detected and the intensity recorded using a counter on a moving arm moving at a constant angular velocity. The resulting trace gives the diffracted beam intensity as a function of degrees 2θ.

Figure 2.6 shows how Bragg's diffraction operates. Two parallel incident plane waves make an angle theta (θ). A beam of maximum intensity will be reflected if these two waves are in phase. The difference in path length between the two reflected waves must then be an integral number of wavelengths, (λ). This relationship is expressed mathematically using Bragg's law [15]:

$$n\lambda = 2d \sin \theta$$

Equation 2.4

Where *n* is an integer determined by the order given, and *d* is the spacing between planes of the atomic lattice.

2.1.6.1   XRD Experimental Parameters

X-ray Diffraction analysis was performed at the Materials and Engineering Research Institute at Sheffield Hallam University using a Phillips-expert XRD with Cu X-ray source λ=1.542Å, with a Philips miniprop detector, and standard masks for the x-ray beam (¼ inch divergence slit, ½ inch anti-scatter slit, and a 10cm fixed mask).

The samples were dried, crushed to a powder and analysed on an aluminium mount. A diffraction trace was produced from the analysis of diffraction between 5 and 90 degrees theta.

2.1.7 Scanning Electron Microscopy (SEM)

The scanning electron microscope (SEM) is a method used for obtaining high resolution images of surfaces by scanning a primary beam of high-energy electrons across the surface of a sample. The kinetic energy of these electrons is dissipated as a variety of signals emitted as a result of electron- sample collisions. For example, high resolution SEM micrographs are produced by the detection of secondary electrons, an electron backscatter diffraction detector (EBSD) uses back-scattered electrons to aid the close examination of the crystallographic orientation of crystalline or polycrystalline materials, and an energy dispersive x-ray spectrometer (or EDS) allows the acquisition of qualitative and quantitative elemental information from characteristic x-rays. X-ray emission is the result of the removal of an inner shell electron from the sample after its collision with an incident electron. This causes a higher energy electron to replace it and release energy of a specific wavelength corresponding to that specific element.

Typically, a surface area of between ~5 microns to 1cm can be imaged at any one time with a conventional SEM setup, with a magnification of approximately 10 to 500,000X. A large depth of field yields a 3-dimensional image and reveals details of the surface texture and structure.

Special considerations are as follows:

- Samples must be self-supporting and fit into the microscope chamber. Typically this is around 10cm in width and rarely more than 4cm in height.
- In the majority of cases, the sample must be stable in a vacuum of around 10^{-5} - 10^{-6} torr. Wet samples and most organic materials are likely to outgas as such pressures and are unsuitable for conventional SEM analysis. Such samples can be successfully analysed, however, in specialised "low vacuum" and "environmental" SEMs (LVSEM and ESEM, respectively).
- EDS detectors are not capable of detecting very light elements (Hydrogen, Helium, and Lithium), and many instruments cannot detect elements with atomic numbers lower than 11 [16].
- Unless the instrument is capable of operation in a low vacuum mode, electrically insulating samples must have an electrically-conductive coating such as carbon or gold for study in conventional SEM systems.
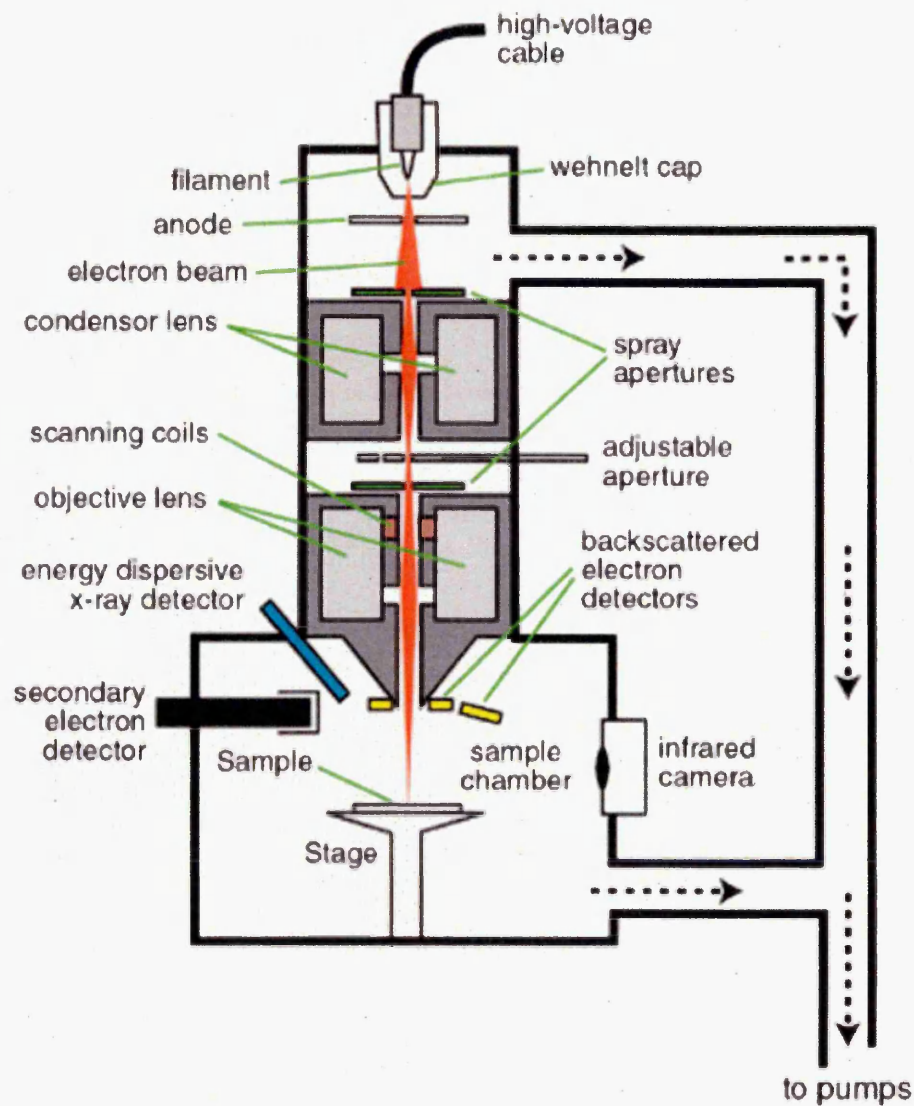
Figure 2.7. Schematic of a Scanning Electron Microscope [17]

In this thesis, all SEM data was collected in low vacuum (LV) mode without the need for carbon coating.

2.1.7.1   SEM Experimental Parameters

The electron micrographs were taken at the Materials and Engineering Research Institute at Sheffield Hallam University by Mr. Stuart Creasey in low vacuum (LV) mode using a FEI NOVA nanoSEM 200 Scanning Electron Microscope. A Helix detector insert was used to obtain the images with an operational water vapour pressure of 0.8-1.2 Torr, together with an accelerating voltage of 5KV and spot size of 4.

2.1.8 Matrix-Assisted Laser Desorption/Ionisation Time-Of-Flight Mass Spectrometry (MALDI-TOF-MS)

Matrix-assisted laser desorption/ ionisation time-of-flight mass spectrometry (MALDI-TOF MS) has become a fast, reliable and reproducible technique in the analysis of biomolecules and polymers. Analytes are mixed with a "matrix" – a low molecular weight compound with an absorption maximum at the laser wavelength (typically a-cyano-4-hydroxy cinnamic acid, but dependent on the nature of the analyte and type of measurement to be taken) [18-19]. A mixture of matrix and analyte is applied to a metal plate and allowed to dry.

The plate is then inserted into a vacuum chamber via a vacuum lock where the analysis takes place. Pulsed laser radiation (377nm) is focussed onto the sample plate and energy is absorbed by the matrix molecules. A typical MALDI-TOF-MS set-up is shown in figure 2.8.
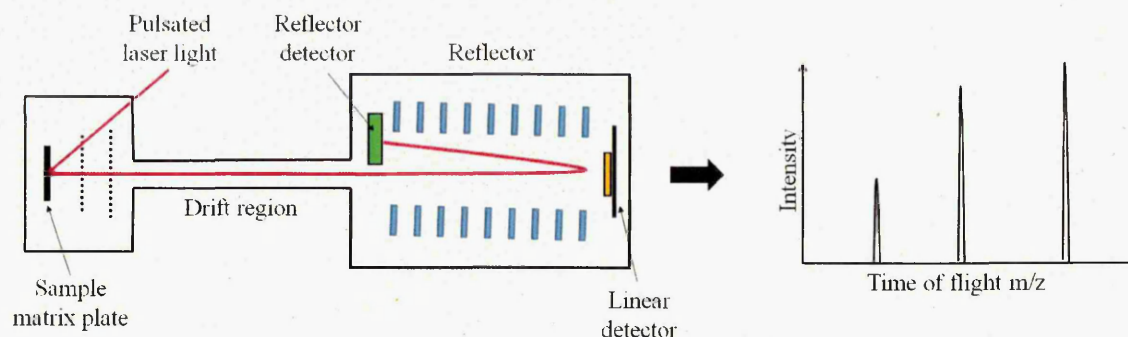
Figure 2.8. Schematic of a Matrix-assisted laser desorption/ ionisation time-of-flight mass spectrometer with a typical spectrum.

As a result, desorption of the matrix and co-crystallised analyte occurs at speed into the "drift region" or the gas phase of the instrument. Concurrently, collisions occur between ionised matrix molecules and analyte molecules, transferring their charges across and producing mainly singly-charged, metastable ions. After desorption, charged analytes are accelerated in an electric field in a high voltage grid. An identical kinetic energy applied to all ions ensures that ions of the same mass travel at the same speed. The ions travel through the drift region under high vacuum until they reach a detector. Lighter ions travel faster and reach the detector earlier than heavier ones; therefore they are separated according to their "time of flight" and hence, size. Flight times are converted to ion masses in mass per charge, or m/z. It is important that these ions are detected prior to their decomposition (typically within 10^{-5} seconds).

63

Reflector tubes are often used to improve resolution by correcting a distribution in start velocity and lengthen the flight path by reversing the drift direction in an electric counter field before reaching the detector [20].

2.1.8.1   MALDI-TOF-MS Experimental Parameters

All mass spectrometric analyses were conducted with an Applied Biosystems Voyager-DE STR instrument with a 2m flight path in positive ion mode. The accelerating voltage was kept at 2500, the delay time was 500 nsec and the shot number was 300.

2.1.9   Dynamic Mechanical Analysis (DMA)

Dynamic Mechanical Analysis, or DMA, is a characterisation technique whereby a small sinusoidal deformation is applied to a sample of a known geometry. The sample's subsequent response to applied stress, frequency and temperature are measured. Because a sinusoidal force is applied, the modulus can be presented as an in-phase component (storage modulus), and an out-of-phase component (loss modulus), as represented in figure 2.9. The storage modulus is indicative of the sample's elastic properties. The ratio of the loss modulus to storage modulus is given as tan delta, or "tan δ" and is very often referred to in literature as "damping". It quantifies the energy dissipation of a sample.
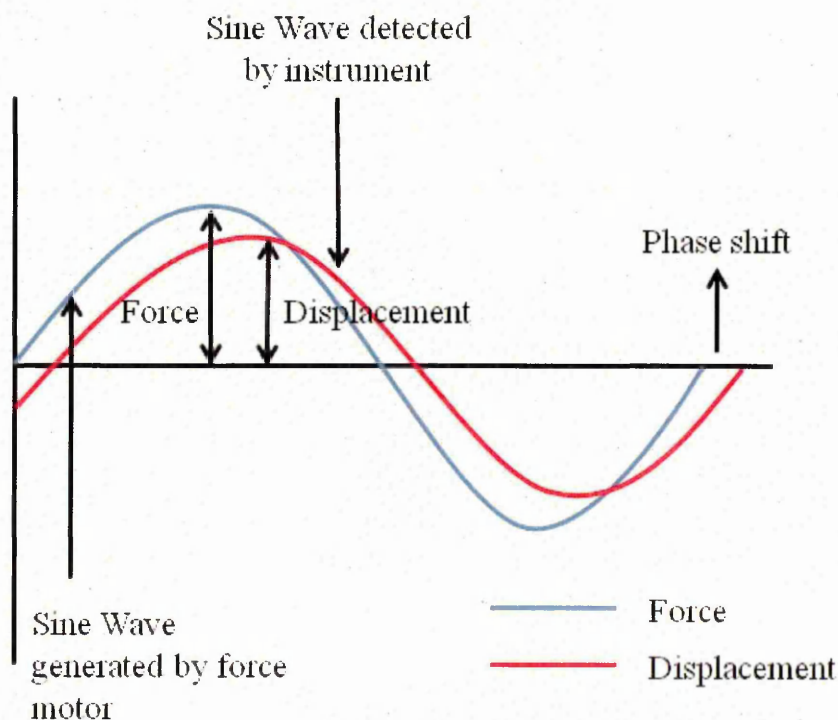
Figure 2.9. The relationship between applied sinusoidal stress and strain of an elastic material measured by DMA, with the resultant phase lag.

64

For the DMA measurements in this thesis, frequency sweep measurements were applied. For this, a sample of known geometry is held between two surfaces. The oscillatory displacement, which is defined by its amplitude and frequency, was applied on one side of the sample and the reaction force was measured at the opposite side. Measuring the amplitude of the sine wave and the lag between the stress and strain sine waves of the material response allows the calculation of the modulus, viscosity and damping of a sample.

An important requirement is that the sample is prepared suitably with reasonable aspect dimensions, and be of even thickness with parallel sides.

2.1.9.1 Dynamic Mechanical Analysis (DMA) Experimental parameters

A PerkinElmer DMA8000 model was used in compression mode at 25°C, at frequencies between 0.1-10 Hz in ambient humidity.

2.2 Materials and Sample Synthesis

2.2.1 Chapter 3 - The Development of a PNIPAM/ Clay Nanocomposite Liquid Gel Precursor

2.2.1.1 Materials Used in Chapter 3

N-Isopropylacrylamide, 99% (NIPAM) monomer was purchased from Sigma-Aldrich chemicals unless otherwise stated, and recrystallised from hexane before being allowed to dry for 2 days at room temperature, unless otherwise stated. The inorganic clay, synthetic hectorite Laponite RD, was supplied by Rockwood additives Ltd and was used without further treatment or purification. 2-2'-azobisisobutyronitrile (AIBN) (Sigma) was recrystallised from methanol and dried in vacuum. Gelatine and hyaluronic acid (bovine vitreous humour, lyophilised) (HA) were supplied by Fluka Analytical and used without further treatment. 1,1,1,3,3,3 hexafluoroisopropanol (HFIP) and sodium chloride (NaCl) were purchased from Sigma-Aldrich (Spain) and used without further treatment. 1,8,9-trihydroxyanthracene (dithranol) was purchased from Sigma UK and used without further treatment. All water was 18 mΩ, distilled and deionised. Water used as a solvent in the gel synthesis was also degassed by purging with nitrogen gas for a minimum of 30 minutes prior to use.

2.2.1.2   Synthesis and Preparation of a PNIPAM/ Clay nanocomposite Hydrogel Precursor Liquid.

All glassware, including sample vials were thoroughly washed, rinsed with acetone and dried in a drying cupboard overnight prior to use. An appropriate amount of laponite clay was weighed before being dispersed in deionised water, which had been previously purged with nitrogen gas for 30 minutes prior to use, and exfoliated under rapid stir for 24 hours. NIPAM monomer and AIBN were weighed and added to the mixture, before stirring for a further 2 hours. Pure PNIPAM formulations were prepared identically, omitting the presence of clay. Pure clay suspensions were prepared by dispersing the appropriate amount of clay in water for 24 hours.

To prepare a hydrogel precursor solution which contains 10% solids of which 1% is clay (otherwise denoted $1C_{10}$), a transparent aqueous solution consisting of water (9g) exfoliated inorganic clay (0.1g) (or 9.1g of the original exfoliated suspension), AIBN (0.009g) and NIPAM (0.9g) was prepared (N.B. In all cases, the ratio of NIPAM to AIBN was kept at 99:1). The nomenclature format is as follows:

$$xC_y$$

Where x is the overall percentage of clay by weight, and y denotes the overall percentage of "solids" (discounting AIBN , therefore clay + NIPAM) by weight of the hydrogel precursor and subsequent gel.

Table 2.1. PNIPAM and PCPH formulations used in chapter 3

Sample code	Overall composition w/w
$0C_{10}$	10% PNIPAM, 90% water
$.25C_{10}$	9.75% PNIPAM, .25% clay, 90% water
$.5C_{10}$	9.5% PNIPAM, .5% clay, 90% water
$1C_{10}$	9% PNIPAM, 1% clay, 90% water
$0C_5$	5% PNIPAM, 95% water
$.25C_5$	4.75% PNIPAM, .25% clay, 95% water
$.5C_5$	4.5% PNIPAM, .5% clay, 95% water
$.5C_0$	.5% clay, 99.5% water
$0C_{10}$	10% PNIPAM, 90% water

PNIPAM samples synthesised without the presence of clay (with sample codes $0C_y$), "y" denotes the percentage of NIPAM by weight of the monomer solution (discounting AIBN, which is always 99/1 wt.-% NIPAM/ AIBN). For example, "$0C_{10}$" indicates a 10g sample of monomer solution prepared using 9g water, 1g NIPAM and 0.01g AIBN. Table 2.1. gives the sample codes and corresponding compositions of all nanocomposite gels examined in this chapter.

Unless otherwise stated, polymerisation was allowed to proceed in an oil bath preset to 80°C for 24 hours. For experiments which require nanocomposite gel (post-PTTNAG) systems, the resulting polymer- clay precursor hydrogel (PCPH) was allowed to cool at room temperature inside glass vials (unless otherwise stated) and subsequently solidify *in situ* for 2 hours prior to use.

2.2.1.3   Formation of the Gelatine-incorporated PCPH

The hydrogel precursor liquid was synthesised as described in Section 2.2.1.2. A gelatine solution was made by warming a 1:1 w/w mixture of gelatine granules and deionised water to 70°C and stirring until smooth. A measured quantity of this solution was combined with the hydrogel precursor solution and carefully stirred in a heated ultrasonic bath (40 KHz at 70°C) for 2 hours until a homogenous pale-yellow viscous liquid, the gelatine-incorporated PNIPAM/ Clay hydrogel precursor, is formed. The gelatine-incorporated PCPH formulations used in this chapter, along with their overall compositions are given in table 2.2.

Table 2.2. The gelatine- incorporated PCPH formulations used in chapter 3

Sample code	Overall composition w/w
$1C_{10}$	9% PNIPAM, 1% clay, 90% water
$1C_{10}G5$	8.55% PNIPAM, 0.95% clay, 88% water, 2.5% gelatine
$1C_{10}G10$	8.1% PNIPAM, 0.9% clay, 86% water, 5% gelatine
$1C_{10}G15$	7.65% PNIPAM, 0.85% clay, 84% water, 7.5% gelatine
$1C_{10}G20$	7.2% PNIPAM, 0.8% clay, 82% water, 10% gelatine
$1C_{10}G25$	6.75% PNIPAM, 0.75% clay, 80% water, 12.5% gelatine

2.2.1.4   Formation of the HA-incorporated PCPH

The hydrogel precursor liquid was synthesised as per Section 2.2.1.2.

An aqueous HA solution was made by firstly preparing a 50:1 w/w mixture of crude HA and deionised water. The mixture was refrigerated for 48 hours, during which time it was removed and stirred vigorously every 12hours. A measured quantity of this solution, which now was a very viscous homogeneous liquid, was then combined with the hydrogel precursor solution and carefully stirred in a heated ultrasonic bath (40 KHz at 40°C) for 1- 2 hours until a homogenous milky liquid, the HA-incorporated PNIPAM/ Clay hydrogel precursor, is formed. The HA-incorporated PCPH formulations used in this chapter, along with their overall compositions are given in table 2.3.

Table 2.3. The hyaluronic acid- incorporated PCPH formulation used in chapter 3

Sample code	Overall composition w/w
$1C_{10}$	9% PNIPAM, 1% clay, 90% water
$1C_{10}HA5$	8.55% PNIPAM, 0.95% clay, 90.4% water, .1% HA
$1C_{10}HA10$	8.1% PNIPAM, 0.9% clay, 90.8% water, .2% HA
$1C_{10}HA15$	7.65% PNIPAM, 0.85% clay, 91.2% water, .3% HA
$1C_{10}HA20$	7.2% PNIPAM, 0.8% clay, 91.6% water, .4% HA
$1C_{10}HA25$	6.75% PNIPAM, 0.75% clay, 92% water, .5% HA

2.2.2   Chapter 4 - The Processability of PNIPAM/ Clay Nanocomposite Liquid Gel Precursor formulations.

2.2.2.1   Materials used in chapter 4

The materials used in this chapter are detailed in section 2.2.1.1. The synthesis, nomenclature format and compositions of PNIPAM/clay PCPH formulations are detailed in section 2.2.1.2, and compositions of PNIPAM/clay/gelatine PCPH formulations are detailed in section 2.2.1.3 of this thesis.

2.2.3 Chapter 5 - The Characterisation of PNIPAM/ Clay Nanocomposite Liquid Gel Precursor Formulations Post- PTTNAG.

2.2.3.1 Materials used in chapter 5

The materials, synthesis, nomenclature format and formulation compositions are detailed in sections 2.2.1.1 and 2.1.1.2.

2.2.4 Chapter 6 – The Influence of Alcoholic Solutions and Dopants on the Phase Behaviour of PNIPAM.

2.2.4.1 Materials used in chapter 6

N-Isopropylacrylamide, 99% (NIPAM) monomer was supplied by Sigma-Aldrich chemicals unless otherwise stated, and recrystallised from hexane before being allowed to dry for 2 days at room temperature, unless otherwise stated. The inorganic clay, synthetic hectorite Laponite RD, was supplied by Rockwood additives Ltd and was used without further treatment or purification. N, N'-methylenebisacrylamide, 99% (BIS) (Sigma) was used as received, Diethoxyacetophenone (Sigma) was used as received and 2-2'-azobisisobutyronitrile (AIBN) (Sigma) was recrystallised from methanol and dried in vacuum. Gelatine and hyaluronic acid (bovine vitreous humour, lyophilised) (HA) were supplied by Fluka Analytical and used without further treatment. Laboratory grade ethanol and methanol were supplied by Sigma Aldrich Chemicals. All water was 18 mΩ, distilled and deionised. Water used as a solvent in the gel synthesis was also degassed by purging with nitrogen gas for a minimum of 2 hours prior to use.

2.2.4.2 Synthesis of thermally- initiated Clay/ PNIPAM Nanocomposite Hydrogels

To prepare a hydrogel precursor solution which contains 10% solids of which 1% is clay (referred to as 1C$_{10}$), a transparent aqueous suspension consisting of water (9g) exfoliated inorganic clay (0.1g) (or 9.1g of the original exfoliated suspension), AIBN (0.009g) and NIPAM (0.9g) was prepared (N.B. In all cases, AIBN concentration is 1% that of NIPAM). Then, polymerisation was allowed to proceed in an oil bath preset to 80°C for 24 hours. The nomenclature format is as follows:

$$xC_y$$

Where x is the overall percentage of clay by weight, and y denotes the overall percentage of "solids" (clay + NIPAM) by weight of the hydrogel precursor and subsequent gel.

For example, ".5C_{10}" indicates a 10g sample of hydrogel precursor prepared using 9g water, 0.95g NIPAM, 0.05g clay, 0.0095g AIBN (Table 2.4). The resulting polymer-clay precursor hydrogel (PCPH) was allowed to cool at room temperature within the glass vials and set *in situ*.

2.2.4.3 Synthesis of ultra-violet (UV) -initiated Clay/ PNIPAM Nanocomposite Hydrogels

The samples were prepared using the protocol outlined in section 6.1.1.2, with the exception that diethoxyacetophenone was used as an initiating agent in place of AIBN. For UV-irradiation initiation, the vials were placed under a UV flux (wavelength 366nm) for 20 hours, turning once after 10 hours. The matrix of sample codes for all clay/ PNIPAM gels examined in this chapter along with their compositions are given in Table 2.4.

Table 2.4. The matrix if all clay/ PNIPAM gels examined in chapter 6

UV initiated	Thermally initiated	Overall composition
.25C_{10}U	.25C_{10}	9.75% PNIPAM, .25% clay, 90% water
.5C_{10}U	.5C_{10}	9.5% PNIPAM, .5% clay, 90% water
1C_{10}U	1C_{10}	9% PNIPAM, 1% clay, 90% water

2.2.4.4 Synthesis of N, N'-methylenebisacrylamide (BIS) cross-linked PNIPAM hydrogels

Organic cross-linking agent N, N'-methylenebisacrylamide (BIS) was weighed before being dissolved in degassed deionised water and stirred for a minimum of 2 hours. Next, NIPAM monomer and initiator were weighed and added to the mixture, before stirring for a further 2 hours. The homogenised solution was injected into 35mm x 10mm glass vials prior to polymerisation.

2.2.4.5 Synthesis of thermally-initiated BIS cross-linked PNIPAM hydrogels

To prepare chemically cross-linked hydrogels that contain 10% solids of which 1% is BIS (or 1BIS_{10}), a transparent aqueous solution consisting of water (9g) BIS (0.1g), AIBN (0.009g) and NIPAM (0.9g) was prepared. Then, polymerisation was allowed to proceed *in situ* in an oil bath preset to 80°C for 24 hours. The nomenclature format is as follows:

$$x\text{BIS}_y$$

Where x is the overall percentage of BIS by weight, and y denotes the overall percentage of "solids" (BIS + NIPAM) by weight of the subsequent gel.

For example, ".5BIS$_{10}$" indicates a 10g sample of chemically cross-linked hydrogel prepared using 9g water, 0.95g NIPAM, 0.05g BIS, and 0.0095g AIBN (Table 2.5).

2.2.4.6   Synthesis of UV-initiated BIS cross-linked PNIPAM hydrogels

The samples were prepared using the protocol outlined in section 6.3.2.1, with the exception that diethoxyacetophenone was used as an initiating agent in place of AIBN. For UV-irradiation initiation, the vials were placed under a UV lamp (wavelength 366nm) for 20 hours, turning once after 10 hours. The matrix of sample codes for all BIS/ PNIPAM gels, examined in this chapter along with their compositions is given in Table 2.5

Table 2.5. The matrix of all BIS/ PNIPAM gels examined in chapter 6

UV initiated	Thermally initiated	Overall composition
.25BIS$_{10}$U	.25BIS$_{10}$	9.75% PNIPAM, .25% clay, 90% water
.5BIS$_{10}$U	.5BIS$_{10}$	9.5% PNIPAM, .5% clay, 90% water
1BIS$_{10}$U	1BIS$_{10}$	9% PNIPAM, 1% clay, 90% water

The resulting hydrogels are a series of translucent, rubbery, rod-shaped gels of varying tensile strengths. Although definitive quantitative observations will be seen in future work, tensile strength of the gels improves with increasing concentration of clay when initiated thermally, and worsens when initiated by UV irradiation. All gels cross-linked with BIS were fragile and needed to be handled with the greatest care, only slight deformation was required to cause splitting and breakage of the gel rod. This is in good agreement with observations made by Haraguchi et al [15].

2.2.4.7   Formation of diluted clay/ PNIPAM nanocomposite hydrogels

All diluted gels were initially synthesised as thermally-initiated PCPHs as described in section 6.1.1.2 and Table 2.4. Whilst still in their liquid state at 80°C, a precise quantity of hot deionised water was added to the PCPH and the mixture was stirred gently before being allowed to cool and solidify at room temperature. The gels were allowed to "set" for at least 4 hours at room temperature in 35mm x 10mm glass vials prior to carefully being sliced into discs of ~2mm thickness. The matrix of the composition of PCPH, the

extent of dilution and overall resulting gel composition examined in this chapter is given in table 2.6.

Table 2.6. The matrix of diluted PCPH gels examined in this chapter.

Sample (from thermally initiated PCPH)	Overall composition
100% .25C$_{10}$	9.75% PNIPAM, .25% clay, 90% water
75% .25C$_{10}$, 25% water	7.3125% PNIPAM, .1875% clay, 92.5% water
50% .25C$_{10}$, 50% water	4.875% PNIPAM, .125% clay, 95% water
100% .5C$_{10}$	9.5% PNIPAM, .5% clay, 90% water
75% .5C$_{10}$, 25% water	7.125% PNIPAM, .375% clay, 92.5% water
50% .5C$_{10}$, 50% water	4.75% PNIPAM, .25% clay, 95% water
100% 1C$_{10}$	9% PNIPAM, 1% clay, 90% water
75% 1C$_{10}$, 25% water	6.75% PNIPAM, .75% clay, 92.5% water
50% 1C$_{10}$, 50% water	4.5% PNIPAM, .5% clay, 95% water

2.2.4.8   Formation of Gelatine – doped clay/ PNIPAM nanocomposite hydrogels

Please refer to section 2.2.1.3.

2.2.4.9   Formation of hyaluronic acid (HA) – doped clay/ PNIPAM nanocomposite hydrogels

Please refer to section 2.2.1.4.

2.2.5   Chapter 7 – PCPH as an injectable, functional therapy for degenerative disc disease.

2.2.5.1   Materials used in chapter 7

The materials used in this chapter to synthesise PNIPAM/ clay PCPH materials are detailed in section 2.2.1.1. The synthesis, nomenclature format and compositions of PNIPAM/clay PCPH formulations are detailed in section 2.2.1.2, and compositions of PNIPAM/clay/gelatine and PNIPAM/clay/HA PCPH formulations are detailed in section 2.2.1.3, and 2.2.1.4, respectively. For materials used for the synthesis of a PNIPAM/ clay/ DMAc PCPH, the materials used are detailed in section 2.2.1.1, with the addition of N, N-Dimethylacrylamide (DMAc) (Aldrich, 99%), which was used as received. For materials used for the synthesis of a PNIPAM/ clay/ DMAc PCPH, the

materials used are detailed in section 2.2.1.1 with the addition of glycidyl methacrylate (GMAc) (Aldrich, 99%), which was used as received.

2.2.5.2. Preparation of a PNIPAM/ clay/ DMAc PCPH

In all cases, the % DMAc in the system refers to the % of overall monomer. Polymerisations were carried out using the protocol detailed in section 2.2.1.2. The nomenclature format is as follows:

$$xC_yDz$$

Where x is the overall percentage of clay by weight, and y denotes the overall percentage of "solids" (discounting AIBN , therefore clay + NIPAM + DMAc), D denotes comonomer DMAc and z is the % DMAc as a function of total monomer by weight. All overall DMAc/PNIPAM PCPH compositions and their sample codes are given in Table 2.7.

Table 2.7. PNIPAM PCPH and DMAc/PNIPAM PCPH formulations used in chapter 7

Sample code	Overall composition w/w
$1C_{10}$	9% NIPAM, 1% clay, 90% water
$1C_{10}D10$	8.1% PNIPAM, .9% DMAc, 1% clay, 90% water
$1C_{10}D13$	7.83% PNIPAM, 1.17% DMAc, 1% clay, 90% water
$1C_{10}D20$	7.2% PNIPAM, 1.8% DMAc, 1% clay, 90% water
$1C_{10}D30$	6.3% PNIPAM, 2.7% DMAc, 1% clay, 90% water

2.2.5.3. Preparation of a PNIPAM/ clay/ GMAc PCPH

In all cases, the % GMAc in the system refers to the % of overall monomer. Polymerisations were carried out using the protocol detailed in section 2.2.1.2. The nomenclature format is as follows: ·

$$xC_yDz$$

Where x is the overall percentage of clay by weight, and y denotes the overall percentage of "solids" (discounting AIBN, therefore clay + NIPAM + GMAc), D denotes

comonomer GMAc and z is the % GMAc as a function of total monomer by weight. All overall GMAc/PNIPAM PCPH compositions and their sample codes are given in Table 2.8.

Table 2.8. PNIPAM PCPH and GMAc/PNIPAM PCPH formulations used in chapter 7

Sample code	Overall composition w/w
$1C_{10}$	9% NIPAM, 1% clay, 90% water
$1C_{10}G20$	7.2% PNIPAM, 1.8% GMAc, 1% clay, 90% water
$1C_{10}G50$	4.5% PNIPAM, 4.5% GMAc, 1% clay, 90% water
$1C_{10}G80$	1.8% PNIPAM, 7.2% GMAc, 1% clay, 90% water

2.10   References

1.   Fundamentals of molecular spectroscopy. 1994: Tata McGraw-Hill Publishing Co.

2.   Coates, J., Interpretation of Infrared Spectra, A Practical Approach, ed. R.A. Meyer. 2000, Chichester: JohnWiley & Sons Ltd.

3.   E.M. Burka, R.C., Imaging ATR spectrometer.: US Patent. 6,141,100.

4.   Chan, K.L.A., Kazarian, K., Attenuated total reflection Fourier transform infrared imaging with variable angles of incidence: A three-dimensional profiling of heterogeneous materials. Applied Spectroscopy, 2007. 61(1): p. 48-54.

5.   Kane, S.R., Ashby, P., Pruitt, L., ATR-FTIR as a Thickness Measurement Technique for Hydrated Polymer-on-Polymer Coatings. Journal of Biomedical Materials Research Part B-Applied Biomaterials, 2009. 91B(2): p. 613-620.

6.   Miseo, E.V., Shimada, S., ATR imaging applied to the analysis of small polymer samples. Spectroscopy, 2004: p. 23-24.

7.   Mueller, M., Paulik, S., In situ ATR-FTIR and SFM studies on the influence of adsorption time on deposition and nanostructure of poly(ethyleneimine)/poly(acrylic acid) multilayers. Macromolecular Symposia, 2008. 265: p. 77-88.

8.   Kazarian, S.G., Chan, K., Sampling approaches in Fourier transform infrared imaging applied to polymers, in Characterization of Polymer Surfaces and Thin Films, K. Grundke, M. Stamm, and H.J. Adler, Editors. 2006. p. 1-6.

9.   Kazarian, S.G., et al., Spectroscopic imaging applied to drug release. Food and Bioproducts Processing, 2005. 83(C2): p. 127-135.

10.   Van der Weerd., et al., Combined approach of FTIR imaging and conventional dissolution tests applied to drug release. Journal of Controlled Release, 2004. 98(2): p. 295-305.

11.   Chan, K.L.A., et al., Applications of Attenuated Total Reflection Infrared Spectroscopic Imaging to Pharmaceutical Formulations. Analytical Chemistry, 2003. 75(9): p. 2140-2146.

12.   Kazarian, S.G., Chan, K., Applications of ATR-FTIR spectroscopic imaging to biomedical samples. Biochimica Et Biophysica Acta-Biomembranes, 2006. 1758(7): p. 858-867.

13.   Ricci, C., Chan, K., Kazarian, S., Combining the tape-lift method and Fourier transform infrared spectroscopic imaging for forensic applications. Applied Spectroscopy, 2006. 60(9): p. 1013-1021.

14.   Earnest, C.M., et al., Measurements, Compositional analysis by thermogravimetry: The development of a standard method. American Society for Testing and Materials. 1988: p. 28-37.

15.   Suryanarayana, C., Norton, M., X-Ray diffraction: a practical approach. 1998: Plenum Press.

16.   Hall, J.L. and C.R. Hawes, Electron microscopy of plant cells. 1991: Academic Press.

17.   Scanning Electron Microscope Laboratory, Northern Arizona University. 2006 10/ 08/2006 [online] accessed 12/03/2012 at: http://www4.nau.edu/microanalysis/Microprobe-SEM/Instrumentation.html.

18.   Goborn, J., a-Cyano-4-hydroxycinnamic acid affinity sample preparation, a protocol for MALDI-MS peptide analysis in proteomics. Analytical Chemistry, 2001. 73: p. 434- 438.

19.   Zhang, N., Doucette, A., Li, L., Two-layer sample preparation method for MALDI mass spectrometric analysis of protein and peptide samples containing sodium dodecyl sulfate. Analytical Chemistry, 2001. 73(13): p. 2968-2975.

20.   Bakhtiar, R., Nelson, R., Electrospray ionization and matrix-assisted laser desorption ionization mass spectrometry - Emerging technologies in biomedical sciences. Biochemical Pharmacology, 2000. 59(8): p. 891-905.

3

The Development of a PNIPAM/ Clay Nanocomposite Liquid Gel Precursor

Chapter 3 - The Development of a PNIPAM/ Clay Nanocomposite Liquid Gel Precursor.

3.1   Introduction

Many potential functions of PNIPAM can be achieved by producing gels with specific behavioural profiles which can be tailored through cross-link type, initiation method and incorporation of copolymers. The full utility of PNIPAM gel is realised when these gels are specifically tailored for their intended purpose. For example, flat sheets, films and various "shapes" of PNIPAM have been produced by; end-grafting PNIPAM bushes on surfaces [1], using a rheologically complex spin coating technique [2] attaching to a support by photo cross-linking of preformed polymer chains [3], photo polymerisation *in situ* in the presence of a cross-linking agent [4], or initiation of polymerisation from self-assembled monolayers [5]. Haraguchi [6] synthesised PNIPAM sheets *in situ* via thermal free radical initiation by bringing the aq. monomer/ initiator solution up to the disassociation temperature of the initiator and allowing polymerisation to proceed in the desired shape. All of the aforementioned techniques require several processing steps, some degree of specialist equipment and expertise and therefore moderate financial cost.

Haraguchi successfully synthesised clay/ PNIPAM gels *in situ* [6] in the form of flat sheets at ambient temperature using potassium persulfate (KPS) as a thermally-dissociated free-radical initiating agent with tetramethylethylenediamine (TEMED) as an accelerator. Numerous attempts in the presented research to devise a method of polymerising PNIPAM sheets *in situ* at high temperatures (specifically 60-80 °C to allow dissociation of AIBN) whilst keeping the system devoid of oxygen (and thus preventing chain growth termination) were met with failure, largely due to pressurisation issues and the thermal expansion of the gel during propagation causing any air-tight seal to become dislodged.

The problem was solved with the following novel discovery: When clay/PNIPAM formulations are subject to thermally initiated free-radical polymerisation, polymer propagation and the process of cross-linking occur separately. After 20-25 minutes at 80°C, the NIPAM/ clay/ AIBN/ water solution quickly and spontaneously loses its transparency, transforming from a clear monomeric suspension to a watery milk-like

liquid. It is after this point that subsequent cooling of the liquid (which shall henceforth be referred to as the polymer-clay precursor hydrogel or PCPH) to a temperature below the LCST of the polymer (~33°C for PNIPAM), results in the spontaneous formation of a transparent gel, a process which shall henceforth be referred to as "phase transition triggered nanoparticle anchored gelation", or PTTNAG. The PTTNAG of the PCPH and subsequent formation of the gel is permanent and the gel does not re-liquefy when the temperature is increased, but is instead a fully thermally switchable PNIPAM/ clay nanocomposite hydrogel capable of all the very high swelling/ deswelling capacity and optical transparency changes reported by Haraguchi [7-12].

In this chapter we examine this phenomenon in depth and put forward possible reasons for its occurrence. Conclusions regarding electrostatic interactions during PTTNAG are drawn from attenuated total reflectance – Fourier transform infrared spectroscopy (ATR-FTIR), the viscosity of the PCPH is investigated using Ostwald viscometery, mechanism of polymerisation *in situ*, as well as z-average hydrodynamic diameter of aqueous particles during polymerisation and PTTNAG is determined using dynamic light scattering (DLS).

3.2 · Preparation of a PNIPAM/ clay nanocomposite liquid gel precursor

The materials and methods used to synthesise PNIPAM/ Clay/gelatine nanocomposite liquid gel precursor are given in section 2.2.1.1.

3.3 Monitoring the PTTNAG of PNIPAM/ Clay Nanocomposite Liquid Gel Precursor using Attenuated Total Reflectance Fourier Transform Infrared Spectroscopy (ATR-FTIR).

The dominant intermolecular force in a very large number of natural and synthetic polymers is hydrogen bonding. It carries huge influence on behaviours such as phase transition, melting temperature and glass transition temperature (Tg). ATR-FTIR is a simple, effective and very widely utilised technique in the investigation of hydrogen bonding in polymeric systems and is also ideally suited to the acquisition of structural information. Although infrared spectroscopy is very sensitive to changes in hydrogen bonding, intermolecular and intramolecular O-H oscillator coupling results in highly complex water spectra (coupling is observed between symmetric v(OH) and antisymmetric v(OH) and between O-H oscillators on other molecules). In order to

achieve isolation of distinct O-H vibrations, decoupling of vibrational modes using mixtures of HOD and H_2O or D_2O have been examined [13]. Two separate models exist which explain spectral bands for water. The mixture model represents water molecules as existing in two states; hydrogen bonded and non-hydrogen bonded, and the continuum model where the spectral band consists of a continuum of progressively strengthening hydrogen bonds as the electromagnetic frequency decreases.

A great deal of spectroscopic work has been published which addresses the binding states of water in polymers, which behaves quite anomalously when compared to pure, "free" water. Techniques employed for this purpose include FTIR [14-23], Raman [24-28] , NMR [29-33], and neutron scattering [34-38]. The nature of water present in polymers depends on several factors, including component fraction and polymer hydrophilicity. Up to four water hydration levels or "states" have been reported, and the literature has been well reviewed [39].

IR spectroscopy has been a particularly useful tool in the determination of hydrogen bond change during polymer hydration, particularly the study of hydration and hydrogen bonds of amide groups [40]. The timescale for the formation and destruction of hydrogen bonds (10^{-12}s) is longer than that of vibration (10^{-14}s) [18], which enables the observation of several $\nu(OH)$ absorbance bands manifested from separate hydrogen bond types [18]. Absorbance bands arising from water-water and polymer-water interactions are broadened and intensified with increasing water concentration. Simultaneously, peak centre shift of $\nu(OH)$ bands to lower frequencies are observable, whilst the $\nu(OH)$ peak centre shifts to a higher frequency [19, 41]. Generally speaking, a change in hydrogen bond strength is observable in ATR-FTIR spectra as "shifting "of the corresponding band; weakening bonds shift the band to higher wavenumbers, strengthening bonds shift the band to lower wavenumbers [18].

ATR-FTIR was used to probe the thermal phase transition of PNIPAM and accompanying PTTNAG behaviour of PCPH suspensions. The parameters for data collection are given in section 2.1.1. A $1C_{10}$ PCPH suspension was prepared as detailed in Section 2.2.1.2. Blue-tac was used to create a ~3mm-deep circular well which just covered the heating stage and crystal of the ATR. The stage thermocouple was set to 40°C and left to equilibrate for 20 minutes before a further background spectrum was taken. This process was repeated to obtain backgrounds at 38°C, 36°C, 34°C, 32°C, 30°C, 28°C, 26°C, and 24°C. After re-equilibration at 40°C, enough hot $1C_{10}$ PCPH was

80

pipetted carefully into the well to fill it completely. A warm glass plate was placed over the top of the well carefully as to omit any trapped air and create an air-tight seal around the top of the well. The apparatus was left to equilibrate at 40°C for 30 minutes before the measurement was taken. The background was ratioed against the measurement spectrum obtained at 40°C. The process was repeated at 2°C decrements, subtracting the spectrum from the corresponding background each time. Since the resolution of these experiments is 4 wavenumbers cm^{-1} and observed shifts begin at 2 wavenumbers, close repeatability must be demonstrated. 5 repeats of the experiment were performed, and a t test was carried out to determine whether there existed a significant difference between each observed shift and the average of those shifts (table 3.1). The absolute value of the t Stat is lower than the t Critical two-tail for all data sets, and the probability that the null hypothesis is true is larger than Alpha (0.05). Therefore the null hypothesis is affirmed that there is no statistical difference between the values obtained for each wavenumber shift and their average.

Table 3.1. Average observed IR frequencies and assignments of a $1C_{10}$ PCPH at 40°C (above LCST of PNIPAM) and subsequent $1C_{10}$ PNIPAM/ clay hydrogel at 24°C (below LCST of PNIPAM), along with t Stat and t Critical statistical values. n=5.

Assignment	40°C	24°C	Wavenumber shift cm^{-1}	t Stat	t Critical
$\nu_{as}(CH_2)$	2937	2938.6	+1.6	-0.35	3.18
$\nu_{as}(CH_3)$	2977.4	2983.4	+6	1	3.18
Amide I	1632.4	1630.2	-2.2	0.5	3.18
Amide II	1556	1560.8	+4.8	-0.2	3.18
$\nu(Si-O)$	999.4	1001.4	+2	-0.2	3.18

81
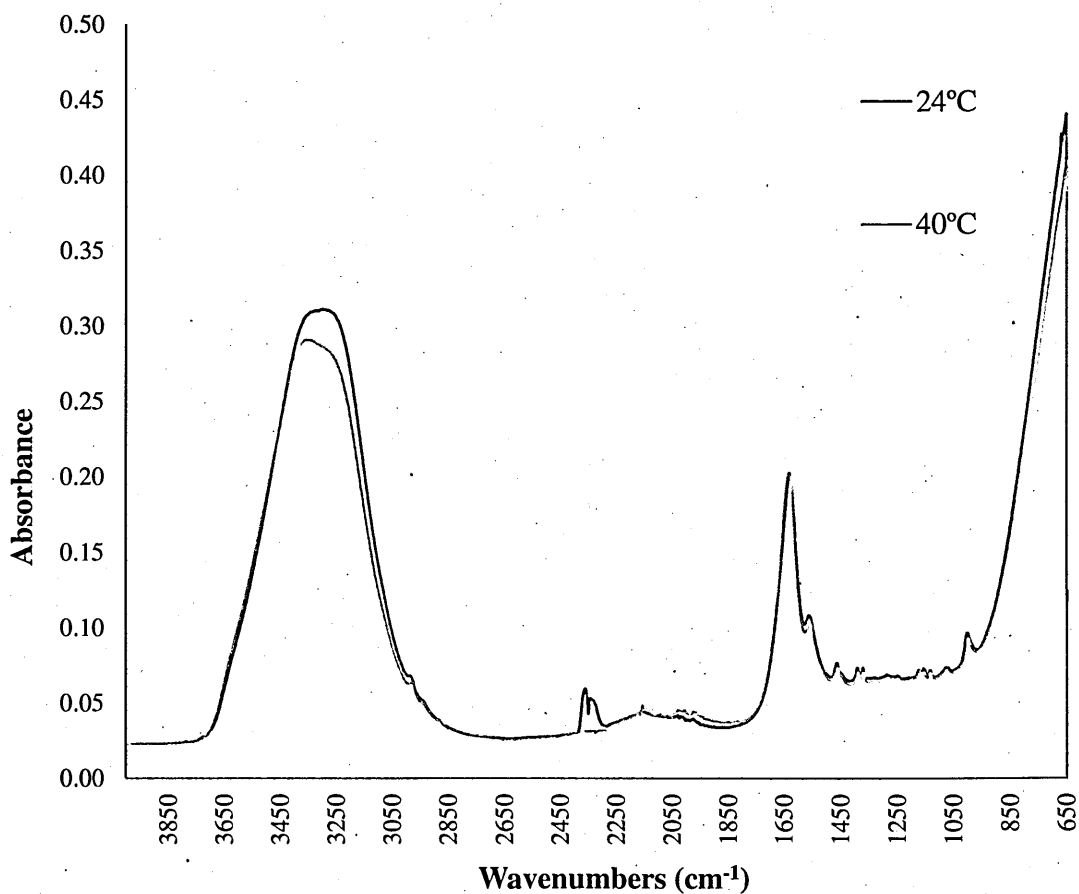
Figure 3.1. Typical full ATR spectra of a 1C$_{10}$ PCPH at 40°C and subsequent PNIPAM/ clay nanocomposite hydrogel when the PCPH is cooled to 24°C.

For clarity, only spectra for the highest and lowest experimental temperatures are shown. The full ATR-FTIR spectra are shown in figure 3.1. Bands of interest were expanded for closer inspection and are shown across figures 3.2 – 3.5. Wavenumbers and wavenumber shifts of peaks observed in these spectra are given in table 3.1.
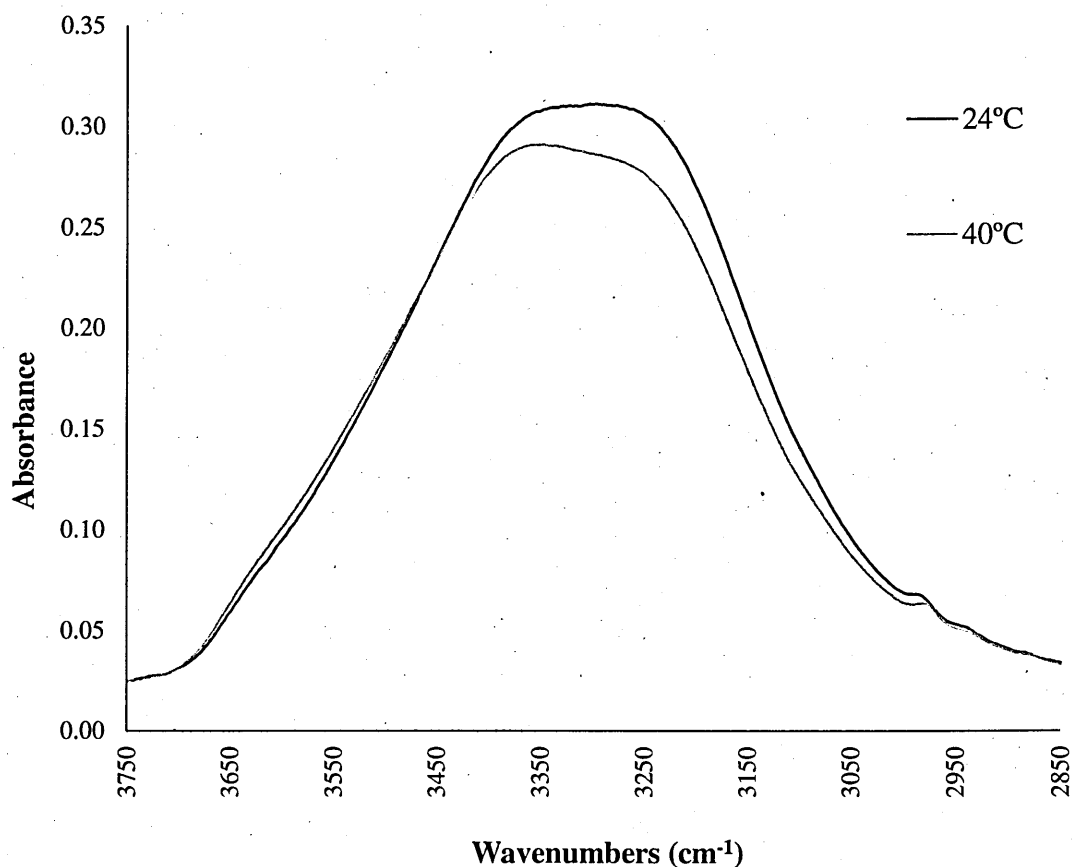
Figure 3.2. Comparison of typical ATR-FTIR v(OH) band intensities and evolving band shape of a $1C_{10}$ PCPH at 40°C and subsequent PNIPAM/ clay nanocomposite hydrogel when the PCPH is cooled to 24°C.

Polar functional groups absorb strongly in the mid infrared region, and the infrared intensity is governed by the magnitude of the change in dipole during vibration. Figure 3.2 shows the v(OH) band for the sample at 40°C and 24°C. Band intensity change is explained by the change in net dipole magnitude. A less intense v(OH) at 40°C is indicative of fewer water- water and water-polymer interactions in a relatively high energy system. As the temperature is reduced from 40°C to 24°C, changes the relative band proportions are observable, also changing the band shape. A greater intensity at lower wavenumbers changes the band shape, which as mentioned previously, is indicative of strengthening hydrogen bonding interactive forces. Therefore, when the amount of energy in the system is decreased, the capacity for hydrogen bond formation is increased [42].
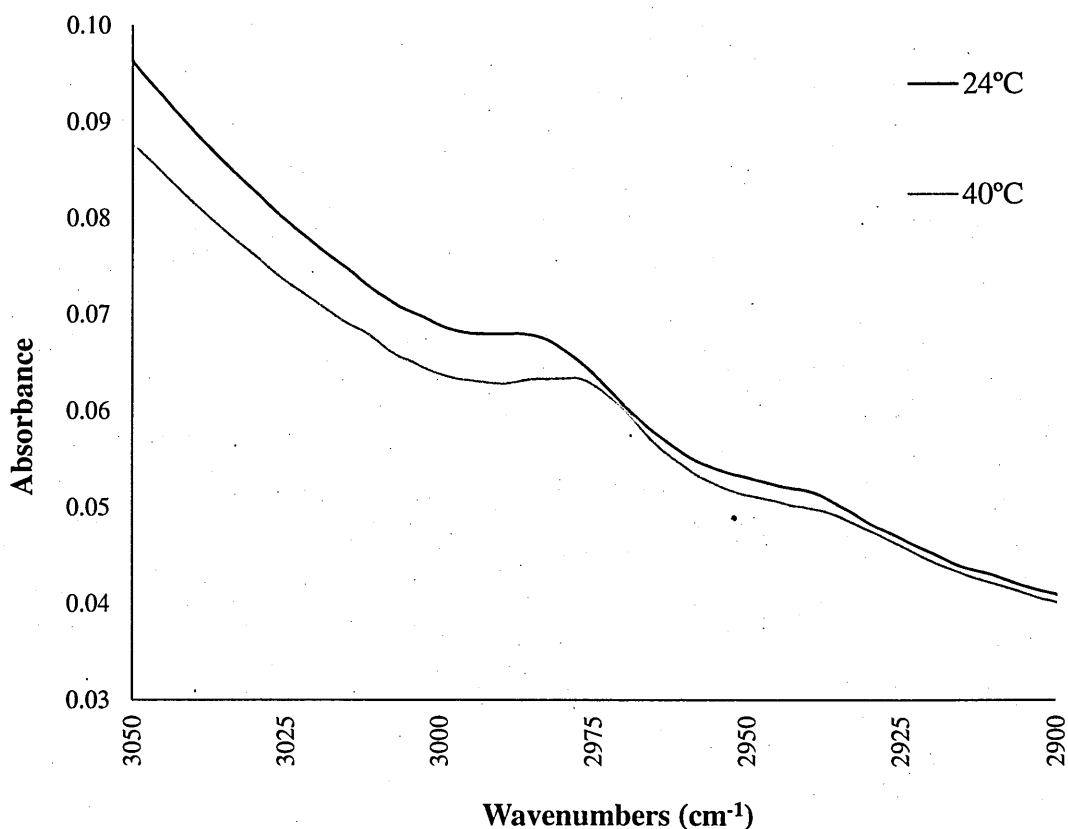
Figure 3.3. Comparison of typical ATR-FTIR $\nu_{as}(CH_2)$ and $\nu_{as}(CH_3)$ band intensities and evolving band shape of a $1C_{10}$ PCPH at 40°C and subsequent PNIPAM/ clay nanocomposite hydrogel when the PCPH is cooled to 24°C.

The two spectral bands shown in figure 3.3 at *ca.* 2983 cm^{-1} and 2931 cm^{-1} are assigned to antisymmetric methylene $\nu_{as}(CH_2)$ and symmetric methyl $\nu_s(CH)$, respectively. A shift to higher wavenumbers during temperature decrease is accompanied by an shift in peak position for $\nu_{as}(CH_2)$ and $\nu_{as}(CH_3)$ absorptions by 1.6 and 6 wavenumbers respectively (see table 3.1). As a positive shift in wavenumber is indicative of weakening hydrogen bond interactions, in turn revealing dehydration of the CH_3 and CH_2 groups which a conclusive indication of phase transition [43-46].

84
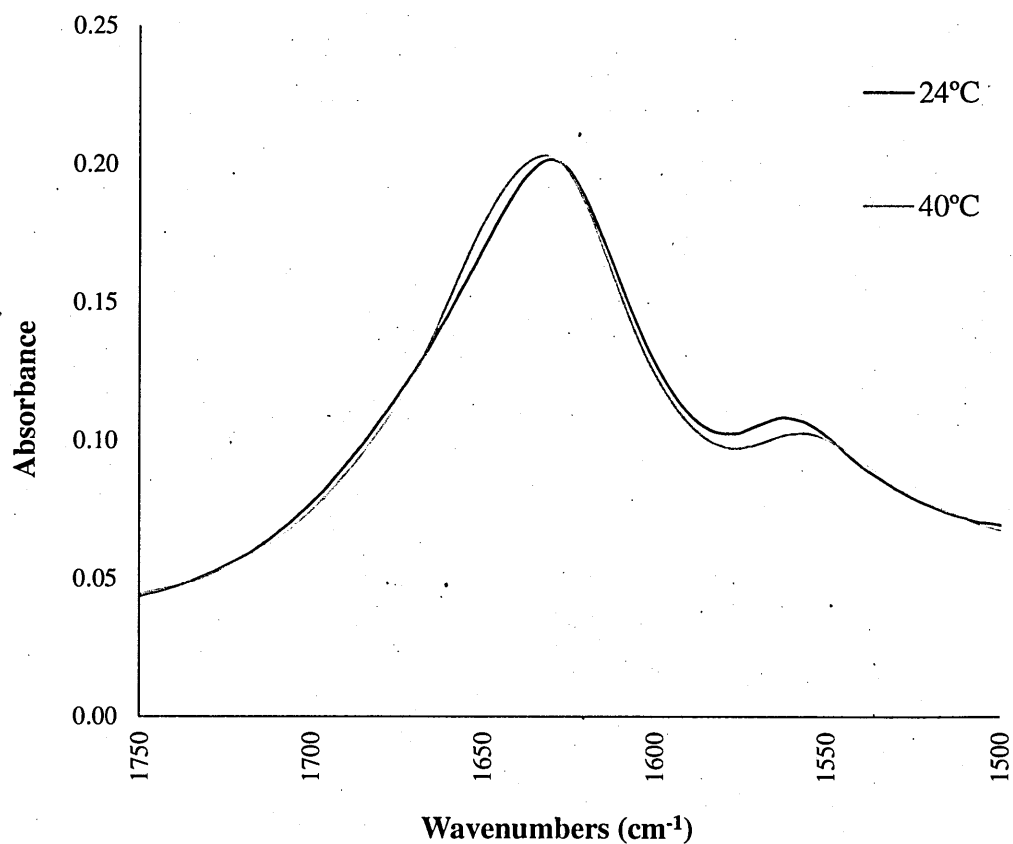
Figure 3.4. Comparison of typical ATR-FTIR Amide I and Amide II band intensities and evolving band shape of a 1C$_{10}$ PCPH at 40°C and subsequent PNIPAM/ clay nanocomposite hydrogel when the PCPH is cooled to 24°C.

The strong absorbance band located between 1580cm^{-1} and 1700cm^{-1} in figure 3.7 consists of 2 overlapping bands, the amide I C=O stretching vibration at 1646cm^{-1} and δ (OH) at1630cm^{-1}. There is no change in δ(OH) as a function of temperature, so any thermal shifts in this band can be attributed to the C=O vibration. The peak position is highly dependent on the carbonyl environment, and will shift depending on the strength of hydrogen bonding within it [44-45]. At 40°C, the PNIPAM chains are in the globule conformation and less carbonyl sites are available to form hydrogen bonds with water. At 24°C, the PNIPAM chains are in the coil conformation; water has better access to the polymers and can hydrogen bond at and around a larger number of carbonyl sites. This explains the 2.2 wavenumber negative shift to lower wavenumber from 1632.4 to 1630.2 cm^{-1} above and below the LCST of PNIPAM in this system (see table 3.1). Conversely, the Amide II v(NH) band shifts from 1556 cm^{-1} to 1560.8 cm^{-1} wavenumbers upon the cooling and subsequent hydration of PNIPAM. The analysis of these 2 diagnostic bands determines conclusively that the PNIPAM has undergone globule to coil phase transition between 40°C to 24°C [44-45, 47].

Figure 3.5. Comparison of the ATR-FTIR ν(Si-O) (1001 wavenumbers) band intensities and evolving band shape of a $1C_{10}$ PCPH at 40°C and subsequent PNIPAM/ clay nanocomposite hydrogel when the PCPH is cooled to 24°C.
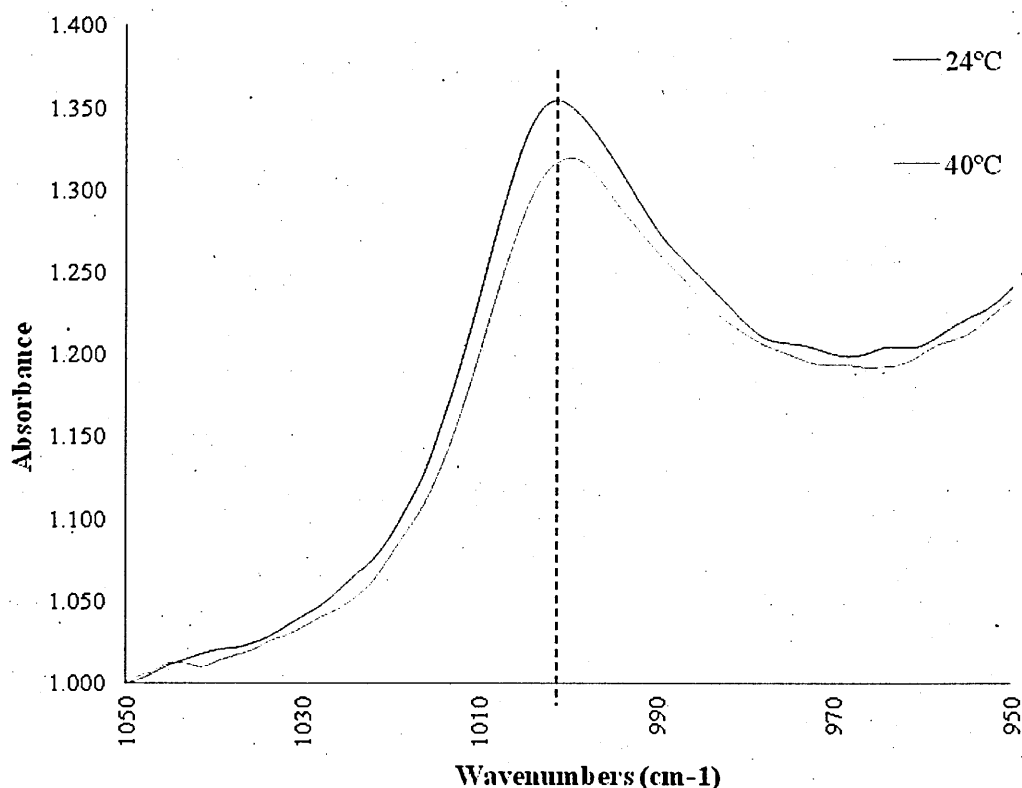
The spectral band at *ca.* $1001cm^{-1}$ in figure 3.5 is assigned to ν(Si-O) of the laponite clay, and is associated with Si in a tetrahedral environment (figure 1.13). Weakening Si-O/ hydrogen bond interactions are observed as a 2 wavenumber increase as temperature decreases. The hydrogen bonds in this instance are those donated by the NH groups of PNIPAM. A the temperature decreases, the number of Si- O- NH interactions decrease as the globule-state PNIPAM adopts the coil conformation and extends outward into the aqueous matrix.

3.4 Viscosity determination of a standard PCPH suspension.

A $1C_{10}$ PCPH suspension was synthesised as detailed in Section 2.2.1.2. The dynamic viscosity of the PCPH suspension at 54°C was measured using a simple glass capillary Ostwald viscometer, which consists of a U-shaped glass tube where one arm of the glass tubing contains a precise narrow capillary of a known length and radius.

The time taken for a fixed volume of liquid to pass through the viscometer under the influence of gravity was recorded and the following equation was used to calculate viscosity, with water at 54°C used as the reference liquid:

$$\eta_s = \eta_w \frac{t_s \rho_s}{t_w \rho_w}$$

Equation 3.1.

Where: η = dynamic viscosity (Pa s), ρ = density (kg m^{-3}) and t= time (s). Subscripts $_s$ and $_w$ represent sample and water, respectively.

For comparison, values for water and sunflower oil were generated using an identical method. Densities were calculated by weighing a fixed volume of liquid at 54°C to 4 dp.

All flow times were generated from liquids equilibrated at 54°C for 15 minutes prior to analysis, and all experiments were performed in triplicate with a fresh sample used for each measurement. The values given in table 3.2 consist of the average of 3 measurements.

Table 3.2. The dynamic viscosity of water, 1C10 PCPH and sunflower oil as determined by Ostwald viscometery, n=3.

Liquid at 54°C	Density Kg$^{3-1}$	Standard Error	Viscosity mPa s	Standard Error
Water	986.1	3.928	0.512	0.008
$1C_{10}$	1059.7	4.163	0.917	0.004
Sunflower Oil	890.8	3.940	20.32	1.307

The measured viscosity of $1C_{10}$ is approximately double that of water at the same temperature, but comparable to that of water at 25°C, demonstrating their similarity in viscosity. This is emphasised with the measured viscosity of sunflower oil, whose viscosity is more than twenty times that of $1C_{10}$.

3.5 Preparation of a PNIPAM/ Clay/ Gelatine Nanocomposite liquid gel precursor

The materials and methods used to synthesise PNIPAM/ Clay/gelatine nanocomposite liquid gel precursor are given in section 2.2.1.3.

3.5.1 Rationale for incorporating gelatine

Gelatine (or gelatin) is primarily used as a gelling agent [48] and creates strong, transparent, flexible and thermoreversible water soluble gels. It is a mixture of peptides and *proteins* and is usually the product of the thermal denaturation of animal bone, skin and ligament- derived collagen, usually in the presence of a dilute acid. Less commonly it is extracted from fish skins.

The range of applications of gelatine matrices and colloids in the food [49], pharmaceutical [50] and photographic [51] industries have made the properties of aqueous and gel state gelatine of significant interest to the polymer scientist and continue to be extensively studied [52-54]. The structure of gelatine consists of multi or single-stranded polypeptides consisting of left-handed polyproline helices containing 50 - 1000 amino acid residues [54].

The relatively inexpensive nature of gelatine, as well as its hydrophilic nature, biocompatibility and ability to withstand the relatively high temperatures necessary to allow the PCPH to remain in a liquid state made it an ideal candidate for initial PCPH doping/ incorporation studies.

3.6 PNIPAM/ Clay/ Hyaluronic Acid nanocomposite liquid gel precursor

The materials and methods used to synthesise PNIPAM/ Clay/ Hyaluronic Acid nanocomposite liquid gel precursor are given in section 2.2.1.4.

3.6.1 Rationale for incorporating Hyaluronic Acid (HA)

Hyaluronic acid is a ubiquitous component of extracellular matrix and is found in all vertebrate connective tissues. It is a structurally linear, viscoelastic, high-molecular-weight (1–2 million Da) glycosaminoglycan copolymer of N-acetyl-D-glucosamine and D-glucuronic acid [55], and plays an integral role in biological processes such as cell proliferation (cell growth and division resulting in an increase in cell number), adhesion and cell motility. HA is continuously digested and synthesised by cells, and directly influences tissue repair [56-57], morphogenesis [58-59], metastasis [60-61] and inflammatory response [57, 62] via cell surface receptor interaction [63-64]. Recent biomedical applications of HA include material implantation, the treatment of arthritis, ophthalmic surgery, wound healing scaffolds and tissue engineering [65]. The range of important biological functions as well as structural properties (due to its viscosity, water retention capabilities and hydrophilic nature) makes HA an obvious candidate as a dopant species in the PCPH technology.

3.7 The physical manifestation of PCPH PTTNAG

PTTNAG in this system refers to the mechanism by which the PCPH solidifies to form the cross-linked hydrogel, the stages of which are shown in figures 3.6 a-f.

Figure 3.6 shows the visible process by which the PCPH undergoes PTTNAG to form a polymer/ clay precursor hydrogel. After 20-25 minutes at 80°C, 15ml of the NIPAM/ clay/AIBN/ water solution spontaneously loses transparency and transforms into a low viscosity opaque liquid, or PCPH, which resembles milk. The PCPH remains in this state indefinitely until it is cooled to a temperature below that of its PTTNAG temperature – at or very close to the LCST of the polymer. In the case of $1C_{10}$ (pictured) this temperature is 33°C. For illustration purposes, 2ml of hot $1C_{10}$ PCPH suspension was drawn from a glass vial with a dropping pipette (a) and transferred drop-wise to a heart-shaped steel mould (b). After a few minutes cooling to room temperature (c), the PCPH begins to undergo PTTNAG, with the cooler outer edges of the mould gelating

first (d). PTTNAG and subsequent solidification is indicated by the spontaneous change in gel opacity. During the course of the following 10 minutes, the gel becomes completely optically transparent (e), and the solid PNIPAM/ clay hydrogel can easily be removed from the mould having taken its precise shape (f). The gel is rubbery in texture and exerts all of the thermally reversible phase-change characteristics of "regular" PNIPAM/ clay nanocomposite materials.
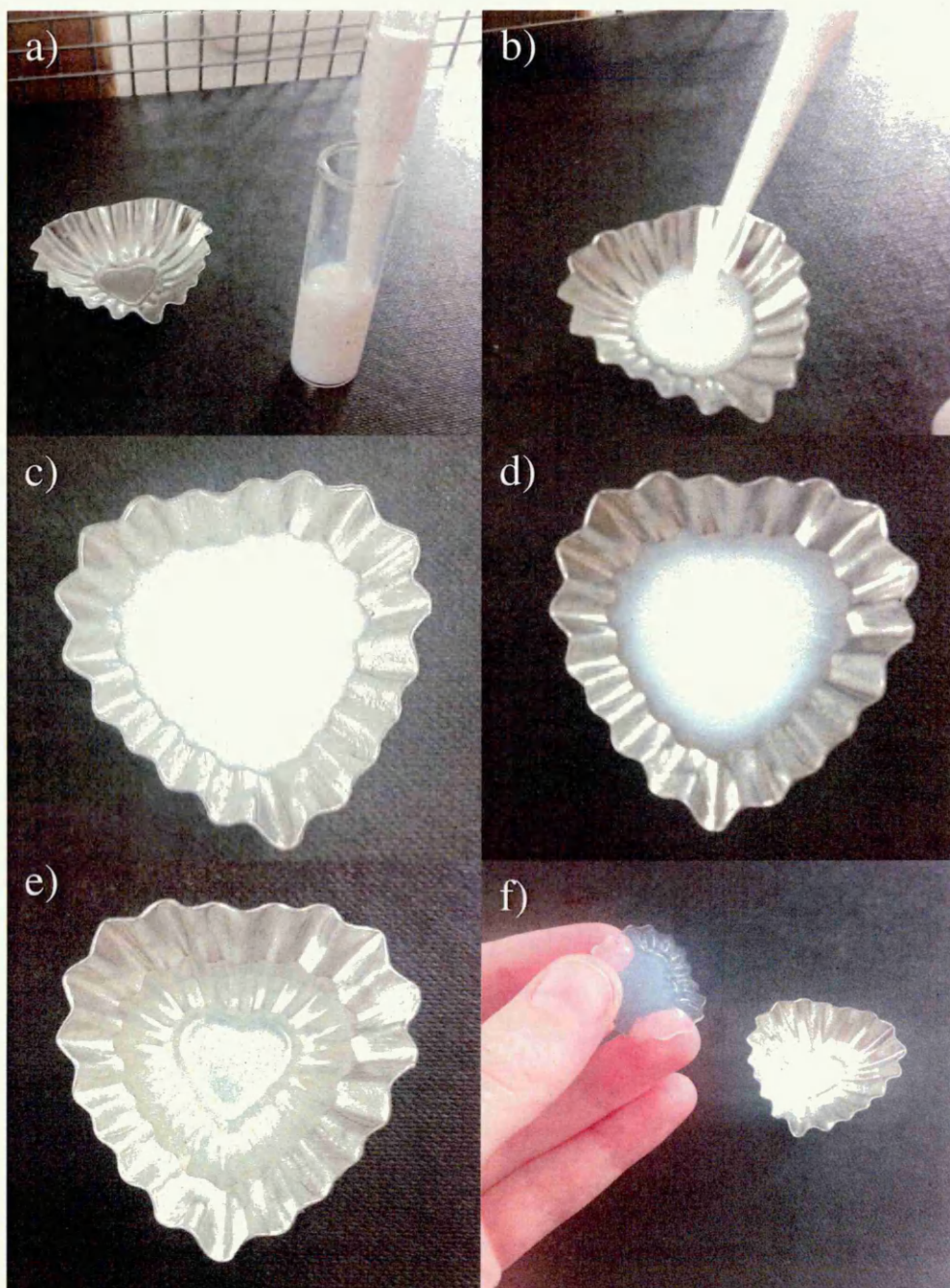
Figure 3.6. Photographs a-f demonstrate the visible PTTNAG steps of the polymer/ clay precursor hydrogel (PCPH).

3.8 Real-time Dynamic Light Scattering (DLS) study of polymerisation and PTTNAG of PCPH of various clay concentrations

In the case of PNIPAM, dynamic light scattering (DLS) has been used to examine the Z- average hydrodynamic diameter (D_H) of microgels (cross-linked latex particles that are swollen in solvent) and nanoparticle/polymer hybrid microgels in dispersion [66-70]. Commonly, PNIPAM microgel particles are synthesised by the free-radical precipitation polymerisation of NIPAM in the presence of a physical cross-linking agent such as methylenebisacrylamide (BIS) [71-76]. DLS has been used to successfully monitor the increase/ decrease in PNIPAM/ BIS microgel D_H as a function of temperature [68, 77].

To understand the process of particle growth in the presented precipitation polymerisation system, DLS was employed to give an approximate calculation of the D_H of particles formed in real time during the initial 6h of polymerisation with and without the presence of clay. The increase in D_H of particles was observed in real time during polymerisation at 80°C, with the D_H being obtained every 3-4 minutes during the polymerisation process. After 6h at 80°C, the instrument settings were altered to record the D_H of the particles every 3 minutes as the solution as it cooled at a rate of 1°C/ 3min. To reduce the negative influence of sample concentration on the reliability of the results, the quantity of solids used in this study are half that of typical formulations, and the sample codes altered accordingly. To avoid dust contamination, the solutions were filtered using syringe filters with pore size of 20 nm immediately before use.

The derived count rate (the back-scattered signal intensity, measured in kilo counts per second (kcps)), which is proportional to the amount of photons reflected from the sample solution, was taken simultaneously.

Z- Average (d.nm) of 0C5 Polymerising at 80°C
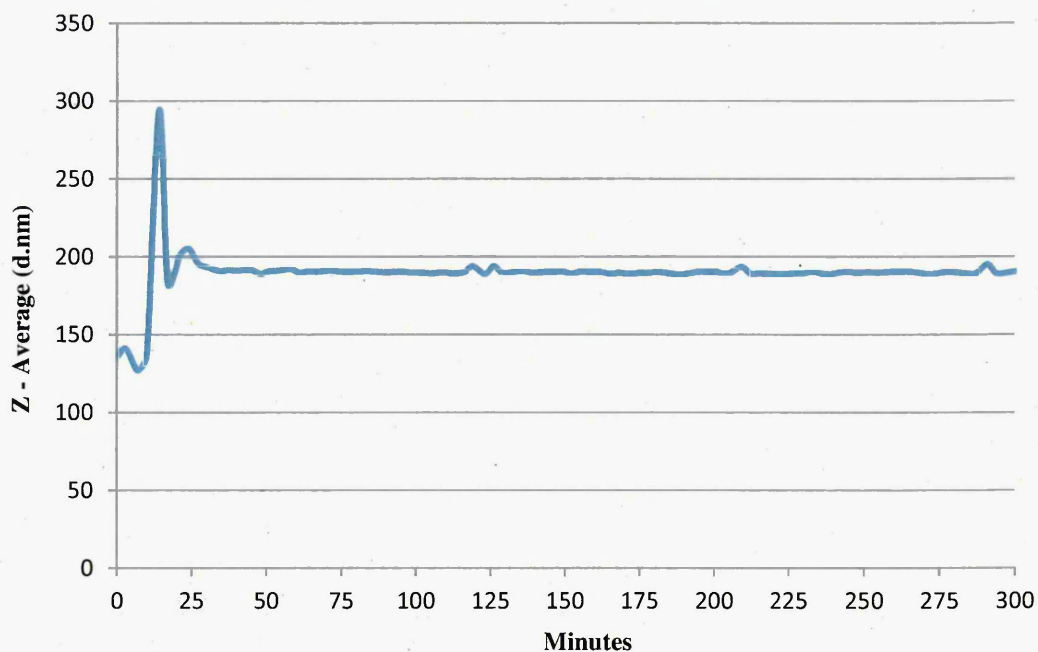
Figure 3.7. The Z-Average diameter of a 0C$_5$ PNIPAM solution (see Section 2.2.1.2 and table 2.1) as observed by DLS during precipitation polymerisation at 80°C.

Derived Count Rate of 0C5 Polymerising at 80°C (kcps)
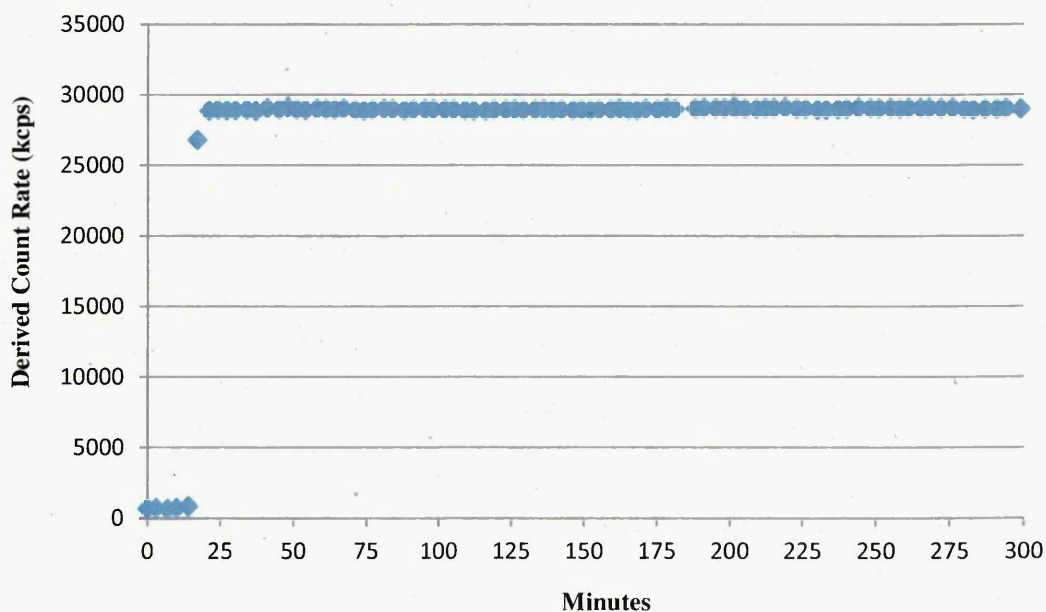
Figure 3.8. The derived count rate of a 0C$_5$ PNIPAM solution (see Section 2.2.1.2 and table 2.1) as observed by DLS during precipitation polymerisation at 80°C.

Z- Average (d.nm) of 0C5 cooling 1°C/3min.
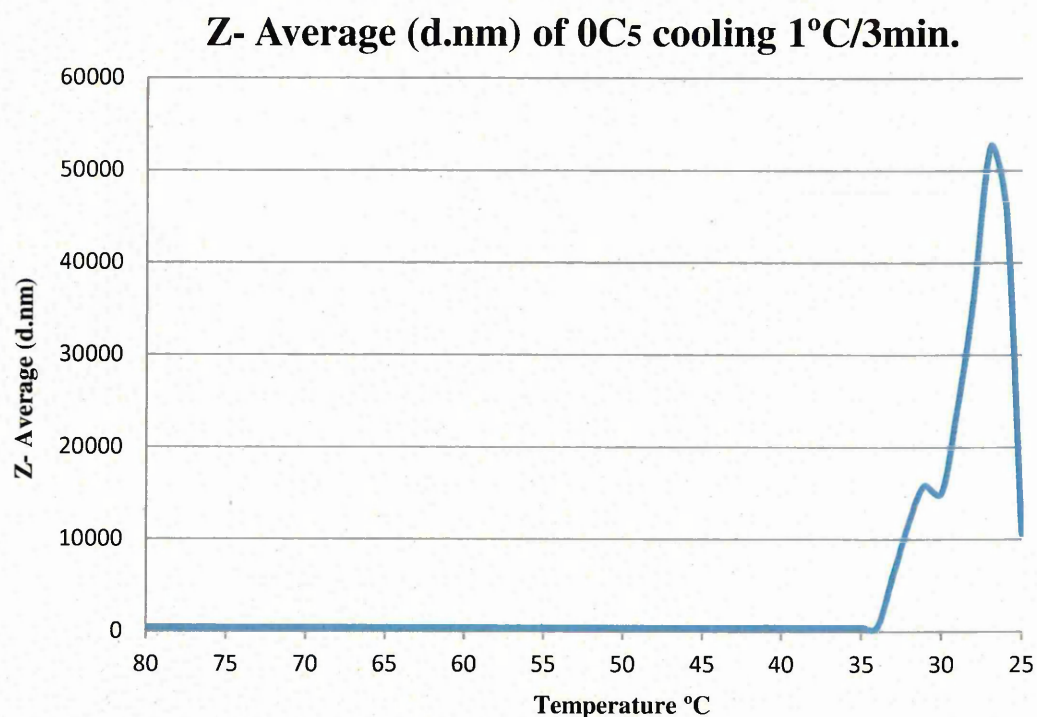
Figure 3.9. The Z-Average diameter measured during the cooling of a 0C₅ PNIPAM solution (see Section 2.2.1.2 and table 2.1) at a rate of 1°C/3 min. The solution had previously been held at 80°C for 6h.

Derived Count Rate of 0C5 cooling 1°C/3min (kcps)

Figure 3.10. The derived count rate measured during the cooling of a 0C₅ PNIPAM solution (see Section 2.2.1.2 and table 2.1) at a rate of 1°C/3 min. The solution had previously been held at 80°C for 6h.

In the $0C_5$ system, the D_H data (figure 3.7) indicates that at t = 0, the water/ monomer/ initiator solution contains particles with a diameter of approximately 170 nm. This observation is logically inaccurate, and can be explained by an insufficient quantity of backscattered light causing the instrument to predict a starting point for the size measurement, and bases this entirely on the polystyrene standards used in the instrument calibration. This is confirmed by the derived count rate at t = 0 for the same measurement (figure 3.8), which at ~700 kcps, is insufficient for meaningful size data to be determined. Therefore, for this particular data set, size values should be ignored and conclusions regarding particle size behaviour should be drawn from the curve shape and relative particle size changes alone. From this data, there is insufficient backscattered light to produce meaningful data until the reaction has proceeded for 17 minutes, by which time the derived count rate has jumped from ~800kps (at 14 minutes) to ~26,800kps. The sudden increase in quantity of backscattered light is indicative of the "crashing out" of PNIPAM particles from the solution. That is, a critical chain length has been reached and the polymer chain has collapsed into a globule-like conformation. The "blip" in the data between 17 and 27 minutes could be attributed to the stabilisation of the particles, or the instrument adjusting to the sudden intensity of backscattered light. After 27 minutes, the particles have reached their final D_H and remain practically unchanged for the following 5 and half hours, which according to this data are ca.60nm larger than the initial recorded value of the monomer solution.

Figures 3.8 and 3.10 show the D_H and derived count rate of $0C_5$ polymerised polymer particles cooling at a rate of 1°C/3min, respectively. The D_H remains largely unchanged during the cooling process between 80°C and 32°C, and the slight decrease in count rate over this temperature change is not significant. Upon cooling beyond 32°C, the Z- D_H is seen to increase very sharply (figure 3.9) whilst the derived count rate is simultaneously significantly reduced (figure 3.10). The cause of this phenomenon is the reformation of water-polymer hydrogen bonds and subsequent reswelling of the PNIPAM particles, which switch sharply from the globule to the coil conformation. The occurrence of globule-to-coil phase transformation is accompanied with a marked increase in optical clarity of PNIPAM solutions, which explains the abrupt decrease in backscattered light and as such, the abrupt decrease in derived count rate.

## Z- Average (d.nm) of .5C₀ at 80°C

Figure 3.11. The Z-Average diameter of a .5C_0 clay solution (see Section 2.2.1.2 and table 2.1) as observed by DLS during precipitation polymerisation at 80°C.
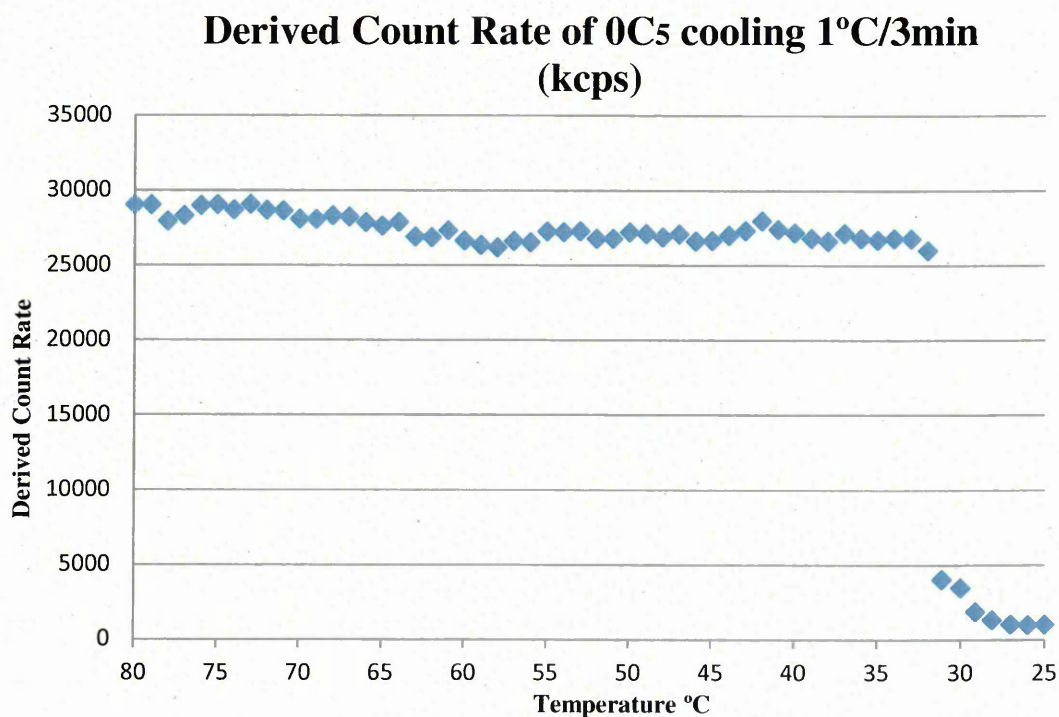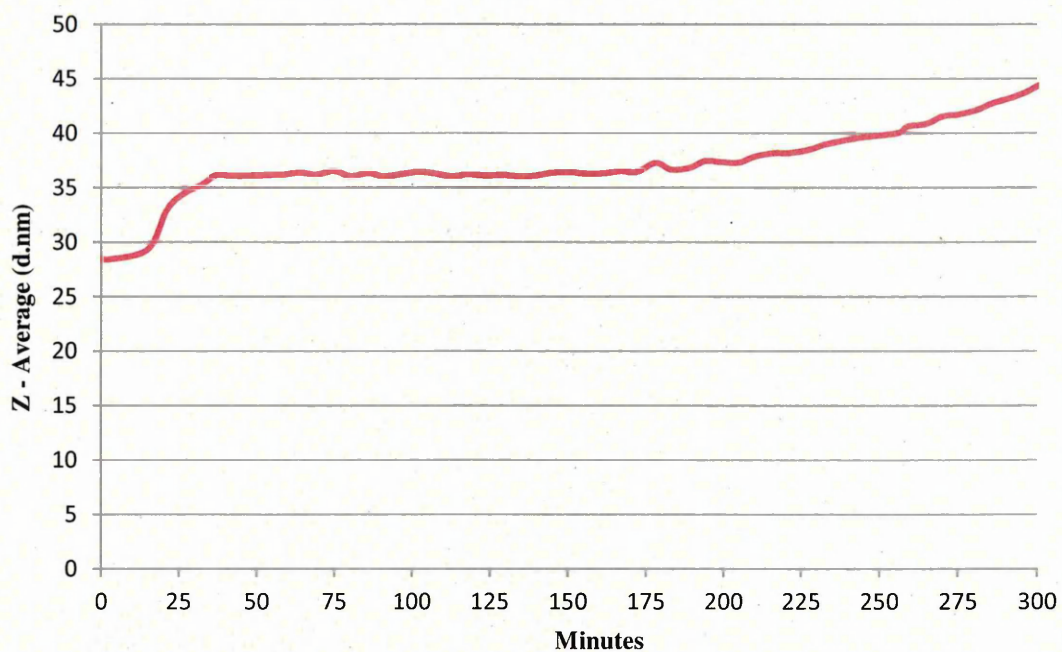
Derived Count Rate of .5C₀ at 80°C
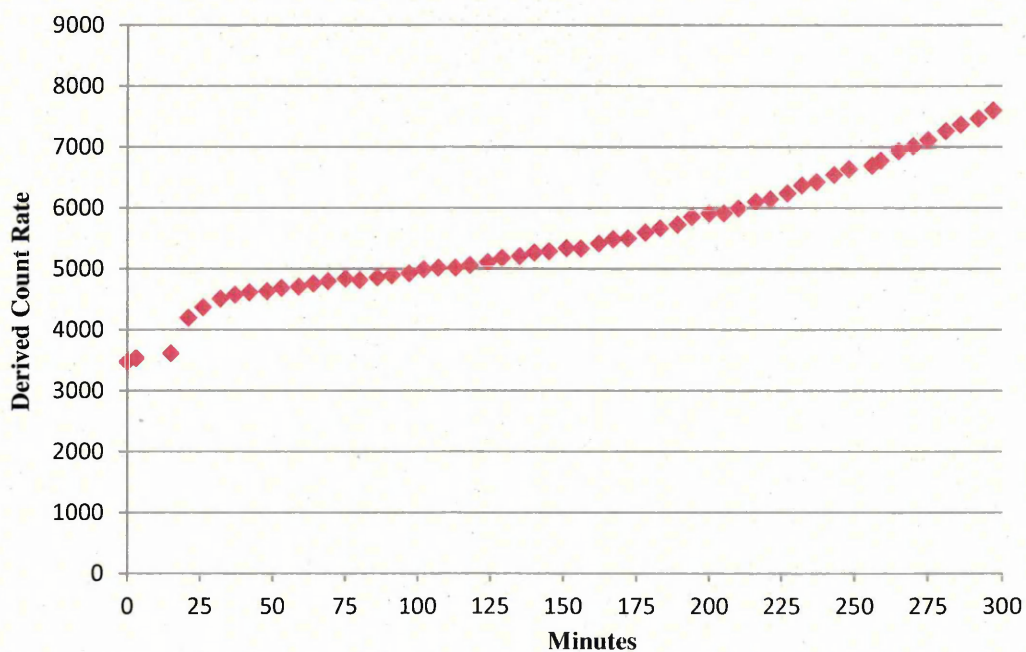
Figure 3.12. The derived count rate of a .5C_0 clay solution (see Section 2.2.1.2 and table 2.1) as observed by DLS as a function of time at 80°C.

Z- Average (d.nm) of .5C₀ cooling 1ºC/3min.
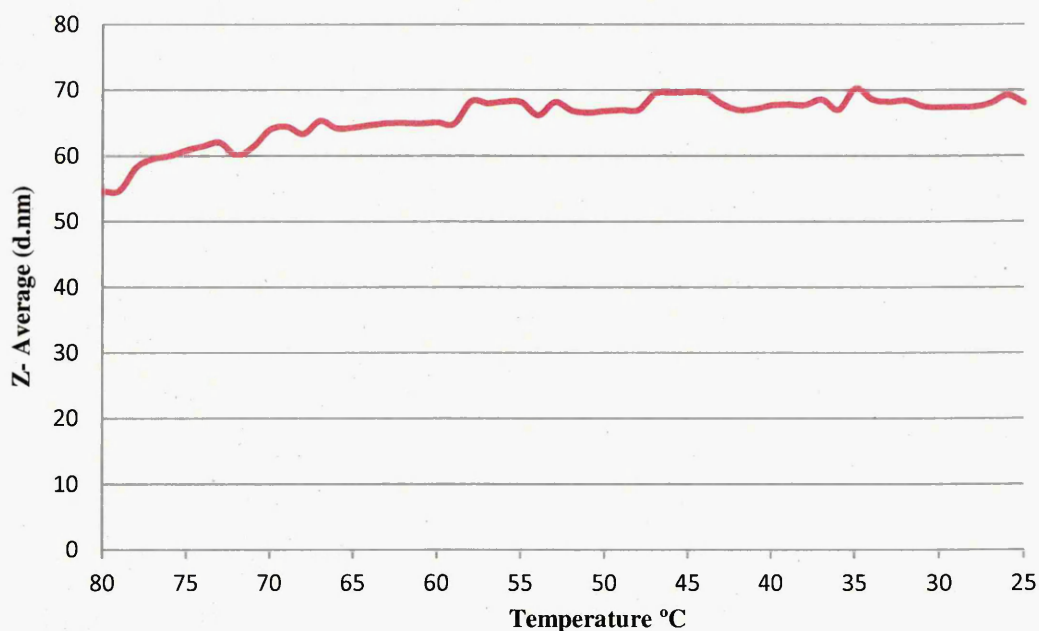
Figure 3.13. The Z-Average diameter of clay particles during the cooling of a .5C$_0$ solution (see Section 2.2.1.2 and table 2.1) at a rate of 1ºC/3 min. The solution had previously been held at 80ºC for 6h.

Derived Count Rate of .5C₀ cooling 1C/ 3min

Figure 3.14. The derived count rate measured during the cooling of a .5C$_0$ solution (see Section 2.2.1.2 and table 2.1) at a rate of 1ºC/3 min. The solution had previously been held at 80ºC for 6h.

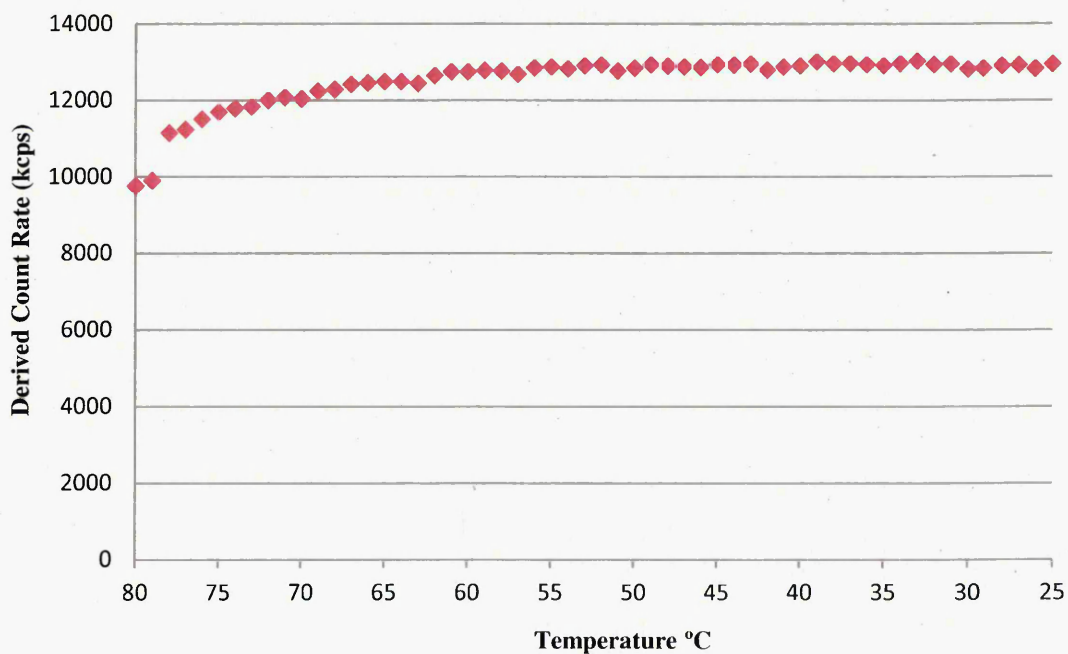In order to understand the effect of high temperature polymerisations on the aggregation behaviour of laponite clay platelets (a manufactured clay with a similar structure to that of hectorite composed of monodisperse plate-like particles of ca. 1nm thickness and ca. 30nm diameter) and to determine whether any of the observed phenomena can be attributed to clay behaviour alone, clay/ water solutions were subject to the same heating/ cooling process as the NIPAM and NIPAM/ clay formulations. The concentration of clay chosen for this experiment was precisely that of .5C_x formulations and the volume otherwise occupied by NIPAM/ AIBN was replaced with water. The solution was exfoliated, degassed and filtered in the same way as all other formulations. The D_H for this solution at t = 0 at 80°C is 28nm (figure 3.11), which begins to increase rapidly after 15 minutes and reaches 36 nm at 37 minutes. The derived count rate (figure 3.12) follows a near identical pattern, indicating a possible aggregation of the clay platelets.

To illustrate the aggregation phenomena of clay particles in water, a model of van der Walls and electrostatic interactions between Laponite platelets was shown in a study by of Kutter et al [78]. This model indicates a negative charge over the face of the laponite platelets and a positive charge distributed around its edge. This results in the formation of a "house of cards" platelet conformation through ionic interactions [79] which is illustrated in figure 3.15.

An important consideration when observing this data is the samples were filtered, and therefore agitated, immediately prior to analysis. It is feasible that the initial abrupt increase in derived count rate and perceived D_H is due to the "settling" of the clay suspension and the initial formation of an aggregated "house of cards" structure. The sustained and steady increase in derived count rate and perceived D_H during the remainder of the experiment is likely to be attributed to observations made previously by Tawari et al [80], who used DLS measurements to conclude that laponite rim charges increase with increasing temperature in aqueous solutions, and Harguchi et al [81] who concluded that among other factors such as clay concentration, the viscosity (and therefore aggregation) of aqueous clay suspensions also show time dependence. As the aggregates grow, they become less mobile and perceived D_H therefore increases.
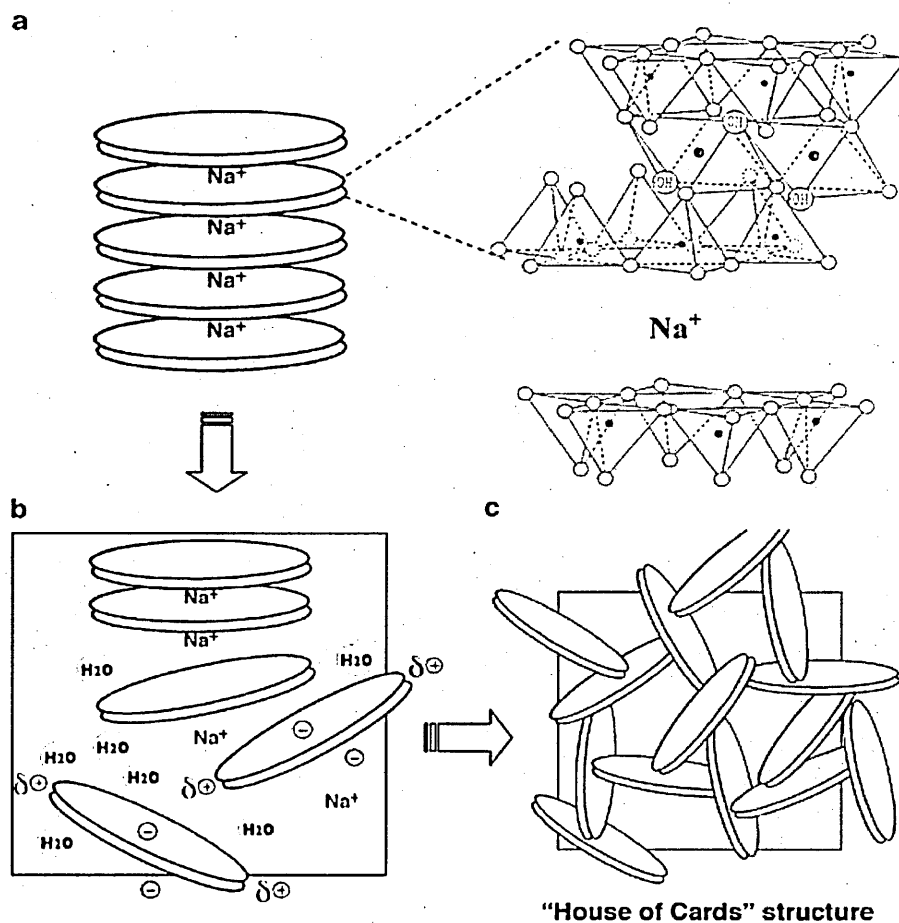
Figure 3.15 Schematic representation of the exfoliation of an aqueous clay suspension (b) from a stacked clay structure (a) and the subsequent formation of the house-of-cards structure (c) [81].

Over the course of the cooling experiments, the D_H and derived count rate (figures 3.13 and 3.14 respectively), show a follow-on increase in clay aggregation which gradually slows and reaches a plateau at temperatures below ~55°C. This could be due to the absence of thermal aggregative effects, or the thermodynamic stabilisation of the system.

Z-Average (d.nm) of .5C5 Polymerising at 80°C
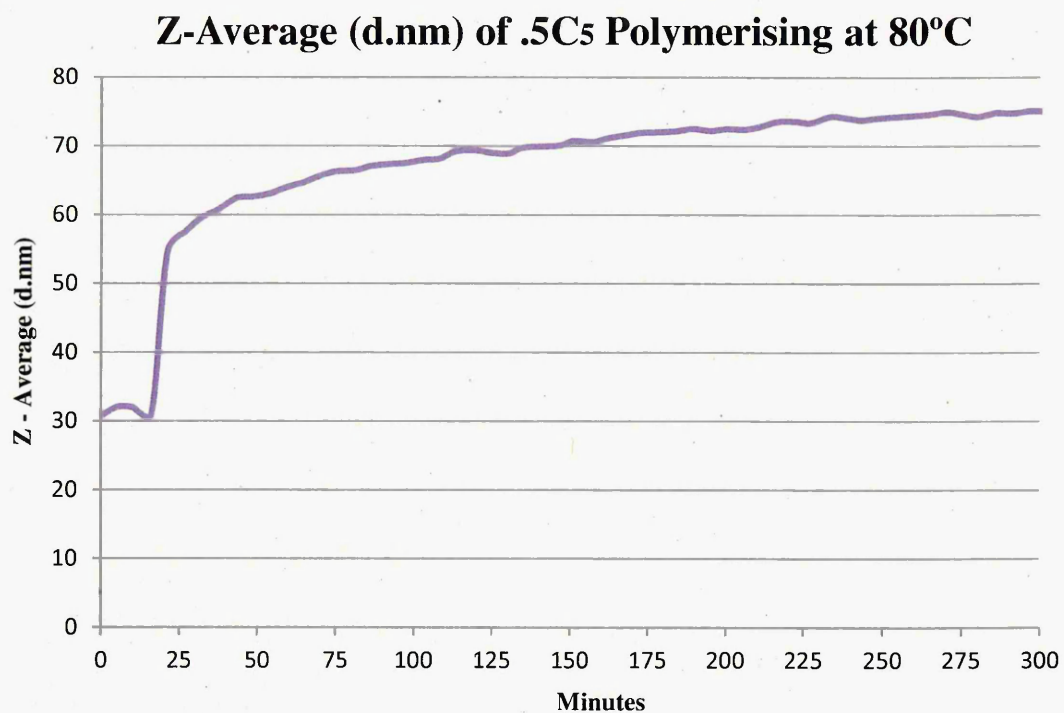
Figure 3.16. The Z-Average diameter of a .5C$_5$ PNIPAM/ clay solution (see Section 2.2.1.2 and table 2.1) as observed by DLS during precipitation polymerisation at 80°C.

Derived Count Rate of .5C5 Polymerising at 80°C (kcps)
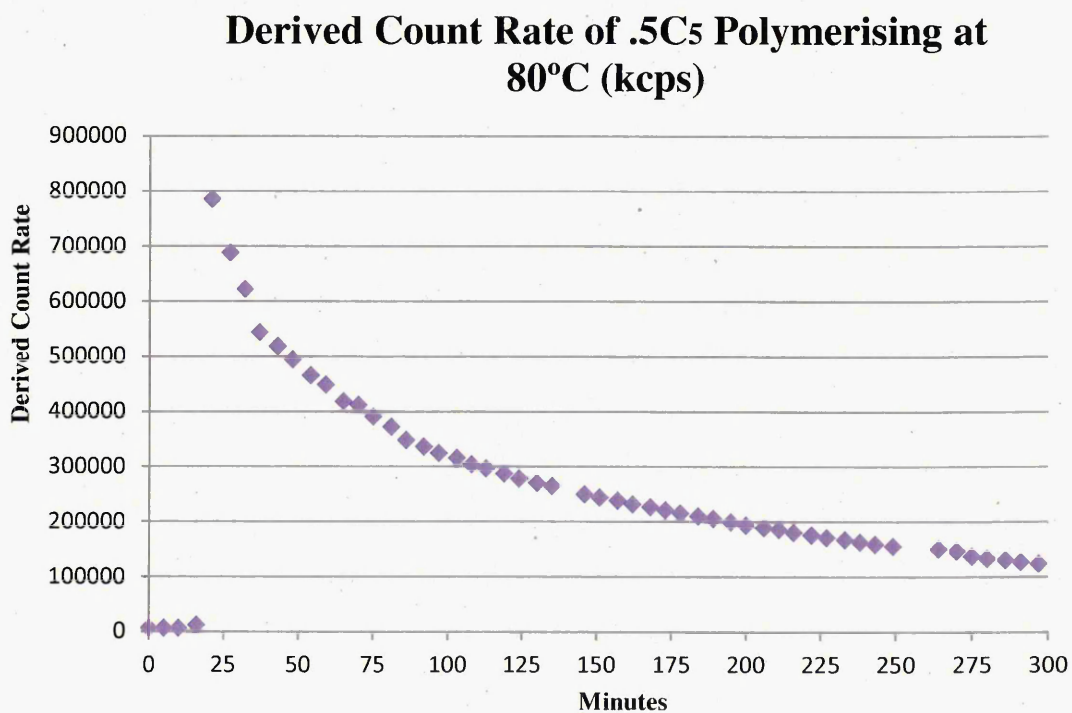
Figure 3.17. The derived count rate of a .5C$_5$ PNIPAM solution (see Section 2.2.1.2 and table 2.1) as observed by DLS during precipitation polymerisation at 80°C.

Z- Average (d.nm) of .5C5 cooling 1°C/3min.
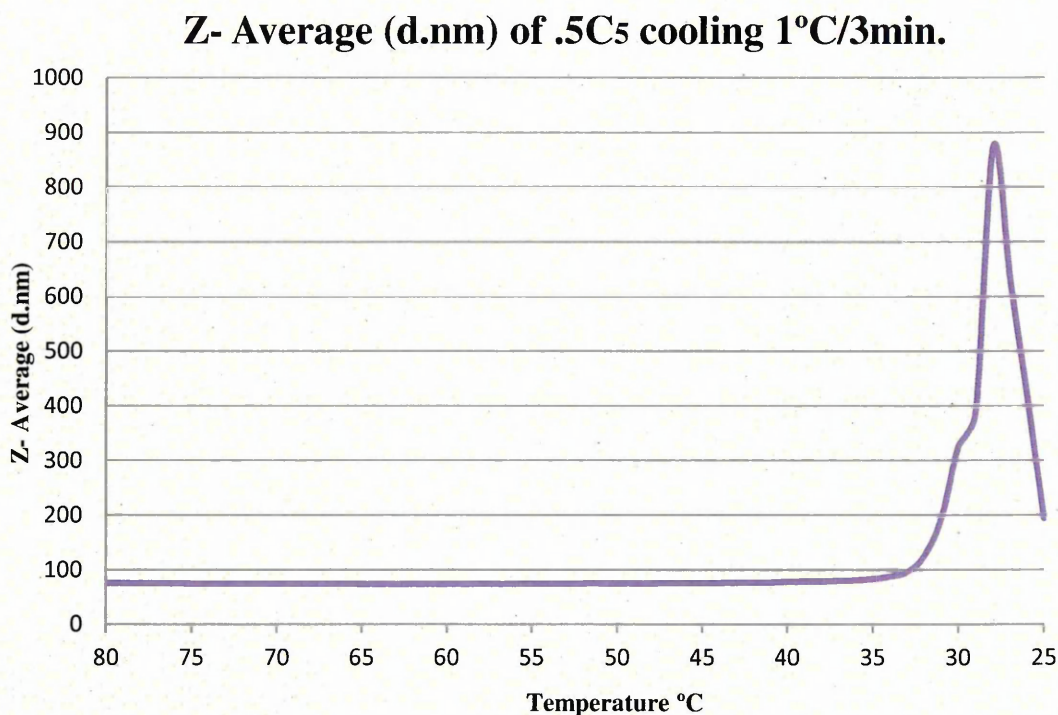
Figure 3.18. The Z-Average diameter of PNIPAM/ clay particles during the cooling of a .5C$_5$ PCPH solution (see Section 2.2.1.2 and table 2.1) at a rate of 1°C/3 min. The PCPH had been synthesised by free radical precipitation polymerisation at 80°C for 6h.

Derived Count Rate of .5C5 cooling 1°C/ 3min (kcps)
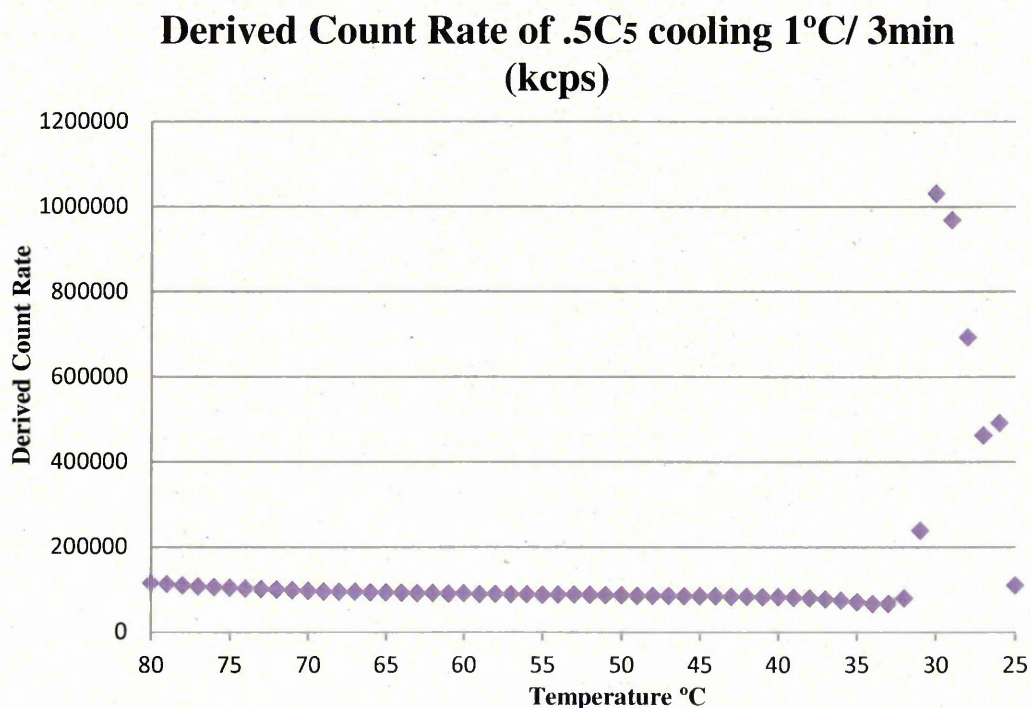
Figure 3.19. The derived count rate measured during the cooling of a .5C$_5$ PCPH solution (see Section 2.2.1.2 and table 2.1) at a rate of 1°C/3 min. The PCPH was previously synthesised by free radical precipitation polymerisation at 80°C for 6h.

101

The D_H and derived count rate (figures 3.16 and 3.17 respectively) of a $.5C_5$ monomeric solution was observed in real time during its polymerisation at 80°C over the course of 6 hours. The DLS instrument records a D_H at $t = 0$ of 30.7nm, which is in good agreement with the previously recorded D_H of laponite in this system (figure 3.11) which was 28nm. The derived count rate at $t = 0$ is ca. 3600 kcps, which is very similar to the count rate to that taken from the clay/ water solution at $t = 0$, which is ca. 3500kcps (figure 3.23) (It should be noted here that the amount of light scattered from monomers during the initial phase of the reaction is negligible and the monomers are considered "invisible" in a light scattering context for DLS). The D_H and derived count rate remain stable (and the monomers/ oligomers remain "invisible") at 80°C up to a critical point at ~19 minutes, where a very sharp increase in both values is seen (786000 kcps count rate and 55 d.nm Z- average at 24 minutes). This is the point at which the polymer chains have reached a critical length and have collapsed into a globule conformation, a phenomenon also observable in clay devoid systems (figures 3.7 and 3.8). Following this, a gradual increase in D_H and simultaneous decrease in scattering intensity is observable. Although seemingly counter-intuitive, this could be attributed to the following factors:

- Scattering intensity depends on both the size of the aggregates and their concentration. PNIPAM globules may have begun to aggregate and large particles do not scatter significantly in the backward direction [82].

- A decrease in scattered light may arise from a refractive index change as PNIPAM molecules undergo transition from random -coil to condensed globule. A low count rate (and hence quantity of scattered light) equates to a low refractive index [83]. It is therefore feasible from this data that the particles/ aggregates are growing in size but are backscattering less light.

Upon cooling (figures 3.18 and 3.19), very little change in either parameter is observable between 80- 33°C, and the system remains stable until cooling proceeds beyond 33°C. It is beyond this temperature that the condensed PNIPAM globules undergo phase transition and adopt the "coil" conformation, the process during which irreversible cross-linking takes place. Since the particles are no longer free to move at this stage, the recorded correlation functions cease to be indicative of particle size, and any data recorded below 33°C should be considered unreliable.
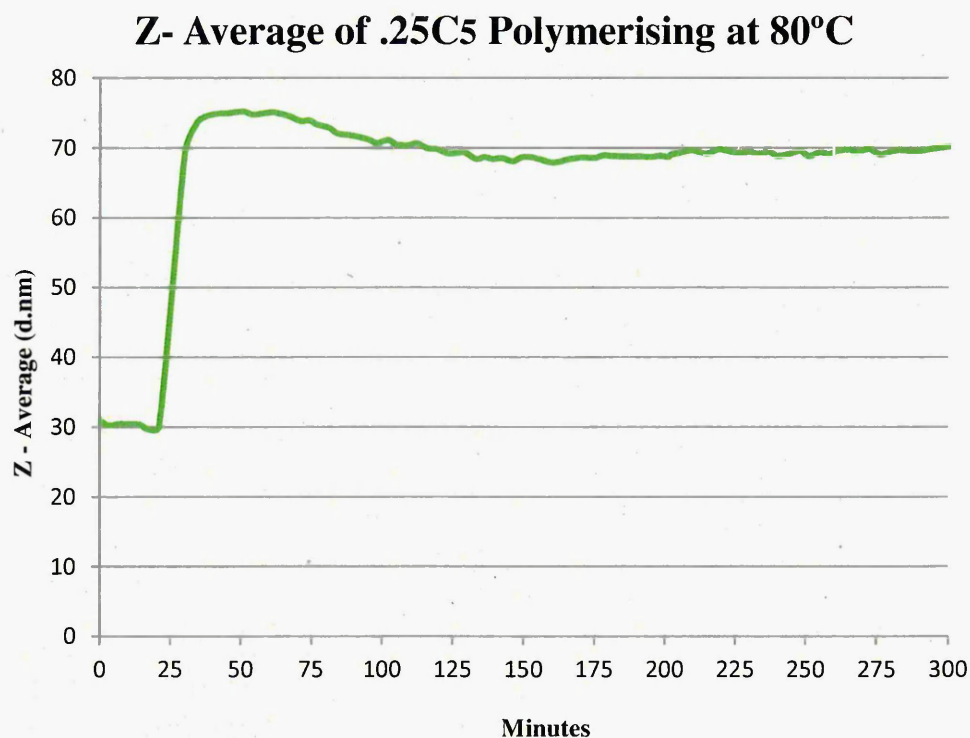
102

Z- Average of .25C5 Polymerising at 80ºC

Figure 3.20. The Z-Average diameter of a .25C$_5$ PNIPAM/ clay solution (see Section 2.2.1.2 and table 2.1) as observed by DLS during precipitation polymerisation at 80ºC.

Derived Count Rate of .25C5 Polymerising at 80ºC (kcps)

Figure 3.21. The derived count rate of a .25C$_5$ PNIPAM solution (see Section 2.2.1.2 and table 2.1) as observed by DLS during precipitation polymerisation at 80ºC.

Z- Average of .25C5 cooling 1°C/3min.
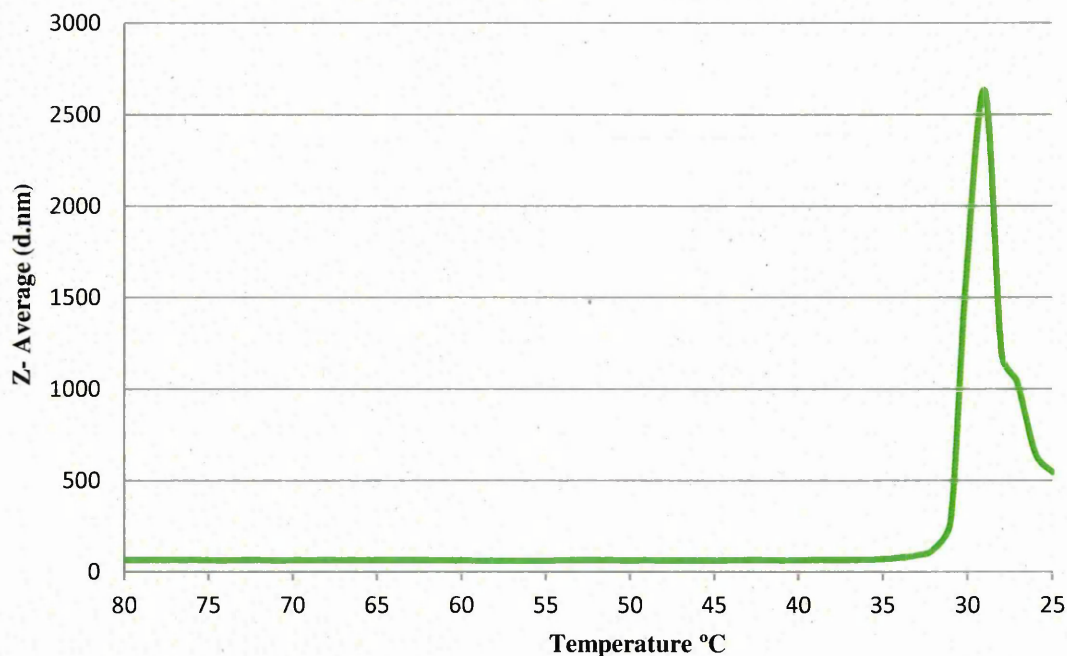
Figure 3.22. The Z-Average diameter of PNIPAM/ clay particles during the cooling of a .25C$_5$ PCPH solution (see Section 2.2.1.2 and table 2.1) at a rate of 1°C/3 min. The PCPH was previously synthesised by free radical precipitation polymerisation at 80°C for 6h.
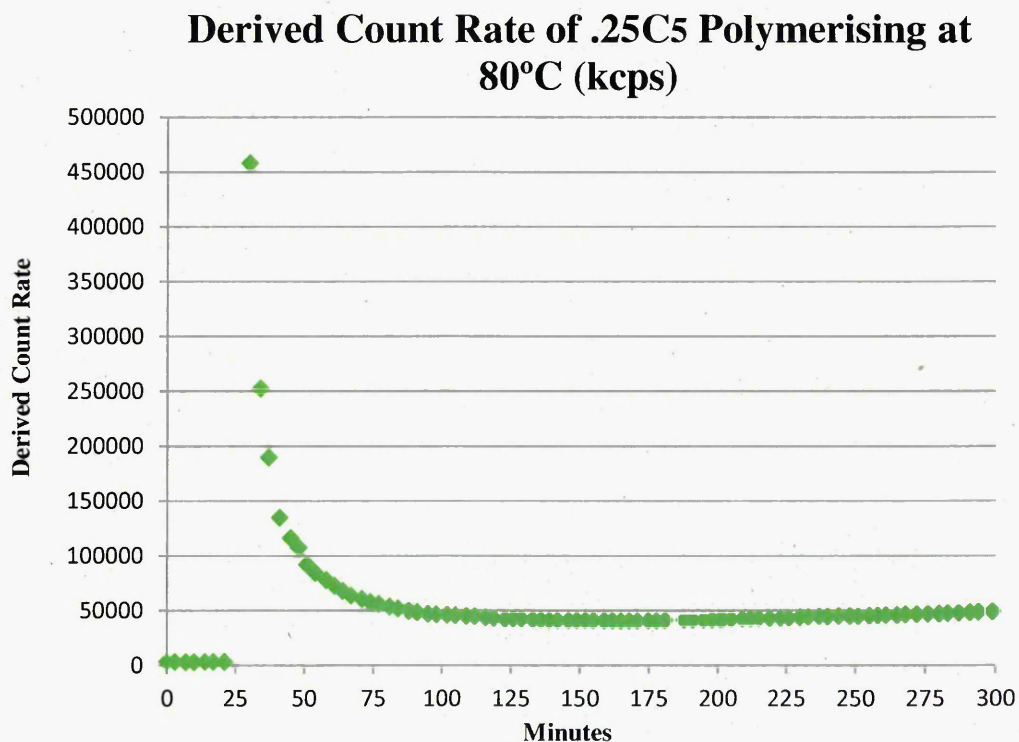
Derived Count Rate of .25C5 cooling 1°C/3min (kcps)
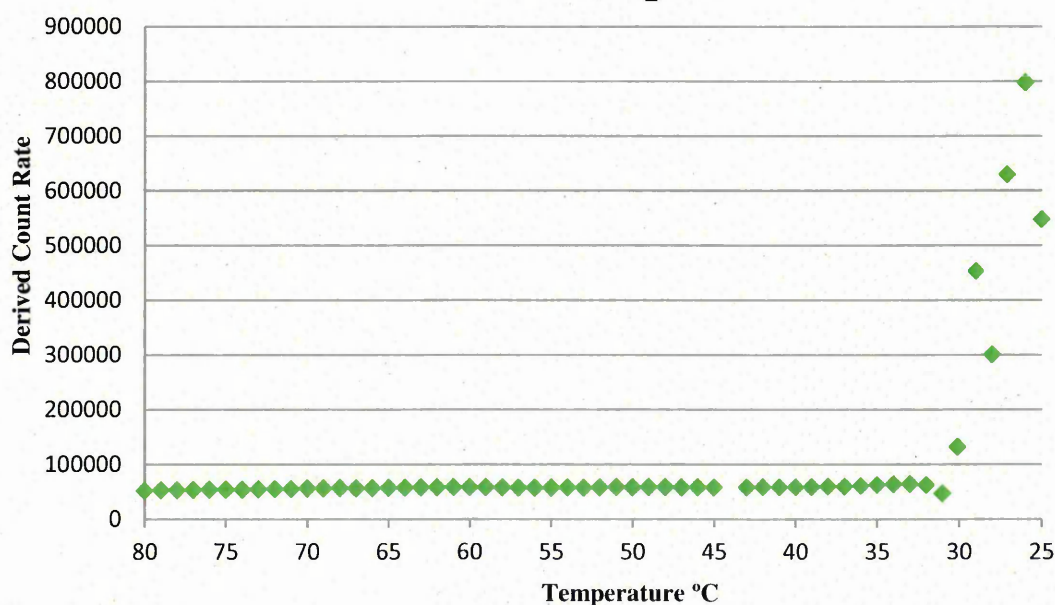
Figure 3.23. The derived count rate measured during the cooling of a .25C$_5$ PCPH solution (see Section 2.2.1.2 and table 2.1) at a rate of 1°C/3 min. The PCPH was previously synthesised by free radical precipitation polymerisation at 80°C for 6h.

The D_H and derived count rate (figures 3.20 and 3.21 respectively) of a .25C$_5$ monomeric solution was observed in real time during its polymerisation at 80°C over the course of 6 hours. The DLS instrument records a D_H at t = 0 of 30.9nm, which is in good agreement with the previously recorded D_H of laponite in this system (figure 3.11) and that of the .5C$_5$ formulation (figure 3.16) which were recorded as 28nm and 30.7nm respectively. The derived count rate at t = 0 is ca. 3600kcps, which is almost identical to that taken for the .5C$_5$ formulation at t = 0 (figure 3.17) and very similar to the count rate to that taken from the clay/ water solution, which was ca. 3500kcps (figure 3.12). This is confirmation that as in the previous data set (.5C5), the amount of light scattered from monomers during the initial phase of the reaction is negligible and the monomers are considered "invisible" for DLS.

The D_H and derived count rate remain stable (and the monomers/ oligomers remain "invisible") at 80°C up to a critical point at ~24 minutes, where a very sharp increase in both values is recorded (458000 kcps count rate and 69 d.nm Z- average at 30minutes). This is indicative of the reaching of a critical chain length which has resulted in the collapse if the polymer chains which have adopted a globule conformation. Although in the previous data set (for the .5C5 formulation), this increase is recorded to occur at 19 minutes, it should be noted that each measurement takes approximately 4 minutes and therefore each data point should be given an approximate + and – 2 minute error. Following this, a small decrease in D_H and sharp simultaneous decrease in scattering intensity is recorded. As noted in the .5C5 data, the decrease in scattering intensity could be attributed to the aggregation of the PNIPAM/ clay particles and which do not scatter significantly in the backward direction [82], or a refractive index change as PNIPAM molecules undergo transition from random -coil to condensed globule [83].

Upon cooling (figures 3.33 and 3.34), as observed in the .5C5 data, very little change in either D_H or count rate is observable between 80- 33°C. As mentioned previously, beyond 33°C the condensed PNIPAM globules undergo phase transition and adopt the "coil" conformation and irreversible cross-linking takes place. Since the particles are no longer free to move at this stage, the recorded correlation functions cease to be indicative of particle size, and any data recorded below 33°C should be considered unreliable.

3.9   Proposed mechanism of polymerisation of a PCPH

The fact that linear PNIPAM undergoes phase transition at temperatures above ~30-35°C causing the chains to separate and collapse [84] can be exploited in high temperature precipitation polymerisations of PNIPAM. The technique has been used to successfully produce monodisperse micron and submicron PNIPAM hydrogel particles in a single phase without the need for surfactants [76, 85] which are required for room temperature emulsion polymerisations [86]. PNIPAM-based microgels first appeared in literature as the result of 'surfactant-free emulsion polymerisation' of NIPAM and *N,N'-*methylenebisacrylamide (BIS) in aqueous media, by Pelton *et al* [76]. Successful PNIPAM particle formation was achieved at 60–70°C, temperatures at which the persulfate initiator dissociates and propagating PNIPAM chains phase separate to form colloidal precursor particles. The procedure has been replicated by several authors [87-92]. The mechanism proceeds as follows; a hydrophilic sulfate radical engages a water-soluble NIPAM monomer molecule and initiates a free-radical polymerisation. When the PNIPAM chain reaches a critical chain length, the growing chain undergoes phase transition and collapses into a colloidally unstable PNIPAM precursor globule particle. At this stage, the intact microgel particle morphology of the PNIPAM can be ensured with the use of a chemical cross-linking agent such as BIS. The cross-linker plays a crucial role in preventing the dissolution of the polymer particle when it is cooled below the LCST of PNIPAM. The globule particles aggregate and colloidally stabilise themselves electrostatically, as hydrophilic sulfate groups with which the polymer chains are terminated concentrate at the surface of the aggregate, until they form a colloidally stable particle.

In 2002, Haraguchi *et al* [12] reported a novel nanocomposite PNIPAM-based hydrogel which was cross-linked with exfoliated inorganic clay particles and polymerised by free-radical polymerisation in aqueous media *in situ* using potassium persulfate (KPS) as an initiator at 20°C. The gels exhibited excellent transparency, a rapid swelling/deswelling rate and improved mechanical properties when compared to their chemically cross-linked predecessors. In subsequent years, the concept has been replicated and modified with different monomeric species [93], clay types and concentrations [94-95], and using cationic exchange to modify the clay surface [96]. The mechanism of the PNIPAM/ clay composite formation was considered to be as follows; The KPS initiator, with a divalent anion, ionically interacts with the surface of

the clay platelet and as a result, the polymer chains begin propagation at the clay surface and grow outwards, with one end always firmly anchored to the clay. The polymer chains are thought to then extend to, and form interactions with, other neighbouring clay platelets *in situ*. The net result is a stable, cross-linked 3-dimensional PNIPAM/ clay hydrogel network.

KPS and ammonium persulfate (APS) are commonly used for the free radical polymerisation of PNIPAM, and both possess a divalent anionic structure. AIBN does not contain an anionic group, and since cross-linking of clay/ PNIPAM nanocomposite systems was thought to be based on clay/ initiator interactions, AIBN is not routinely used as an initiator during the synthesis of clay nanocomposite hydrogels. Recently, however, Wang *et al* [93] successfully used AIBN to initiate the synthesis of poly(N,N'-dimethylacrylamide) (PDMAc)/ clay nanocomposite hydrogels (and as a side note, unexpectedly found that they possessed superior mechanical properties to identical gels prepared with KPS).

In the presented system, PNIPAM particles were formed using AIBN as an initiator in the presence of clay at 80°C, whereby elements from both aforementioned synthetic procedures are combined to create a previously unreported system. In the absence of clay/ AIBN ionic interactions, initiation is thought to occur in the aqueous phase, separate from the clay particles (figure 3.24a). Polymerisation proceeds (figure 3.24b), and electrostatic interactions between the electropositive NH groups of PNIPAM and electronegative clay surfaces cause precipitation to proceed very close to the clay platelet surface. At a critical chain length, the polymer separates from the aqueous phase to form tightly-packed PNIPAM globules around the individual clay platelets, thus forming colloidal precursor particles (figure 3.24c). Since AIBN is hydrophobic, it is more favourable for the AIBN to reside within the PNIPAM particles at elevated temperatures. At the same time, the polar groups on the collapsed PNIPAM particles preferentially present on the outer surface, which reside in close proximity to the clay forming electrostatic interactions with it, as is shown spectroscopically in section 3.4. As long as this PNIPAM/ clay suspension remains at temperatures above the LCST of PNIPAM, the polymer remains in a hydrophobic "globule" conformation and the polymer/ clay particles exist discreetly in a colloidal suspension. The suspension remains colloidally stable at temperatures higher than that of the LCST of the polymer.
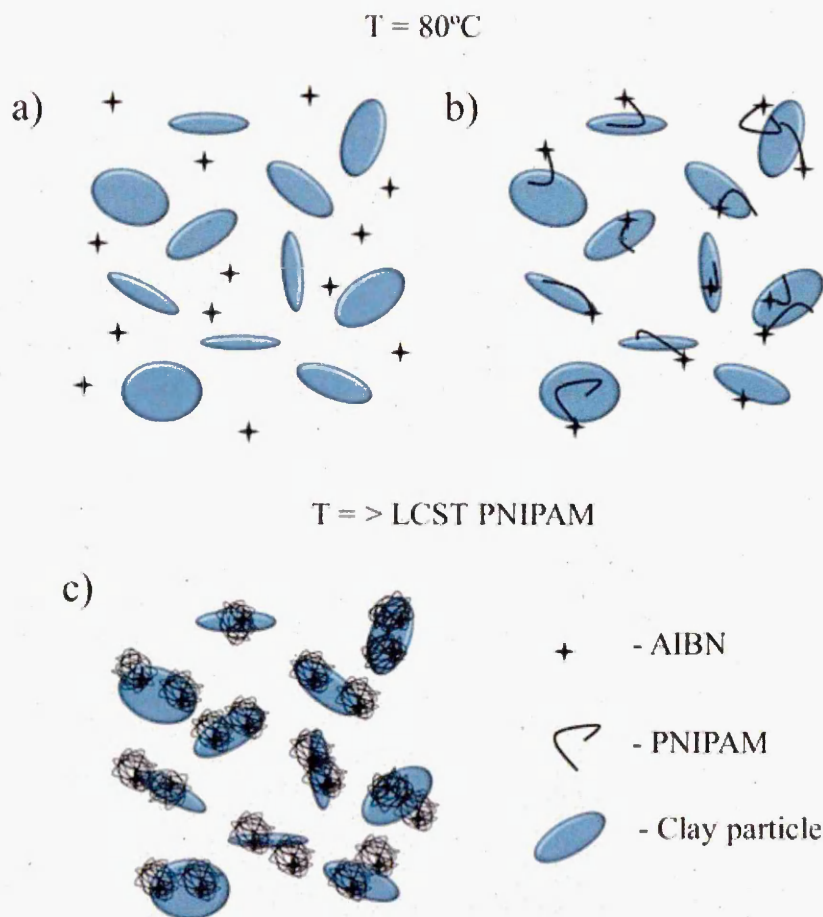
Figure 3.24. Schematic of the proposed mechanism of polymerisation of a typical PCPH suspension (monomers not shown). a) AIBN and clay platelets existing separately in monomer solution, b) free-radical initiation of NIPAM, c) precipitation of PNIPAM at critical chain length, PNIPAM globule particles reside in close proximity to the clay particles via electrostatic interactions.

3.10   Proposed mechanism of PTTNAG of a PCPH

The PTTNAG mechanism is thought to be the physical manifestation of the following theory:

"Globule" (hydrophobic) state PNIPAM chains residing in close proximity to the clay (figure 3.25a) platelets transform to a "coil" (hydrophilic) state when the temperature is lowered to that which is below the LCST of PNIPAM (figure 3.25b). In the coil conformation, polymer chains extend between and attach to neighbouring exfoliated clay particles, forming strong direct PNIPAM- clay anchor points as well as polymer-polymer entanglements (figure 3.25c).
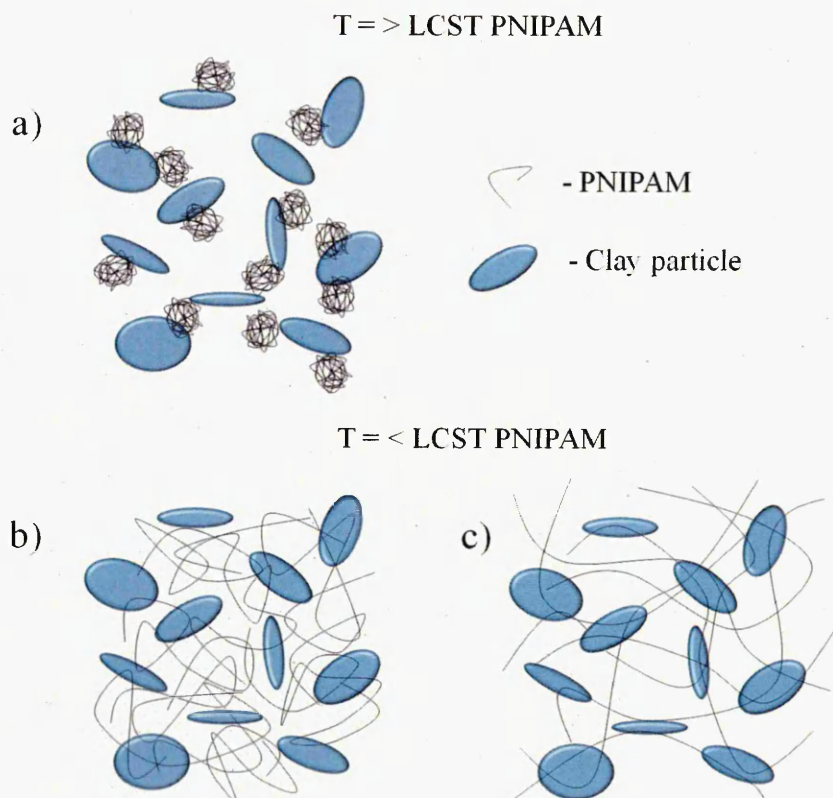
Figure 3.25. Schematic of the proposed a) structure of PCPH suspension, b) & c) mechanism of PCPH PTTNAG and c) resulting network structure model of a typical PNIPAM/ clay nanocomposite hydrogel.

3.11   Summary

In 2002, Haraguchi [97] successfully developed a unique PNIPAM / clay nanocomposite hydrogel system with highly utilisable swelling/ deswelling, optical and mechanical characteristics. His methodology involved the KPS-initiated *in situ* free radical polymerisation of PNIPAM in the presence of a degassed, exfoliated clay suspension at room temperature. The materials produced were proven candidates for cell cultivation platforms [6] and effective wound management materials for artificial wounds in adult goats [98], but only after "extensive dialysation against fresh water to remove residual monomers" [6, 98]. The processability of the system was restricted to maintaining the monomeric suspension at low temperatures and allowing the polymerisation to proceed inside an oxygen-devoid vessel of the desired shape. Although literature points toward many avenues in the endeavour of commercial material processing, it is inherently difficult to process cross-linked materials and approaches are usually made by *in situ* polymer synthesis or stimuli responsive gelation.

109

This work has presented the development of a series of novel PNIPAM-based nanocomposite materials and their applications. The "base" material is a fully polymerised, low viscosity liquid (a PNIPAM/ clay precursor hydrogel, or PCPH) and remains thus indefinitely until cooled beyond a predetermined temperature, whereupon the low viscosity liquid undergoes PTTNAG spontaneously and irreversibly. The material it forms is a thermally-responsive hydrogel which not only contains and absorbs large amounts of water, but has excellent optical and swelling/ deswelling properties- attributes which are explored in detail in chapter 6.The PCPH can be doped with biological polymers in the liquid phase. Upon cooling and subsequent PTTNAG, the resulting gel is a homogenous, stimuli-responsive multi-component polymer nanocomposite network.

Dynamic light scattering (DLS) was employed to shed light on the mechanisms of polymerisation and PTTNAG. It would appear that the polymers reside in close proximity to the clay platelets and collapse close to the clay surface upon reaching a critical chain length at *ca.* 24 minutes, forming discreet polymer/ clay particles which indefinitely remain as such at elevated temperatures. These particles may colloidally stabilise over time to form larger aggregates in solution. Upon cooling, the polymer chains undergo globule - to - coil transition and "unravel" from the clay surface, indicated by a very large and sharp increase in hydrodynamic diameter at 32-33°C. This is further supported by spectroscopic data which reveals a decrease in Si-O/ Hydrogen bonding during PTTNAG. Although DLS cannot provide any further inferences than this, it is predicted that the mechanism of PTTNAG involves the interaction of PNIPAM with neighbouring clay platelets, enabling the clay to act as a multi-functional cross-linker, a phenomenon which has been detailed in literature [7-8, 81, 97, 99-104]. This may be accompanied by polymer-polymer interactions and entanglements.

3.13   References

1.   Turan, E., Demirci, S., Caykara, T., Synthesis of thermoresponsive poly(N-isopropylacrylamide) brush on silicon wafer surface via atom transfer radical polymerization. Thin Solid Films, 2010. 518(21): p. 5950-5954.

2.   Makharza, S., et al., Structural and Thermal Analysis of Copper-Doped Poly(N-isopropylacrylamide) Films. International Journal of Polymer Analysis and Characterization, 2010. 15(4): p. 254-265.

3.   Hoffmann, J., et al., Photopatterning of thermally sensitive hydrogels useful for microactuators. Sensors and Actuators a-Physical, 1999. 77(2): p. 139-144.

4.   Singh, D., et al., Synthesis and characterization of poly(N-isopropylacrylamide) films by photopolymerization. Polymers for Advanced Technologies, 2006. 17(3): p. 186-192.

5.   Plunkett, K.N., et al., PNIPAM Chain Collapse Depends on the Molecular Weight and Grafting Density. Langmuir, 2006. 22(9): p. 4259-4266.

6.   Haraguchi, K., et al., Control of Cell Cultivation and Cell Sheet Detachment on the Surface of Polymer/Clay Nanocomposite Hydrogels. Biomacromolecules, 2006. 7(11): p. 3267-3275.

7.   Haraguchi, K., Synthesis and properties of soft nanocomposite materials with novel organic/inorganic network structures. Polymer Journal, 2011. 43(3): p. 223-241.

8.   Haraguchi, K., Nanocomposite hydrogels. Current Opinion in Solid State & Materials Science, 2007. 11(3-4): p. 47-54.

9.   Haraguchi, K., et al., Polymer-clay nanocomposites exhibiting abnormal necking phenomena accompanied by extremely large reversible elongations and excellent transparency. Advanced Materials, 2006. 18(17): p. 2250-2258.

10.   Haraguchi, K., Li, H., The Effect of Water Content on the Ultimate Properties of Rubbery Nanocomposite Gels. Journal of Polymer Science Part B-Polymer Physics, 2009. 47(23): p. 2328-2340.

11.   Haraguchi, K., Li, H., Song, L., The unique optical and physical properties of soft, transparent, stimulus-sensitive nanocomposite gels - art. no. 665400, in Liquid Crystals XI, I.C. Khoo, Editor. 2007. p. O6540-O6540.

12.   Haraguchi, K., Takehisa,T., Nanocomposite Hydrogels: A Unique Organic–Inorganic Network Structure with Extraordinary Mechanical, Optical, and Swelling/De-swelling Properties. Advanced Materials, 2002. 14(16): p. 1120-1124.

13.   Libnau, F.O., Christy, A., Kvalheim, O., Determination of the equilibrium constant and resolution of the HOD spectrum by alternationg least-squares and infrared analysis. Applied Spectroscopy, 1995. 49(10): p. 1431-1437.

14.   Deng, C.S., Sammon, C., Yarwood, J., Sorption and perturbation of water at polyelectrolyte interfaces. Paper 5 - effects of water isotopic dilution. Polymer, 2003. 44(7): p. 2057-2065.

15.   Hajatdoost, S., Sammon, C., Yarwood, J., FTIR-ATR studies of diffusion and perturbation of water in polyelectrolyte thin films. Part 4. Diffusion, perturbation and swelling processes for ionic solutions in SPEES/PES membranes. Polymer, 2002. 43(6): p. 1821-1827.

16.   Pereira, M.R., Yarwood, J., An FTIR-ATR approach to the study of diffusion of water on polysulfone polymeric membranes. 9th International Conference on Fourier Transform Spectroscopy, ed. J.E.W.H. Bertie. Vol. 2089. 1993. 466-467.

17.   Pereira, M.R., Yarwood, J., ATR-FTIR spectroscopic studies of the structure and permeability of sulfonated poly(ether sulfone) membranes .1. Interfacial water-polymer interactions. Journal of the Chemical Society-Faraday Transactions, 1996. 92(15): p. 2731-2735.

18.   Sammon, C., et al., Vibrational spectroscopic studies of the dynamics and perturbation of water in polymeric films. Journal of Molecular Liquids, 2002. 101(1-3): p. 35-54.

19.   Sammon, C., Deng, C., Yarwood, J., Polymer-water interactions. Origin of perturbed infrared intensities of water in polymeric systems. Polymer, 2003. 44(9): p. 2669-2677.

20.   Sammon, C., Everall, N., Yarwood, J., The diffusion of water into PET followed in-situ using FT-IR ATR. Macromolecular Symposia, 1997. 119: p. 189-196.

21.   Sammon, C., et al., ATR-FTIR study of the diffusion and interaction of water and electrolyte solutions in polymeric membranes. Journal of Molecular Liquids, 2002. 96-7: p. 305-315.

22.   Sammon, C., et al., FTIR-ATR studies of the structure and dynamics of water molecules in polymeric matrixes. A comparison of PET and PVC. Journal of Physical Chemistry B, 1998. 102(18): p. 3402-3411.

23.   Sammon, C., Everall, N., Yarwood, J., A FTIR-ATR study of liquid diffusion processes in PET films: comparison of water with simple alcohols. Polymer, 2000. 41(7): p. 2521-2534.

24.   Christensen, M., et al., Water structure in polyethylene glycols for preservation of wooden artefacts. A NIR-FT-Raman spectroscopic investigation. Journal of Molecular Structure, 2005. 735: p. 267-270.

25.   Nakaoki, T., Yamashita, J., Bound states of water in poly(vinyl alcohol) hydrogel prepared by repeated freezing and melting method. Journal of Molecular Structure, 2008. 875(1-3): p. 282-287.

26.   Nickolov, Z.S., et al., Total internal reflection Raman spectroscopy as a method to study water structure near langmuir-blodgett films. Journal of Raman Spectroscopy, 1993. 24(7): p. 411-416.

27.   Ostrovskii, D.I., et al., Water sorption properties of and the state of water in PVDF-based proton conducting membranes. Solid State Ionics, 1997. 97(1-4): p. 315-321.

28.   Sekine, Y. et al., Structural changes of water in a hydrogel during dehydration. Journal of Chemical Physics, 2009. 130(3): p. 130-137

29.   Jeong, S.Y., Han, O., A solid-state NMR study of water in poly(vinyl butyral) by magic angle spinning. Bulletin of the Korean Chemical Society, 2007. 28(4): p. 662-666.

30.   Liu, W.G., et al., Thermal and NMR investigation of the change in the states of water caused by volume phase transition of gelatin gel. Polymer International, 2000. 49(12): p. 1624-1628.

31.   Machida, Y., et al., A structural study of water in a poly(vinyl alcohol) gel by O-17 NMR spectroscopy. Journal of Molecular Structure, 2000. 554(1): p. 81-90.

32.   Reuvers, N.J.W., et al., Quantitative Water Uptake Study in Thin Nylon-6 Films with NMR Imaging. Macromolecules, 2012. 45(4): p. 1937-1945.

33.   Zainuddin, et al., The states, diffusion, and concentration distribution of water in radiation-formed PVA/PVP hydrogels. Soft Materials, 2004. 2(2-3): p. 195-212.

34.   Borodin, O., et al., Temperature dependence of water dynamics in poly(ethylene oxide)/water solutions from molecular dynamics simulations and quasielastic neutron scattering experiments. Journal of Physical Chemistry B, 2002. 106(20): p. 5184-5193.

35.   Krakovsky, I., Szekely, N., SANS and DSC study of water distribution in epoxy-based hydrogels. European Polymer Journal, 2011. 47(12): p. 2177-2188.

36.   Laurati, M., et al., Dynamics of Water Absorbed in Polyamides. Macromolecules, 2012. 45(3): p. 1676-1687.

37.   Mosdale, R., G., et al., Water profile determination in a running proton exchange membrane fuel cell using small-angle neutron scattering. Journal of Membrane Science, 1996. 118(2): p. 269-277.

38.   Perelli-Cippo, E., et al., Investigation of high-energy inelastic neutron scattering from liquid water confined in silica xerogel. Physica B-Condensed Matter, 2006. 385-86: p. 1095-1097.

39.   Coyle, F.M., et al., Dynamics of water molecules in polymers. Journal of Molecular Liquids, 1996. 69(0): p. 95-116.

40.   Ozaki, Y., et al., Application of two-dimensional near-infrared correlation spectroscopy to protein research. Vibrational Spectroscopy, 1999. 20(2): p. 127-132.

41.   Kusanagi, H., Yukawa, S., Fourier transform infra-red spectroscopic studies of water molecules sorbed in solid polymers. Polymer, 1994. 35(26): p. 5637-5640.

42.   Sammon, C., et al., ATR-FTIR studies of a thermo-responsive ABA triblock copolymer gelator in aqueous solution. Polymer, 2006. 47(17): p. 6123-6130.

43.	Su, Y.L., et al., Association behavior of PEO-PPO-PEO block copolymers in water orrprganic solvent observed by FTIR spectroscopy. Molecular Simulation, 2003. 29(12): p. 803-808.

44.	Maeda, Y., et al., Change in hydration state during the coil-globule transition of aqueous solutions of poly(N-isopropylacrylamide) as evidenced by FTIR spectroscopy. Langmuir, 2000. 16(19): p. 7503-7509.

45.	Maeda, Y., et al., Changes in the hydration states of poly(N-alkylacrylamide)s during their phase transitions in water observed by FTIR spectroscopy. Macromolecules, 2001. 34(5): p. 1391-1399.

46.	Su, Y.L., et al., FTIR spectroscopic investigation of effects of temperature and concentration on PEO-PPO-PEO block copolymer properties in aqueous solutions. Macromolecules, 2002. 35(16): p. 6426-6431.

47.	Doppers, L.M., et al., FTIR-ATR studies of the sorption and diffusion of acetone/water mixtures in poly(vinyl alcohol). Polymer, 2006. 47(8): p. 2714-2722.

48.	Hill, S.E., Ledward, D., Mitchell, J., Functional properties of food macromolecules. (Google ebook) 1998: Aspen.

49.	Dickinson, E., Wasan, D., Editorial overview. Current Opinion in Colloid & Interface Science, 1996. 1(6): p. 709-711.

50.	Marty, J.J., et al., Nanoparticles--a new colloidal drug delivery system. Pharmaceutica Acta Helvetiae, 1978. 53(1): p. 17-23.

51.	Howe, A.M., Some aspects of colloids in photography. Current Opinion in Colloid & Interface Science, 2000. 5(5–6): p. 288-300.

52.	Normand, V., et al., Gelation Kinetics of Gelatin: A Master Curve and Network Modeling. Macromolecules, 2000. 33(3): p. 1063-1071.

53.	Clark, A., Ross-Murphy, S., Structural and mechanical properties of biopolymer gels. Biopolymers. 1987, Springer Berlin / Heidelberg. p. 57-192.

54.	Joly-Duhamel, C., et al., All Gelatin Networks: 1. Biodiversity and Physical Chemistry. Langmuir, 2002. 18(19): p. 7208-7217.

55.	Lindahl, G.E., et al., Activation of Fibroblast Procollagen α1(I) Transcription by Mechanical Strain Is Transforming Growth Factor-β-dependent and Involves Increased Binding of CCAAT-binding Factor (CBF/NF-Y) at the Proximal Promoter. Journal of Biological Chemistry, 2002. 277(8): p. 6153-6161.

56.	Hubbell, J.A., Hydrogel systems for barriers and local drug delivery in the control of wound healing. Journal of Controlled Release, 1996. 39(2–3): p. 305-313.

57.	Weigel, P.H., et al., The role of hyaluronic acid in inflammation and wound healing. International Journal of Tissue Reactions-Experimental and Clinical Aspects, 1988. 10(6): p. 355-365.

58. Azuma, N., et al., Histochemical studies on hyaluronic acid in the developing human retina. Graefes Archive for Clinical and Experimental Ophthalmology, 1990. 228(2): p. 158-160.

59. Pohl, M., et al., Role of hyaluronan and CD44 in in vitro branching morphogenesis of ureteric bud cells. Developmental Biology, 2000. 224(2): p. 312-325.

60. Entwistle, J., et al., HA receptors: Regulators of signalling to the cytoskeleton. Journal of Cellular Biochemistry, 1996. 61(4): p. 569-577.

61. Ladeda, V., et al., Function and Expression of CD44 during Spreading, Migration, and Invasion of Murine Carcinoma Cells. Experimental Cell Research, 1998. 242(2): p. 515-527.

62. Ortonne, J.P., A controlled study of the activity of hyaluronic acid in the treatment of venous leg ulcers. Journal of Dermatological Treatment, 1996. 7(2): p. 75-81.

63. Zhang, S., et al., The Hyaluronan Receptor RHAMM Regulates Extracellular-regulated Kinase. Journal of Biological Chemistry, 1998. 273(18): p. 11342-11348.

64. Tammi, R., et al., Hyaluronan Bound to CD44 on Keratinocytes Is Displaced by Hyaluronan Decasaccharides and Not Hexasaccharides. Journal of Biological Chemistry, 1998. 273(44): p. 28878-28888.

65. Kim, J., et al., Characterization of low-molecular-weight hyaluronic acid-based hydrogel and differential stem cell responses in the hydrogel microenvironments. Journal of Biomedical Materials Research Part A, 2009. 88A(4): p. 967-975.

66. Andersson, M., Maunu,S., Structural studies of Poly(N-isopropylacrylamide) microgels: Effect of SDS surfactant concentration in the microgel synthesis. Journal of Polymer Science Part B-Polymer Physics, 2006. 44(23): p. 3305-3314.

67. Karg, M., Hellweg, T., New "smart" poly(NIPAM) microgels and nanoparticle microgel hybrids: Properties and advances in characterisation. Current Opinion in Colloid & Interface Science, 2009. 14(6): p. 438-450.

68. Kratz, K., Hellweg, T., Eimer, W., Structural changes in PNIPAM microgel particles as seen by SANS, DLS, and EM techniques. Polymer, 2001. 42(15): p. 6631-6639.

69. Ma, X.M., et al., Different deswelling behavior of temperature-sensitive microgels of poly(N-isopropylacrylamide) crosslinked by polyethyleneglycol dimethacrylates. Journal of Colloid and Interface Science, 2004. 276(1): p. 53-59.

70. Varga, I., et al., Effect of Cross-Link Density on the Internal Structure of Poly(N-isopropylacrylamide) Microgels. The Journal of Physical Chemistry B, 2001. 105(38): p. 9071-9076.

71. Saunders, B.R., On the Structure of Poly(N-isopropylacrylamide) Microgel Particles. Langmuir, 2004. 20(10): p. 3925-3932.

72. Wu, X., et al., The kinetics of poly(N-isopropylacrylamide) microgel latex formation. Colloid & Polymer Science, 1994. 272(4): p. 467-477.

73.   Acciaro, R., T. et al., Preparation of Monodisperse Poly(N-isopropylacrylamide) Microgel Particles with Homogenous Cross-Link Density Distribution. Langmuir, 2011. 27(12): p. 7917-7925.

74.   Goodwin, J.W., et al., Control of particle size in the formation of polymer latices. Br Polym J, 1978. 10(3): p. 173-180.

75.   Pelton, R., Temperature-sensitive aqueous microgels. Advances in Colloid and Interface Science, 2000. 85(1): p. 1-33.

76.   Pelton, R.H., Chibante, P., Preparation of aqueous latices with N-isopropylacrylamide. Colloids and Surfaces, 1986. 20(3): p. 247-256.

77.   Varga, I., et al., Effect of cross-link density on the internal structure of Poly(N-isopropylacrylamide) microgels. Journal of Physical Chemistry B, 2001. 105(38): p. 9071-9076.

78.   Kutter, S., et al., Structure and phase behavior of a model clay dispersion: A molecular-dynamics investigation. Journal of Chemical Physics, 2000. 112(1): p. 311-322.

79.   Dijkstra, M., et al., Gelation of a Clay Colloid Suspension. Physical Review Letters, 1995. 75(11): p. 2236-2239.

80.   Tawari, S.L., et al., Electrical double-layer effects on the Brownian diffusivity and aggregation rate of Laponite clay particles. Journal of Colloid and Interface Science, 2001. 240(1): p. 54-66.

81.   Haraguchi, K., et al., Mechanism of forming organic/inorganic network structures during in-situ free-radical polymerization in PNIPA-clay nanocomposite hydrogels. Macromolecules, 2005. 38(8): p. 3482-3490.

82.   Santiago, P.S., et al., Dynamic light scattering and optical absorption spectroscopy study of pH and temperature stabilities of the extracellular hemoglobin of Glossoscolex paulistus. Biophysical Journal, 2008. 94(6): p. 2228-2240.

83.   Malvern. Polymer Characterisation Using Light Scattering Techniques and Equipment From Malvern Instruments. 10.05.2005 [online] accessed 01.05.2012 at: http://www.azonano.com/article.aspx?ArticleID=1232.

84.   Heskins, M., Guilet, J., Solution properties of poly(N -isopropylacrylamide). J Macromol Sci Part A Pure Appl Chem. 1968. 2(8) p. 1441-1455.

85.   Jańczewski, D., et al., Introduction of Quantum Dots into PNIPAM microspheres by precipitation polymerization above LCST. European Polymer Journal, 2009. 45(7): p. 1912-1917.

86.   Chu, L.Y., et al., Preparation of micron-sized monodispersed thermoresponsive core-shell microcapsules. Langmuir, 2002. 18(5): p. 1856-1864.

87.   Bokias, G., et al., Molar mass control of poly(N-isopropylacrylamide) and poly(acrylic acid) in aqueous polymerizations initiated by redox initiators based on persulfates. Macromolecular Chemistry and Physics, 1998. 199(7): p. 1387-1392.

88.   Kawaguchi, H., et al., Hydrogel microspheres III. Temperature-dependent adsorption of proteins on poly-N-isopropylacrylamide hydrogel microspheres. Colloid & Polymer Science, 1992. 270(1): p. 53-57.

89.   Zhou, G., et al., Synthesis and characterization of surface-cyanofunctionalized poly(N-isopropylacrylamide) latexes. Colloid and Polymer Science, 1998. 276(12): p. 1131-1139.

90.   Wu, C., et al., Volume phase transition of spherical microgel particles. Angewandte Makromolekulare Chemie, 1996. 240: p. 123-136.

91.   Öle Kiminta, et al., The rheology of deformable and thermoresponsive microgel particles. Polymer, 1995. 36(25): p. 4827-4831.

92.   Murray, M.J., Snowden, M.J., The preparation, characterisation and applications of colloidal microgels. Advances in Colloid and Interface Science, 1995. 54(0): p. 73-91.

93.   Wang, Y., et al., PDMAA/Clay nanocomposite hydrogels based on two different initiations. Colloids and Surfaces A: Physicochemical and Engineering Aspects, 2011. 390(1–3): p. 20-24.

94.   Sur, G.S., et al., Synthesis and LCST behavior of thermosensitive poly (N-isopropylacrylamide)-clay nanocomposites. Journal of Industrial and Engineering Chemistry, 2003. 9(1): p. 58-62.

95.   Zhuk, A., et al., Multiresponsive Clay-Containing Layer-by-Layer Films. ACS Nano, 2011. 5(11): p. 8790-8799.

96.   Kim, J.P., et al., Synthesis of thermoresponsive poly(N-isopropylacrylamide)/clay nanocomposites. Polymer-Korea, 2001. 25(2): p. 263-269.

97.   Haraguchi, K., Takehisa, T., Nanocomposite hydrogels: A unique organic-inorganic network structure with extraordinary mechanical, optical, and swelling/de-swelling properties. Advanced Materials, 2002. 14(16): p. 1120-1124.

98.   Zhou, Y.M., et al., Nanocomposite hydrogels: a novel Wound dressings. 2010 3rd International Conference on Biomedical Engineering and Informatics, ed. W.Z.M.W.L.S.Y. Yu. 2010. 432-434.

99.   Haraguchi, K., Stimuli-responsive nanocomposite gels. Colloid and Polymer Science, 2011. 289(5-6): p. 455-473.

100.   Haraguchi, K., Li, H., Mechanical properties and structure of polymer-clay nanocomposite gels with high clay content. Macromolecules, 2006. 39(5): p. 1898-1905.

101.   Haraguchi, K., Uyama, K., Tanimoto, H., Self-healing in Nanocomposite Hydrogels. Macromolecular Rapid Communications, 2011. 32(16): p. 1253-1258.

102.   Miyazaki, S., et al., Clay concentration dependence of microstructure in deformed poly(N-isopropylacrylamide)-clay nanocomposite gels. Macromolecules, 2006. 39(23): p. 8112-8120.

103.   Shibayama, M., et al., Structure and Dynamics of Poly(N-isopropylacrylamide)–Clay Nanocomposite Gels. Macromolecules, 2004. 37(25): p. 9606-9612.

104.   Xu, Y., Li, G., Haraguchi, K., Gel Formation and Molecular Characteristics of Poly(N-isopropylacrylamide) Prepared by Free-Radical Redox Polymerization in Aqueous Solution. Macromolecular Chemistry and Physics, 2010. 211(9): p. 977-987.

4

The Processability of PNIPAM/ Clay Nanocomposite Liquid Gel Precursor Formulations

Chapter 4 - The Processability of PNIPAM/ Clay Nanocomposite Liquid Gel Precursor formulations.

4.1   Introduction

A major technical issue for PNIPAM/ clay nanocomposite materials is their processability, more specifically, the straightforward creation of physical shapes and forms which make them adept for their intended purpose. In this chapter, the processability of PNIPAM/ clay-based hydrogels achieved through the PCPH technology described in chapter 3 is demonstrated. The successful electrospinning of cross-linked PNIPAM/ clay-based fiber mats, which have not previously been reported in literature, and the industrial extrusion of continuous PNIPAM/ clay thin films in a manner also previously unreported, effectively demonstrates the versatility and processability of this material.

4.2   Materials used in this Chapter and the Synthesis and Preparation of the PCPH

The materials used in this chapter as well as materials synthesis are detailed in section 2.2.2.1.

4.3   A Novel Method for the Electrospinning of Fine Fibre Mats of PNIPAM/ Clay Hanocomposite Hydrogels.

Interest in electrospinning has gained popularity in recent years as a method for fabricating polymeric nanofibres, due to the growing interest in technologies which exploit nanoscale properties. Electrospun polymer fibres, which generally have diameters ranging from 3 nm to more than 5 μm [1], have a very large surface area to volume ratio as well as vastly improved mechanical properties and flexibility when compared to alternative polymer forms. These characteristics allow for their potential use as catalytic nanofibres, filtration media and fibre-based nanosensors [2]. In the medical field, electrospun polymers have been investigated as wound dressing materials and tissue engineering scaffolds since they emulate the nanoscale characteristics of native extracellular matrix [1-3].
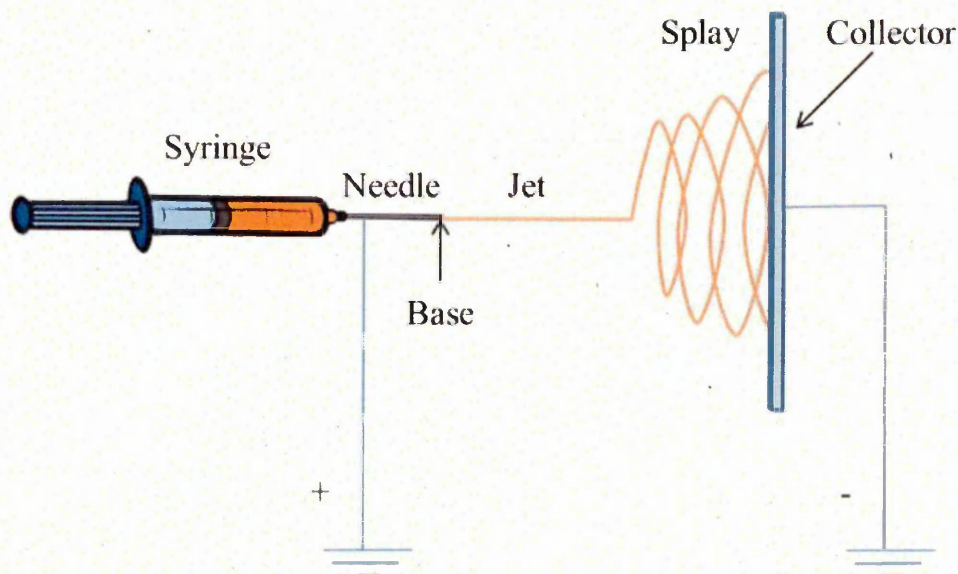
Figure 4.1. A schematic representation of a typical electrospinning apparatus.

The electrospinning phenomenon is illustrated in figure 4.1, and was detailed by Reneker et al, who described the extruded polymer as being composed of four regions: the base, jet, splay, and collector [4]. At the base, the polymer solution emerges from the needle tip in the form of a small "Taylor cone". The precise dimensions and shape of the Taylor cone depend largely upon the strength of the electric field and surface tension of the liquid polymer- it is possible for a polymer jet to be ejected from a flat surface if the electric field is sufficiently strong.

The electrical charging of the polymer jet occurs at the base, and electric forces accelerate the liquid polymer jet toward the collector, stretching and decreasing the diameter of the jet as it moves away from the needle. The evaporation of solvents may also occur at this stage, further decreasing the jet diameter [2]. Reneker *et al* [4] presented a hypothesis detailing a radial charge repulsion which subsequently results in the splaying of polymer fibres of consistent charge and diameter onto the collector. The result is a non-woven fabric (mat) made of easily processable electrospun polymer nanofibres.

It has been well documented in literature that electrospinnabilty, fibre diameter and subsequent properties of a range of polymers strongly depend on a number of factors, including polymer solution viscosity, concentration, solvent composition and presence of additives such as salts. The main objectives of this exercise were to (i) test the capabilities of the PCPH as a candidate for electrospinning, and (ii) to explore the possibility of development and optimisation of the PNIPAM/ clay electrospun mats in

121

order to produce novel PNIPAM based nanomaterials with highly desirable industrial properties.

4.3.1 Electrospinning procedure

The synthesis of the PCPH formulations used in this work was performed my Dr. Subodh Sabnis of Sheffield Hallam University, under direction.

The hydrogel precursor liquid formulations $1C_{10}$ and $1C_{10}G15$ were synthesised and prepared as described in sections 3.3 (see table 2.1) and 3.6.1 (see table 2.2), respectively. The electrospinning apparatus was manufactured and assembled by Yflow Ltd. (Spain), supplied by Nanobiomatters S.L. (Spain). A stainless steel needle with an internal diameter 0.9mm was fitted to a 5ml syringe and connected to the positive electrode of a variable high voltage power supply, whilst the negative electrode was connected to an aluminium foil- covered copper grid, used as the collector. The syringe was placed inside a digitally- controlled syringe pump in a horizontal position pointing toward the collector. The liquid PCPH was helped to remain at sufficient elevated temperatures thus avoiding premature solidification with the use of a thermocoupled heated "wrap", set to 50°C and placed around the syringe and part of the needle. The tip-to-collector distance was 10cm, and experiments were carried out in stable conditions in air at 50°C and 60% relative humidity by enclosing the apparatus in a temperature and humidity-controlled chamber. Any residual solvent remaining in the fibres was left to evaporate at room temperature.

Initial electrospinning trials were carried out using $1C_{10}$ at room temperature at a voltage of 14kV. It was immediately noted that the viscosity of the $1C_{10}$ PCPH alone was not sufficient to produce a continuous jet. The $1C_{10}G15$ formulation (table 2.2) was chosen for the subsequent trial as sufficient gelatine content was anticipated to increase the PCPH viscosity to such a degree that electrospinning could occur, as well as the added advantage of functionalising the electrospun fibres with a biologically relevant macromolecule. Fibres were successfully produced at a voltage of 11kV. SEM images of the resulting fibre mat as well as morphological details can be found in section 4.3.2 and figure 4.2.

The solvent 1,1,1,3,3,3-hexafluoro-2-propanol (HFIP) was added to the $1C_{10}G15$ formulation for the third trial in order to investigate any morphological changes it would impart on the resulting mat. HFIP is commonly utilised solvent in electrospinning protocol and it plays a dual role in polymer solubilisation, with a mildly acidic

secondary alcohol hydroxyl serving to break hydrogen bonding and hydrophobic interactions being disrupted with two trifluoromethyl groups [5]. A 9/1 wt.-% $1C_{10}G15$ PCPH/ HFIP solution was prepared and magnetically stirred at 50°C for 15 minutes. Fibres were successfully produced at a voltage of 11kV. SEM images of the resulting fibre mat as well as morphological details can be found in section 4.3.2 and figure 4.3.

It has been shown that that the conductivity of a solution is an integral factor in influencing the spinning current and fibre diameter. Salts strongly affect the electrospinning process by enhancing the conductivity of the polymer solution and subsequently altering the properties of the fibres produced [6-8]. For the fourth trial, a 9/1 wt.-% $1C_{10}G15$/ 1.42 m NaCl solution was prepared and magnetically stirred at 50°C for 15 minutes. Fibres were successfully produced at a voltage of 11kV. SEM images of the resulting fibre mat as well as morphological details can be found in section 4.3.2 and figure 4.4.

4.3.2 Fibre morphology

The effects of solution and processing variables such as concentration, viscosity, solvent, voltage, conductivity, tip-to-collector distance and feed rate on electrospun fibre morphology have been examined for a range of polymeric systems [4, 9-12]. For many polymer/ solvent systems, an increase in solution viscosity or concentration reduces beading defects and somewhat increases the overall electrospun fibre diameter [10]. For the presented system, comparisons with previous observations should be made tentatively, as the polymer behaviours and mechanism of solidification are entirely different.
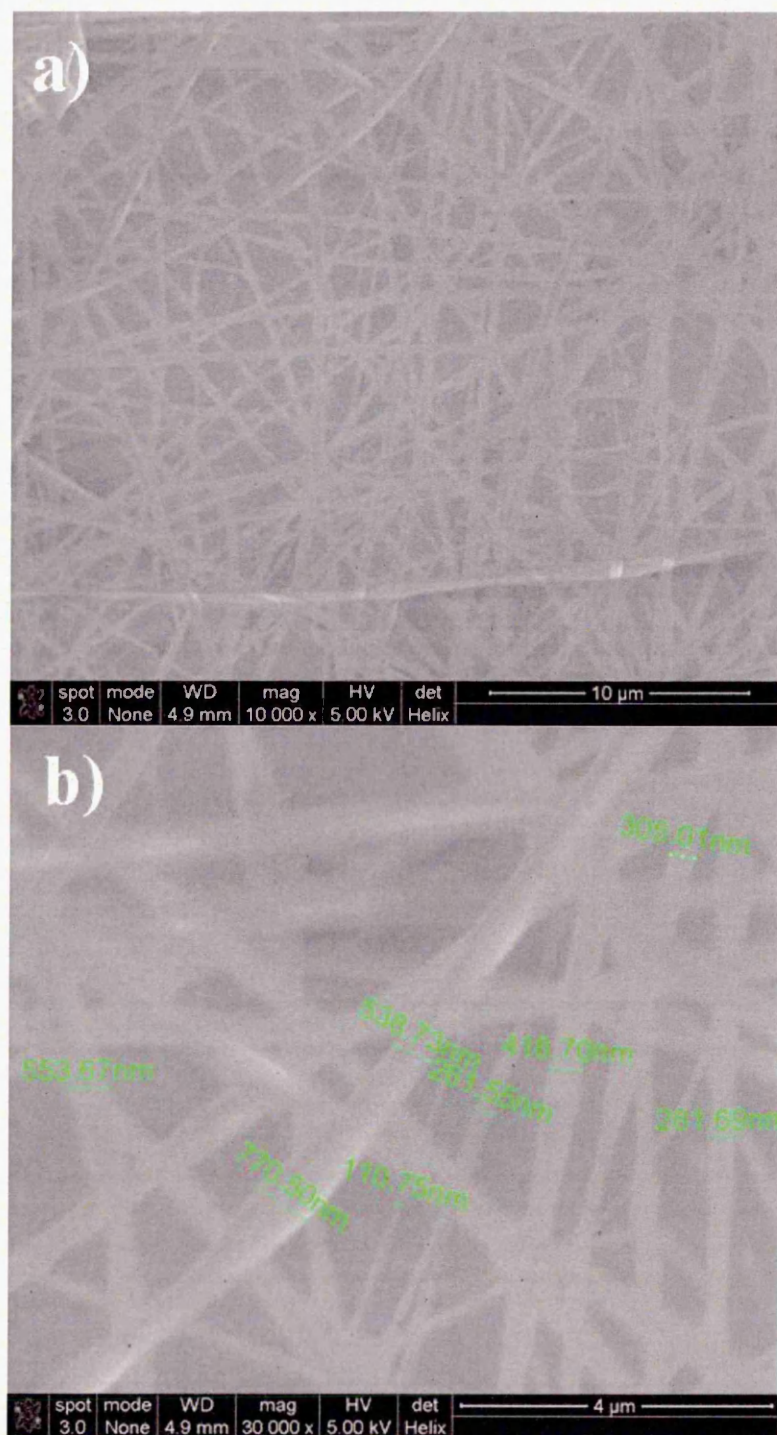
Figure 4.2 shows SEM images of the electrospun $1C_{10}G15$ PCPH formulation obtained in trial 2. The mat consisted of large areas containing polymer bead defects and fibres of significant size variation, some with flat, ribbon-like morphologies with rough fibre surfaces (a). There appears to be a high degree of variation in fibre diameter in areas of more uniform tubular-like fibres, which have a cross-section of ~150 – ~760 nm (b).

123
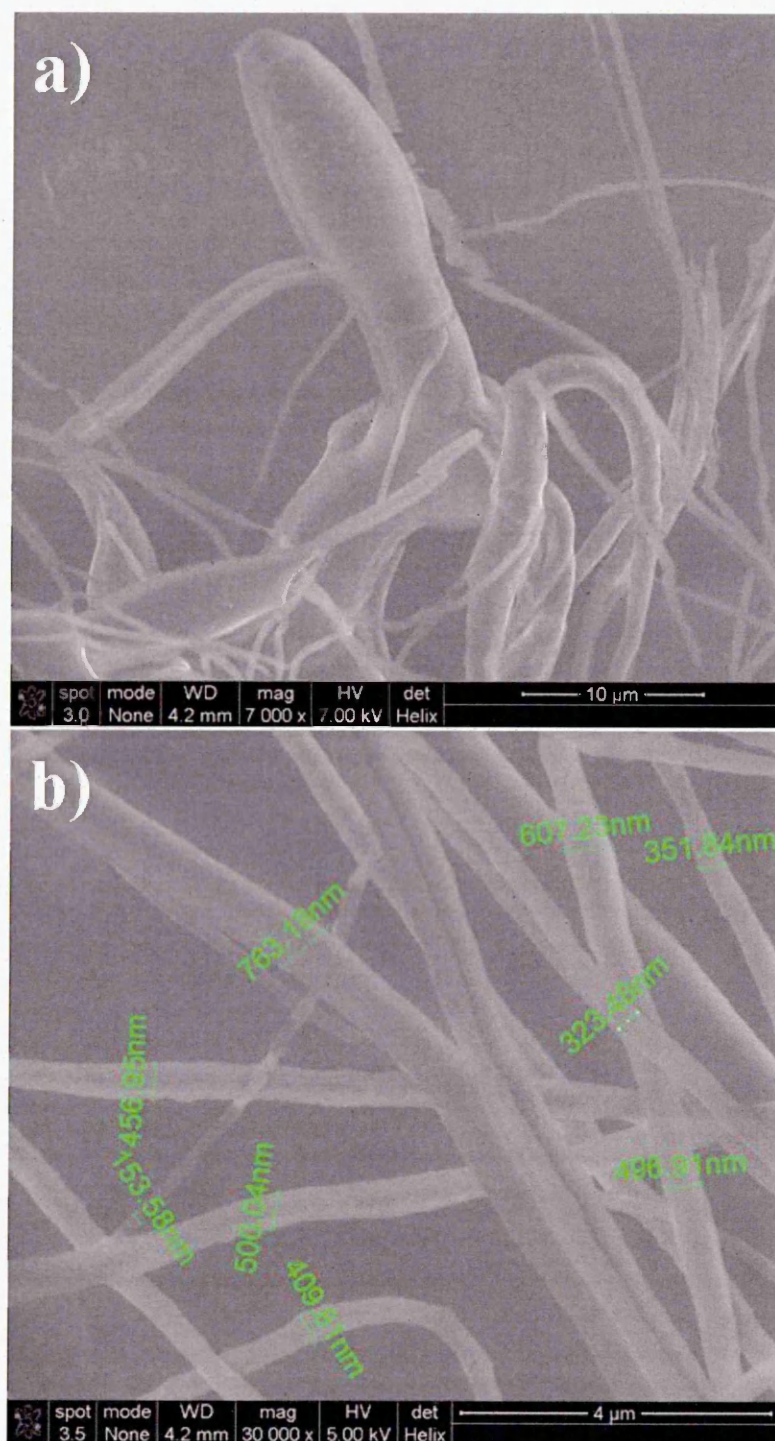
Figure 4.2. Typical SEM micrographs of electrospun fibre mats obtained with the $1C_{10}G15$ PCPH formulation at 7000x (a) and 30,000x (b) magnification.

Figure 4.3 shows SEM images of the electrospun 9/1 wt.-% $1C_{10}G15$ PCPH/ HFIP formulation obtained in trial 3. It was observed that although the fibre diameter distribution is large and strikingly similar to the electrospun $1C_{10}G15$ formulation (~

110nm – ~ 770 nm), fibre beading was greatly reduced, and neat, smooth, continuous ribbon-like fibre formation is evident.
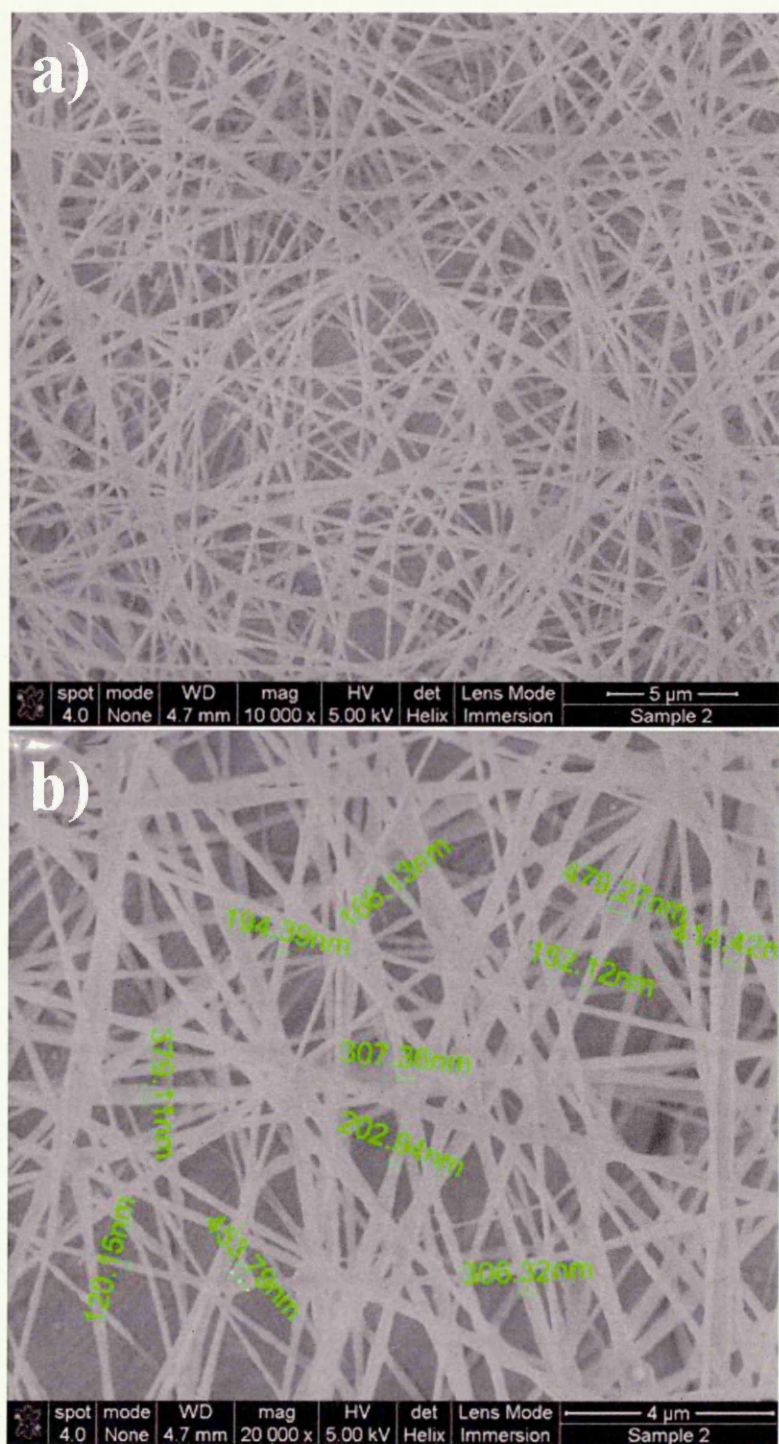

Figure 4.3. Typical SEM micrographs of electrospun fibre mats obtained with 9/1 wt.-% 1C$_{10}$G15 PCPH/ HFIP at 10,000x (a) and 30,000x (b) magnification.

Figure 4.4 shows SEM images of the electrospun 9/1 wt.-% 1C$_{10}$G15 PCPH/ NaCl formulation obtained in trial 3. The average diameters of 1C$_{10}$G15 fibre mats were

lower when NaCl was used as an additive when compared to HFIP. The fibres are continuous, straight, and smooth, and fibre diameter distributions are narrow when

Figure 4.4. Typical SEM micrographs of electrospun fibre mats obtained with 9/1 wt.-% 1C$_{10}$G15 PCPH/ NaCl solution at 10,000x (a) and 20,000x (b) magnification.

compared to other formulations used in the study. This narrow size distribution observation is in good agreement with other studies involving the electrospinning of salt

126

incorporated polymer solutions [6, 13], and is thought to be a result of enhanced conductivity of the polymer jet which in turn enhances jet elongation.

Atomic force microscopy (AFM) could also be carried out on the fibres in order to better resolve the topology of the fibres. It may give a better understanding fluid mechanical effects and possible fibre skin formations, as well as alternative collapse modes (ribbon-like fibres can be a product of fibre collapse during solvent evaporation). Furthermore, the distribution of dispersed clay nanoparticles within the fibres could be examined using bright field TEM imaging. It is anticipated that extensional forces applied by the electrospinning process may cause the clay nanoparticles to align along the axis of the fibre, as reported previously [14-16].

4.4   A novel method for the industrial casting of thin films of PNIPAM/ clay nanocomposite hydrogels.

Smith & Nephew Extruded Films (SNEF) are independent manufacturers within the global manufacturer Smith & Nephew PLC and the producers of extruded films, tapes, apertured meshes and nets, with experience in providing innovative solutions in intelligent polymer technology. Their manufacturing site in Gilberdyke, UK has a large production capacity including custom net and film production, as well as adhesive coating and foam casting [17]. The trial line used for the PCPH and subsequent PNIPAM/ clay films was a bespoke "Cutinova" setup (also referred to as a "PU gel casting line") which is depicted in figure 4.5. The temperature of the casting room was kept cool (19°C) to help the PTTNAG process and the humidity was recorded as 29-30% relative.

The purpose of the film casting trial day was to establish the viability of the PCPH as a candidate for film production on an industrial scale. 600mls of $1C_{10}$ PCPH (in separate 100ml sample jars) were produced for the trial. For COSHH and health and safety reasons, one 100ml batch per day was synthesised over 6 days and maintained at 80°C prior to the trial. Sample 1 was initiated 7 days prior to the trial and samples were labelled in numerical order on subsequent days, with sample 6 being initiated the day before the trial.

Poly-coated silicone release papers from Loparex BV were drawn through the Cutinova apparatus as shown in figure 3.8 and 3.9a. These papers were waterproof and stable to the moisture levels and temperatures required for casting the material.

The PCPH was very gradually manually poured onto the casting table (figures 4.5 and 4.6 b and c) where it was drawn through a gap between the coating bar and casting table between the 2 sheets of release paper at a speed of 0.6m/ min^{-1}. This coating method is known in the industry as a "spreading box"- a coating bar method where coat weight is controlled by the dimensions of a gap. A continuous sheet of PCPH (and subsequent nanocomposite hydrogel sheet) sandwiched between the 2 release papers was created and was allowed to cool and undergo PTTNAG on top of the steel slats inside the "drying tunnel" of the setup (which was turned off for this trial) for 1-2 hours (figures 4.5 and 4.6 e and f). The winding bar was used for speed control only and product was not rewound. After this time, the release paper was peeled back to reveal the transparent, uniform PNIPAM/ clay film (figure 4.6g and h). Films of 300μm, 500μm, 800μm 1000μm were successfully manufactured with this process by adjusting the height of the gap, with mechanical stability of the films improving respectively.
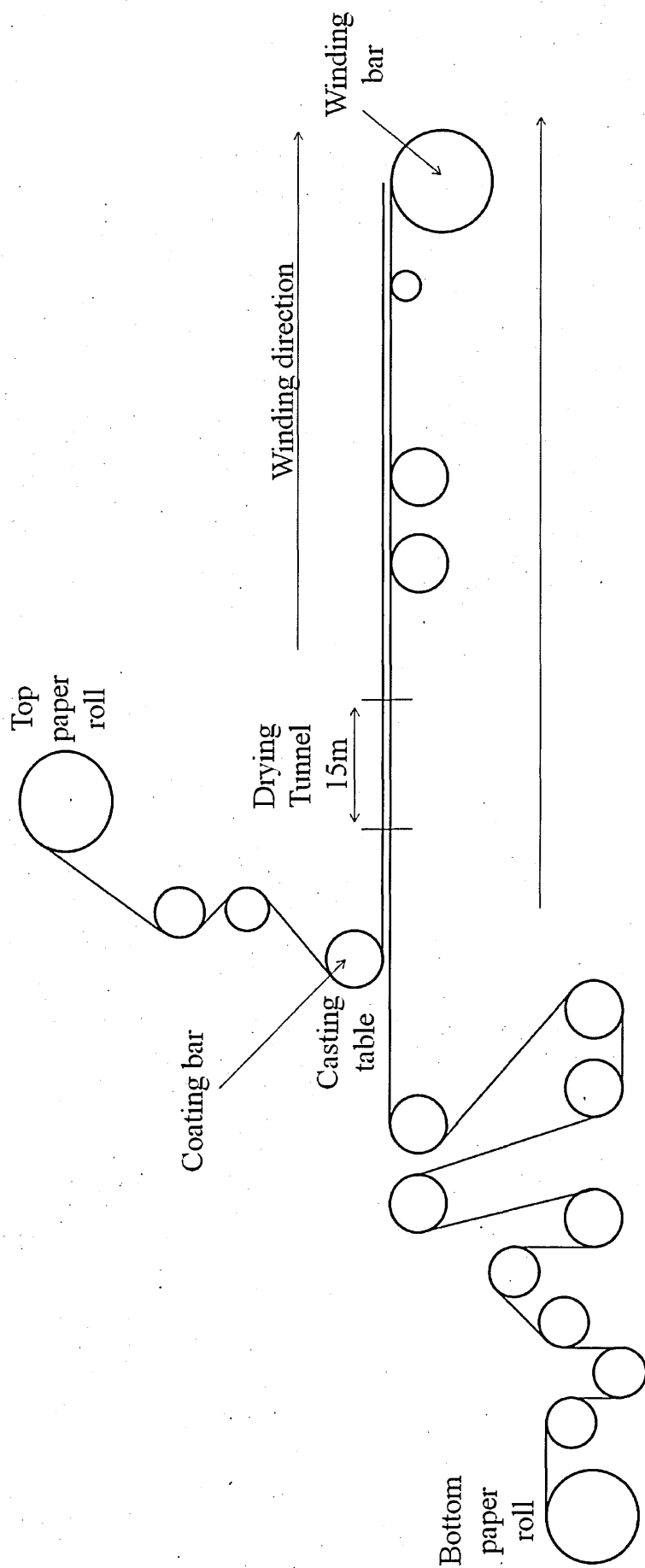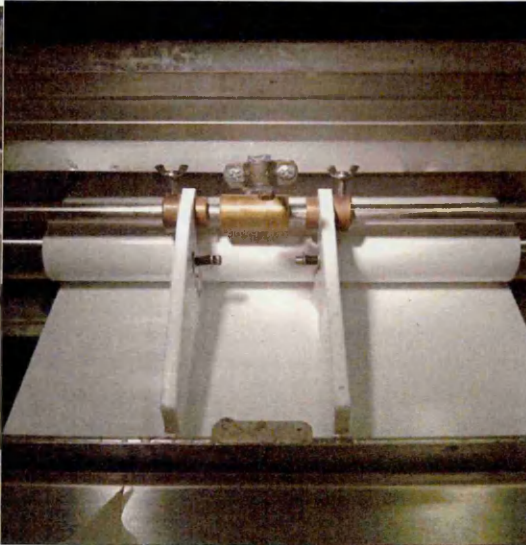
Figure 4.5. A schematic representation of the gel casting line at SNEF, a bespoke piece of equipment also known as the "Cutinova" setup, on which the liquid PNIPAM/ clay casting trials took place.

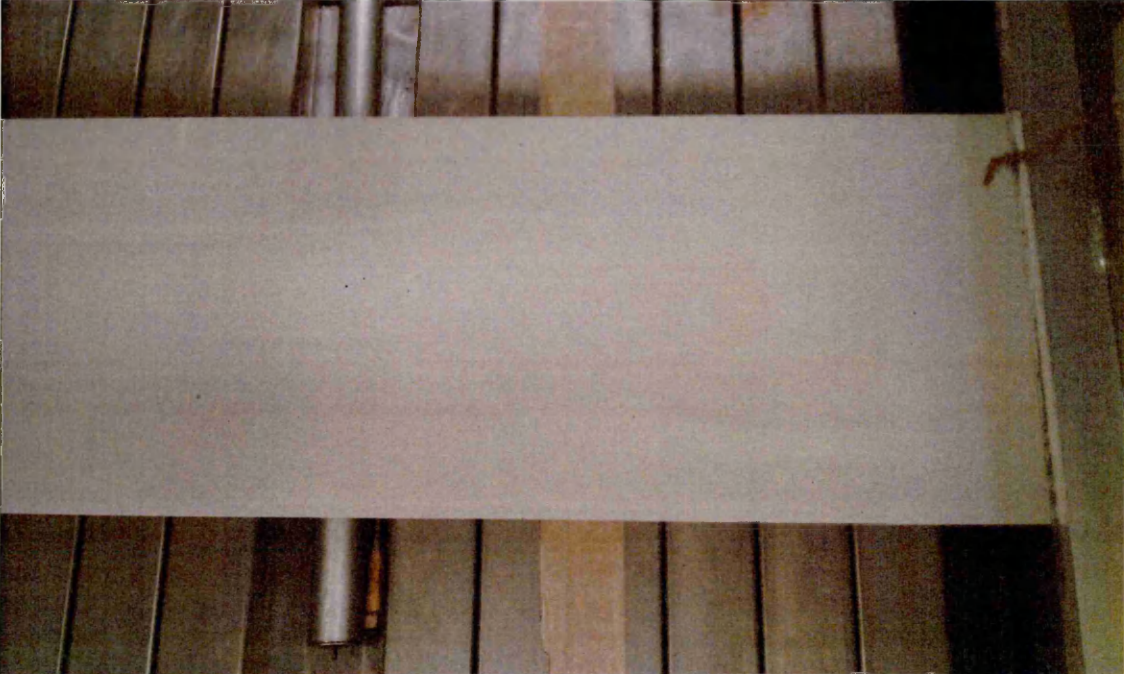e)

f)

g)

h)

Figure 4.6. The various equipment and production steps at SNEF with which flat films of PNIPAM/ clay nanocomposite gel were manufactured in a one-step process directly from 1C$_{10}$ PCPH formulations.

Figure 4.6. shows the gel-casting process at SNEF, showing a) top and bottom poly-coated silicone release papers rolls (above and below respectively), b) the "spreading box" apparatus showing the two guard plates between which the PCPH (c) is gradually poured. The PCPH is squeezed through a precise predetermined size gap between the coating bar and casting table between the upper and lower coated silicone release papers, which are simultaneously pulled through the tunnel (d and e) by the winding bar at a speed of 0.6m/ min^{-1}. The nanocomposite film, sandwiched between two silicone release papers is allowed to cool on top of the steel "slats" of the drying tunnel (f) before the paper is peeled back to reveal the transparent, uniform PNIPAM/ clay film (g and h, both showing film of 1000µm thickness).

4.5   Summary

Previous reports on the electrospinning PNIPAM are limited, but show that the polymer can be electrospun into fine fiber mats by dissolving commercially produced linear PNIPAM in various solvents, such as methanol [18], water, acetone, THF [19], and DMF [20] prior to electrospinning the resulting solution. Despite this, the non-cross-linked networks of such mats would not be capable of retaining any of their fibrous structure upon reswelling, rendering the useful stimuli responsive properties of PNIPAM in solution effectively useless. In this chapter, the production of novel fine (100-800nm), uniform, cross-linked PNIPAM/ clay nanocomposite fibers of various compositions is presented. The facile incorporation of additives to the solution prior to electrospinning is related to the morphologies of the resulting fibers.

The only PNIPAM/ clay hydrogel sheets apparent in literature have been synthesised by warming a monomer/ initiator/ accelerator solution inside a flat mould to temperature above which initiator dissociation occurs, and allowing polymerisation to proceed *in situ* [21]. Inconveniently, this method requires the complete encapsulation of the entire apparatus in an oxygen-free, nitrogen atmosphere and whereby the solution is highly toxic until fully polymerised. The method does not facilitate the addition of dopants prior to PTTNAG and the resulting sheets must be purified extensively after synthesis to remove unreacted species. Here is presented a novel, simple, safe and convenient method of producing thin films of PNIPAM/ clay nanocomposite hydrogel of uniform and controllable thickness (as thin as300µm) on an industrial scale, using industrial film- extrusion apparatus.

4.6 Chapter 4 References

1.   Subbiah, T., et al., Electrospinning of nanofibers. Journal of Applied Polymer Science, 2005. 96(2): p. 557-569.

2.   Huang, Z.M., et al., A review on polymer nanofibers by electrospinning and their applications in nanocomposites. Composites Science and Technology, 2003. 63(15): p. 2223-2253.

3.   Frenot, A., Chronakis, I., Polymer nanofibers assembled by electrospinning. Current Opinion in Colloid & Interface Science, 2003. 8(1): p. 64-75.

4.   Reneker, D.H., Chun, I., Nanometre diameter fibres of polymer, produced by electrospinning. Nanotechnology, 1996. 7(3): p. 216-223.

5.   Dong, B., et al., Electrospinning of Collagen Nanofiber Scaffolds from Benign Solvents. Macromolecular Rapid Communications, 2009. 30(7): p. 539-542.

6.   Dao, A.T., et al., Effect of sodium chloride on the needle electrospinning of poly (vinyl alcohol). Nanocon 2009, Conference Proceedings. 2009. 202-206.

7.   Theron, S.A., et al., Experimental investigation of the governing parameters in the electrospinning of polymer solutions. Polymer, 2004. 45(6): p. 2017-2030.

8.   Demir, M.M., et al., Electrospinning of polyurethane fibers. Polymer, 2002. 43(11): p. 3303-3309.

9.   Bhardwaj, N., Kundu, S., Electrospinning: A fascinating fiber fabrication technique. Biotechnology Advances, 2010. 28(3): p. 325-347.

10.   Fong, H., Chun, I., Reneker, D., Beaded nanofibers formed during electrospinning. Polymer, 1999. 40(16): p. 4585-4592.

11.   Jarusuwannapoom, T., et al., Effect of solvents on electro-spinnability of polystyrene solutions and morphological appearance of resulting electrospun polystyrene fibers. European Polymer Journal, 2005. 41(3): p. 409-421.

12.   Yang, Y., et al., Experimental investigation of the governing parameters in the electrospinning of polyethylene oxide solution. Ieee Transactions on Dielectrics and Electrical Insulation, 2006. 13(3): p. 580-585.

13.   Lee, C.K., et al., The influence of added ionic salt on nanofiber uniformity for electrospinning of electrolyte polymer. Synthetic Metals, 2005. 154(1-3): p. 209-212.

14.   Ji, Y., et al., Structure and nanomechanical characterization of electrospun PS/clay nanocomposite fibers. Langmuir, 2006. 22(3): p. 1321-1328.

15.   Fong, H., et al., Generation of electrospun fibers of nylon 6 and nylon 6-montmorillonite nanocomposite. Polymer, 2002. 43(3): p. 775-780.

16.   Li, L., et al., Formation and properties of nylon-6 and nylon-6/montmorillonite composite nanofibers. Polymer, 2006. 47(17): p. 6208-6217.

134

17.   Smith&Nephew. Profile overview. [online] Accessed 01.05.2012 from: http://global.smith-nephew.com/snef/9650.htm.

18.   Okuzaki, H., et al., Non-woven fabric of poly(N-isopropylacrylamide) nanofibers fabricated by electrospinning. Synthetic Metals, 2009. 159(21-22): p. 2273-2276.

19.   Rockwood, D.N., et al., Characterization of electrospun poly(N-isopropyl acrylamide) fibers. Polymer, 2008. 49(18): p. 4025-4032.

20.   Chen, H., Hsieh, Y., Ultrafine hydrogel fibers with dual temperature- and pH-responsive swelling behaviors. Journal of Polymer Science Part A: Polymer Chemistry, 2004. 42(24): p. 6331-6339.

21.   Haraguchi, K., Takehisa, T., Ebato, M., Control of Cell Cultivation and Cell Sheet Detachment on the Surface of Polymer/Clay Nanocomposite Hydrogels. Biomacromolecules, 2006. 7(11): p. 3267-3275.

5

The Characterisation of PNIPAM/ Clay Nanocomposite Liquid Gel Precursor Formulations Post- PTTNAG

Chapter 5 - The Characterisation of PNIPAM/ Clay Nanocomposite Liquid Gel Precursor Formulations Post-PTTNAG.

5.1 Introduction

This chapter explores the characterisation carried out on PCPHs post PTTNAG. Clay distribution of the PNIPAM/ clay formulations of various clay concentrations is determined using X-ray diffraction (XRD), and their thermal stability examined using thermogravimetric analysis (TGA). Mechanical properties of various gel formulations with and without biologically active dopants are compared using data obtained from dynamic mechanical analysis (DMA). Limitations of certain Molecular weight (M_w) characterisation approaches are also presented and discussed.

Clay concentrations present in the samples are confirmed using ATR-FTIR, and an ATR-FTIR study of the formation and destruction of hydrogen bonding in PNIPAM/ clay, PNIPAM/ clay / gelatine and PNIPAM/ clay Hyaluronic acid (HA) hydrogel formulations during dehydration at 27 °C is presented.

5.2 Materials used in this chapter and the synthesis and Preparation of a PNIPAM/ Clay nanocomposite hydrogel precursor liquid
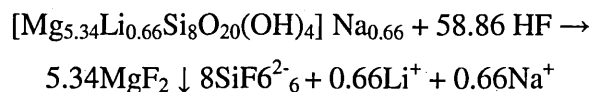
The materials, synthesis, nomenclature format and formulation compositions are detailed in section 2.2.3.1.

5.3 Separation of PNIPAM from clay nanocomposite hydrogels by Hydrofluoric Acid (HF) digestion.

In order to remove the clay from the PNIPAM/ clay network and thus allow molecular weight data to be obtained and compared between PNIPAM gel systems synthesised with various clay loadings, hydrofluoric acid (HF) was chosen to digest and remove the clay particles.

HF reacts with most silica- based minerals, including clays and quartz, and aqueous HF solutions decompose clay platelets in PNIPAM/ clay gels [1]. The reaction between HF and Laponite is thought to be:

$$[Mg_{5.34}Li_{0.66}Si_8O_{20}(OH)_4]\,Na_{0.66} + 58.86\,HF \rightarrow$$

$$5.34MgF_2 \downarrow 8SiF6^{2-}_6 + 0.66Li^+ + 0.66Na^+$$

Equation 5.1.

Removal of clay from the PNIPAM/ clay system can be verified by monitoring the loss of intensity of the v(Si-O) band in ATR spectra.

The removal of clay from PNIPAM gels has been successfully performed previously by Haraguchi et al [1], who selected an adequate HF concentration (0.2wt %) to completely decompose the clay whilst posing no damage to the PNIPAM chains. Haraguchi's system differed from the one presented only in method of synthesis, and therefore it was deemed appropriate to select the same HF concentration in the following procedure;

In order to observe the effect of clay loading on the molecular characteristics of PNIPAM/ clay gels, $.25C_{10}$, $.5C_{10}$ and $1C_{10}$ were prepared using the protocol described in Section 2.2.1.2. The gels were cut into cubes of ~ 5mm x 5mm x 5mm and placed into an excess of aqueous HF under rapid stir. The amount of aqueous HF solution required was 30ml (HF = 0.2 wt %) per 1g of the gel. This was sufficient to induce clay decomposition. After 24h of constant stirring, the linear PNIPAM was retrieved from the solution by inducing PNIPAM phase- transition at 50°C. Purification was achieved by alternating the temperature between 20 - 50°C, and exchanging water at 50°C. The handling of HF (the digestion and purification steps) in this procedure was carried out by Daniel Capon, Senior Technologist at Glass Technology Services Ltd, Sheffield.

The linear PNIPAM obtained from an xC_y nanocomposite gel is denoted as xC_y^{-C}.

Spectroscopic data of the xC_y^{-C} polymers show that despite HF treatment, a small v(Si-O) ~1000 cm^{-1} (figure 5.1) is observed and indicates that although the majority of the clay was decomposed, a small amount remains. As such, no GPC data could be obtained or compared for the clay cross-linked PNIPAM gels.
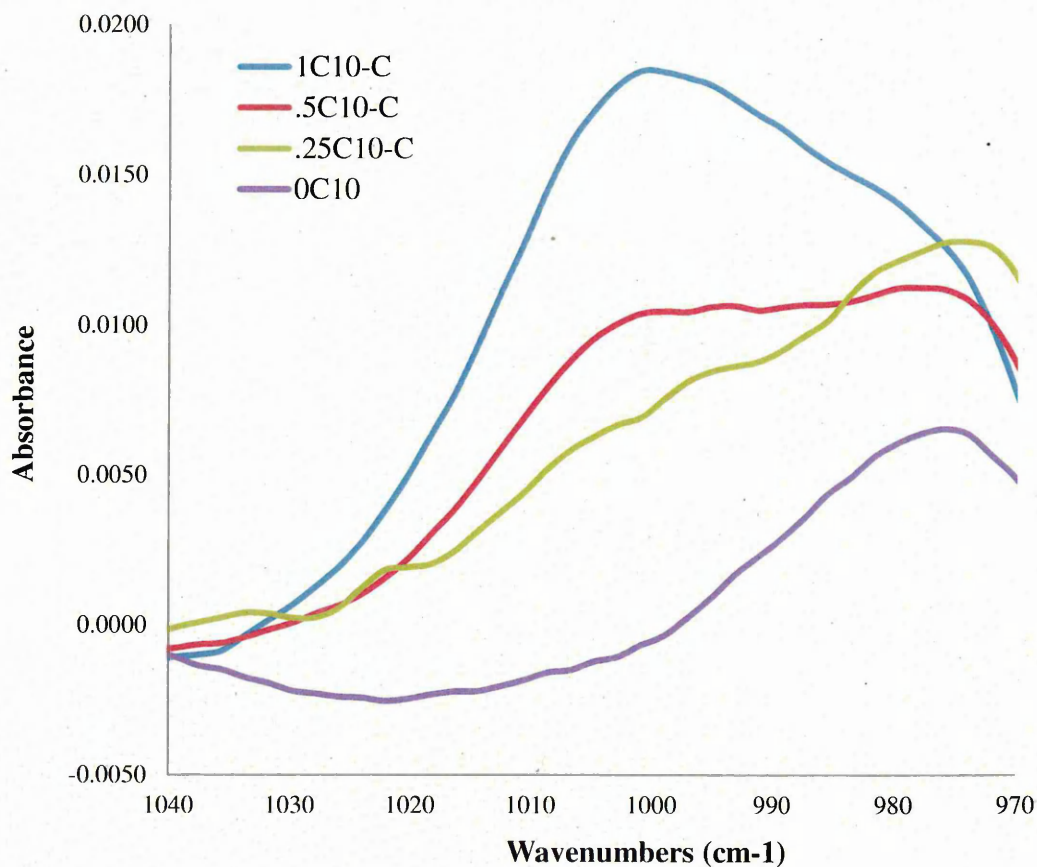
Figure 5.1. ATR-FTIR spectra of .25C$_{10}$$^{-C}$, .5C$_{10}$$^{-C}$ and 1C$_{10}$$^{-C}$ polymers which have been dried overnight at 80°C prior to analysis. v(Si-O) vibrations ~1000 cm^{-1} in all systems are clearly observable when compared to the pure polymer system 0C10.

A greater degree of success with regards to clay removal may be achieved in future work by increasing the HF concentration from = 0.2 wt % to 0.25 wt%, and extending the stirring period to 36-48h.

5.4 Gel permeation Chromatography (GPC) analysis of linear PNIPAM at various stages of polymerisation.

To follow the propagation of the PNIPAM chains during synthesis, gel permeation chromatography (GPC) analysis was employed to attempt to determine molecular weights and molecular weight distribution of pure PNIPAM at various time intervals (1, 2 , 5 and 24 hours) during polymerisation. In light of the difficulties encountered during the removal of clay from the PNIPAM nanocomposite materials (section 5.3), only pure, linear PNIPAM ($0C_{10}$) was included in this study. The polymers were synthesised as described in section 3.2. After the precise required polymerisation time had elapsed, the sample was removed from the hot oil bath and immediately quenched in an ice bath. The aqueous polymers were dried at room temperature overnight and ground to a grainy consistency (the samples were not completely dried at a higher temperature for reasons discussed later). 5mg of each sample was added to 5ml GPC grade tetrahydrofuran (THF) (Fisher Scientific) in separate sample vials and stabilised with 250ppm butylated hydroxytoluene (BHT) (Aldrich). The solutions were swirled gently for 24h to dissolve (although they appeared simply to swell). Each sample was injected into the GPC system through a 0.45µm sieve.
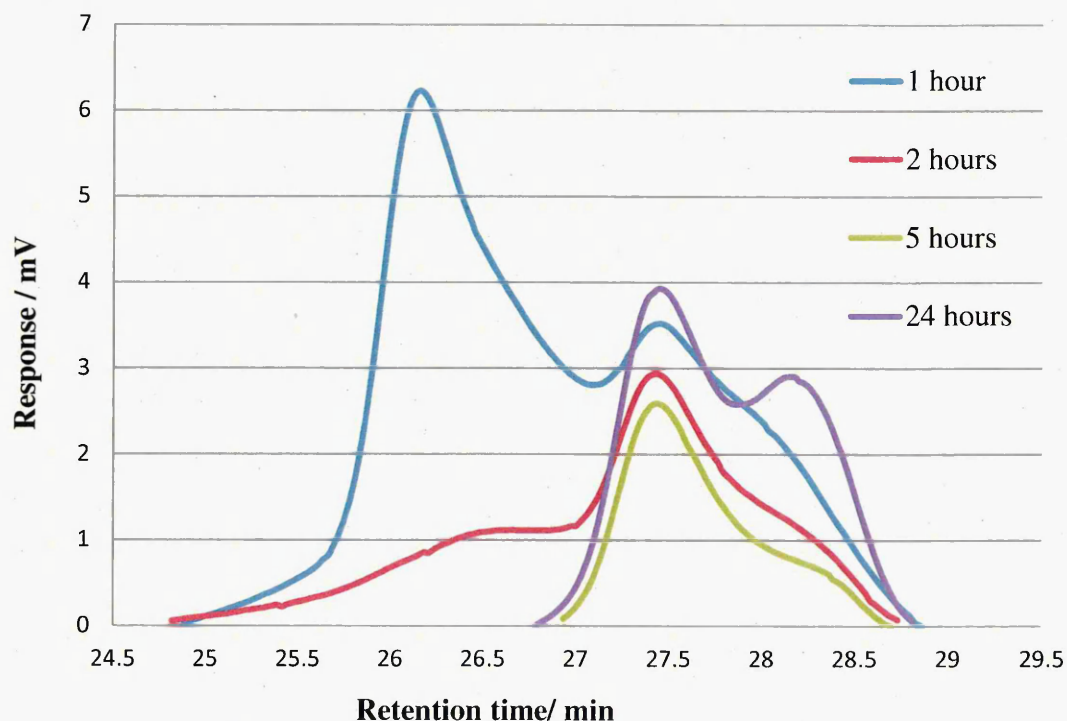
Figure 5.2. Influence of polymerisation time on GPC chromatograms of $0C_{10}$ PNIPAM polymers, based on polystyrene standards. PNIPAM

concentration = 1 mg/ ml^{-1}, and flow rate = 1 ml/ min^{-1}. Filter pore size = 0.45 μm and 2 μm (guard column).

Table 5.1. Average molecular weight (M$_w$) and molecular weight distribution (M$_w$/ M$_n$) data obtained for linear PNIPAM by GPC.

Polymerisation time	M$_w$	M$_n$	M$_w$/M$_n$ (MWD)
1 hour	P1= 651	P1= 590	P1= 1.10
	P2= 224	P2= 204	P2= 1.11
2 hours	P1= 377	P1= 267	P1= 1.41
5 hours	P1= 231	P1= 215	P1= 1.10
24 hours	P1= 257	P1= 250	P1= 1.03
	P2= 150	P2= 146	P2= 1.03

GPC chromatographs of the samples are shown in figure 5.2, and the corresponding molecular weight (M$_w$) and molecular weight distribution (M$_w$/ M$_n$) data is shown in table 5.1. The average M$_w$ in all systems is not only unexpectedly very low, but appears to decrease as polymerisation time increases, which is counter-intuitive. The erroneous nature of these results can be explained by the reasons outlined below.

Literature gives an array of solvents which have been used as GPC mobile phases for PNIPAM. These include THF [2-5], DMF[6], chloroform [7], methanol [8], and water [9-10]. There exists, however, some uncertainties regarding the accuracy of measurement data obtained for PNIPAM analysis. These uncertainties are thought to be linked to problems such as to chain aggregation [11], filtration [10, 12-13] and solvent effects [10]. Xu *et al* [13] reported particular difficulty analysing PNIPAM by THF-phase GPC and attributes the data irreproducibility to the lack of solubility, which results on the trapping of PNIPAM by the filter and/or guard column. It is reasonable to conclude that solubility and polymer trapping issues are at play in the data presented in figure 5.2. It is likely that only very short chain polymers and oligomers in the samples were sufficiently solubilised to pass through the guard column filter. Further to this, Ganachaud *et al* [11] concluded that completely drying PNIPAM causes chain aggregation which is not undone when the sample is dissolved in THF, and it could be possible that air drying at room temperature is also sufficient to induce such aggregation.

In addition to solvent issues, inaccurate molecular weights will be obtained if the standards used in the calibration and the sample are of a different chemistry.

141

GPC does not separate polymer chains on the basis of M_w, but on their size in solution. During GPC calculations, it is assumed that a particular M_w corresponds to a particular polymer coil size in solution (hence retention time), as shown by the calibration. Polymers of different chemistry coil differently in solution, forming polymer spheres of different size and therefore have a different size/ M_w relationship. Therefore, only relative M_w could have been achieved with this system.

More data are needed to make mechanistic inferences on the M_w of PNIPAM in the presented system. Possible future approaches are discussed in chapter 8.

5.5 Matrix-Assisted laser desorption/ ionisation time-of-flight mass spectrometry (MALDI TOF MS) analysis of PNIPAM/ clay films

Sometimes, number-average molecular weight (M_n) and polydispersity values can be calculated by appropriate averaging of peak heights from matrix-assisted laser desorption/ionisation time of flight mass spectrometry (MALDI-TOF-MS), and the technique can be used to determine the terminal structure of polymers.

In this study, PNIPAM/ clay nanocomposite films were cast from the PCPH formulations $.25C_{10}$, $.5C_{10}$ and $1C_{10}$ (table 2.1 and Section 2.2.1.2), using PTFE moulds with the dimensions 10 x30x5mm. The films were removed from the moulds and left to air dry at room temperature for 2 days, becoming flat, transparent sheets of .4- .5mm thickness. Pure PNIPAM film obtained from a $0C_{10}$ formulation (table 2.1 and Section 2.2.1.2) was obtained by pouring the reacted aqueous polymer mixture into an identical mould and drying under the same conditions.

Samples were fixed onto a stainless steel slide and 2 spots of matrix, 1,8,9-trihydroxyanthracene (dithranol) (Aldrich, 97%) were placed on the surface of each sample. The sample spots were scanned averaging ~50 shots per spectrum with constant laser intensity.

The MALDI-TOF MS spectra for all samples obtained in this study is shown in figure 5.2.What would be expected in the MALDI-TOF MS spectra are a series of peaks with a regular interval of 113.08, which corresponds to molar mass of the monomer unit. What appears instead, however, is a series of regularly-spaced peaks corresponding to the dithranol matrix (table 5.2). The detection of the matrix and not of the analyte may be owed to a number of contributing factors. One of the integral requirements of solvents that are used in MALDI sample preparation is their ability to dissolve all

142

components of the sample. It is possible that suitable solubility was not achieved in this case. Also, analysis of PNIPAM via this method is difficult due to its lack of ionic character, and therefore laser desorption would only yield neutral gas phase molecular species. A future approach to this problem would involve the addition of a suitable catonisation agent or salt solution (such as NaCl or KCl), to form charged analyte clusters.
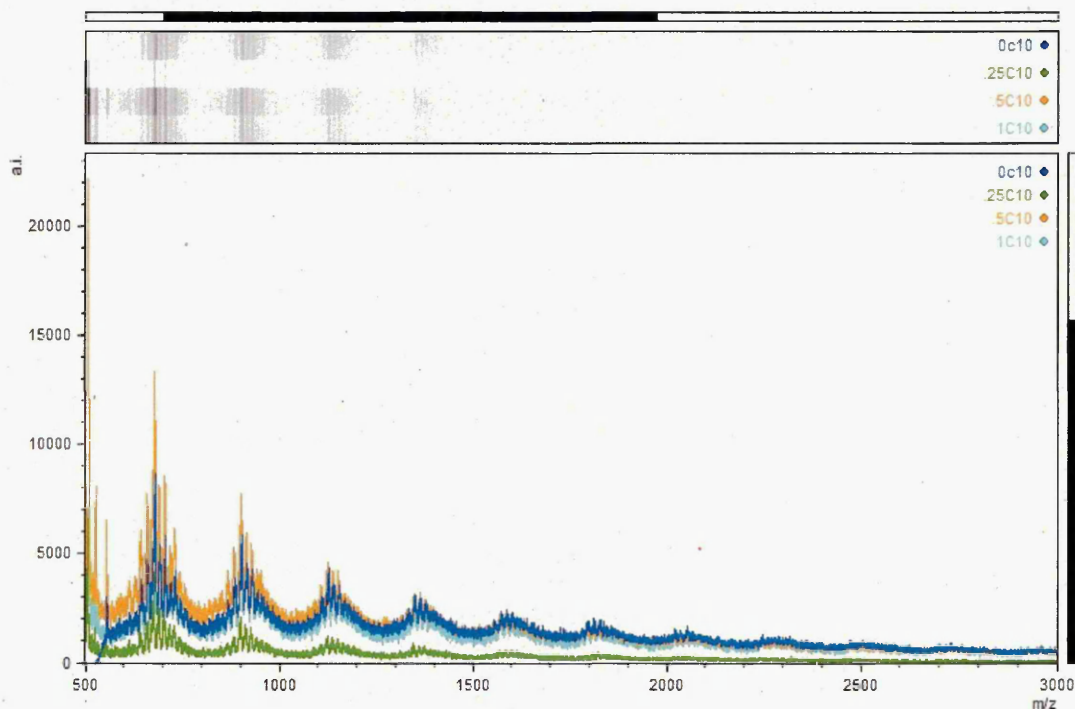
Figure 5.3. MALDI TOF-MS mass spectra of dried films of 0C10, .25C10, .5C10 and 1C10 PNIPAM/ clay nanocomposite hydrogels. In all instances, the regularly-spaced peaks are indicative of dithranol matrix clusters and no polymer was detectable.

Table 5.2. m/z and intensity values recorded for the MALDI TOF-MS peaks shown in figure 3.11 for the .5C10 PNIPAM/ clay film. For all samples, the m/z values recorded were near identical. The m/z values are very close multiples of the Mw of dithranol, which is 226.23. This is indicative of the detection of dithranol matrix clusters.

m/z	Intensity
685	8721
905	9015
1131	4005
1357	2759
1582	2047
1810	1602

143

5.6 Thermogravimetric Analysis (TGA) of dry PNIPAM/ clay nanocomposites.

In this study, TGA was performed to observe thermal degradation of the polymer samples with respect to their clay content, and to observe the effects of clay content on the thermostability of the polymer/ clay composites.

Lab: Vicky Boyes   METTLER TOLEDO STAR^e SW 7.01
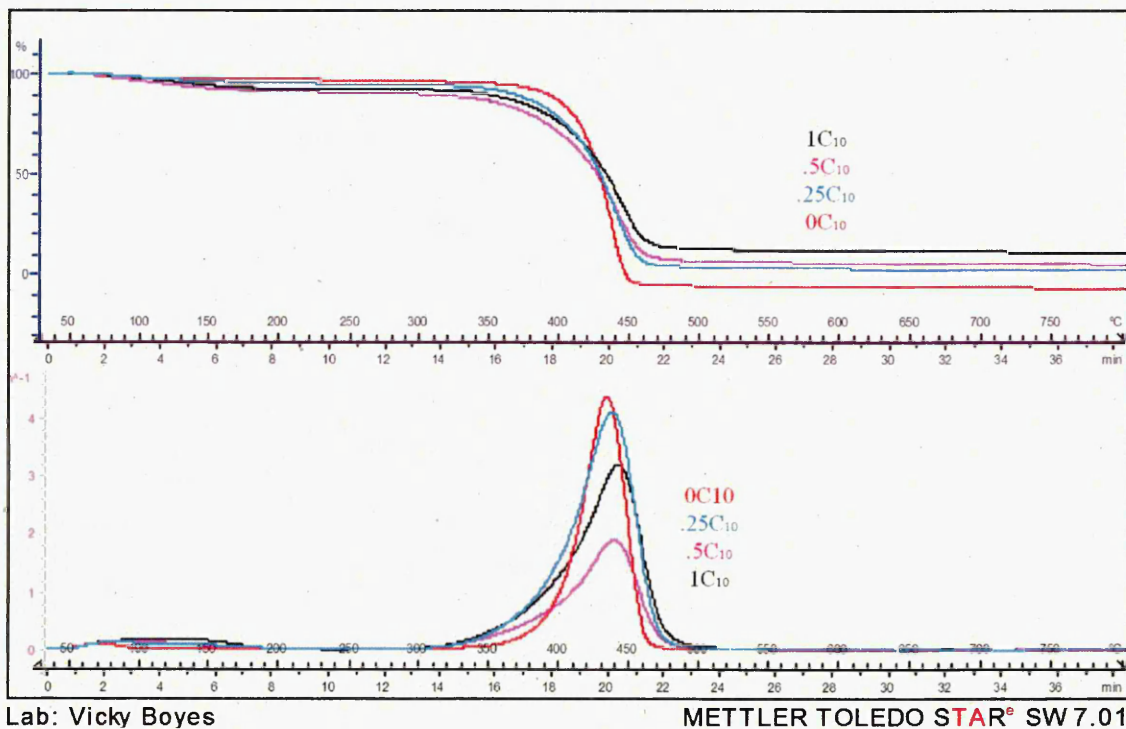
Fig.5.4. TGA data of thermally initiated PNIPAM & clay cross-linked PNIPAM of various clay concentrations.

Thermogravimetric analysis results for PNIPAM and the clay nanocomposites are shown in 5.4. All samples in this study were synthesised as described in Section 2.2.1.2 before being dried at 80°C for 24h, crushed to a granular consistency using a mortar and pestle, then dried for a further 12h before being crushed once more to a powder. The top trace shows the normalised % weight of the sample plotted against temperature. The lower traces show a negative derivative of these results, to show the changes in rate of decomposition more clearly. Both sets of data show pyrolysis (heat-induced chemical decomposition) in a single step process with a peak maximum at approximately 430°C for all gels. In both sets of data, decomposition of pure PNIPAM begins at 360°C and has reached completion at 500°C, whereas the nanocomposite materials begin decomposition at the slightly lower temperature of around 320°C, with pyrolysis complete at 500°C. The more gradual weight changes of the nanocomposite materials

144

indicate improved thermal stability when compared to the pure polymer, and the clay platelets appear to have had a shielding effect and slowed down the decomposition rate. As expected, the stability of the inorganic component meant that residual sample weight at the end of the experiment increases in accordance with clay content. The only anomaly in this finding is the behaviour of pure PNIPAM initiated by UV, as it has a higher than expected residual weight. A possible future approach to this experiment would be to re-run the sample in an O_2 atmosphere, removing any char which could contribute to the residual weight of the samples.

5.7 X-Ray Diffraction (XRD) data of dry PNIPAM/ clay nanocomposites.

When X-rays interact with regular, repeated structures which have approximately the same repeat distance as X-ray wavelength, diffraction occurs. Crystalline solids have interatomic distances of just a few angstroms, which is the approximate wavelength of X-ray radiation. X-rays are diffracted from minerals (such as clay) which have regular repeated structures, and XRD analysis was used to determine degree of clay exfoliation and/ or intercalation of clay in dried clay/ polymer nanocomposite samples. It is expected that disordered exfoliated clay nanocomposites would produce no diffraction pattern due to a lack of an ordered internal structure; whereas an unexfoliated phase separated microcomposite (or system of "stacked" clay platelets) would produce a strong diffraction pattern. An ordered intercalated nanocomposite produces signal intensity dependent on the extent of platelet ordering and subsequent diffraction.

All polymer samples in this study were synthesised as described in Section 2.2.1.2 before being dried at 80°C for 24h, ground to a granular consistency using a mortar and pestle, then dried for a further 12h before being ground once more to a powder. The powder was placed inside the well of an aluminium sample holder and pressed firmly to achieve a flat sample surface. The data are shown in figure 5.5.

Laponite clay is notoriously difficult to observe using XRD as it has weak reflections due to imperfect platelet registration and small size [14]. Observing intercalation of Laponite in PNIPAM nanocomposites is especially difficult as the broad diffraction pattern of the polymer masks the Laponite peaks at $2\theta = 9°$ and $2\theta = 19°$. The crystalline peaks at 9° in both sets of data loosely follow a pattern of decreasing

XRD Analysis data of dry Clay/PNIPAM Hydrogels of Various Clay Concentrations
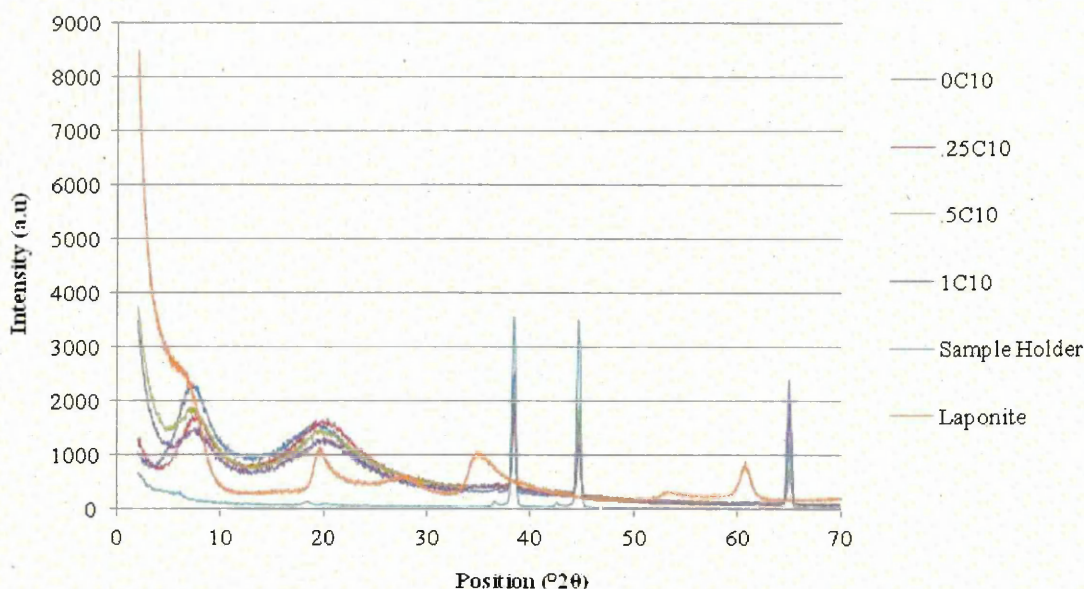
Figure.5.5. XRD data of fure laponite clay, the sample holder, linear PNIPAM & clay cross-linked PNIPAM of various clay concentrations (see table 2.1).

intensity with increasing clay content. This is opposite to what one would normally predict, as increased number of clay platelets should, in theory, result in increased number of repeated structures and therefore increase in diffraction intensity. It is possible that the observations made here are attributed to a regular, ordered polymer structure which is being disrupted by the presence of exfoliated clay platelets. If the experimental parameters were perfect (more specifically, the sample was ground into a very fine powder and pressed to form a flat sample surface), it could be assumed that an increasing baseline is an indication of good clay exfoliation within the polymer network. Since the parameters were imperfect (extraordinary hardness of the dried gel made grinding extremely difficult, resulting in a possible inhomogeneous sample density and uneven sample surface), it is impossible to derive tentative conclusions from these baseline observations. If there were no parallel planes within the structure of the material (i.e. the clay was well exfoliated and the polymer amorphous), what would be observed is a smooth, featureless diffraction pattern, curved with a high baseline.

## 5.8 ATR-FTIR spectroscopic analysis of dry PNIPAM/ clay nanocomposite and doped nanocomposite films.

5.8.1 ATR-FTIR analysis of PNIPAM/ clay nanocomposite materials

Shown in figure 5.6 are the ATR-FTIR spectra of PNIPAM and its clay nanocomposites of various clay concentrations. All samples were synthesised as described in Section 2.2.1.2 before being dried at 80°C for 24h, crushed to a granular consistency using a mortar and pestle, then dried for a further 12h before being crushed once more to a powder.

This sample treatment prior to data collection allowed for improved sample/ crystal contact and helped significantly reduce the large v(OH) vibration associated with sorbed water which masks the characteristic v(NH) band of PNIPAM at ~3300cm^{-1}. The pure PNIPAM material is also characterised by the amide I band at ~1649 cm^{-1} and amide II band at ~1546 cm^{-1}. For the clay nanocomposites, the band ~1000 cm^{-1} is assignable to the stretching vibration of Si-O in the clay. The intensity of the Si-O band increased with increasing concentration of clay, as expected.

This sample treatment prior to data collection allowed for improved sample/ crystal contact and helped significantly reduce the large v(OH) vibration associated with sorbed water which masks the characteristic v(NH) band of PNIPAM at ~3300cm^{-1}. The pure PNIPAM material is also characterised by the amide I band at ~1649 cm^{-1} and amide II band at ~1546 cm^{-1}. For the clay nanocomposites, the band ~1000 cm^{-1} is assignable to the stretching vibration of Si-O in the clay. The intensity of the Si-O band increased with increasing concentration of clay, as expected.

An integrated area plot of the Si-O/ Amide I ratio versus clay content (figure 5.7) shows a linear relationship as predicted by the Beer- Lambert law.
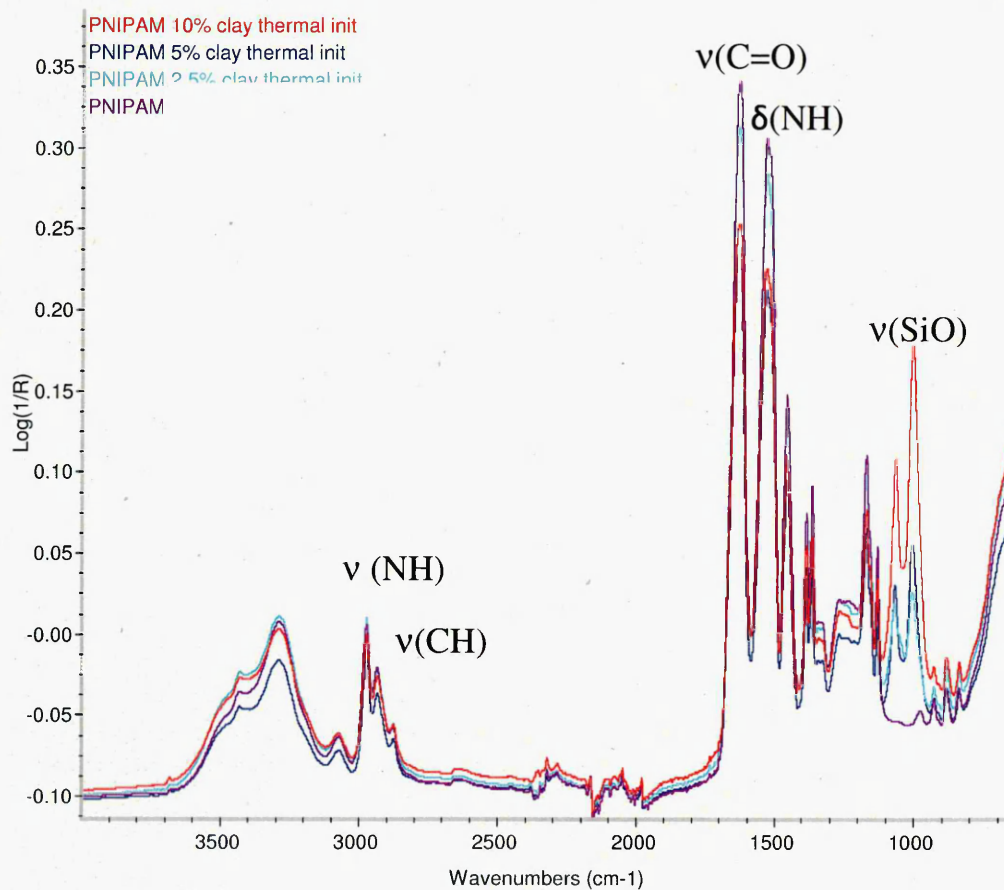
Figure 5.6. FTIR spectra of dry PNIPAM/ clay hydrogels of various clay concentrations.
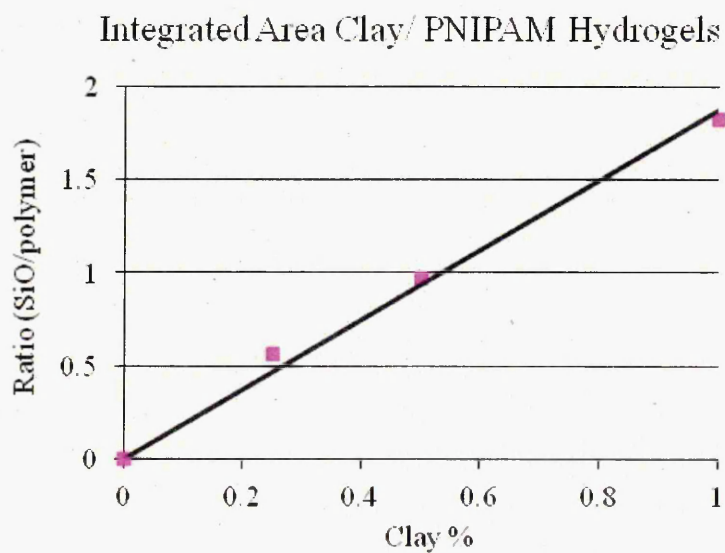
Figure 5.7. An integrated area plot of the Si-O/ polymer FTIR bands of dry Clay/ PNIPAM hydrogels of various clay concentrations.

5.8.2 ATR-FTIR monitoring of the ambient dehydration of various hydrogel formulations.

In this section, the water evaporation dynamics from "pure", gelatine- doped and hyaluronic acid- doped PNIPAM films were studied by following the real- time dehydration of thin films using attenuated total reflectance Fourier- transform infrared spectroscopy (ATR-FTIR). As model systems $1C_{10}$; $1C_{10}G10$ and $1C_{10}HA10$ formulations (see Section 2.2.1.2 of this thesis for precise compositions) were examined. The dynamics of water-polymer interactions in PNIPAM hydrogels have been described in literature [15-17].

5.8.2.1 Conformational states of water molecules in polymers and water movement in polymers

The understanding of water/ polymer interactive behaviour is crucial to the development of behaviour specific polymeric systems, and the "states" of water existing in, evaporating from, and being absorbed into such systems has been of significant interest [18-31]. The presence of a polymer can transform water behaviour, and the association of the two phases (whether physical or chemical) dictates this behaviour.

The general theory of water conformation in polymeric systems involves the division of possible water states into 3 categories [19-26]."Non-freezable bound" water is thought to be associated, through hydrogen bonds, with polar polymeric functional groups. As the name describes, the bonds are very strong and this water is not possible to freeze. "Freezable bound" water exhibits a characteristic lower phase transition temperature than that of bulk or "unbound" water. "Free" or unbound water is thought to exist free of electrostatic influence from the polymer chains. The freezable bound and non-freezable bound water fractions are collectively referred to as the "bound water" content.

Diffusion is the process by which atoms or molecules migrate through space with the absence of a bulk flow. Commonly, the cause of this movement is the presence of a concentration gradient, during which the component concentrations are continually altered until equilibrium is reached [32]. The diffusion of liquids through solids has been of key interest in the field of materials science for more than a century, beginning with the empirical formulation of Fickian diffusion which examines the effect of concentration gradient of a system on the resulting a diffusion flux. Later, Einstein would postulate revolutionary theories regarding the relationship between spontaneous movement of liquids through matter and random molecular movement.

The movement of liquid in polymeric systems have been studied extensively with techniques such as gravimetry [33], dynamic light scattering [34-37], membrane permeation [38-39] fluorescence spectroscopy [40-43], NMR [44-46] and ATR-FTIR [23, 27, 47-49]. The understanding of principles governing these phenomena has led to the development of several theoretical models and enhanced understanding of polymer structure and behaviour. The specifics all of such models are beyond the scope of this thesis but have been reviewed by Masaro et al [50] and Duda [51]. Although the swelling kinetics and behaviour of various hydrogel types have been extensively studied, the availability of information regarding the kinetics of hydrogel dehydration is comparatively poor.

For polymers, the mechanism of dehydration is complex and depends fundamentally on structural parameters such as the reordering of the polymer chains during solute escape (and hence polymer structure and chemistry), the nature and density of cross-links and branches, and the nature and levels of fillers and other additives [31, 52-54].

5.8.2.2 Rate of dehydration measured by attenuated total reflection Fourier transform infrared spectroscopy

Real-time Fourier transform infrared attenuated total reflectance (FTIR-ATR) spectroscopy has proven a convenient, reliable and accurate method to study sorption kinetics in polymers [55]. Unlike data provided by gravimetric methods, FTIR-ATR spectroscopy provides short time data such as time-dependent alterations in local environment for the polymer and penetrant, such as penetrant-polymer and penetrant-penetrant hydrogen bonding [56].

Barbari et al showed that diffusion coefficients for polymers obtained from FTIR-ATR spectroscopy were in good agreement of those measured gravimetrically, lying well within their experimental error [56-57]. It is therefore implied that that diffusion coefficient values obtained gravimetrically can be indicative of those obtained spectroscopically, and vice versa. In ATR measurements, the intensity of absorbance of a particular functional group correlates directly to the concentration of that functional group within the evanescent field. The equivalent relationship in FTIR-ATR spectroscopic experiments is more complex than that of gravimetric data because of the exponential decay of the evanescent field extending into the polymer. Fieldson et al [58] used ATR- FTIR to measure the diffusion of water through polyacrylonitrile, and

devised an equation which allowed the convolution of the evanescent electric wave field [51].

The most common approach of measuring solvent sorption and evaporation in polymers using ATR involves the close adherence of a polymer film to the ATR crystal and presenting a gas or liquid to the exposed side. Despite its numerous advantages associated with ATR monitoring of these systems, sufficient contact can often be difficult to maintain during polymer structural rearrangement and delamination can occur.

5.8.2.3 The data fitting process

In order to obtain diffusion coefficient values with the short term approximation of the Fieldson equation [51] (equation 5.2), data were plotted against the square root of time and the slope of the linear section was calculated by applying a linear trendline to this section.

$$\frac{Mt}{M\infty} = \frac{2}{L}\sqrt{\frac{D}{\pi}}\,\sqrt{t}$$

Equation 5.2

Where M_t is the mass sorbed at time t, M_∞ is the mass sorbed at equilibrium, D is the diffusion coefficient, and L is the sample thickness.

The relationship between the slope of the linear trendline, sample thickness and diffusion coefficient D is given by:

$$m = \frac{2}{L}\sqrt{\frac{D}{\pi}}$$

Equation 5.3

Which can be rearranged to give the diffusion coefficient:

$$D = \pi\left(\frac{mL}{2}\right)^2$$

Equation 5.4

The delay in appearance of structural changes within the evanescent field is derived from the intercept "y" value.

151

5.8.2.4 ATR-FTIR monitoring of the dehydration of 1C10 hydrogels.

A $1C_{10}$ PCPH suspension was synthesised as described in Section 2.2.1.2. 50μl of $1C_{10}$ was pipetted onto the ATR crystal which had been preset to 27°C, and a PTFE mould of exactly 1mm thickness was immediately placed on top. As the PCPH cooled, it undergoes PTTNAG precisely in conformation to the mould depth. After exactly 10 minutes, the mould was removed revealing the disk-shaped hydrogel adhered to the ATR crystal. Data collection was immediately commenced with 64 scans per spectrum at a resolution of $4cm^{-1}$ on a Thermo Nicolet Nexus instrument, and the spectra were ratioed against a single beam spectrum of the clean crystal at 27°C. Using a series setup, a spectrum was taken automatically every 15m for 720m (12h), with all parameters kept constant throughout. Figure 5.8 shows a series of reference spectra of all of the individual components used in the formulations characterised in this section. Figure 5.9 shows a selection of the drying $1C_{10}$ spectra in their entirety, and figures 5.10- 5.13 shows expansions of these spectra to highlight the observable peak intensity changes and peak shifts during the drying process.
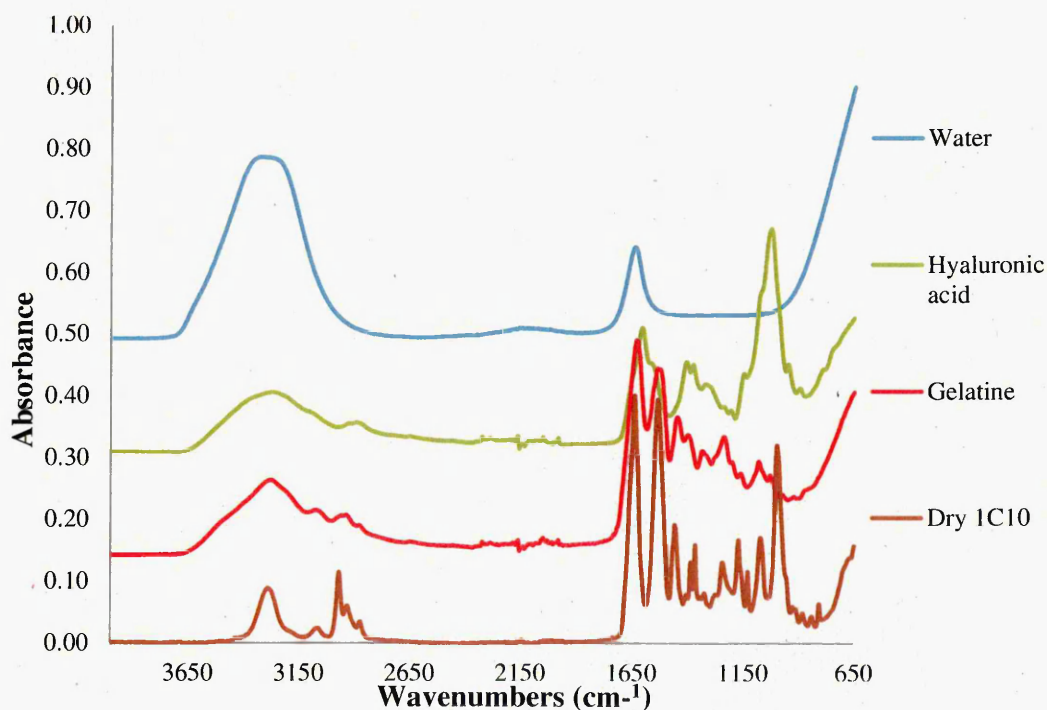
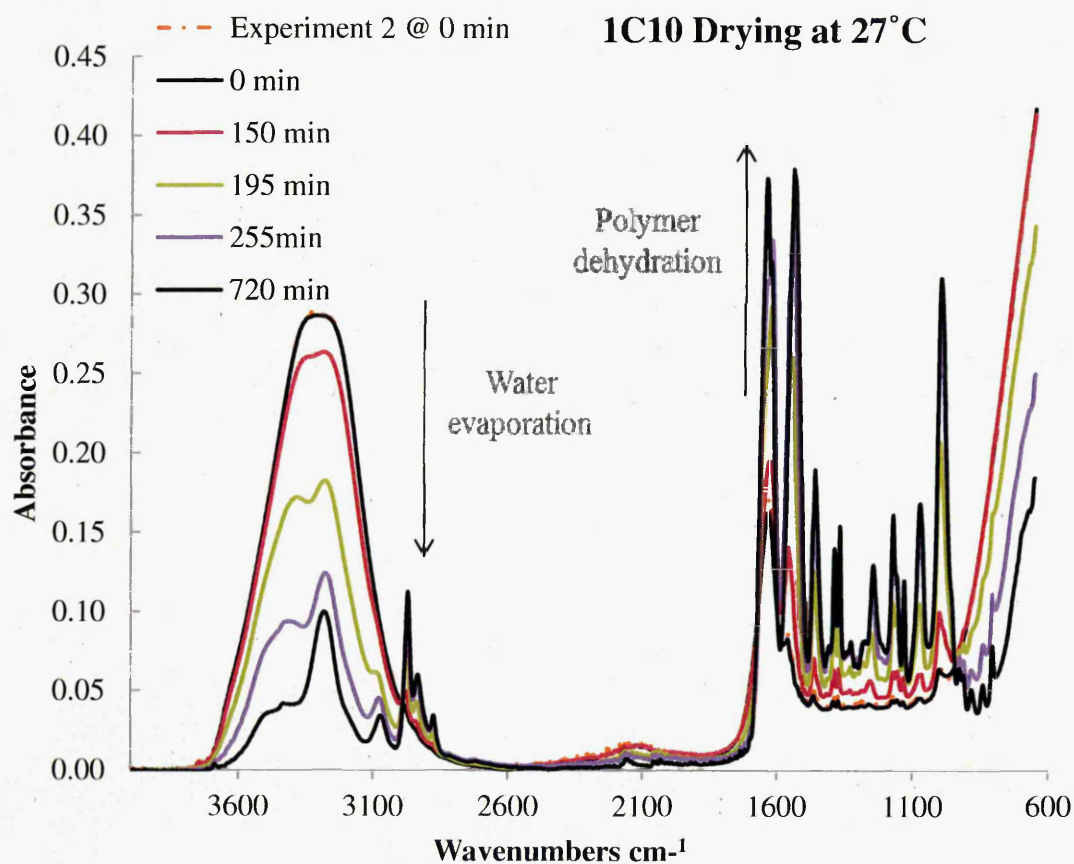**Figure 5.8. Reference spectra of water, hyaluronic acid, gelatine and dry $1C_{10}$ taken at 27°C.**

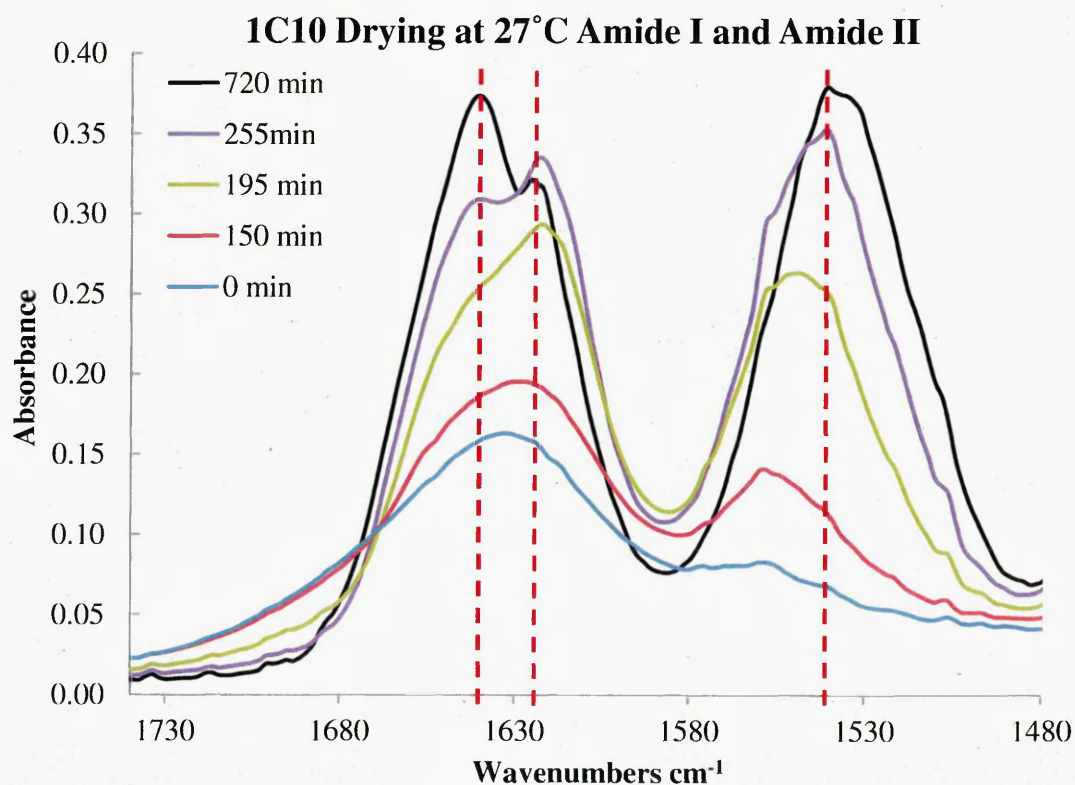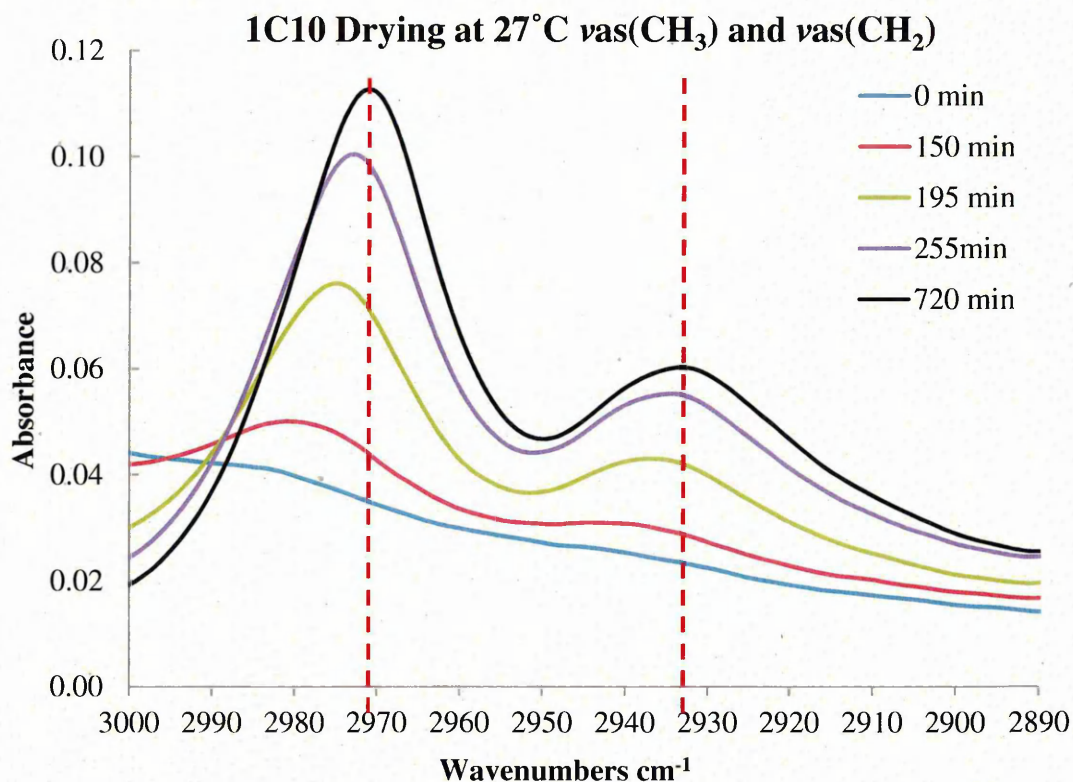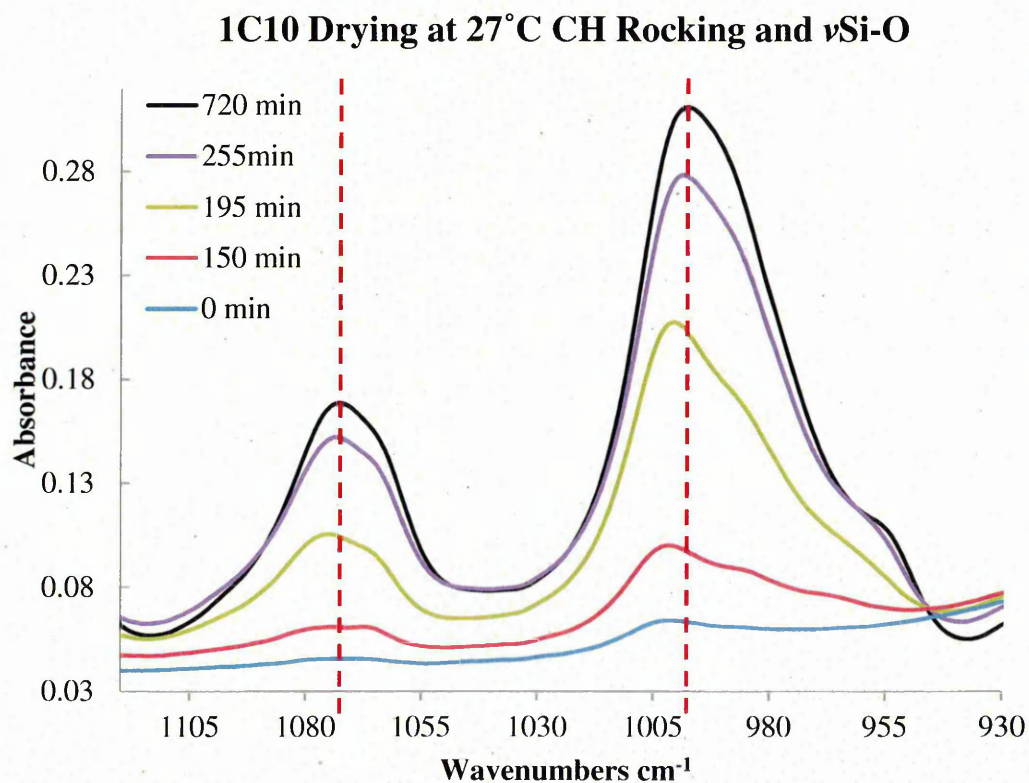**Figure 5.9. Full spectra of water evaporating from a 1C$_{10}$ hydrogel at 27˚C.**

Figure 5.10. Amide I and Amide II spectral bands (from left to right) taken during the drying of a 1C$_{10}$ hydrogel at 27˚C.
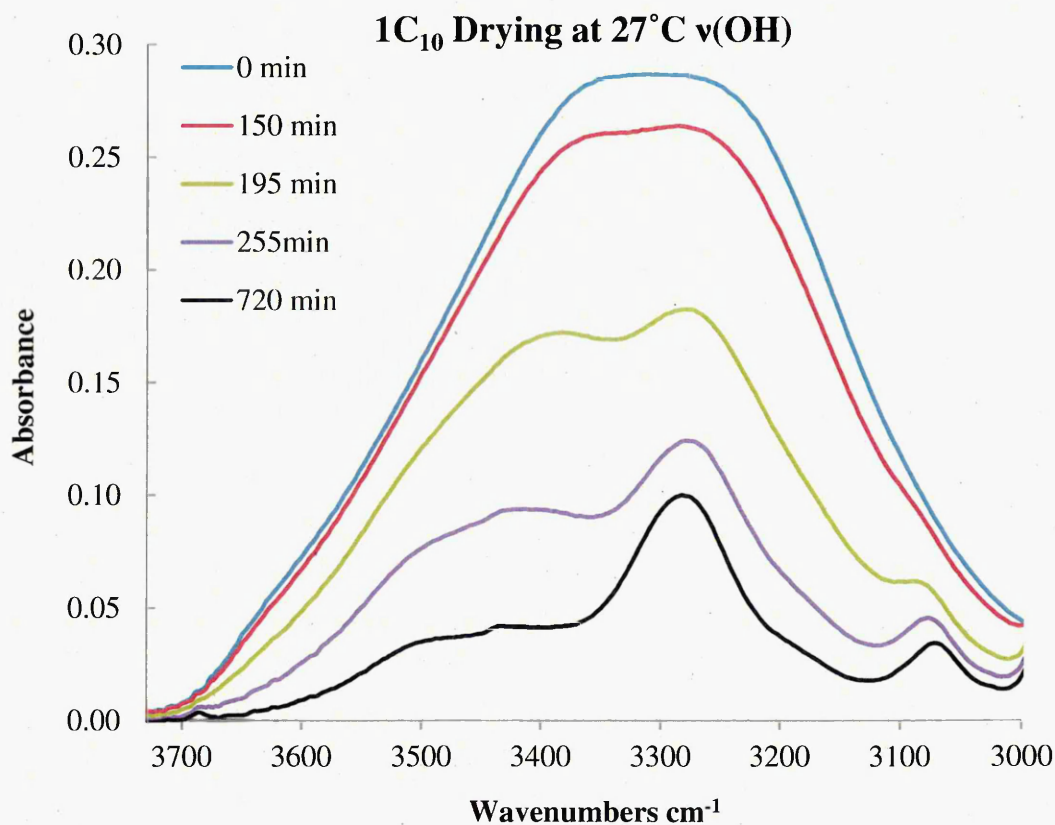
Figure 5.11. $\nu_{as}(CH_3)$ and $\nu_{as}(CH_2)$ spectral bands (from left to right) taken during the drying of a $1C_{10}$ hydrogel at 27˚C.
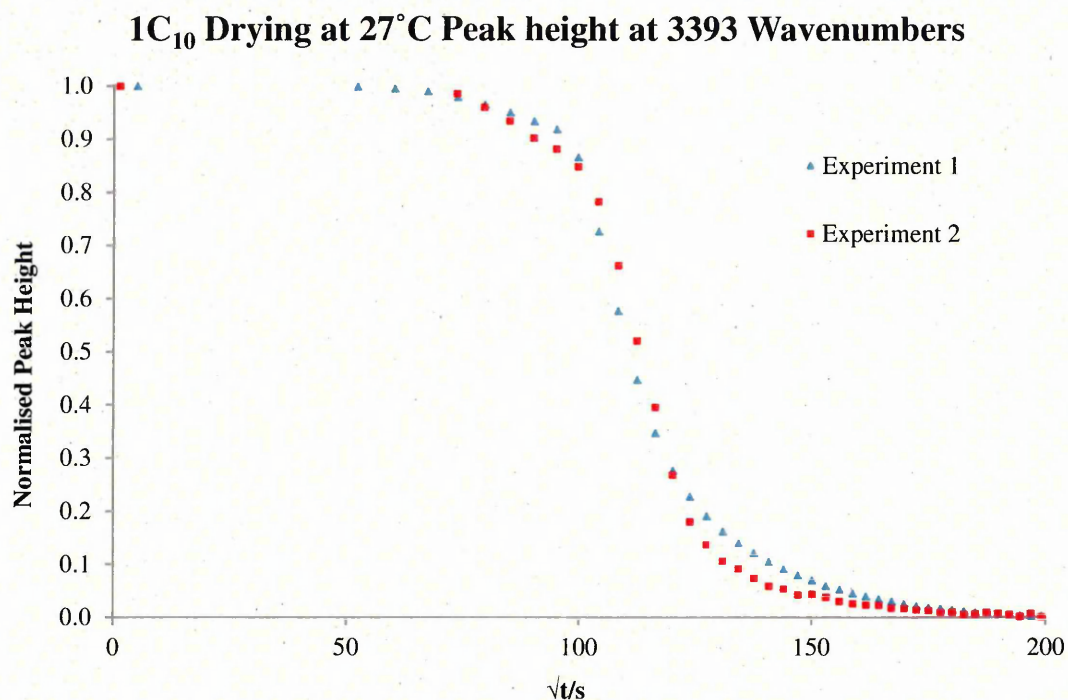

Figure 5.12. CH Rocking and $\nu(Si\text{-}O)$ spectral bands (from left to right) taken during the drying of a $1C_{10}$ hydrogel at 27˚C.

154

Table 5.3. Observed IR frequencies and assignments of a $1C_{10}$ hydrogel disc after 0min and 720min drying at 27 °C.
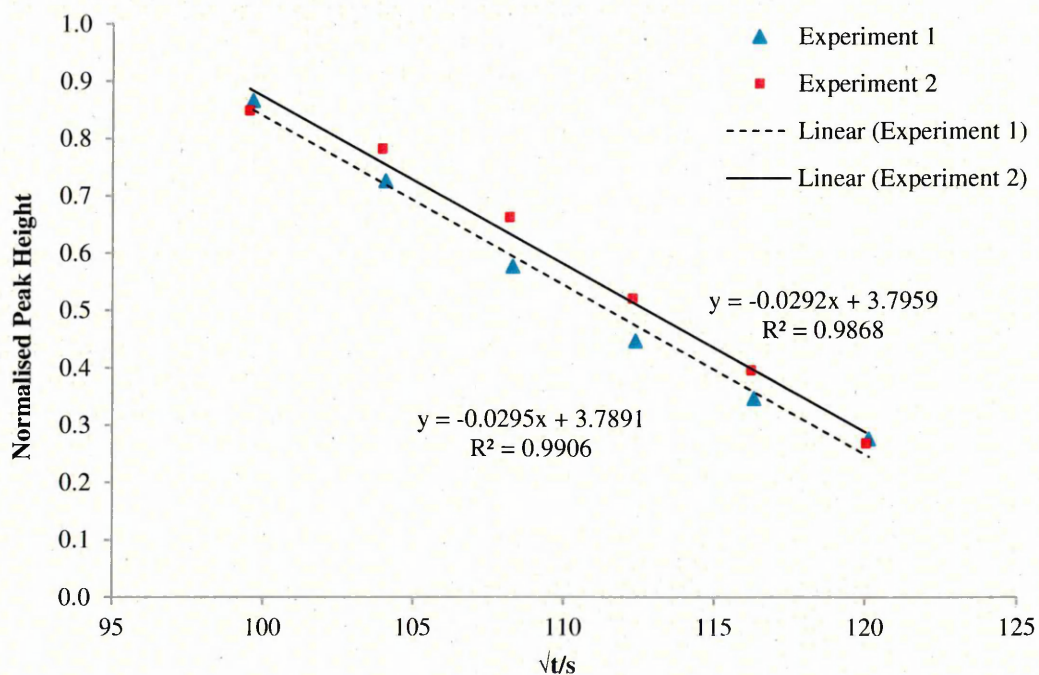
Assignment	Frequency/ cm^{-1}		Wavenumber shift cm^{-1}
	0 min	720 min	
H- bonded Amide I	1633	1639	+6
Amide I	1633	1622	-11
Amide II	1556	1541	-15
$v_{as}(CH_3)$	2981	2972	-9
$v_{as}(CH_2)$	2939	2933	-6
CH Rocking	1078	1072	-6
$v(Si-O)$	1001	999	-2

Figure 5.13. v(OH) (3700-300cm^{-1}) and v(OH) with visible v(NH) (3270cm^{-1}) taken during the drying of a $1C_{10}$ hydrogel at 27°C.

1C$_{10}$ Drying at 27°C Peak height at 3393 Wavenumbers

Figure 5.14.Kinetic profile of evaporation of water from a 1C$_{10}$ hydrogel into the atmosphere as a function of √time.

$$y = -0.0292x + 3.7959$$
$$R^2 = 0.9868$$

$$y = -0.0295x + 3.7891$$
$$R^2 = 0.9906$$

Figure 5.15. Kinetic profile of evaporation of water from a 1C$_{10}$ hydrogel into the atmosphere as a function of √time, including intercept "Y" and R^2.

156

Table 5.4. Diffusion coefficient "D" and intercept values obtained for the drying of $1C_{10}$.

|	Sample Thickness (cm)	Intercept	D value $(cm_2 \ s^{-1})$
Experiment 1	0.009	128.3	1.26E-04
Experiment 2	0.009	129.6	1.28E-04

5.8.2.5 ATR-FTIR monitoring of the dehydration of 1C10G10 hydrogels.

A $1C_{10}G10$ PCPH suspension was synthesised as described in section 2.1.1.3.2. 50μl of $1C_{10}$ was pipetted onto the ATR crystal which had been preset to 27°C, and a PTFE mould of exactly 1mm thickness was immediately placed on top. As the PCPH cooled, it undergoes PTTNAG precisely in conformation to the mould depth. After exactly 10 minutes, the mould was removed revealing the disk-shaped hydrogel adhered to the ATR crystal. Data collection was immediately commenced with 64 scans per spectrum at a resolution of $4cm^{-1}$ on a Thermo Nicolet Nexus instrument, and the spectra were ratioed against a single beam spectrum of the clean crystal at 27°C. Using a series setup, a spectrum was taken automatically every 15m for 720m (12h), with all parameters kept constant throughout. Figure 5.8 shows a series of reference spectra of all of the individual components used in the formulations characterised in this section. Figure 5.16 shows a selection of the drying $1C_{10}G10$ spectra in their entirety, and figures 5.17-5.19 shows expansions of these spectra to highlight the observable peak intensity changes and peak shifts during the drying process.
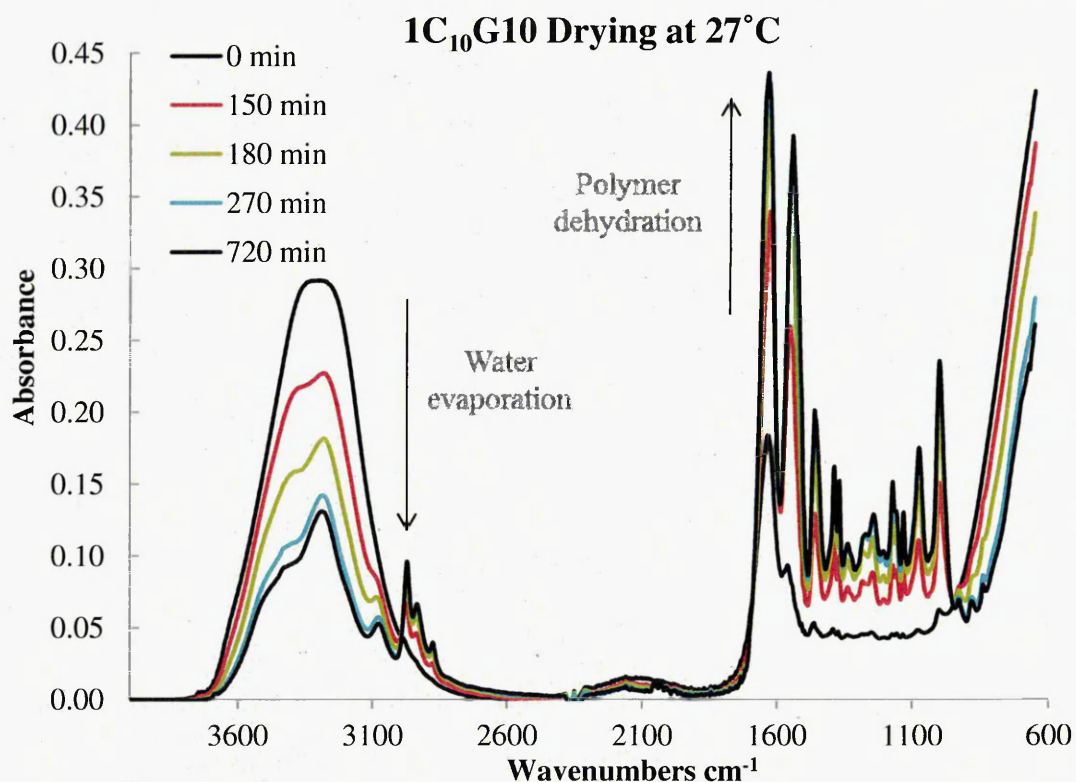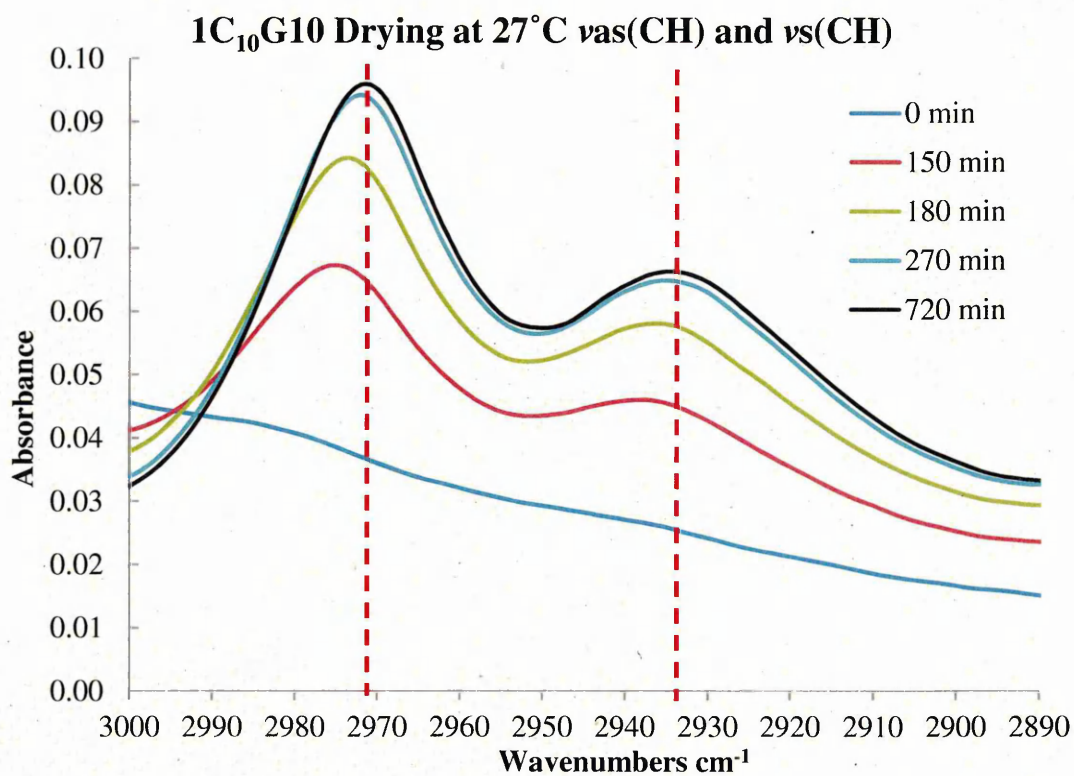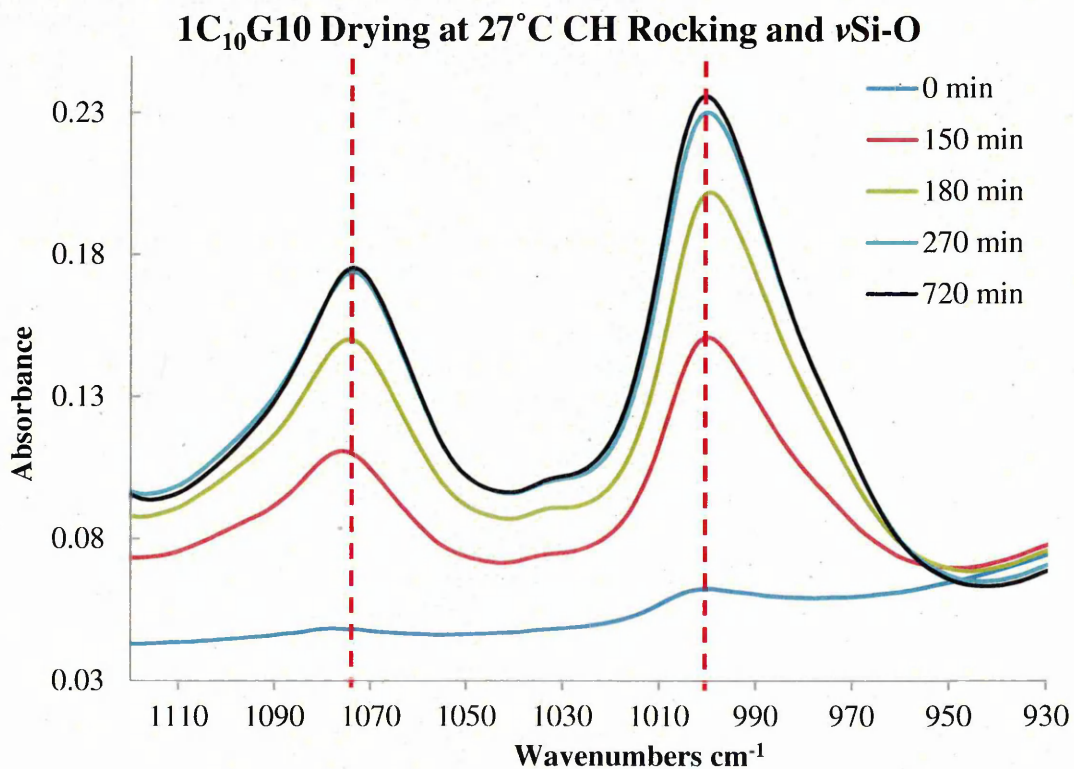
Figure 5.16. Full spectra of water evaporating from a $1C_{10}G10$ hydrogel at 27°C.
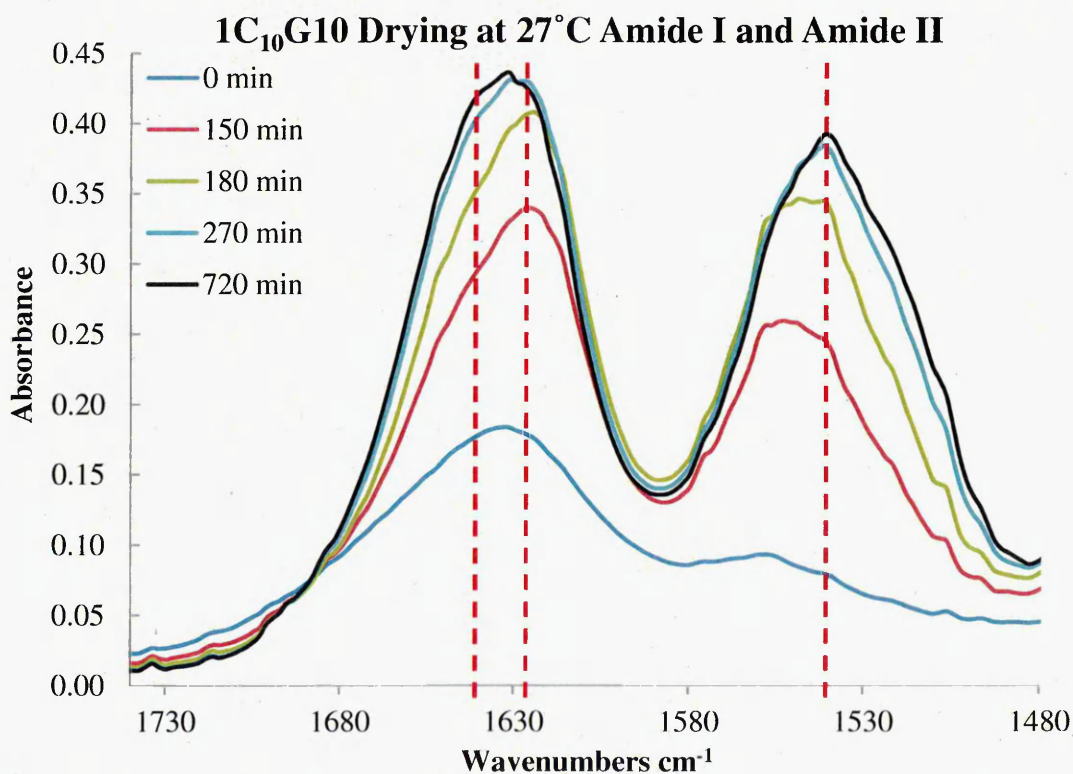
Figure 5.17 Amide I and Amide II spectral bands (from left to right) taken during the drying of a $1C_{10}G10$ hydrogel at 27°C.

158

Figure 5.18. $\nu_{as}(CH_3)$ and $\nu_{as}(CH_2)$ spectral bands (from left to right) taken during the drying of a $1C_{10}G10$ hydrogel at 27°C.

Figure 5.19. CH Rocking and $\nu(Si\text{-}O)$ spectral bands (from left to right) taken during the drying of a $1C_{10}G10$ hydrogel at 27°C.

Table 5.5. Observed IR frequencies and assignments of a 1C$_{10}$G10 hydrogel disc after 0min and 720min drying at 27 °C.

Assignment	Frequency/ cm^{-1}		Wavenumber shift cm^{-1}
	0 min	720 min	
H- Bonded Amide I	1633	1639	+6
Amide I	1633	1628	-5
Amide II	1556	1540	-16
$\nu_{as}(CH_3)$	2980	2972	-8
$\nu_{as}(CH_2)$	2939	2933	-6
CH Rocking	1078	1072	-6
$\nu(Si\text{-}O)$	1001	999	-2
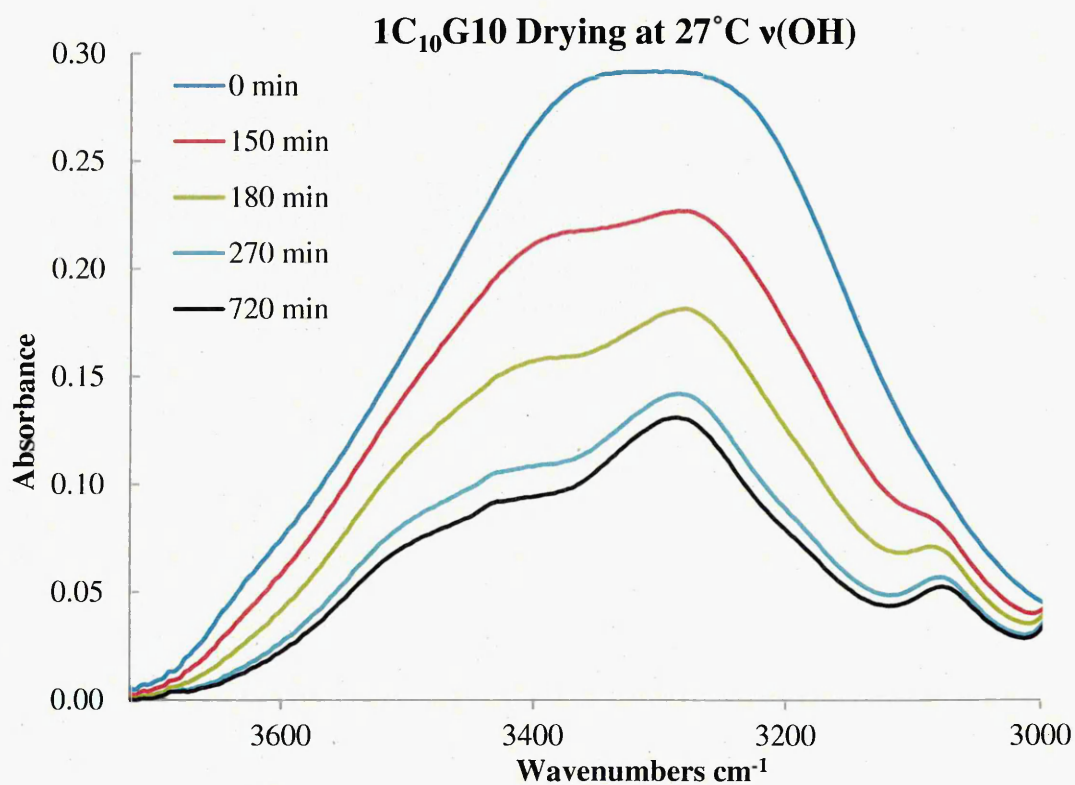
Figure 5.20. ν(OH) (3700-300cm^{-1}) and ν(OH) with visible ν(NH) (3270cm^{-1}) taken during the drying of a 1C$_{10}$G10 hydrogel at 27°C.

160

1C$_{10}$G10 Drying at 27°C Peak height at 3393 Wavenumbers
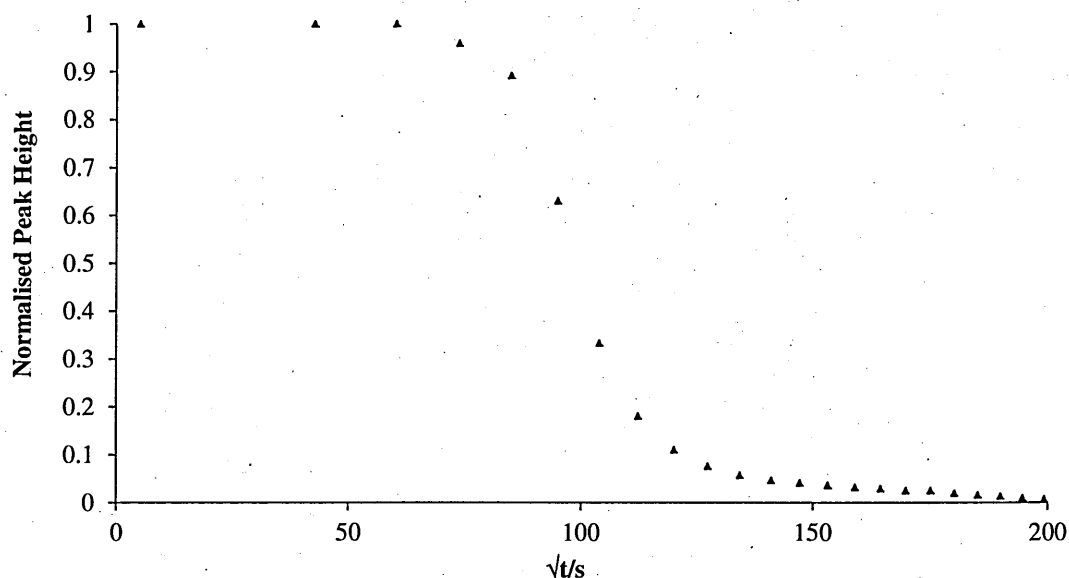
Figure 5.21. Kinetic profile of evaporation of water from a 1C$_{10}$G10 hydrogel into the atmosphere as a function of √time.

$$y = -0.0267x + 3.1514$$
$$R^2 = 0.9907$$
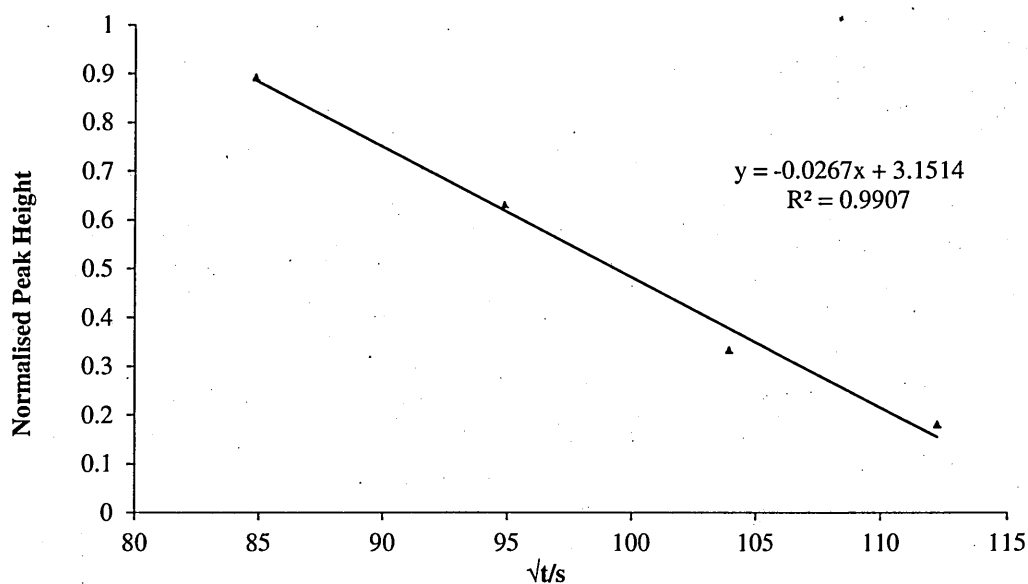
Figure 5.22. Kinetic profile of evaporation of water from a 1C$_{10}$G10 hydrogel into the atmosphere as a function of √time, including intercept "Y" and R^2.

Table 5.6. Diffusion coefficient "D" and intercept values obtained for the drying of 1C$_{10}$G10.

	Sample Thickness (cm)	Intercept	D value (cm$_2$ s^{-1})
Experiment 1	0.012	117.9	2.35E-04

5.8.2.6   ATR-FTIR monitoring of the dehydration of 1C10HA10 hydrogels.

A 1C$_{10}$HA10 PCPH suspension was synthesised as described in section 2.1.1.4.2. 50µl of 1C$_{10}$ was pipetted onto the ATR crystal which had been preset to 27°C, and a PTFE mould of exactly 1mm thickness was immediately placed on top. As the PCPH cools, it undergoes PTTNAG in conformation to the mould depth. After exactly 10 minutes, the mould was removed revealing the disk-shaped hydrogel adhered to the ATR crystal. Data collection was immediately commenced with 64 scans per spectrum at a resolution of 4cm^{-1} on a Thermo Nicolet Nexus instrument, and the spectra were ratioed against a single beam spectrum of the clean crystal at 27°C. Using a series setup, a spectrum was taken automatically every 15m for 720m (12h), with all parameters kept constant throughout. Figure 5.8 shows a series of reference spectra of all of the individual components used in the formulations characterised in this section. Figure 5.23 shows a selection of the drying 1C$_{10}$HA10 spectra in their entirety, and figures 5.24- 5.26 shows expansions of these spectra to highlight the observable peak intensity changes and peak shifts during the drying process.
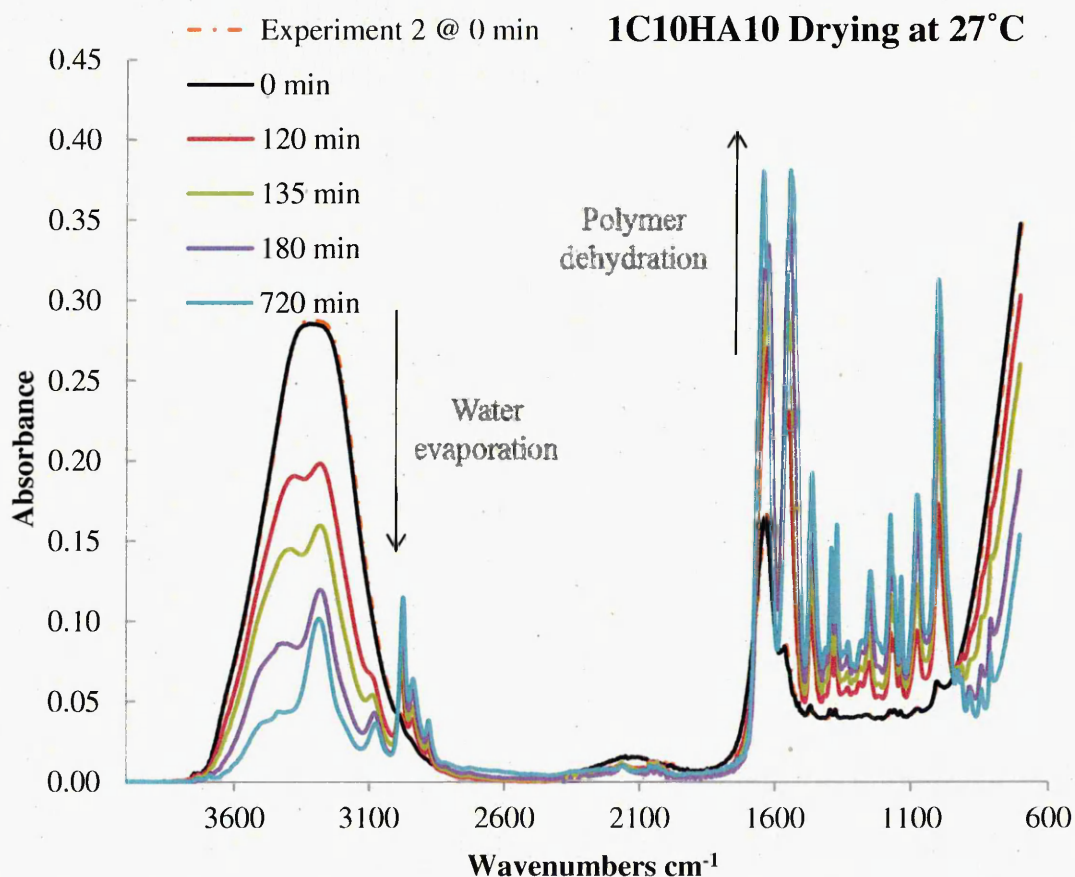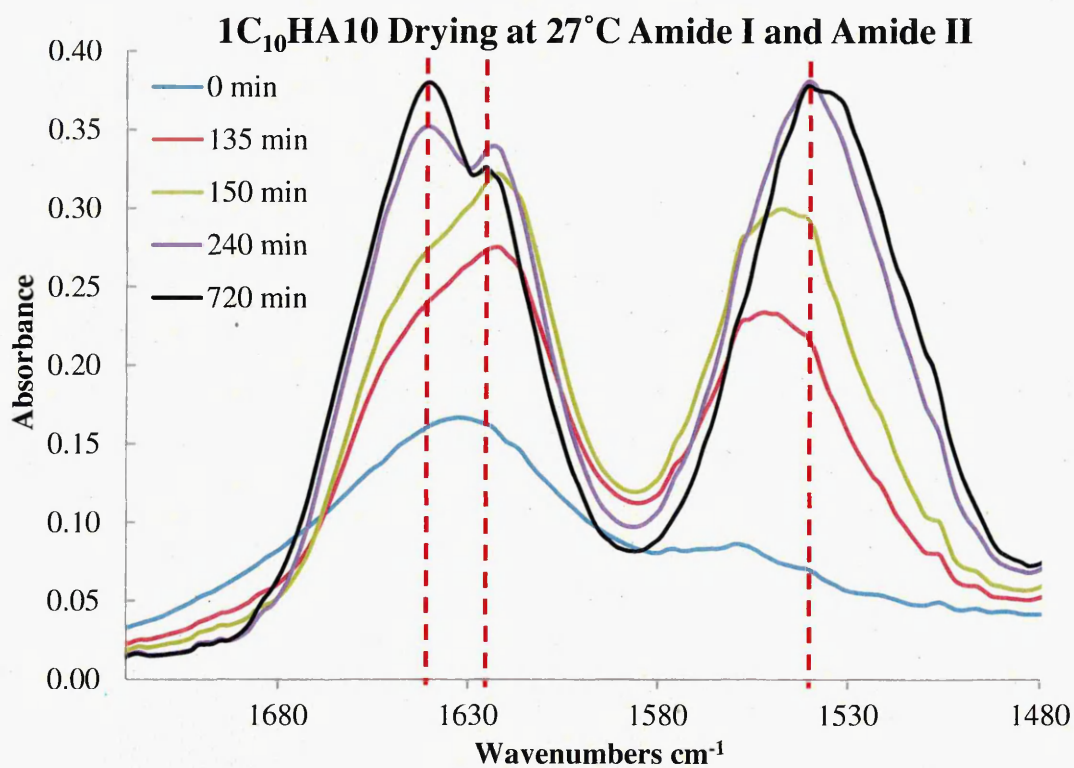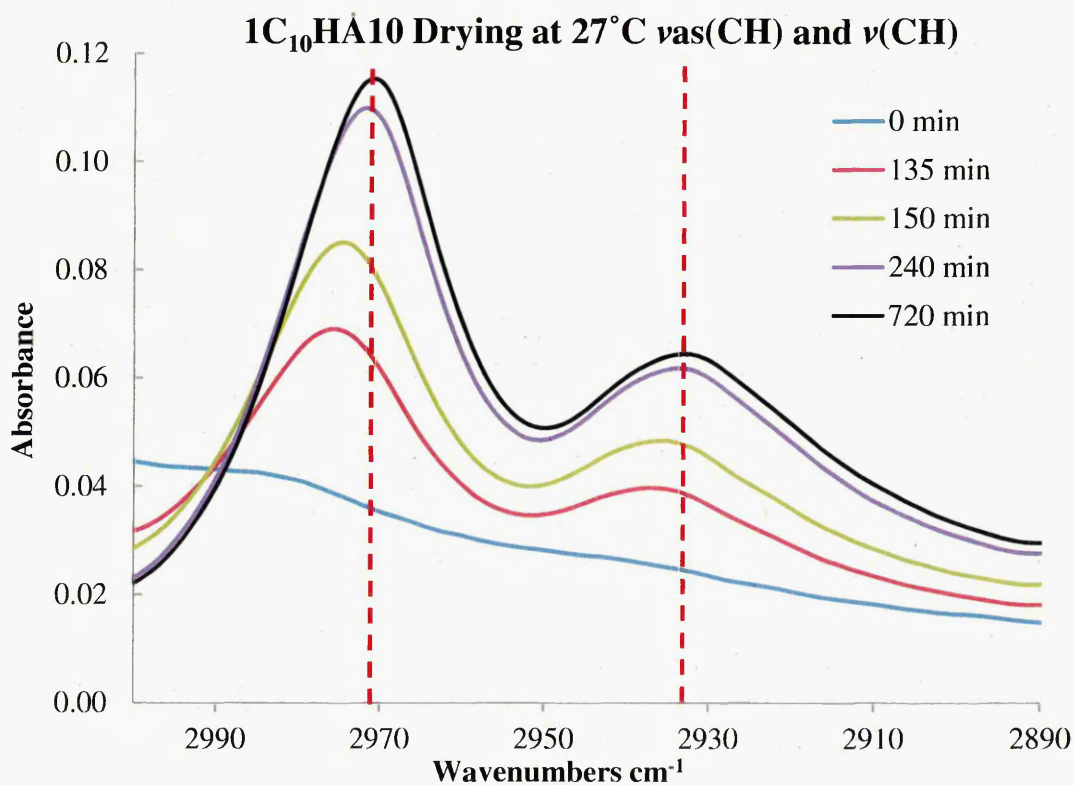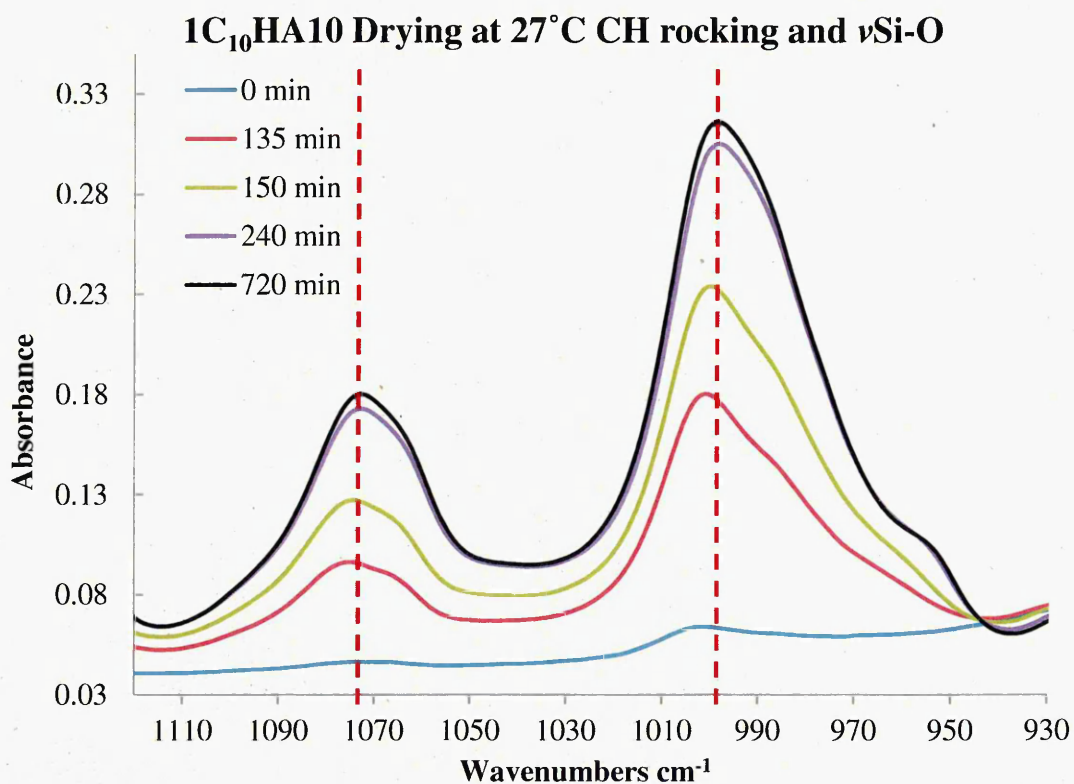

Figure 5.23. Full spectra of water evaporating from a 1C$_{10}$HA10 hydrogel at 27°C.

Figure 5.24. Amide I and Amide II spectral bands (from left to right) taken during the drying of a 1C$_{10}$HA10 hydrogel at 27°C.

Figure 5.25. v_{as}(CH$_3$) and v_{as}(CH$_2$) spectral bands (from left to right) taken during the drying of a 1C$_{10}$HA10 hydrogel at 27°C.

163

Figure 5.26. CH Rocking and v(Si-O) spectral bands (from left to right) taken during the drying of a 1C$_{10}$HA10 hydrogel at 27˚C.

Table 5.7. Observed IR frequencies and assignments of a 1C$_{10}$HA10 hydrogel disc after 0min and 720min drying at 27 ºC.

Assignment	Frequency/ cm^{-1}		
	0 min	720 min	Wavenumber shift cm^{-1}
H- Bonded Amide I	1633	1639	+6
Amide I	1633	1628	-5
Amide II	1558	1541	-17
v_{as}(CH$_3$)	2981	2974	-8
v_{as}(CH$_2$)	2939	2935	-4
CH Rocking	1078	1076	-2
v(Si-O)	1004	1001	-3
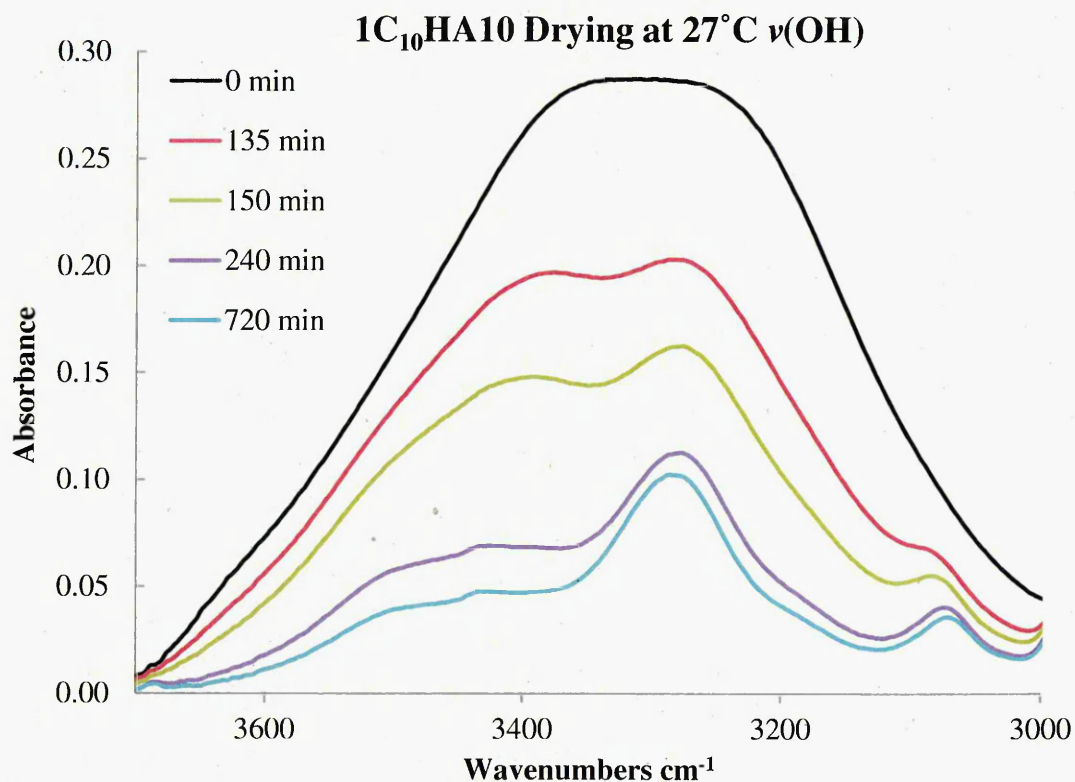
Figure 5.27. $v(OH)$ (3700-300cm^{-1}) and $v(OH)$ with visible $v(NH)$ (3270cm^{-1}) taken during the drying of a 1C$_{10}$HA10 hydrogel at 27°C.
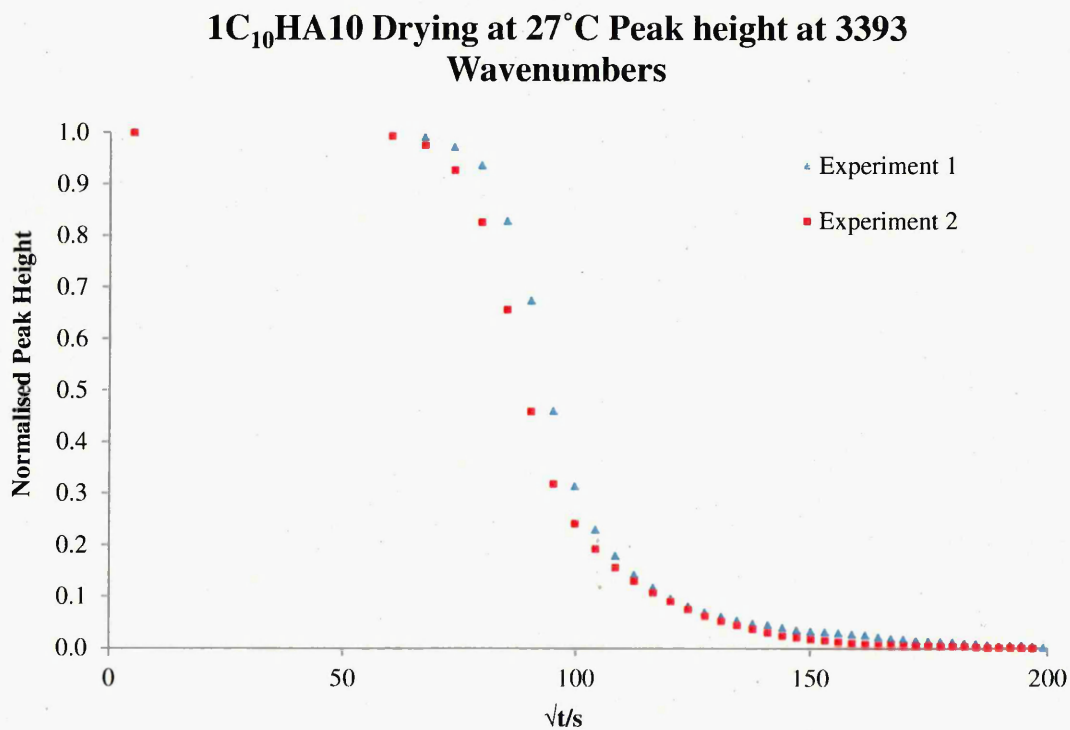
Figure 5.28. Kinetic profile of evaporation of water from a 1C$_{10}$HA10 hydrogel into the atmosphere as a function of √time.
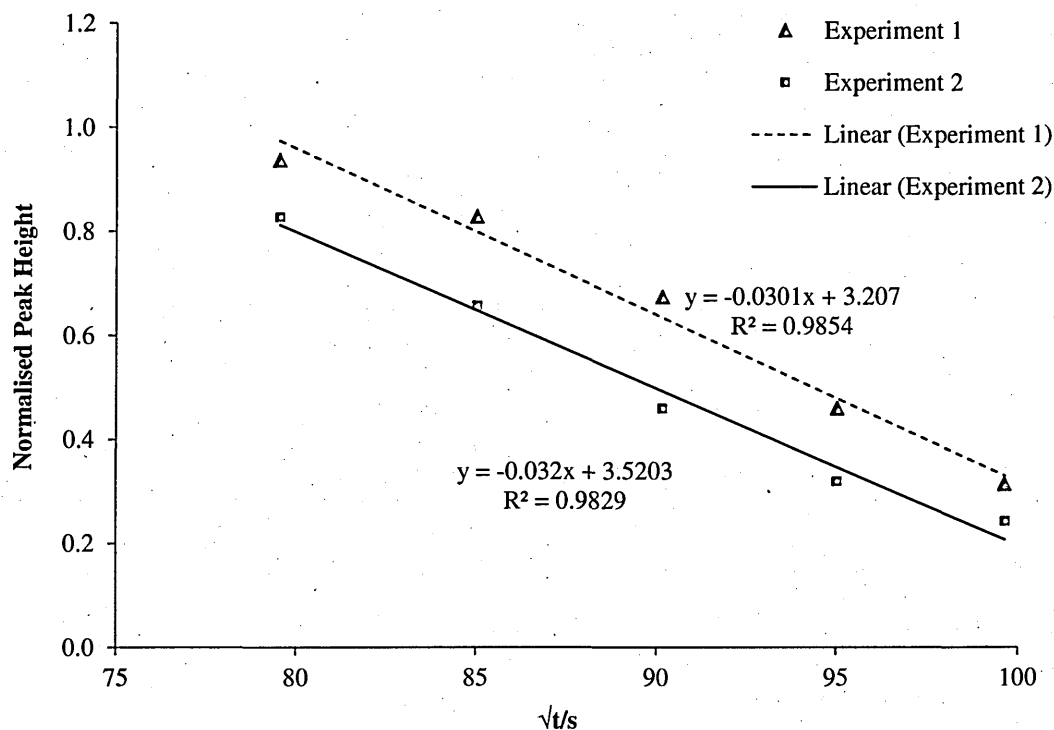
Figure 5.29. Kinetic profile of evaporation of water from a $1C_{10}HA10$ hydrogel into the atmosphere as a function of √time, including intercept "Y" and R^2.

Table 5.8. Diffusion coefficient "D" and intercept values obtained for the drying of $1C_{10}HA10$.

	Sample Thickness (cm)	Intercept	D value (cm$_2$ s^{-1})
Experiment 1	0.011	109.60	1.84E-04
Experiment 2	0.011	106.27	1.79E-04

5.8.2.7 Discussion

The objective of this study was to monitor in real time the evaporation of the aqueous solvent from the PNIPAM- based hydrogels. Several experimental attempts were made for each formulation; and the data sets shown are those for which the starting spectra were near identical, making the data directly comparable. For the $1C_{10}G10$ formulation, for which the data is presented in section 5.8.2.5, only a single experiment endured to completion without delamination occurring. Typically, in the case of $1C_{10}G10$ formulations, contact was lost between sample and crystal between 3-6 hours. Delamination of other formulations during drying was also commonplace, typically occurring at 8-10 hours. Due to the post-drying treatment of the samples required for further analysis, the samples used to collect the data could not be removed in order to

166

obtain exact sample thickness. The thickness was approximated by allowing the drying of 3 separate samples of identical dimensions and composition and under the same conditions as those analysed, and recording an average thickness across the sample centre. The thicknesses were consistent in all cases with an error of +/- .003mm or less.

Hydrogen bonding as a result of hydration principally occurs at electronegative atoms on polar groups, e.g. the oxygen atoms of hydroxyl and carbonyl groups and nitrogen atoms of amino groups. In general terms, a change in hydrogen bond strength is observable in ATR-FTIR spectra as spectral "shifting" of the corresponding band; repulsive forces shift the band to higher wavenumbers, and attractive forces shift the band to lower wavenumbers [18].

Tables 5.3, 5.5 and 5.7 give the characteristic peak wavenumbers and spectral shifts during the dehydration of $1C_{10}$, $1C_{10}G10$ and $1C_{10}HA10$ formulations, respectively. The main spectroscopic changes observable for spectra shown for all formulations in this study are changes in intensity and band position associated with the polymer and water. These can be associated directly to the redistribution of water molecules during dehydration. In all cases, "Free" or "unbound" water will escape first, leaving increasing proportions of bound and unfreezable water classes, thus inducing negative band shifts. As the density of the hydrogel increases and water vaporises from the gel surface, the number of attractive interactions between hydrophobic groups (hydrophobic polymer-polymer interactions) also increases [59]. Su et al found that the $v_{as}(CH_3)$ at $2981cm^{-1}$ is particularly sensitive to hydrophobic interactions in PPO-PEO copolymer systems [60], and records a wavenumber shift of $\sim 10cm^{-1}$. In this data collected for all 3 formulations, wavenumber shifts of 8- $9cm^{-1}$ strongly supports the hydrophobic-hydrophobic interactive theory during the drying of our polymers. This can almost certainly be attributed to the close methyl-methyl group proximities during polymer dehydration.

The peak of the Amide I (C=O) vibration at $1633cm^{-1}$ is expected to shift toward a lower wavenumber upon hydration due to an increase in hydrogen bonding hydration and to a higher wavenumber upon dehydration. Observable in this data is the apparent peak splitting of this band during the drying of all formulations, indicative of the formation of 2 carbonyl populations - one "free" and one strongly hydrogen-bonded to water. This manifests itself as an apparent positive shift of the free population and negative shift of the hydrogen-bound populations. The peak centre of the hydrated carbonylgroup is $\sim 1639cm^{-1}$ and that of the free group is $\sim 1628cm^{-1}$. The magnitude of

167

this difference (11cm^{-1}) is very similar to that observed by Iwamoto *et al* [30] during the drying of Nylon 6, who recorded a carbonyl split of 13cm^{-1} during the dry air purge of a thin Nylon-6 film.

All other band shifts in all spectra are negative, indicative of increasing prevalence of stronger hydrogen bond interactions at all spectroscopically visible hydrogen-bonding loci.

Figures 5.13, 5.20 and 5.27 show the v(OH) of spectra between 0 and 720min as the 1C$_{10}$, 1C$_{10}$G10 and 1C$_{10}$HA10 formulations dry at 27°C, respectively. The peak height at 3393 wavenumbers (chosen for its non-interference from the v(NH) at 3270cm^{-1}) was plotted against the square-root of time, and this typical dehydration curve is shown in figures 5.14, 5.21 and 5.28 , respectively. Expansion of the linear slope together with the corresponding y and R^2 values are given in figures 5.15, 5.22 and 5.28. Pseudo diffusion coefficients were obtained from the short time approximation of Fickian diffusion detailed in section 5.8.2.3, and are given in tables 5.4, 5.6 and 5.8. Also included in these tables are the intercept values obtained during the data-fit process. Values obtained for the slope of drying are not significantly different between data sets and therefore replacing a percentage of PNIPAM / clay within the systems with either gelatine or HA solution does not affect the rate at which water evaporates from the evanescent field. Interestingly, values obtained for the y *intercepts* (the point at which the trendline crosses the y axis) do show significant variation between data sets. The linear drying slope during the drying of 1C$_{10}$ gels occurs between 165-240 minutes, that of 1C$_{10}$G10 occurs between 120-210 minutes and that obtained for 1C10HA10 gels occurs between 105- 165 minutes, and giving average intercepts of 128.95, 117.9 and107.94 respectively. A similar effect was observed by Muthudoss [29] who, using ATR-FTIR recorded similar D values within data-sets, yet simultaneous temperature-dependent intercept shifts during the evaporation of various solvents from solid pharmaceutical dispersions. Since the vibrational spectra represent the molecular constituents and interactions within the evanescent field (dp is in the order of 1-2µm at 1000 cm^{-1}, and because of the wavelength dependence the penetration depth increases by a factor of 10 between 4000 and 400 cm^{-1}), the "delay" in evaporation time can be attributed to the restriction of interstitial water escape from regions within a few µm of the crystal surface during the drying process. Tables 3.1, 3.4 and 3.5 give the precise compositions of the respective gels. The comparatively faster water loss from HA and gelatine-doped gels could be partly due not only to their more loosely-crosslinked
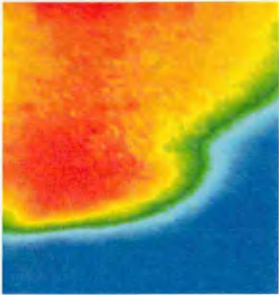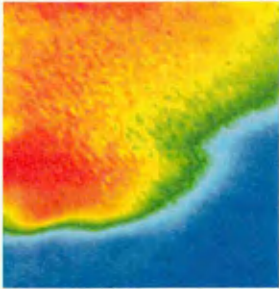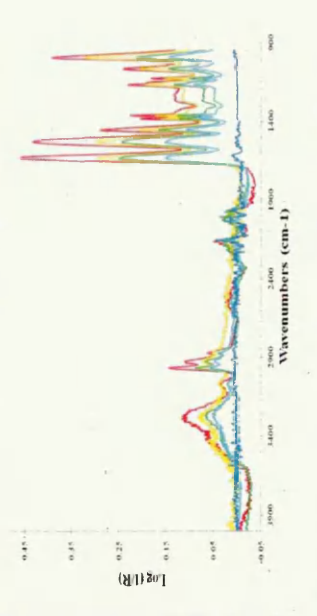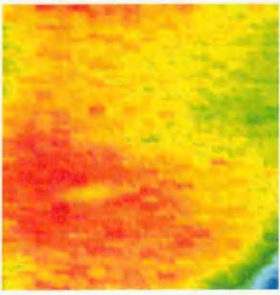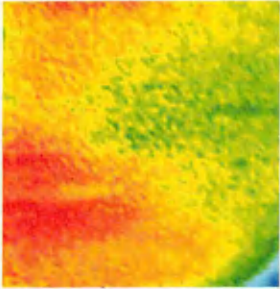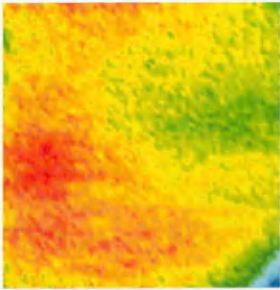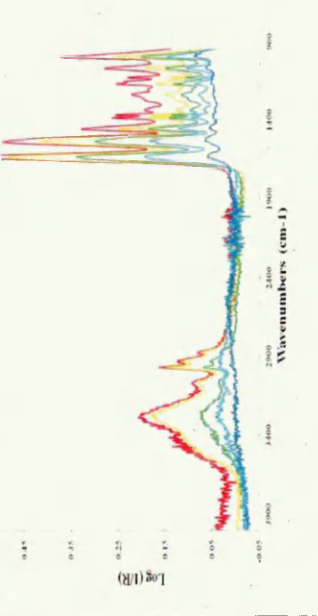
structure (as they both contain 10% less clay than their $1C_{10}$ counterpart), but because of the fact that the clay itself is very hydrophilic and highly swellable in nature [61]. A looser polymer matrix in addition to a lower quantity of clay-bound water could feasibly assist the dehydration process of the doped systems. HA-doped gels reach a maximum dehydration rate faster than those doped with gelatine, despite an identical clay concentration. This observation could be attributed to the higher water content of the former (90.8%) compared to the latter (86%), which in turn will incur larger interstitial "unbound" water-filled spaces. Tentative conclusions require further experiments and generation of statistical error data in order to draw more reliable and scientifically-sound conclusions, however.

5.8.3   ATR-FTIR imaging of doped PNIPAM/ clay nanocomposites.
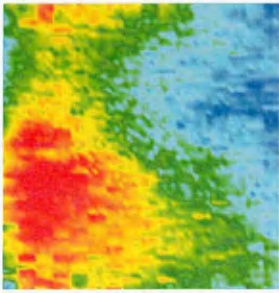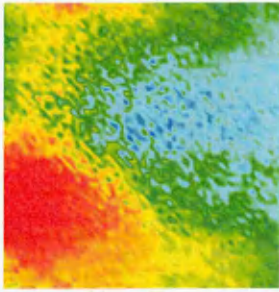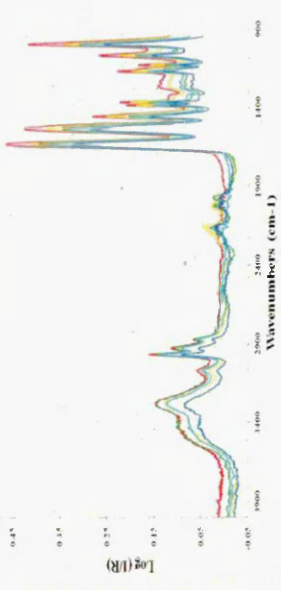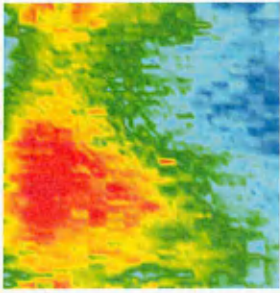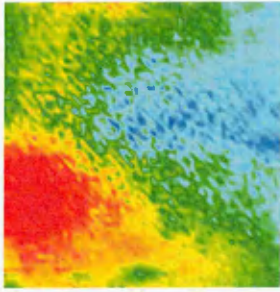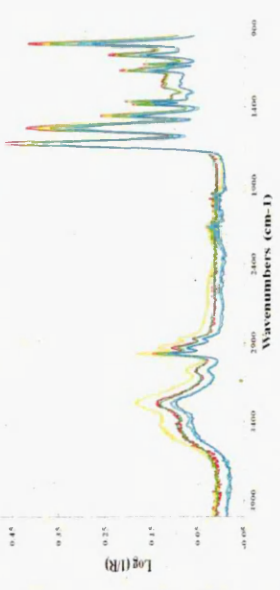
Commonly, and as described in sections 5.8.1 and 5.8.2, ATR- FTIR spectroscopy is carried out on a single sample surface point which is determined to be chemically indicative of the whole sample under observation. In certain cases however, such as polymer blends or layer interfaces, chemical data are required in a spatial or lateral (2-dimensional) context. Imaging ATR-FTIR is a relatively recent alternative approach to conventional ATR-FTIR as it offers the ability to achieve simultaneous multiple laterally resolved spectra using a focal plane array detector. The technique allows images to be generated which show the distribution of a specific peak area or intensity, peak area or intensity ratio or more complex principal component analysis, whivh in turn is related to the distribution a particular component within the system. FTIR relies on the characteristic absorbance of corresponding molecular vibrations in a sample and therefore does not require any labelling methods or dyes in order to visualise separate chemical components within a sample. Each pixel of the spatially resolved chemical image is re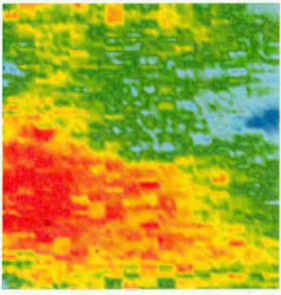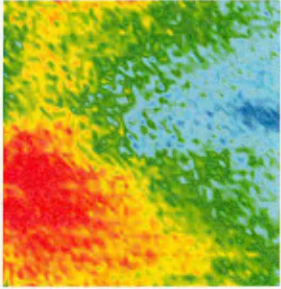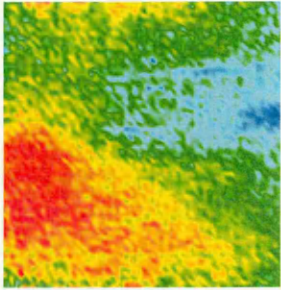presentative of a single data point and are coloured according an arbitary scale depending on the numerical value assigned to them by the image generation method used.

The technique was chosen to determine the spatial distribution of PNIPAM, clay and dopant species separately within the doped PCPH gels in order to investigate domains within the systems. For these experiments, the samples were prepared as described in sections3.3, table 2.1, section 2.1.1.3.2, table 2.2, section 2.1.1.4.2 and table 2.3. A thin (~300µm) layer of each sample was cast onto a metal substrate and allowed to dry at room temperature. The samples were carefully removed from the substrate and placed

onto the diamond ATR crystal. Since the technique requires the sample to be in optical contact with the crystal, controlled pressure was applied to the sample. Each spectrum was collected by accumulating 128 scans at a resolution of 4 cm^{-1}, and the images, along with their constituent spectra are shown in figures 3.9 and 3.10. The image field of view was 640 x 640µm, and the measured spatial resolution was 18µm.

Figure 5.30. ATR-FTIR images of air-dried $1C_{10}$ control, $1C_{10}G10$ and $1C_{10}G20$ polymer films and some of some typical constituent spectra, taken at room temperature. The images show the corresponding peak areas for characteristic PNIPAM, clay and gelatine bands, respectively. The spectra (right) indicate that a variation in peak height across the images are attributed to differences in quality of sample/ crystal contact and all samples possess good homogeneity of all components.

171

Sample	PNIPAM	Clay	HA	Raw Data
a) 1C$_{10}$HA10			N/A	
b) 1C$_{10}$HA20			N/A	

Figure 5.31. ATR-FTIR images of air-dried 1C$_{10}$HA10 and 1C$_{10}$HA20 polymer films and some of some typical constituent spectra, taken at room temperature. Since no characteristic HA band could be found, the images show the corresponding peak areas for characteristic PNIPAM and clay bands. The spectra (right) indicate that a variation in peak height across the images are attributed to slight variation in quality of sample/ crystal contact and all samples possess good homogeneity of both components. With the absence of and polymer/ clay "voids" within the images, it was deduced that the HA must also me homogeneously distributed within the system.

172

Images were constructed based on the area of the $\delta(CH_3)$ vibration of PNIPAM (1480-1415 cm^{-1}), the v(Si-O) vibration of laponite (1034-951 cm^{-1}), and the amide-III vibration of gelatine (1298- 1192 cm^{-1}). The $\delta(CH_3)$ vibration of PNIPAM was chosen instead of the more commonly used amide I and amide II bands to avoid overlap with gelatine peaks. The $\delta(CH_3)$ vibration has a lower vibrational contribution from gelatine. Some typical spectra showing the bands with which the images were generated are also shown in figures 5.30 and 5.31. In all instances, it is observable that apparent variations in peak area for all components are not attributed to domain separation of the components, but to variations in the optical quality of crystal/ sample contact. This is especially evident in figures 3.9a and 3.9b, where areas of green and light blue are of very poor contact, and dark blue areas have virtually none. For HA-doped PNIPAM samples (figures 3.40a and b), no characteristic HA bands, including the very small vibration located at 1410cm^{-1} shown in section 3.8.2, could be located in any of the image spectra during these experiments. The very strong characteristic HA vibrational band at 1033 cm^{-1} is not identifiable in this data due to overlap with the v(Si-O) of laponite. The distribution of all components is therefore determined by the respective spatial distributions of clay and PNIPAM, which are both clearly identifiable and homogenous in this data, with no voids in the polymer or clay distribution.

Since the images indicate qualitative and not quantitative data and the colour scales are allocated arbitrarily for each image, the variation in colour within an image is only comparable to other colours within that image. Evidently, there is no "real" variation in gel composition in within the field of view for any of the systems under study and they are deemed to be homogeneous on the micron length scale. Multivariate curve resolution (MCR) analysis [62], which is a collection of techniques which help determine the number of components in a mixture, their concentrations and response profiles to help resolve them, was applied to the data in this study and confirmed the homogeneity of all formulations.

5.9 Dynamic Mechanical Analysis (DMA) frequency scan data of PNIPAM/ clay and doped PNIPAM/ clay hydrogels.

Polymeric hydrogels have found use in several biomedical devices both in medical and veterinary disciplines, most popularly as drug delivery vehicles and wound management devices. It has been previously demonstrated that the mechanical properties of such devices directly influence their clinical behaviour and performance [63-64]. It is therefore crucial to characterise the rheological/ mechanical properties of any material intended for biomedical applications to as part of the formulation, design and therefore performance optimisation protocol.

Amongst the many techniques employed to mechanically analyse polymers [65], dynamic mechanical methods are non- destructive and enable accurate and rapid determination of the viscoelastic properties of polymeric systems.

Some very commonly used DMA terminology is defined as follows:

Storage modulus- refers to a material's resistance to deformation (given in Pa).

Tan delta (δ) – refers to the ratio of the storage modulus to loss modulus. It quantifies of the presence and extent of elasticity in a material.

Strain- refers to the amount by which the sample is deformed.

Damping- a measure of the internal friction of a material which is indicative of the amount of energy loss from a material as dissipated heat.

Stress- refers to the force per unit area (given in Pa) required to bring about sample deformation.

DMA was carried out to investigate the viscoelastic properties of PNIPAM/ clay hydrogels as well as those with added dopants as described in sections 3.6 and 3.7. In all cases, the liquid PCPH was freshly synthesised using the protocols described in sections 3.6 and 3.7 and sonicated at 80°C for 30 minutes to remove any trapped air. The appropriate amount of PCPH was carefully transferred to a mould (a small glass Petri dish) with a depth of 4.5mm, filling it to the brim. After approximately 2 minutes at room temperature, the PCPH cooled sufficiently to undergo phase transition, lose its opacity and solidify to the precise dimensions of the mould. The mould was then air-sealed and stored at room temperature for 24h. A

circular biopsy punch with a 4.5mm internal diameter was used to punch cylindrical samples from the hydrogel, thus maintaining sample dimension consistency. The geometry of the samples was measured, and they were then clamped between the DMA compression plates. A PerkinElmer DMA8000 model was used in compression mode at room temperature (recorded as 25.2°C - 25.5°C) and the spectra were acquired during a frequency scan between 0.1 and 10 Hz. The displacement for each experiment was set to 0.05mm.Each experiment was performed 3 times using a fresh sample each time. A sample of bovine nucleus pulposus, a component of spinal disc tissue discussed in detail in chapter 7, was analysed using identical parameters by Dr. Kerstin Mader of the Materials and Engineering Research Institute at Sheffield Hallam University for comparison. The average storage modulus (Pa) and tan δ were plotted against frequency with standard error shown. The results are given in figure 5.32 and 5.33, respectively.
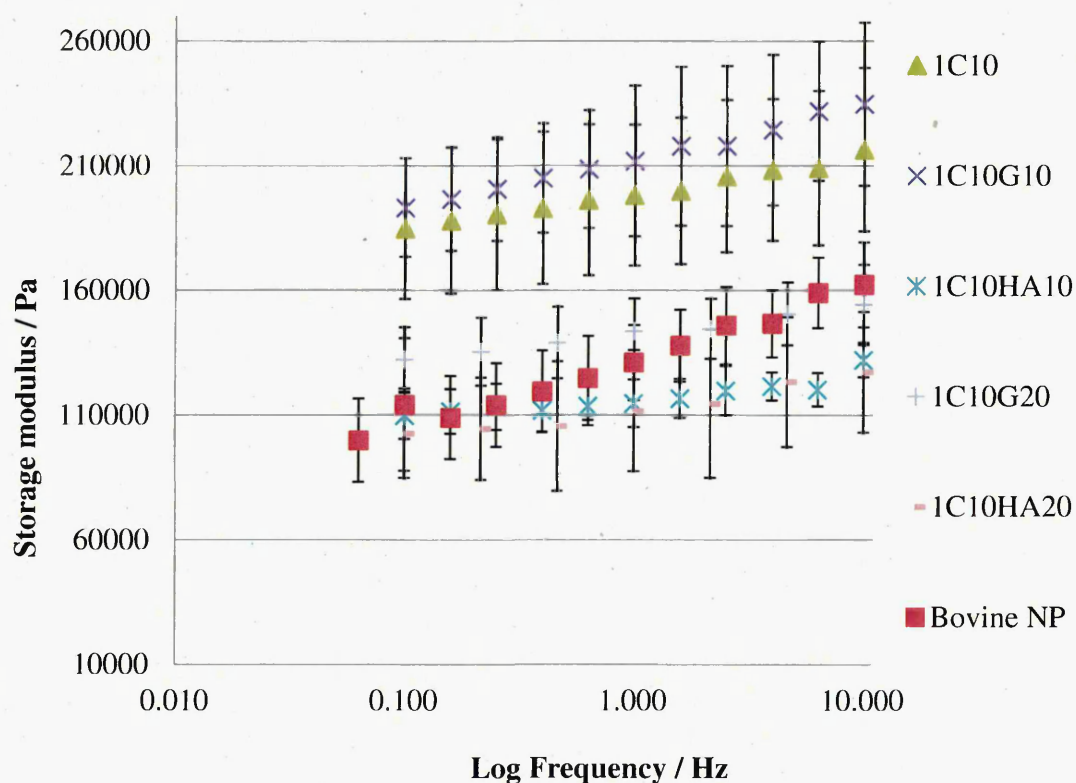
Figure 5.32. Frequency sweep data obtained using DMA for the PNIPAM/ clay hydrogel and its doped variants, showing their relative storage moduli (Pa). The experiments were performed at room temperature. n=3.

During a frequency scan, oscillatory stress is applied to the sample and the resultant storage modulus is plotted as a function of frequency. DMA characterisation revealed that storage

modulus for all formulations very gradually increased with increasing frequency (in other words, the material becomes marginally less elastic and "tougher" at higher oscillatory frequencies, which is typical viscoelastic behaviour). Also, the viscoelastic behaviour of the PNIPAM/ clay formulations more resembled that bovine NP tissue with increasing HA content, not only by a decrease in storage modulus, but also displaying a greater degree of linear viscoelasticity during compression [66]. Whilst the viscoelastic behaviour of formulations containing 10% gelatine solution ($1C_{10}G10$) closely resemble that the standard clay/ polymer ($1C_{10}$) formulation, further increasing the gelatine solution concentration to 20% ($1C_{10}G20$) induces a decrease the storage modulus of the material, more closely bringing it in line with that of bovine NP tissue.

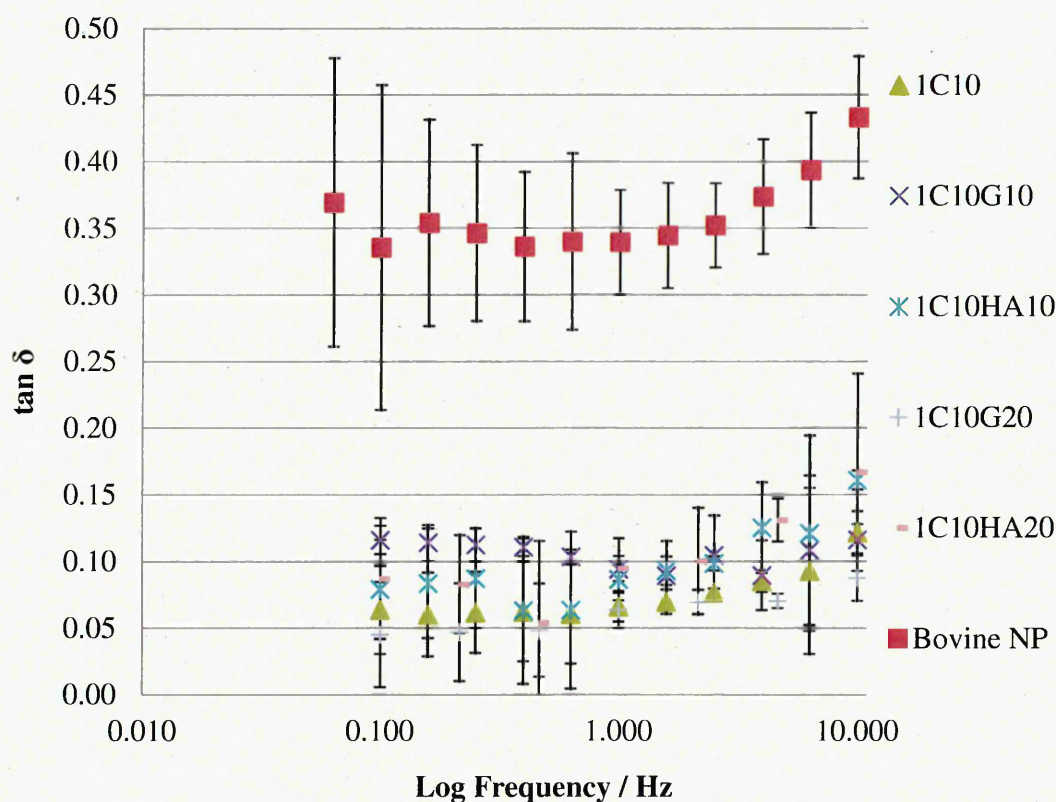**Figure 5.33. Frequency sweep data obtained using DMA for the PNIPAM/ clay hydrogel and its doped variants, showing their relative tan δ values. The experiments were performed at room temperature. n=3.**

The tangent of phase difference, "tan δ" or "damping ratio", provides information regarding energy dissipation properties of the gels (in this case as a function of frequency), and is given

175

by the ratio G" (loss modulus)/G' (storage modulus), the elastic and inelastic components respectively.

In principal, the larger the tan δ, the greater the dampening force. This reduces the amplitude of the oscillatory force, effectively reducing the "shock of impact".

Figure 5.33 shows the relationship between tan δ and oscillatory frequency of various gel formulations in comparison to bovine NP tissue. The overlapping standard error of the PNIPAM based gels make them largely indistinguishable from a damping perspective, although all formulations exhibit a marginal increase in tan δ at higher frequencies. The tan δ values obtained for bovine NP far exceed those of any of the gel formulations, indicating that they possess markedly higher energy dissipation properties. The energy dissipation properties of the bovine NP also improve with increasing frequency, by a magnitude comparable to the PNIPAM-based gels. This may be related to the hierarchal structure within the native NP, where fibres on the mm scale are interconnected with nanofibres.

5.10   Summary

Approaches undertaken to determine M_w and molecular weight distribution of the polymers have been met with very limited success, owing to the nature and behaviour of the polymer during and following the precipitation polymerisation process. Several characterisation approaches have been proposed for future work, focussing primarily on different approaches to existing techniques.

The ability of PNIPAM to form strong cohesive entanglements when cooled after precipitation polymerisation may help explain the difficulty in dissolving the polymer for M_w analysis.

The accuracy of clay content of the resulting gels has been demonstrated by ATR-FTIR integration and XRD analysis proves excellent clay platelet distribution. It was established using ATR-FTIR that kinetic of isothermal dehydration of various hydrogel formulations can be controlled with the addition of biologically active dopants. This is thought to be due to cross-link density and initial water volume fraction of the starting film. Although some initial data sets indicate consistency, more data and a larger sample matrix is required to draw definitive conclusions with regards to the mechanism of this process and the factors which influence it.

The dynamic mechanical properties of several PNIPAM/ clay/ biological dopant gel formulations have been compared to bovine nucleus pulposus tissue. The viscoelasticity of

the gels can be tailored with varying the nature and quantity of dopant materials. Of the gel formulations examined, those containing a hyaluronic acid (HA) solution most closely resemble bovine spinal disc tissue from a viscoelastic perspective. In addition to this, tan δ data concludes that bovine disc tissue possesses a far greater capacity for energy or impact dissipation than any of the PNIPAM-based gel formulations, regardless of dopant nature or concentration. The cytocompatibility of all formulations and their feasibility as medical devices, specifically spinal disc tissue scaffolds, is examined in detail in chapter 7.

5.11   References

1.   Haraguchi, K., Xu, U., Li, G., Molecular Characteristics of Poly(N-isopropylacrylamide) Separated from Nanocomposite Gels by Removal of Clay from the Polymer/Clay Network. Macromolecular Rapid Communications, 2010. 31(8): p. 718-723.

2.   Schild, H.G., Tirrell,. Microcalorimetric detection of lower critical solution temperatures in aqueous polymer solutions. The Journal of Physical Chemistry, 1990. 94(10): p. 4352-4356.

3.   Furyk, S., et al., Effects of end group polarity and molecular weight on the lower critical solution temperature of poly(N-isopropylacrylamide). Journal of Polymer Science Part A: Polymer Chemistry, 2006. 44(4): p. 1492-1501.

4.   Ringsdorf, H., et al., Fluorescence studies of hydrophobically modified poly(N-isopropylacrylamides). Macromolecules, 1991. 24(7): p. 1678-1686.

5.   Zhang, Y., et al., Effects of Hofmeister Anions on the LCST of PNIPAM as a Function of Molecular Weight†. The Journal of Physical Chemistry C, 2007. 111(25): p. 8916-8924.

6.   Bisht, H.S., et al., Temperature-Controlled Properties of DNA Complexes with Poly(ethylenimine)-graft-poly(N-isopropylacrylamide). Biomacromolecules, 2006. 7(4): p. 1169-1178.

7.   Virtanen, J., Tenhu, H., Thermal Properties of Poly(N-isopropylacrylamide)-g-poly(ethylene oxide) in Aqueous Solutions: Influence of the Number and Distribution of the Grafts. Macromolecules, 2000. 33(16): p. 5970-5975.

8.   Chen, G., Hoffman, A., A new temperature- and pH-responsive copolymer for possible use in protein conjugation. Macromolecular Chemistry and Physics, 1995. 196(4): p. 1251-1259.

9.   Motokawa, R., et al., Time-resolved gel permeation chromatographic study on poly(N-isopropylacrylamide)-block-poly(ethylene glycol) prepared by soap-free emulsion polymerization. Polymer, 2004. 45(26): p. 9019-9022.

10.   Terada, T., et al., Raman spectroscopic study on water in aqueous solutions of temperature-responsive polymers: Poly(N-isopropylacrylamide) and poly[N-(3-ethoxypropyl)acrylamide]. Macromolecular Chemistry and Physics, 1994. 195(9): p. 3261-3270.

11.   Ganachaud, F., et al., Molecular weight characterization of poly(N-isopropylacrylamide) prepared by living free-radical polymerization. Macromolecules, 2000. 33(18): p. 6738-6745.

12.   Haraguchi, K., et al., Poly(N-isopropylacrylamide) Prepared by Free-Radical Polymerization in Aqueous Solutions and in Nanocomposite Hydrogels. Macromolecular Symposia, 2011. 306-307(1): p. 33-48.

13.   Xu, Y., et al., Gel Formation and Molecular Characteristics of Poly(N-isopropylacrylamide) Prepared by Free-Radical Redox Polymerization in Aqueous Solution. Macromolecular Chemistry and Physics, 2010. 211(9): p. 977-987.

14.   Clegg, F., Personal communication. Dec 2011.

15.   Tamai, Y., et al., Molecular dynamics study of water in hydrogels. Molecular Simulation, 1996. 16(4-6): p. 359-374.

16.   Tamai, Y., H. et al., Molecular dynamics study of polymer-water interaction in hydrogels .1. Hydrogen-bond structure. Macromolecules, 1996. 29(21): p. 6750-6760.

17.   Tamai, Y., Tanaka, H., Nakanishi, K., Molecular dynamics study of polymer-water interaction in hydrogels .2. Hydrogen-bond dynamics. Macromolecules, 1996. 29(21): p. 6761-6769.

18.   Sammon, C., et al., Vibrational spectroscopic studies of the dynamics and perturbation of water in polymeric films. Journal of Molecular Liquids, 2002. 101(1-3): p. 35-54.

19.   Shibukawa, M., et al., Liquid chromatography and differential scanning calorimetry studies on the states of water in hydrophilic polymer gel packings in relation to retention selectivity. Journal of Chromatography A, 1999. 832(1-2): p. 17-27.

20.   Jin, Y., Wang, W., Su, Z., Spectroscopic study on water diffusion in aromatic polyamide thin film. Journal of Membrane Science, 2011. 379(1-2): p. 121-130.

21.   Baba, T., et al., Solute retention and the states of water in polyethylene glycol and poly(vinyl alcohol) gels. Journal of Chromatography A, 2004. 1040(1): p. 45-51.

22.   Peng, L., et al., Investigation of the states of water and OH groups on the surface of silica. Colloids and Surfaces a-Physicochemical and Engineering Aspects, 2009. 334(1-3): p. 112-115.

23.   Shen, Y., et al., Two-dimensional ATR-FTIR spectroscopic study on the water diffusion behavior in polyimide/silica nanocomposite. Chinese Journal of Chemical Physics, 2006. 19(6): p. 481-484.

24.   Guan, L., H. Xu, and D. Huang, The investigation on states of water in different hydrophilic polymers by DSC and FTIR. Journal of Polymer Research, 2011. 18(4): p. 681-689.

25.   Hwang, B.-J., et al., Analysis of states of water in poly (vinyl alcohol) based DMFC membranes using FTIR and DSC. Journal of Membrane Science, 2011. 369(1-2): p. 88-95.

26.   Sturcova, A., et al., Role of hydration and water coordination in micellization of Pluronic block copolymers. Journal of Colloid and Interface Science, 2010. 352(2): p. 415-423.

27.   Doppers, L.M., Breen, C., Sammon, C., Diffusion of water and acetone into poly(vinyl alcohol)-clay nanocomposites using ATR-FTIR. Vibrational Spectroscopy, 2004. 35(1-2): p. 27-32.

28.   Sammon, C., et al., Polymer-water interactions. Origin of perturbed infrared intensities of water in polymeric systems. Polymer, 2003. 44(9): p. 2669-2677.

29.   Muthudoss, P., Application of FTIR imaging and spectroscopy to solid dosage formulations, in Materials and Engineering Research Institute. 2011, Sheffield Hallam University: Sheffield.

30.   Iwamoto, R., Murase, H., Infrared spectroscopic study of the interactions of nylon-6 with water. Journal of Polymer Science Part B-Polymer Physics, 2003. 41(14): p. 1722-1729.

31.   Adnadjevic, B., J. et al., The kinetics of isothermal dehydration of equilibrium swollen hydrogel of poly(acrylic-c0-methacrylic acid). Hemijska Industrija, 2009. 63(5): p. 585-591.

32.   Crank, J., The Mathematics of Diffusion. 2nd ed. 1994, Oxford: Clarenden Press.

33.   Hu, D.S.G., Chou, K.J.N., Kinetics of water swelling and development of porous structure in ionic poly(acrylonitrileacrylamide-acrylic acid) hydrogels. Polymer, 1996. 37(6): p. 1019-1025.

34.   Konak, C., et al., Dynamic light scattering from polymer solutions and gels at the gelation threshold. Polymer, 1991. 32(6): p. 1077-1079.

35.   Matsuoka, H., et al., Rotational diffusion of ellipsoidal latex particles in dispersion as studied by depolarized dynamic light scattering. Colloids and Surfaces a-Physicochemical and Engineering Aspects, 1996. 109: p. 137-145.

36.   Tsunashima, Y., Particle diffusion and convection observed by dynamic light scattering from aqueous suspensions of polystyrene latex particles in simple shear flow. Journal of the Physical Society of Japan, 1992. 61(8): p. 2763-2771.

37.   Zuo, J., et al., Dynamic behavior and mass transport in polyacrylic acid gel by dynamic light scattering. Chinese Chemical Letters, 2002. 13(5): p. 448-451.

38.   Oliveira, G., et al., Alcohol enhanced permeation in model membranes. Part I. Thermodynamic and kinetic analyses of membrane permeation. International Journal of Pharmaceutics, 2010. 393(1-2): p. 61-67.

39.   Velicky, M., et al., In situ artificial membrane permeation assay under hydrodynamic control: Correlation between drug in vitro permeability and fraction absorbed in humans. European Journal of Pharmaceutical Sciences, 2011. 44(3): p. 299-309.

40.   Anandan, C., et al., Study of the diffusion of pyrene in silicone polymer coatings by steady state fluorescence technique: effects of pyrene concentration. European Polymer Journal, 2004. 40(8): p. 1833-1840.

41.   Coenjarts, C., et al., Exploratory approaches to the study of acid diffusion and acid loss from polymer films using absorption and fluorescence spectroscopy, in Microlithography 1999: Advances in Resist Technology and Processing Xvi, Pts 1 and 2, W. Conley, Editor. 1999. p. 1062-1073.

42.   Miller, K.E., et al., Mobility sensitive flourescence probes for quantitative monitoring of water sorption and diffusion in polymer coatings. Journal of Polymer Science Part B-Polymer Physics, 1995. 33(17): p. 2343-2349.

43.   Murthy, A.V.R., et al., Probing the Role of Chain Length on the Diffusion Dynamics of pi-Conjugated Polymers by Fluorescence Correlation Spectroscopy. Journal of Physical Chemistry B, 2011. 115(37): p. 10779-10788.

44.   Fujara, F., et al., Translational and rotational diffusion in supercooled orthoterphenyl close to the glass transition. Zeitschrift Fur Physik B-Condensed Matter, 1992. 88(2): p. 195-204.

45.   Schmidt-Rohr, K., Clauss, J., Spiess, H., Correlation of structure, mobility and morphological information in heterogeneous polymer materials by 2-dimensional wideline separation NMR-spectroscopy. Macromolecules, 1992. 25(12): p. 3273-3277.

46.   Zawodzinski, T.A., et al., Determination of water diffusion coefficients in perflourosulfonate ionomeric membranes. Journal of Physical Chemistry, 1991. 95(15): p. 6040-6044.

47.   Dobbyn, V., et al., Measurement of the rates of diffusion of halomethanes into polymer films using ATR-FTIR spectroscopy. International Journal of Environmental Analytical Chemistry, 2003. 83(7-8): p. 643-652.

48.   Jones, Y.K., et al., ATR-FTIR spectroscopic analysis of sorption of aqueous analytes into polymer coatings used with guided SH-SAW sensors. Ieee Sensors Journal, 2005. 5(6): p. 1175-1184.

49.   Yi, X.H., et al., Diffusion measurements using ATR-FTIR spectroscopy: Acetone diffusion in polypropylene - Use of penetrant fluid pressure to improve sample/IRE contact. Journal of Polymer Science Part B-Polymer Physics, 2000. 38(13): p. 1773-1787.

50.   Masaro, L., Zhu, X., Physical models of diffusion for polymer solutions, gels and solids. Progress in Polymer Science, 1999. 24(5): p. 731-775.

51.   Duda, J.L., Molecular diffusion in polymeric systems. Pure & Applied Chemistry, 1985. 57(11): p. 1681—1690.

52.   Adnadevic, B., et al., Normalized Weibull distribution function for modelling the kinetics of non-isothermal dehydration of equilibrium swollen poly(acrylic acid) hydrogel. Chemical Engineering Journal, 2007. 130(1): p. 11-17.

53.   Gonzalez-Meijome, J.M., et al., Qualitative and quantitative characterization of the In Vitro dehydration process of hydrogel contact lenses. Journal of Biomedical Materials Research Part B-Applied Biomaterials, 2007. 83B(2): p. 512-526.

54.   Jankovic, B., et al., Isothermal kinetics of dehydration of equilibrium swollen poly(acrylic acid) hydrogel. Journal of Thermal Analysis and Calorimetry, 2008. 92(3): p. 821-827.

55.   Elabd, Y.A., et al., Time-resolved Fourier transform infrared/attenuated total reflection spectroscopy for the measurement of molecular diffusion in polymers. Journal of Polymer Science Part B: Polymer Physics, 2003. 41(22): p. 2794-2807.

56.   Guo, J.C., Barbari, T., Unified Dual Mode Description of Small Molecule Sorption and Desorption Kinetics in a Glassy Polymer. Macromolecules, 2009. 42(15): p. 5700-5708.

57.   Hong, S.U., et al., Multicomponent diffusion of methyl ethyl ketone and toluene in polyisobutylene from vapor sorption FTIR-ATR spectroscopy. Journal of Polymer Science Part B: Polymer Physics, 1998. 36(2): p. 337-344.

58.   Fieldson, G.T., Barbari, T., Analysis of diffusion in polymers using attenuated total reflectance Fourier-transform infrared spectroscopy. Abstracts of Papers of the American Chemical Society, 1994. 208: p. 80-PMSE.

59.   Sammon, C., et al., ATR-FTIR studies of a thermo-responsive ABA triblock copolymer gelator in aqueous solution. Polymer, 2006. 47(17): p. 6123-6130.

60.   Su, Y.L., et al., Association behavior of PEO-PPO-PEO block copolymers in water orrprganic solvent observed by FTIR spectroscopy. Molecular Simulation, 2003. 29(12): p. 803-808.

61.   Martinez, V.M., et al., Characterization of supported solid thin films of laponite clay. Intercalation of rhodamine 6G laser dye. Langmuir, 2004. 20(14): p. 5709-5717.

62.   Andrew, J.J., Hancewicz, T., Rapid analysis of Raman image data using two-way multivariate curve resolution. Applied Spectroscopy, 1998. 52(6): p. 797-807.

63.   Jones, D.S., et al., Textural, viscoelastic and mucoadhesive properties of pharmaceutical gels composed of cellulose polymers. International Journal of Pharmaceutics, 1997. 151(2): p. 223-233.

64.   Jones, D.S., et al., Textural analysis and flow rheometry of novel, bioadhesive antimicrobial oral gels. Pharmaceutical Research, 1997. 14(4): p. 450-457.

65.   Craig, D.Q.M. and F.A. Johnson, Pharmaceutical applications of dynamic mechanical thermal analysis. Thermochimica Acta, 1995. 248(C): p. 97-115.

66.   Holmes, A.D., Hukins, D., Analysis of load relaxation in compressed segments of lumbar spine. Medical Engineering & Physics, 1996. 18(2): p. 99-104.

6

The Influence of Alcoholic Solutions and Dopants on the Phase Behaviour of PNIPAM

Chapter 6 – The Influence of Alcoholic Solutions and Dopants on the Phase Behavior of PNIPAM.

6.1   Introduction

Typically, a hydrogel consists of a 3- dimensional cross-linked polymer structure which exists in equilibrium with a solvent medium [1-2], whereby the solvent occupies a far larger volume fraction than the polymer. Hydrogels exhibit observable osmotic swelling or deswelling kinetics depending on the hydrodynamic relationship between polymer and solvent, which potentially give rise to dramatic volume phase transitions. Such transitions have been observed for physically and chemically cross-linked hydrogels in a variety of thermodynamic conditions [3-11].

As explained in chapter 1, the LCST observed in PNIPAM systems and accompanying changes in morphological polymer conformation arise from changes in the delicate balance between hydrogen bonding and hydrophobic interactions in aqueous media. Physical changes at LCST, such as degree of swelling, change in optical transparency and mechanical modulus can be modified and engineered by altering cross-link concentration and type, polymerisation method and incorporating different monomer species as a copolymer network. As the temperature is raised, increasingly unfavourable entropic contributions are made to the Gibbs free energy of mixing, and eventually these contributions override the favourable enthalpy attributed to hydrogen bonds between the polymer and water. As such, the LCST of PNIPAM is attributed strongly to the composition of the medium with which it interacts. Some cosolvents modify water structures and conformations, affecting the delicate hydrogen bonding and hydrophobic interactions in PNIPAM systems. For example, aforementioned physical changes are also observed when the gels are placed in alcoholic solutions.

Pure water and pure lower alcohols are good solvents for PNIPAM, but mixtures of the two over a certain concentration range are not. It is thought that water molecules form a disordered tetrahedral (clathrate) structure around an alcohol molecule, and Onori *et al* and Zhu *et al* [12-13] found that a greater number of water molecules were required to form such a clathrate structure around EtOH than MeOH. In water alone, water molecules form cage-like structures around isopropyl groups of the PNIPAM chains whilst forming hydrogen bonds with the amide groups. With the addition of an alcohol, it is the removal of water molecules swelling the PNIPAM chains in order to favourably form clathrate hydrate

conformations around the alcohol molecules which causes the gel to collapse, as hydrogen bonding and hydrophobic interactions are disrupted. Reswelling occurs when the volume fraction of alcohol molecules exceeds a critical concentration (x_{min}), such that they can no longer be encapsulated in the clathrate structure. The alcohol molecules then interact directly with the PNIPAM chains [14].

In this chapter we examine the dependence of the PNIPAM network composition (cross-link, type, cross-link density, addition of biologically active dopants and extra water in the liquid precursor phase), initiation method and solvent composition (as a function of type and volume fraction of alcohol) as well as increase in temperature on the de/reswelling behaviour of PNIPAM gels.

6.2 Materials used in this chapter

Materials used in this chapter are detailed in section 2.2.4.1. The synthesis and sample preparation for all formulations is described in sections 2.2.4.2- 2.2.4.9.

6.3 Characterisation techniques used in this chapter

6.3.1 Temperature-dependent deswelling of PNIPAM hydrogels

The temperature-dependent volume change of cross-linked PNIPAM gels was measured as follows;

A PNIPAM cylindrical rod of the given composition and initiation method with the dimensions 35mm x 10mm was synthesised according to the appropriate method given in section 6.6. The rods were sliced perpendicularly to their length to yield circular discs with a thickness of ~2mm. The gel discs were placed into individual glass vials, each containing 20ml of water. The vials were placed into a water bath which was set to 20°C, 30°C, 32 °C, 34°C, 36°C, 38°C, 40°C and 50°C respectively during the course of the experiments. The temperature range used in this experiment was designed to cross over the LCST of PNIPAM, with smaller increments in temperature over the range of particular interest. The apparatus was allowed to thermally stabilise and the gels to reach equilibrium for a minimum of 24 hours before each measurement was taken. The gel diameter (with a starting diameter of. 10mm) was recorded to the nearest 0.5mm. The experiments were performed in triplicate, each with independently synthesised samples and fresh water. The mean of these experiments were plotted as a function of % total deswelling.

The temperature-dependent volume change of gelatine and hyaluronic acid doped PNIPAM gels were measured as follows;

A gelatine or hyaluronic acid - doped PNIPAM/ clay hydrogel precursor of the appropriate composition, as described in section 6.4, were made. Precisely 0.265ml of the solution was pipetted into a cylindrical mould of 13mm diameter in order to create gel discs of 2mm thickness. The moulds were sealed and the gels were allowed to "set" at room temperature for at least 4 hours. The gels were carefully removed from the moulds and one disc of each composition was sealed inside an individual glass vial containing 20ml water. The vials were placed into a water bath which was set to 20°C, 30°C, 32 °C, 34°C, 36°C, 38°C, 40°C and 50°C respectively during the course of the experiments. The apparatus was allowed to thermally stabilise and the gels to reach equilibrium for a minimum of 24 hours before each measurement was taken. The gel diameter (with a starting diameter of 13mm) was recorded to the nearest 0.5mm. The experiments were performed in triplicate, each with independently synthesised samples and fresh water. Average results were plotted as a function of % total deswelling.

6.3.2   Alcohol-induced deswelling observations of PNIPAM hydrogels.

The alcohol induced volume change of cross-linked PNIPAM gels was measured as follows;

Cylindrical gel rods of each composition and initiation method were sliced into disks of approximately 2mm thickness. One disc of each composition was sealed inside an individual glass vial containing a 20ml aqueous solution of either 0% 20%, 40%, 60%, 80% or 100% alcohol, and left to equilibrate for 28 days. The diameter of the gel was recorded to the nearest 0.5mm. The experiments were performed using ethanol and methanol solutions and were repeated in triplicate for each, with fresh samples and solutions used each time. The average result was taken and plotted as a function of % deswelling.

The alcohol induced volume change of cross-linked PNIPAM gels was measured as follows;

A gelatine or hyaluronic acid - doped PNIPAM/ clay hydrogel precursor of the appropriate composition, as described in section 6.4, were made. Precisely 0.265ml of the solution was pippetted into a cylindrical mould of 13mm diameter in order to create gel discs of 2mm thickness. The moulds were sealed and the gels were allowed to "set" at room temperature for at least 4 hours. The gels were carefully removed from the moulds and one disc of each composition was sealed inside an individual glass vial containing a 20ml aqueous solution of

186

either 0% 20%, 40%, 60%, 80% or 100% alcohol, and left to equilibrate for 28 days. The diameter of the gel was recorded to the nearest 0.5mm. The experiments were performed using ethanol and methanol solutions and were repeated in triplicate for each, with fresh samples and solutions used each time. The average result was taken and plotted as a function of % deswelling.

6.4 Results and discussion

6.4.1 Thermally induced deswelling of clay cross-linked PNIPAM gels

In order to determine the thermal deswelling properties of PNIPAM/ clay nanocomposites, the diameters of ~2mm thick circular PNIPAM discs of various clay loadings were measured after 24h of equilibration at various temperatures, covering the LCST range of PNIPAM. The starting diameter of the freshly prepared discs was 10mm.

Figure 6.1 shows the overall percentage deswelling of thermally-initiated clay cross-linked PNIPAM at various clay concentrations as a function of temperature. All gels undergo significant volume phase transition at temperatures higher than 30°C, afterwhich they follow a crosslink concentration-dependent deswelling trend. Low clay concentrations appear to allow for deswelling to a greater degree at lower temperatures ($.25C_{10}$ reaching 40% its original volume during complete phase transition at 34-38°C) and gels with higher clay concentrations gels achieve a slower, more sustained rate of deswelling, with $1C_{10}$ gels reaching complete deswelling (around 40% original volume) at a temperature between 40-50°C.

The distinct behaviour change upon alteration of clay loading in this particular system prompted an experiment to determine whether this effect could produce a dramatic macroscopic control of behaviour of the gel upon heating. The temperature at which the separation of deswelling behaviour was most pronounced (34°C) (figure 6.1) was chosen for this experiment. A square PTFE mould was engineered and into it was poured a measured volume of $1C_{10}$, $.5C_{10}$ and $.25C_{10}$ respectively, with each layer left to cool and solidify for 4 hours before adding the next (figure 6.2).

Thermally Initiated PNIPAM/ Clay Gels - Deswelling on Temperature Increase
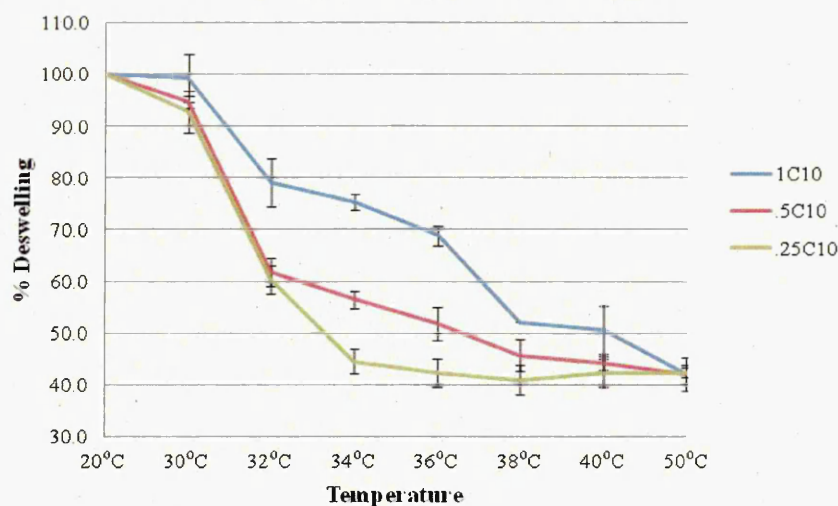
Figure 6.1. The % deswelling of thermally-initiated clay cross-linked PNIPAM of various clay concentrations upon increasing temperature, n = 3.
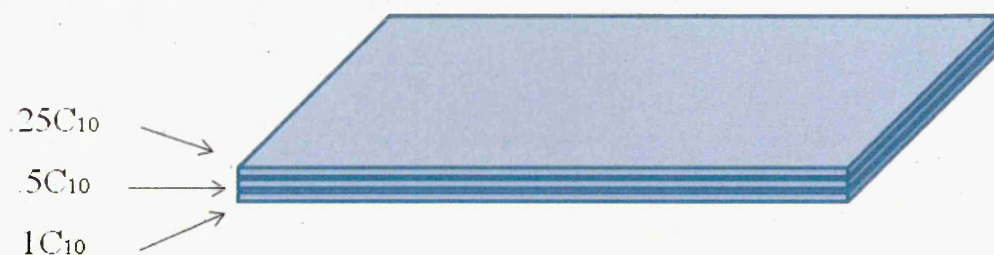
Figure 6.2. A schematic of the triple later sheet formed for this experiment. Each layer contained progressivlely less clay in order to observe whether the combined deswelling action of each would result in a curving of the gel sheet.

The triple-layer gel sheet was removed from the mould and placed into a clean water bath which was subsequently warmed to 34°C.

The high variation in swelling behaviour of the different layers forced the gel sheet to curl back on itself, almost forming a ball (figure 6.3). The effect was completely reversible and the sheet reswelled to its original square flat sheet form when apparatus was cooled.
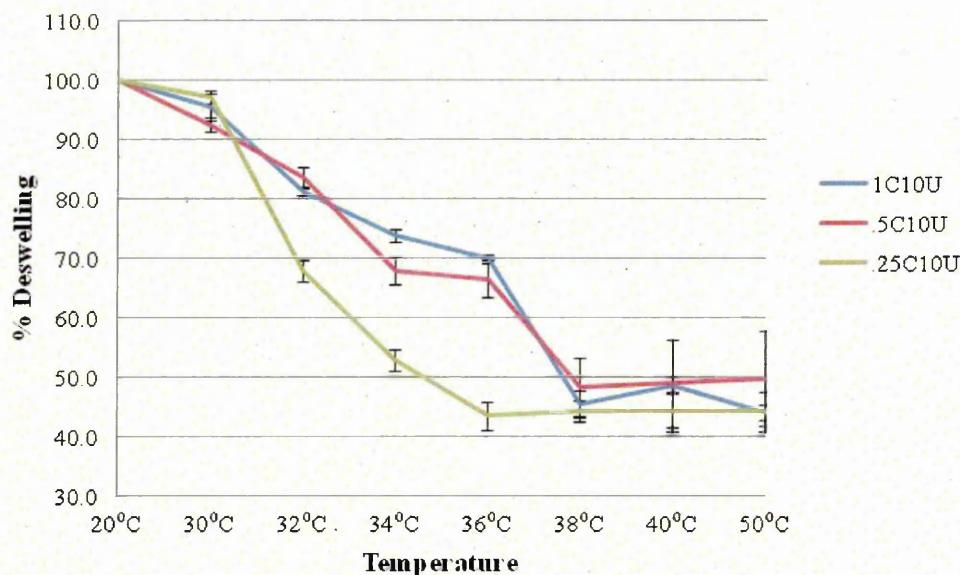
Figure 6.3. Photographs of the gels before and after heating to 34°C. The separate dewelling behaviours of each layer caused the gel sheet to curl dramatically.

UV Initiated PNIPAM/ Clay Gels - Deswelling on Temperature Increase

Figure 6.6. The % deswelling of UV-initiated clay cross-linked PNIPAM of various clay concentrations upon increasing temperature, n = 3.

Figure 6.4 shows the overall percentage of deswelling of UV-initiated clay cross-linked PNIPAM at various clay concentrations. Much like their thermally-initiated counterparts, all UV intitiated gels undergo rapid deswelling at temperatures above 30°C, with gels of a low cross-linking density deswelling to a greater degree at a lower temperatures. .5C$_{10}$U and 1C$_{10}$U gels display very similar and slow deswelling behaviour relative to the .25C$_{10}$U formulation. Complete desewelling in all UV -initiated clay gels is achieved at around 36°C before what appears to be a slight reswelling of the gel, although the overlap of error bars shows that this may not be a consclusive finding.

6.4.2 Thermally induced deswelling of BIS cross-linked PNIPAM gels

In order to determine the thermal deswelling properties of BIS cross-linked PNIPAM gels, the diameters of ~2mm thick circular PNIPAM discs of various BIS concentrations were measured after 24h of equilibration at various temperatures covering the LCST range of PNIPAM. The starting diameter of the freshly prepared discs was 10mm.

Figure 6.5 shows the overall percentage of deswelling of thermally-initiated BIS cross-linked PNIPAM at various BIS concentrations. As expected, the chemically cross-linked gels

**Thermally Initiated PNIPAM/ BIS gels-
Deswelling on Temperature Increase**

Legend: 1BIS10, .5BIS10, .25BIS10
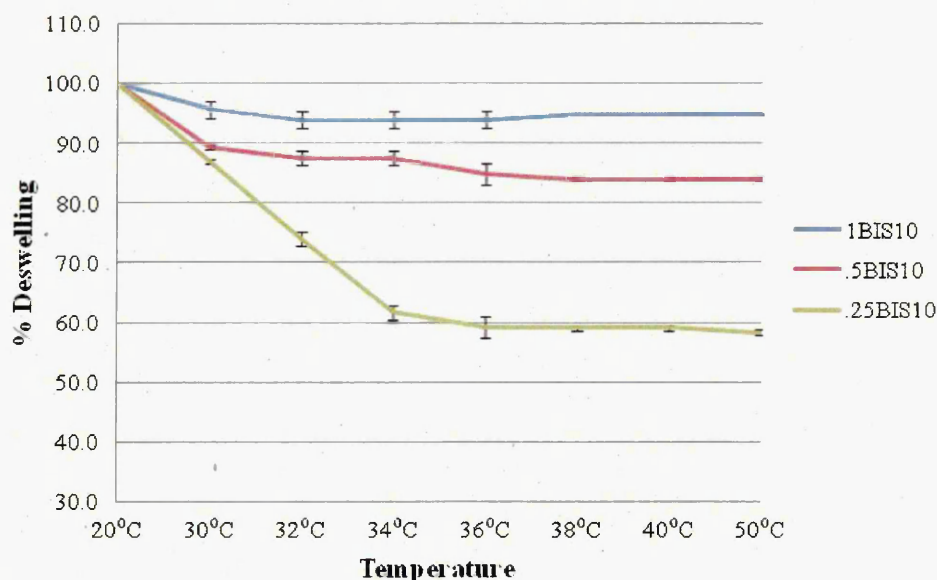
Figure 6.5. The % deswelling of thermally-initiated BIS cross-linked PNIPAM of various clay concentrations upon increasing temperature., n = 3.

deswell to a much smaller extent than those cross-linked with clay. The deswelling rate follows the same pattern of lower cross-linking densities deswelling faster and at lower temperatures, with 10% cross-linked gel deswelling as little as 6%. Unlike any other gel type observed in this study, complete phase transition of all gels is reached at approximately 36°C, with very little or no further deswelling taking place at temperatures above this point. There is also an unusually large distinction between the gel volumes at complete phase transition. Proportionally small error bars in the data for this experiment indicate excellent repeatability and clear distinction in the gels respective deswelling behaviours.

Figure 6.6 shows the overall percentage of deswelling of UV-initiated BIS cross-linked PNIPAM at various BIS concentrations. Upon intitial observation, the deswelling behaviour of these gels does not seem to follow the regular pattern of other gels in this study. However, overlap of standard indictates that there is little difference in the deswelling behaviour between samples at temperatures below 34°C. Above 34°C, $1BIS_{10}U$ gels undergo phase transition over a broad temperature range (34-40°C) and to a smaller extent (to approximately 75%), with repect to $.5BIS_{10}U$ gels which exhibit behaviour very similar to $.25BIS_{10}U$ gels, deswelling more sharply between 34-38°C.

UV Initiated PNIPAM/ BIS Gels - Deswelling on Temperature Increase

Figure 6.6. The % deswelling of UV-initiated BIS cross-linked PNIPAM of various clay concentrations upon increasing temperature., n = 3.
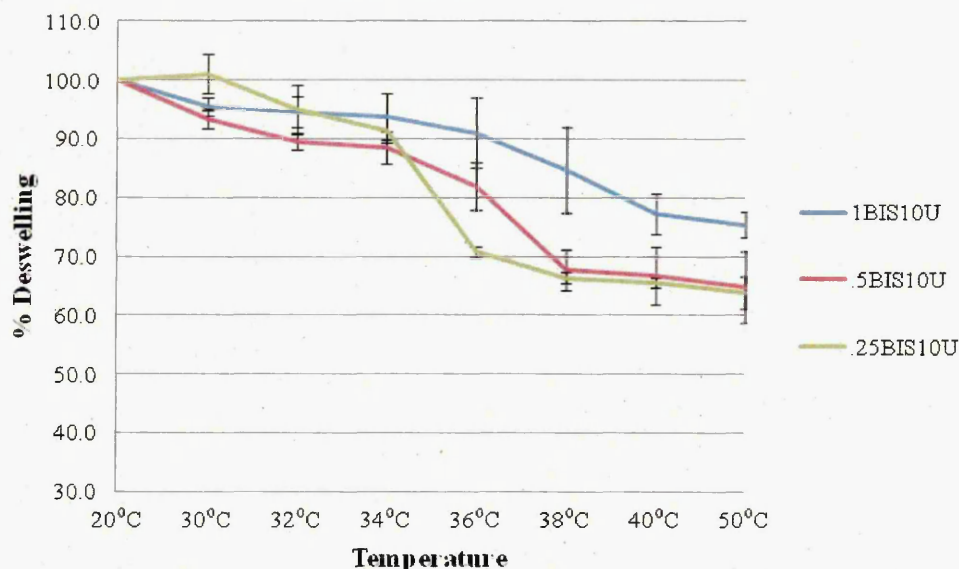
6.4.3 Thermally-induced deswelling of gelatine/ HA-doped clay cross-linked PNIPAM hydrogels

In order to determine the thermal deswelling properties of gelatine- incorporated clay cross-linked PNIPAM gels and quantify possible changes in deswelling behaviour as a direct result of gelatine incorporation, the diameters of 2mm thick circular PNIPAM/ gelatine discs of various gelatine loadings were measured after 24h equilibration at a range of temperatures covering the LCST of PNIPAM. The starting diameter of the freshly prepared discs was 13mm.

Figure 6.7 shows the overall percentage deswelling $1C_{10}Gx$ gels of various gelatine concentrations as a function of temperature.

Gels at all gelatine concentrations deswell to a lesser degree than the $1C_{10}$ control, with most deswelling to around 91% their original size when equilibrated at 32°C, compared to a deswelling of the control of 78-84%. $1C_{10}G5$ exerts a behaviour at this temperature which strikes some balance between the two. Certainly, overlap of standard error concludes that the incorporation of gelatine into the interstitial spaces of the PNIPAM retards deswelling in a consistent manner regardless of gelatine concentration. All $1C_{10}Gx$ gels equilibrate at 50°C

192

1C$_{10}$/ Gelatine Gels- Deswelling on Temperature Increase
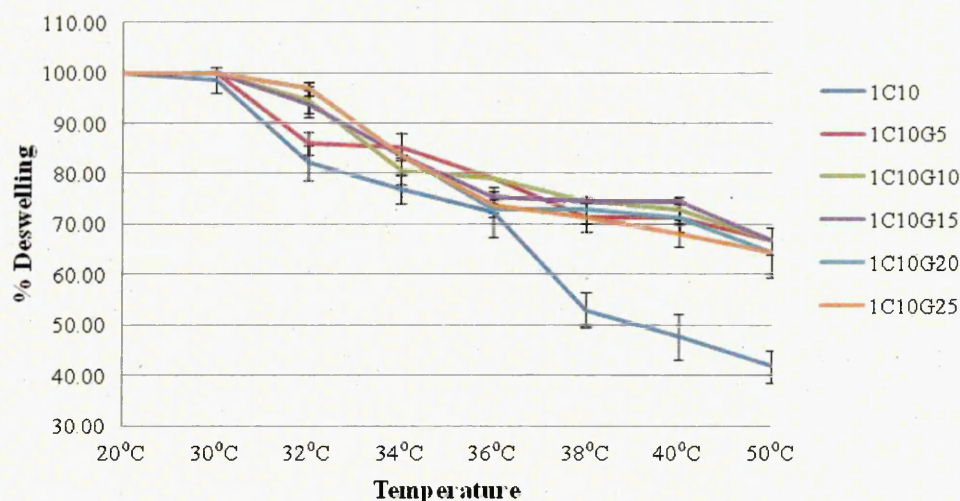
Figure 6.7. The % deswelling of gelatine doped 1C$_{10}$ of various gelatine concentrations upon increasing temperature., n = 3.

having deswollen to 59-69% their original size compared to the gelatine-free control which was significantly more deswollen (38- 45%) at the same temperature.
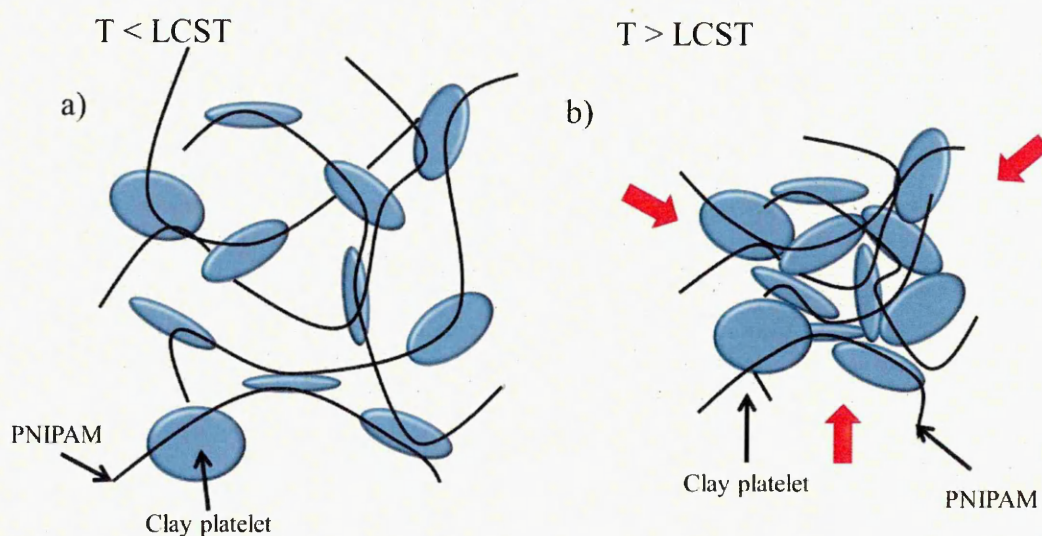
Figure 6.8. A diagrammatic representation of the collapse of a PNIPAM/clay system as it is heated to a temperature beyond its LCST. The gel collapses into a tightly packed hydrophobic network as water is ejected from the interstitial spaces.

Figure 6.8 is a diagrammatic reprsentation of the mechanism of collapse of a standard 1C$_{10}$ gel. As the PNIPAM undergoes phase transition from the coil (swolen and hydrophilic)(a) to

globule (collapsed and hydrophobic) (b) conformation, the 3-dimensional polymer network collapses as thermodynamic forces pull the PNIPAM chains together forming a tightly packed PNIPAM/ clay network. Water is expelled from the network as interstitial spaces shrink.

The observations made in this study with regards to the retardation of collapse with interstitial gelatine can be attributed to one or both of two main considerations:

Firstly, the incorporation of a solid material such as gelatine into the interstitial spaces of the PNIPAM/ clay network (figure 6.9a) could offer a physical barrier to its full deswelling. It is possible that although gelatine solution is thermally reversible, that is to say, gelatine solutions melt under the effect of heat; it is probably not completely expelled from the system but becomes trapped between the polymer chains (figure 6.9b) and hence gives rise to an apparent hindrance in its collapse.

T < LCST   T > LCST

a)   b)

PNIPAM   Gelatine   Clay platelet   Trapped gelatine

Clay platelet   PNIPAM
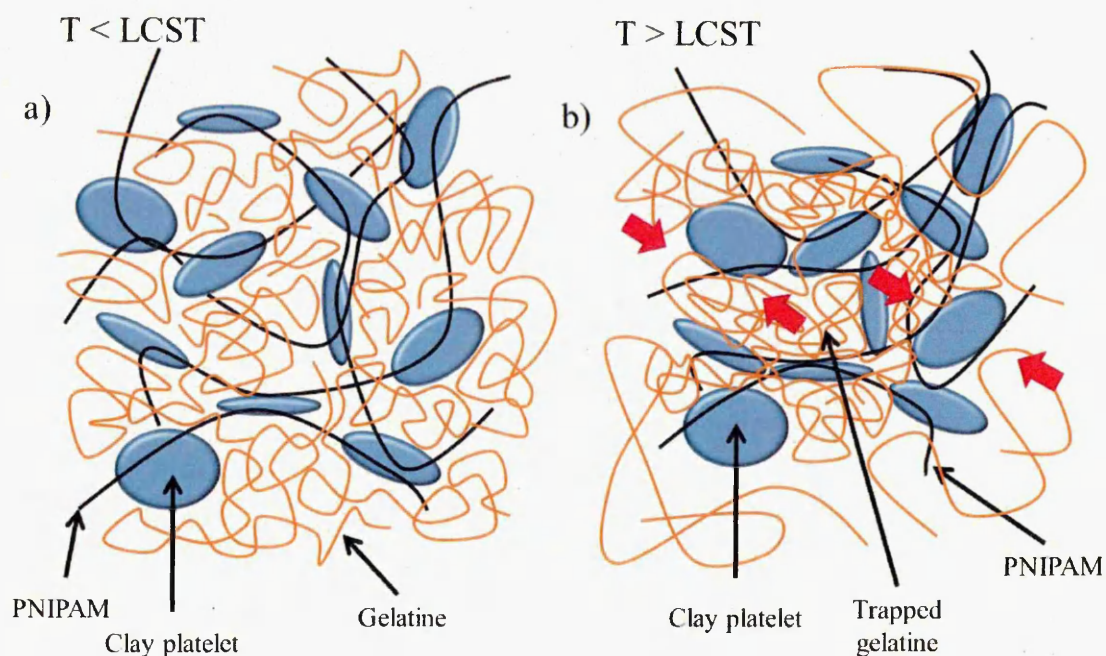
Figure 6.9. A diagrammatic representation of the first proposed mechanism of collapse of a gelatine-incorporated PNIPAM/ clay gel as it is heated to a temperature beyond its LCST.

Secondly, the formation of the gelatine incorporated clay/PNIPAM involves dissolving a gelatine solution into a pre-formed PNIPAM/ clay precursor hydrogel solution (PCPH) before cooling to form a "set" gel (section 2.2.1.3). The extension of PNIPAM chains to neighbouring clay platelets upon cooling and subsequent solidification of the precursor

depends somewhat on free their free interation. If the gelatine chains were to somehow interfere with this free interaction and prevent some crosslinks forming (figure 6.10a) , the resulting gel could contain separate domains of PNIPAM/ clay and gelatine whereby the collapse of separate PNIPAM/ clay domains do not exert influence on one another and "pockets" of gelatine solution appear, across which no or very few PNIPAM chains stretch (figure 6.10b). Since the deswelling measurements involve the macroscopic dimensions of the whole gel, the net recordable result of this occurance would be the apperance of a hindrence in deswelling when perhaps, more accurately, gelatine-filled voids are appearing throughout the network as separate PNIPAM domains collapse. The existence and formation of PNIPAM/ gelaine domains under these conditions could be explored with the use of temdem electron microscopy (TEM) or hot-stage imaging ATR-FTIR in further study.
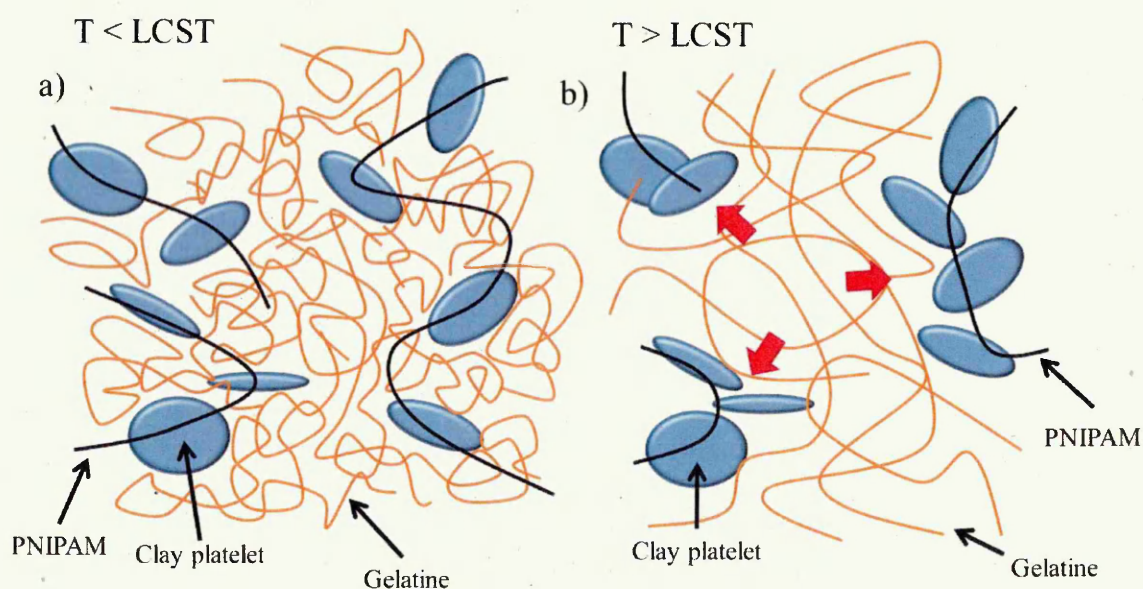
Figure 6.10. A diagrammatic representation of the second proposed mechanism of collapse of a gelatine-incorporated PNIPAM/ clay gel as it is heated to a temperature beyond its LCST.

195
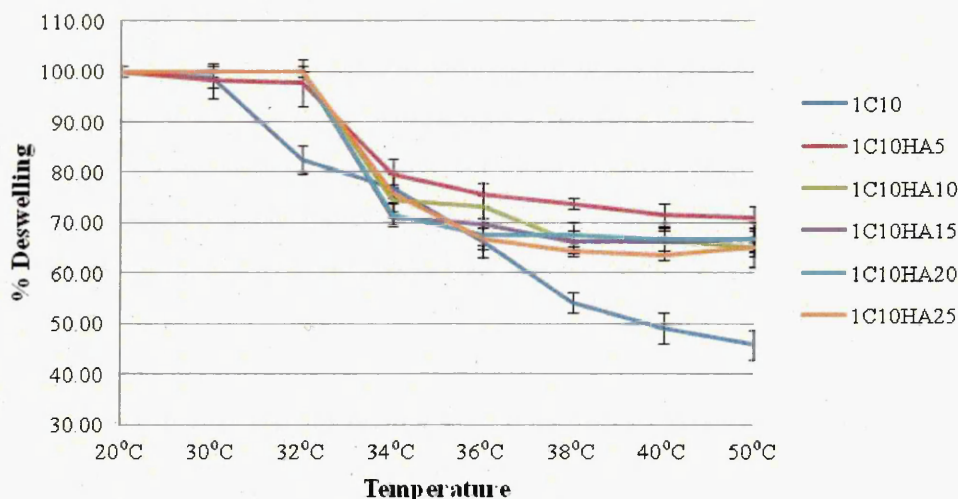
Figure 6.11. The % deswelling of HA doped $1C_{10}$ of various HA concentrations upon increasing temperature., n = 3.

Figure 6.11 shows the overall percentage deswelling $1C_{10}HAx$ gels of various HA concentrations as a function of temperature.

As with the gelatine incorporated gels, all HA incorporated gels exert reduced deswelling capabilities when compared to the $1C_{10}$ control, and an overlap in standard error concludes an almost identical pattern of deswelling as the gelatine gels (shown in figure 6.7) regardless of HA concentration within the polymer matrix. A sharp decrease in gel volume is observable between 32- 34°C before a steady and sustained shrinking is obseved at higher temperatures. At 50°C, all $1C_{10}HAx$ gels were beween 61- 75% their original size, and the HA- free control was 42-49%. Curiously, the behaviours of Gelatine and HA-incorporated gels exert this similar behaviour despite the HA solution being 25 times more dilute than the gelatine solution, and therefore far less of the dopant polymer is available to exert a deswelling hinderance.

Therefore the reasoning behind the effects observed follow two trains of thought; that the incorporation of a dopant species interrupts the formation of PNIPAM/ clay interactions when the PCPH solution is cooled and undergoes PTTNAG, and therefore the hypothesis with regards to domain and void formation for the gelatine incorporated systems is also at play in the HA system (figure 6.10). Also, HA solution usually expands as the temperature rises [16], and the retardation in deswelling of the network could be a result of highly

196

hydrophilic HA existing in direct thermodynamic conflict with an increasingly hydrophobic PNIPAM network upon an increase in temperature, thus preventing some water leaving the interstitial spaces of the PNIPAM/ clay and causing disruption to its collapse.

6.4.4 Thermally induced deswelling of diluted clay/ PNIPAM hydrogels

In order to test the hypotheses made in section 6.4.3, an experiment was devised by which the PCPH system would be diluted and "separated" with pure water, without the addition of dopants, to examine whether this altered their deswelling capabilities.

PCPH solutions of 3 different clay loadings were diluted by precise quantities of water before being allowed to cool and solidify. The diameters of 2mm thick circular PNIPAM/ clay discs of each composition were measured after 24h equilibration at a range of temperatures covering the LCST of the PNIPAM in order to determine their deswelling properties. The starting diameter of the freshly prepared discs was 10mm.
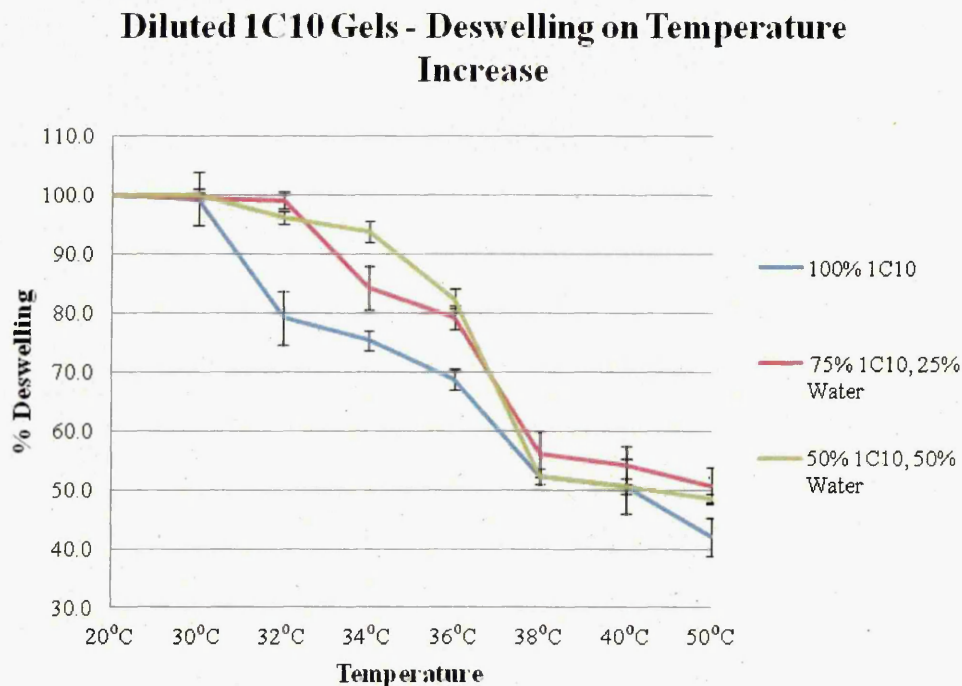
Figure 6.12. The % deswelling of diluted $1C_{10}$ of various water concentrations upon increasing temperature., n = 3.

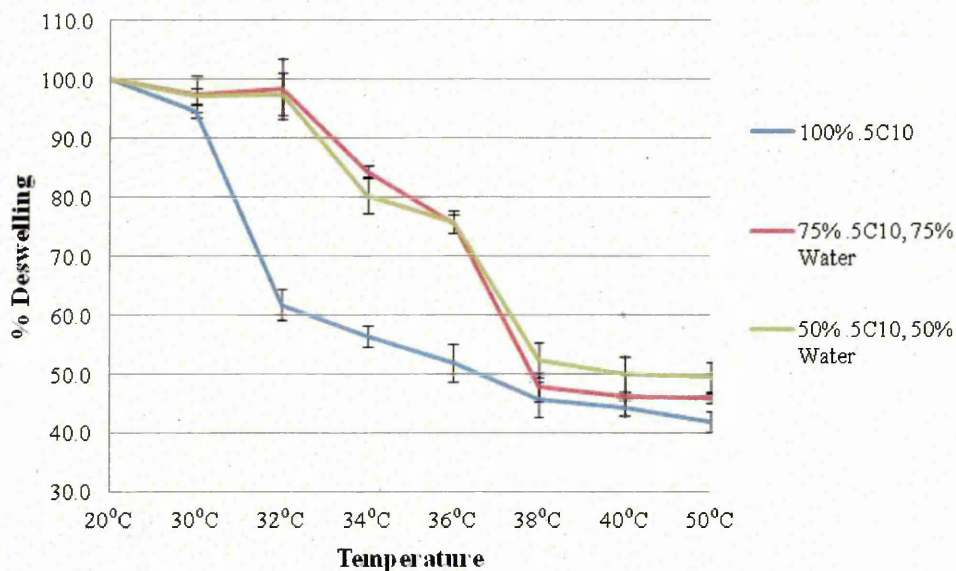**Diluted .5C10 Gels - Deswelling on Temperature Increase**

Figure 6.13. The % deswelling of diluted $.5C_{10}$ of various water concentrations upon increasing temperature., n = 3.

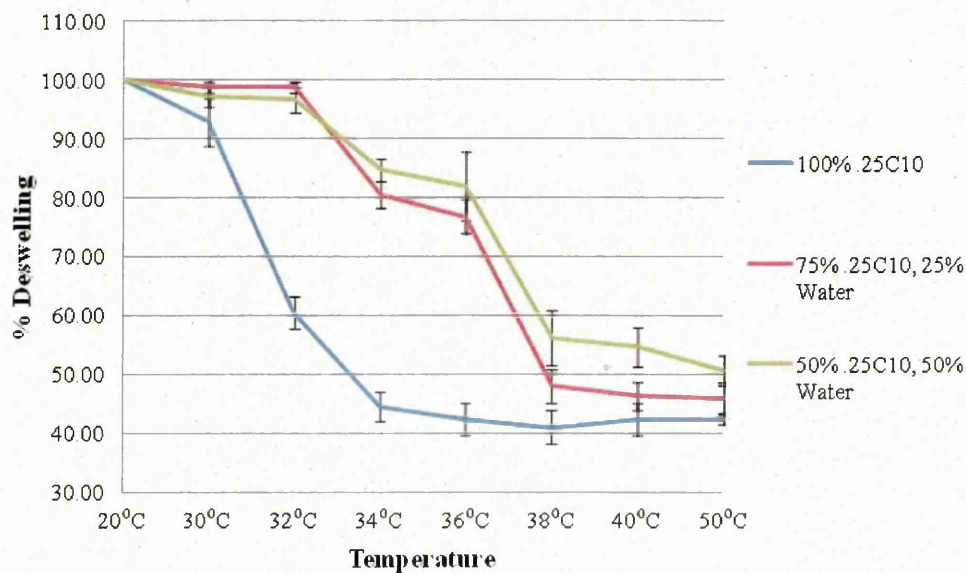**Diluted .25C10 Gels - Deswelling on Temperature Increase**

Figure 6.14. The % deswelling of diluted $.25C_{10}$ of various water concentrations upon increasing temperature., n = 3.

Astonishingly, all diluted gels (figures 6.12 – 6.14) follow a pattern of deswelling different from their original, undiluted form, and this pattern of deswelling was the same regardless of amount of additional water added (up to 50%) or clay loading (.25-1%) of the original PCPH. Curiously still, their behaviours differ slightly but consistently with those of gelatine and HA-doped PNIPAM/ clay gels (section 6.4.3) in that although their collapse is comparatively hindered at temperatures up to 38°C, above this their deswelling behaviours become similar to that of their respective controls (when the gels are doped with HA or gelatine, deswelling at 50°C remains ~15% less than that of their respective controls).

It could therefore be hypothesised that the deswelling mechanism of diluted gels involve 2 separate phases.

Figure 6.15a illustrates the manner in which the undiluted control is proposed to be cross-linked below its LCST. The lengths of the polymer chains are sufficient to anchor neighbouring clay platelets firmly together, thus forming a continuous 3 dimensional polymer/ clay network. Figure 6.15b illustrates the manner in which a diluted gel is proposed to be cross-linked. The lengths of polymer chains are sufficient to join some neighbouring clay platelets, and although the gel appears to be homogeneously cross-linked and has a fair (although reduced) degree of mechanical stability, many of the clay platelets are not anchored to others in close proximity. Figure 6.15c illustrates how the diluted clay/ PNIPAM network is proposed to appear at temperatures just above the LCST of PNIPAM. This is phase I. As water solubility becomes compromised, separate domains (circled) collapse and large water-filled spaces appear between the domains. Although the polymer has undergone phase transition, the size of the whole gel network is comparatively large, and the pseudo-hindrance in deswelling is attributed to the large water-filled voids within the network.
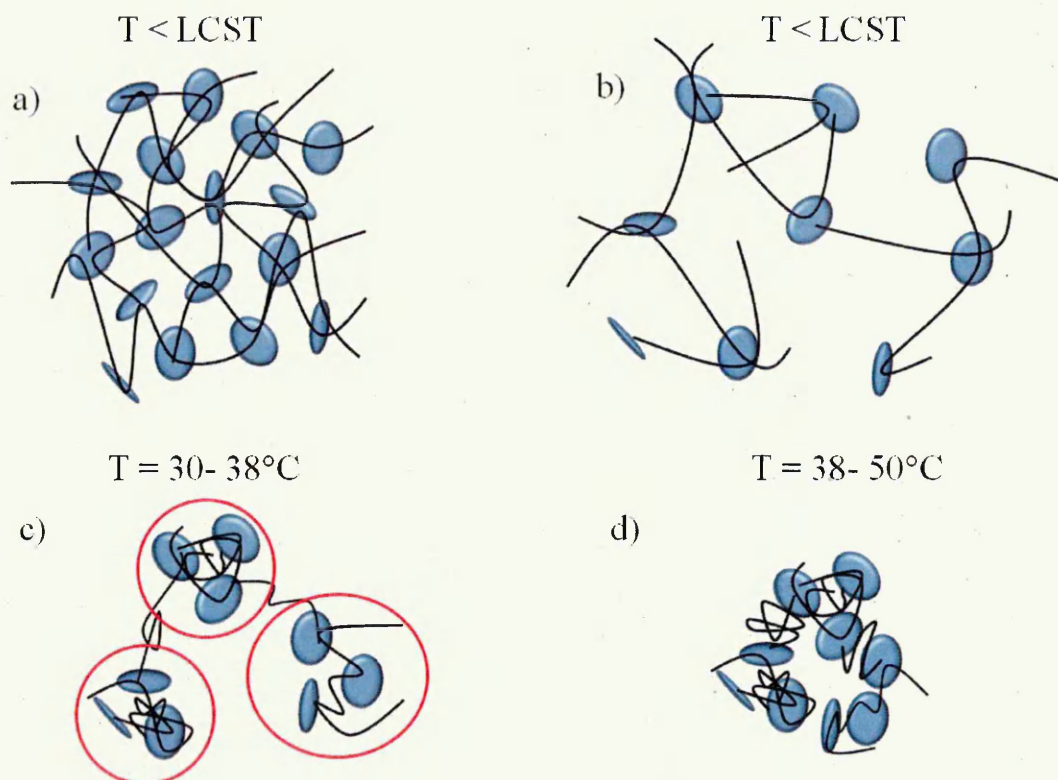
Figure 6.15. A diagrammatic representation of the 2 proposed phases of deswelling of a diluted PNIPAM/ clay hydrogel as it is heated to a temperature beyond its LCST. The proposed structure of an undiluted gel is show for comparion (a). The dilution of the PCPH has prevented some cross-links forming (b) and an increase in temperature causes the collapse of individual domains (circled), leaving large water-filled voids and thus giving the apprearance of a decrease in deswelling capability (c). As the temperature is increased further, an increase in entropy and hydrophobic interactions force the domiains to coagulate, leading to full collapse of the network (d).

Figure 6.15d illustrates how the diluted clay/ PNIPAM network is proposed to appear at temperatures between 38- 50°C. This is phase II. It has been previously shown that after an initial phase separation at LCST, a further increase in temperature enhances the unfavourable contribution of entropy to the PNIPAM system, and further to this, the relative magnitude of this "hydrophobic effect" is directly proportional to thermal input [17-18]. It is proposed that this increase in entropy causes the previously separated domains to coagulate, causing a sharp decrease in gel size and thus emulate the behaviour of the undiluted gel control.

6.4.5 Alcohol volume fraction-dependent deswelling of clay- PNIPAM nanocomposite hydrogels

In order to determine the swelling/ deswelling capacity of clay cross-linked PNIPAM gels as a function of matrix alcohol concentration by cononsolvency, the diameters of ~2mm thick circular PNIPAM discs of various clay densities were taken after their equilibration in various concentrations of ethanol and methanol for 28 days. The starting diameter of the freshly prepared discs was 10mm.

The variation in % deswelling of the gel as a function of the volume fraction of alcohol is shown across figures 6.16 - 6.19.
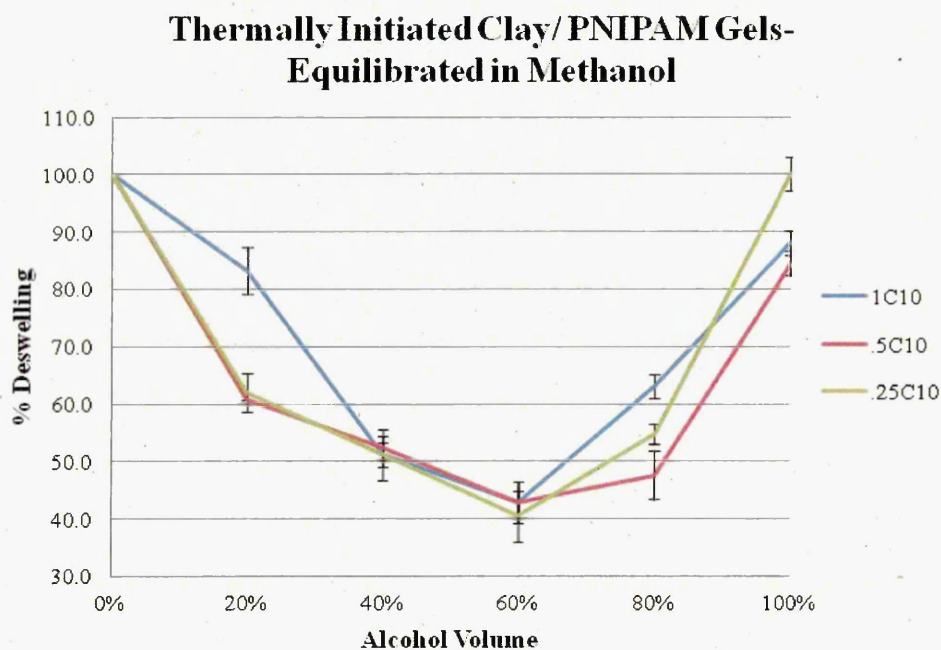
Figure 6.16. The % deswelling of thermally-initiated clay/PNIPAM gels in various methanol concentrations., n = 3.

Figure 6.17. The % deswelling of thermally-initiated clay/PNIPAM gels in various ethanol concentrations. ., n = 3.

uy

Figure 6.18. The % deswelling of UV-initiated clay/PNIPAM gels in various methanol concentrations., n = 3.

202

UV Initiated Clay/ PNIPAM Gels - Equilibrated in Ethanol

Figure 6.19. The % deswelling of UV-initiated clay/PNIPAM gels in various ethanol concentrations., n = 3.

6.4.6 Alcohol volume fraction-dependent deswelling of BIS cross-linked PNIPAM hydrogels

In order to determine the swelling/ deswelling capacity of BIS cross-linked PNIPAM gels as a function of matrix alcohol concentration by cononsolvency, the diameters of ~2mm thick circular PNIPAM discs of various BIS cross-link densities were taken after their equilibration in various concentrations of ethanol and methanol for 28 days. The starting diameter of the freshly prepared discs was 10mm.

The variation in % deswelling of the gel as a function of the volume fraction of alcohol is shown across figures 6.20 - 6.23.

Figure 6.20. The % deswelling of thermally-initiated BIS/PNIPAM gels in various methanol concentrations., n = 3.

Figure 6.21. The % deswelling of thermally-initiated BIS/PNIPAM gels in various ethanol concentrations., n = 3.

UV initiated BIS/ PNIPAM Gels Equilibrated in Methanol

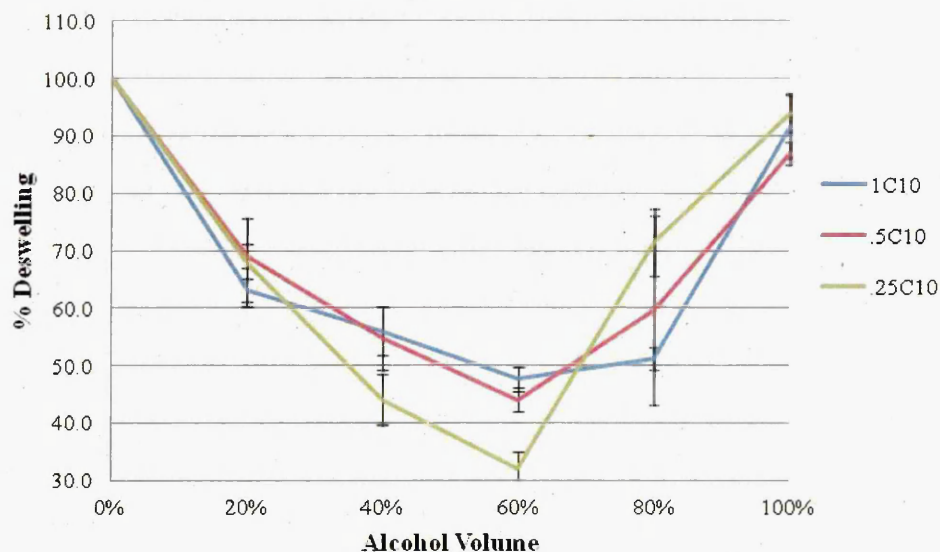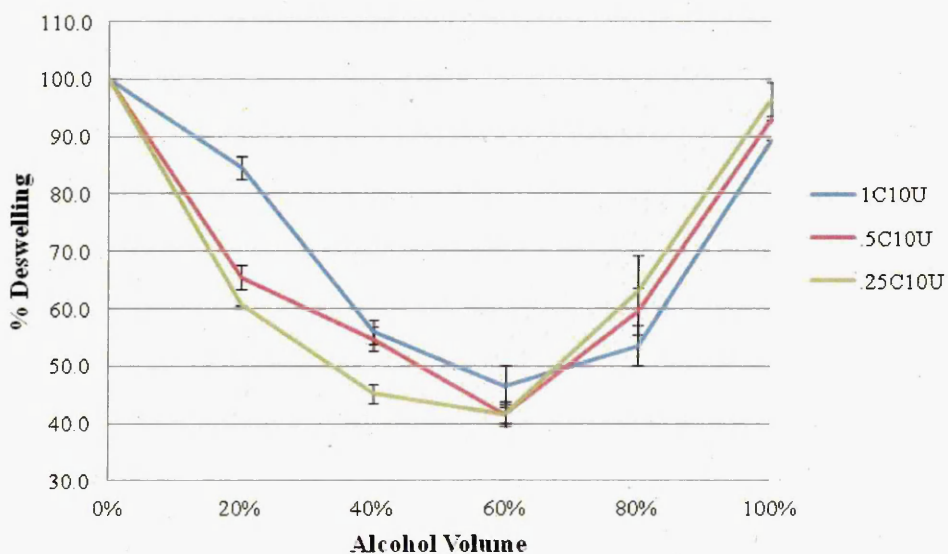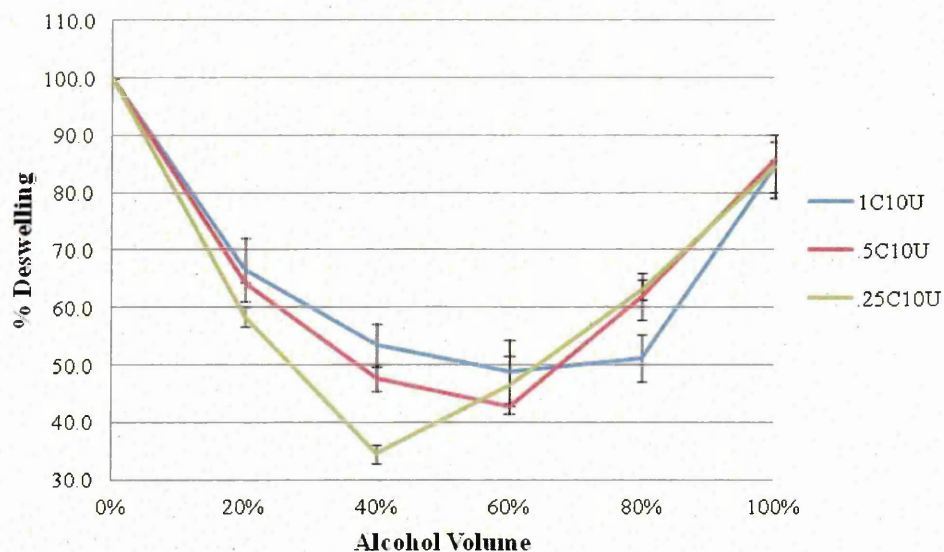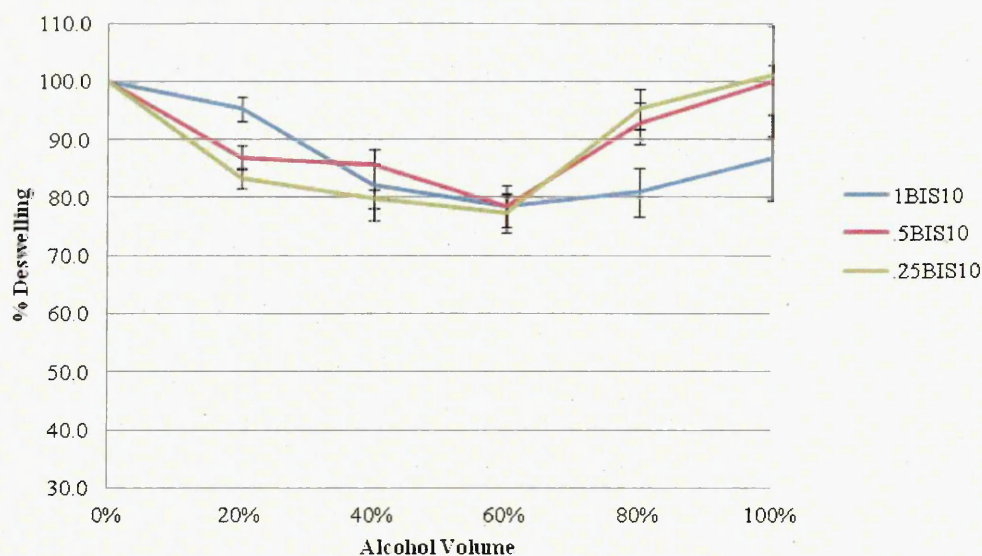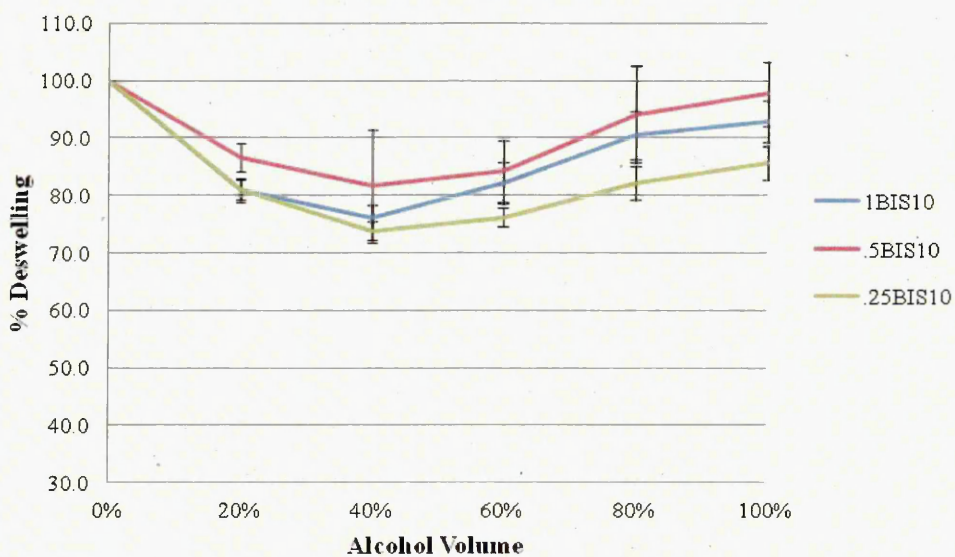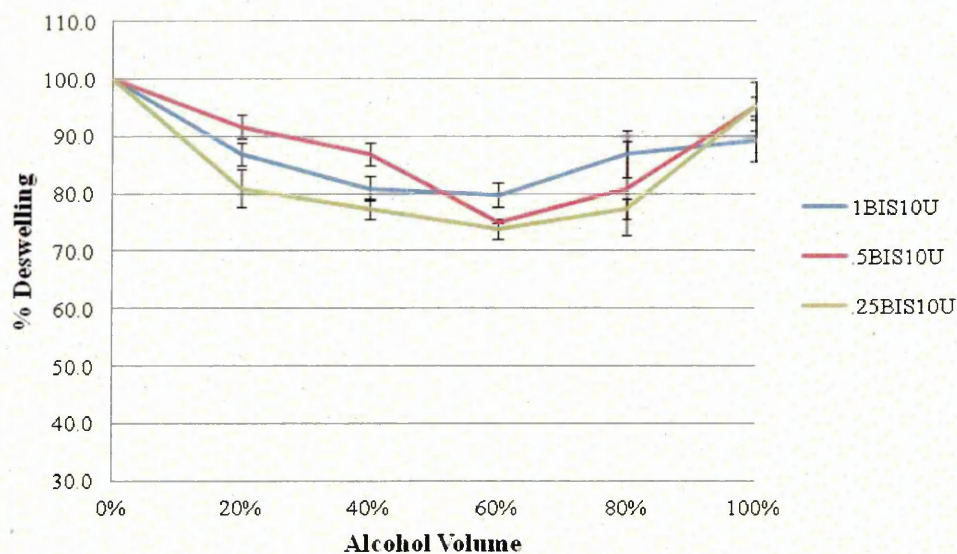Figure 6.22. The % deswelling of UV-initiated BIS/PNIPAM gels in various methanol concentrations., n = 3.

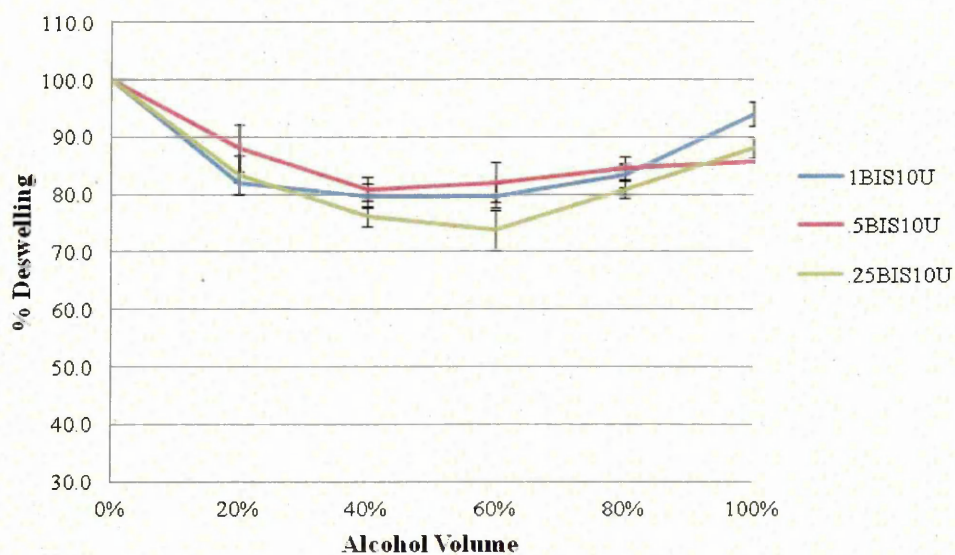**UV Initiated BIS/ PNIPAM Gels Equilibrated in Ethanol**

Figure 6.23. The % deswelling of UV-initiated BIS/PNIPAM gels in various ethanol concentrations., n = 3.

205

Initial results conclude that the two experimental systems (UV and thermally-initiated) afford strikingly similar behaviours despite a distinct difference in their respective behaviour during thermally-induced deswelling. The observed differences in deswelling behaviours argue that the mechanisms involved in thermal and cononsolvency induced collapse are quite different.

In every case, the gels undergo phase separation and collapse to a minimum size in the water-rich region, before reswelling as the alcohol concentration is further increased. It would appear that neat water and neat alcohol are both good solvents for PNIPAM, but the same cannot be said for mixtures of the two. In pure water, water molecules form cage-like structures around the hydrophobic groups around the PNIPAM chains, whilst forming hydrogen bond interactions with the hydrophilic amide groups. It is thought that water molecules form a disordered tetrahedral structure around the alcohol molecules, and further increase in alcohol volume fraction causes the removal of water molecules from the PNIPAM network in favour of forming clathrate hydrates, dehydrating the gels and thus causing them to collapse. This phenomenon is observable in the presented data, with re-entrance swelling behaviour of clay/PNIPAM gels (figures 6.16 – 6.19) occurring more sharply upon equilibration in ethanol solutions than those equilibrated in methanol. The observation that NIPAM gels deswell to a greater extent with an increase in alcohol chain length is consistent with theories presented by Onori *et al* and Zhu *et al* [12, 19] who found that the encapsulation of the alcohol breaks down at lower alcohol volume fractions upon increasing length of the alcohol molecules, explained by the requirement of a greater number of water molecules required to form the clathrate cage. After a point of maximum deswelling, all gels reswell upon increasing the volume fraction of alcohol further. This swelling is thought to occur as a direct result of the clathrate structure encapsulating the alcohol molecules no longer being able to form, allowing the alcohol to interact freely and directly with the PNIPAM chains.

As with heat-induced phase transition experiments, the magnitude of deswelling is heavily influenced by cross-link type, with clay cross-linked gels deswelling to a far greater extent than those cross-linked with BIS. The de- and reswelling behaviour of the BIS/PNIPAM gels (figures 6.20 – 6.23) is highly restricted by the comparative rigidity and inhomogeneous distribution of BIS cross-links when compared to the dynamic "sliding" cross-link interactions afforded by PNIPAM/ clay interactions.

In conclusion, the evidence shows that although cross-link type has a profound effect on swelling/deswelling capacity of the presented PNIPAM-based systems (in agreement with

thermal deswelling data shown in 6.5.1 and 6.5.2); it is independent of alcohol size (at least from methanol to ethanol).

6.4.7 Alcohol volume fraction-dependent deswelling of gelatine- doped clay cross-linked PNIPAM hydrogels

In order to determine the swelling/ deswelling capacity of gelatine- incorporated clay cross-linked PNIPAM gels and quantify possible changes in deswelling behaviour as a direct result of gelatine incorporation and as a function of matrix alcohol concentration, the diameters of 2mm thick circular PNIPAM/ gelatine discs of various gelatine loadings were taken after their equilibration in various concentrations of ethanol and methanol for 28 days. The starting diameter of the freshly prepared discs was 13mm.

The variation in % deswelling of the gel as a function of the volume fraction of alcohol is shown in figures 6.24 and 6.25.
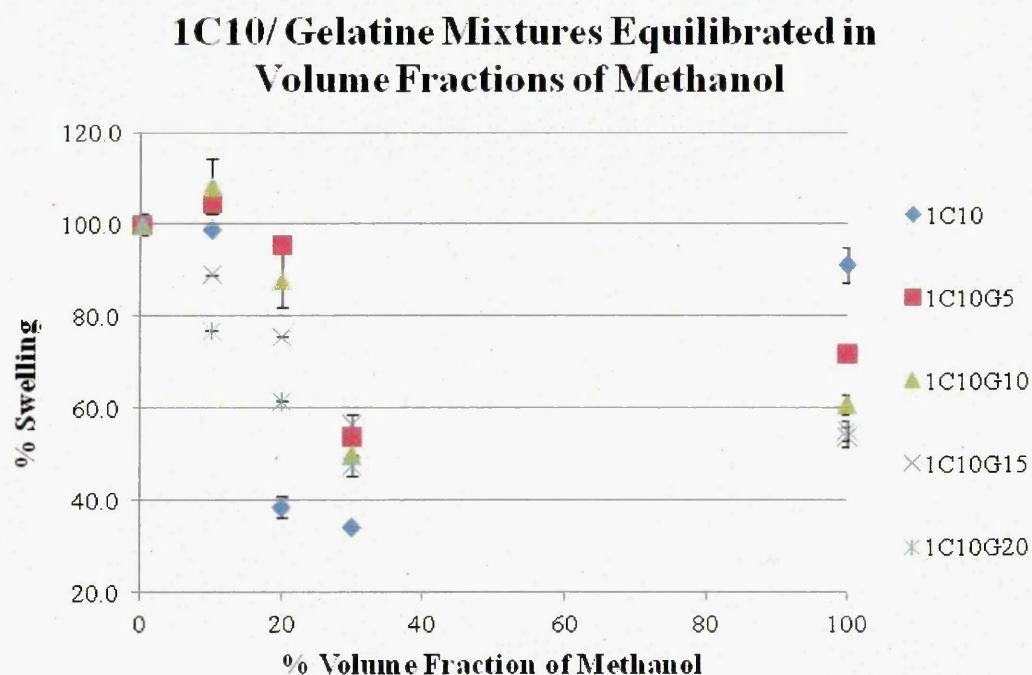
Figure 6.26. The % deswelling of $10C_{10}$/gelatine gels in various methanol concentrations., n = 3.

1C10/ Gelatine Mixtures Equilibrated in Volume fractions of Ethanol
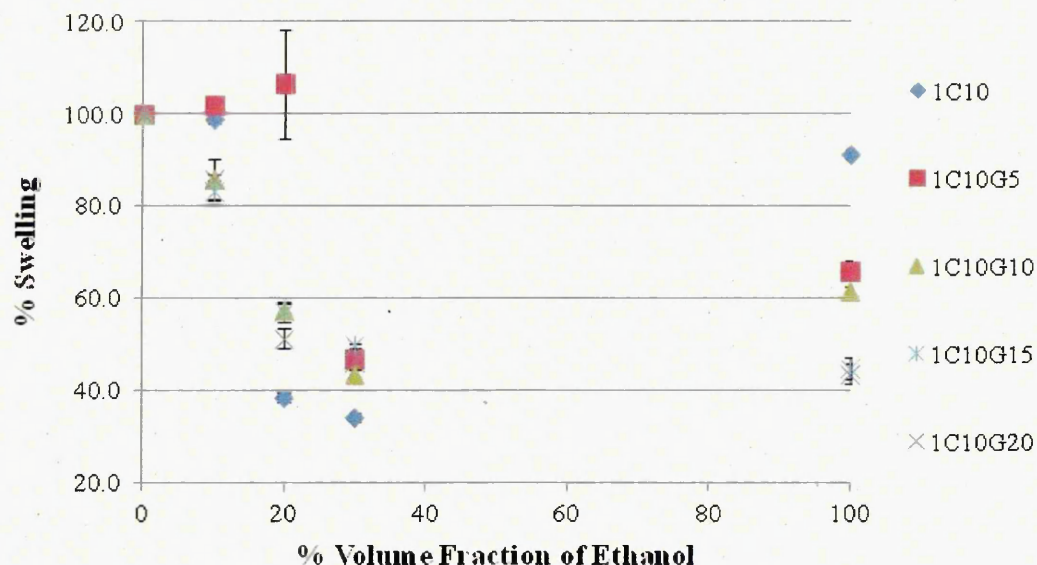
Figure 6.25. The % deswelling of 10C$_{10}$/gelatine gels in various ethanol concentrations. n = 3.

The variation in % deswelling of the gel as a function of the volume fraction of alcohol is shown in figures 6.24 and 6.25. The experiments were performed with 10, 20, 30 and 100% alcohol solutions only, and data outside of these parameters is extrapolated and should be ignored. The purpose of these experiments was to examine the possibility of storing the gels in a sterile environment with a view to utilizing them as medical devices. As shown previously (section 6.5.4), the presence of alcohol causes PNIPAM gels to collapse spontaneously at room temperature by a process of cononsolvency [14], and data presented in section 6.5.3 shows that the presence of gelatine hinders the deswelling process in this type of hydrogel. Here is examined how these two effects combine in alcoholic solutions where the concentration of ethanol (10-30%) may be less likely to be harmful to living tissue.

All gels undergo collapse as alcohol concentration is increased, with the effect being more exaggerated in ethanol systems than those in methanol. This can be explained by the cononsolvency theory proposed by Onori *et al* and Zhu *et al* [12-13], whose models propose that larger alcohol molecules require larger numbers of water molecules to form clathrate hydrate cages around them and indirectly cause PNIPAM to collapse to a higher degree and at a lower alcohol concentration. It could be argued that this effect is responsible for the some degree of separation in gelatine concentration- dependent behaviour in methanol systems (up

to 30% methanol) and the uniformity of deswelling behaviour of all gels in ethanol systems (up to 30% ethanol).

It should be noted here that although water is a good solvent for lower alcohols, gelatine is not soluble in alcohol. By a process called coacervation, summarised in detail in several references [20-23], water molecules preferentially adhere to the alcohol molecules in the presence of gelatine, and the resulting binary mixture is a poor solvent for gelatine [22]. In addition, a decrease in the dielectric constant [23] causes an increase in electrostatic interactions between charged segments the polyion gelatine, and the net result is the collapse of gelatine molecules. This process is separate to that of precipitation, as coacervative solutions are concentrated and polymer-rich, and equilibrium exists between the polymer and supernatant. Re-entrant swelling behaviour of PNIPAM expected at high alcohol concentrations [14] is hindered by the presence of gelatine in all systems.

Swelling Capacity Increase/ Decrease of Gelatine Incorporated PNIPAM in Various Volume Fractions of Methanol Relative to 1C10 Control
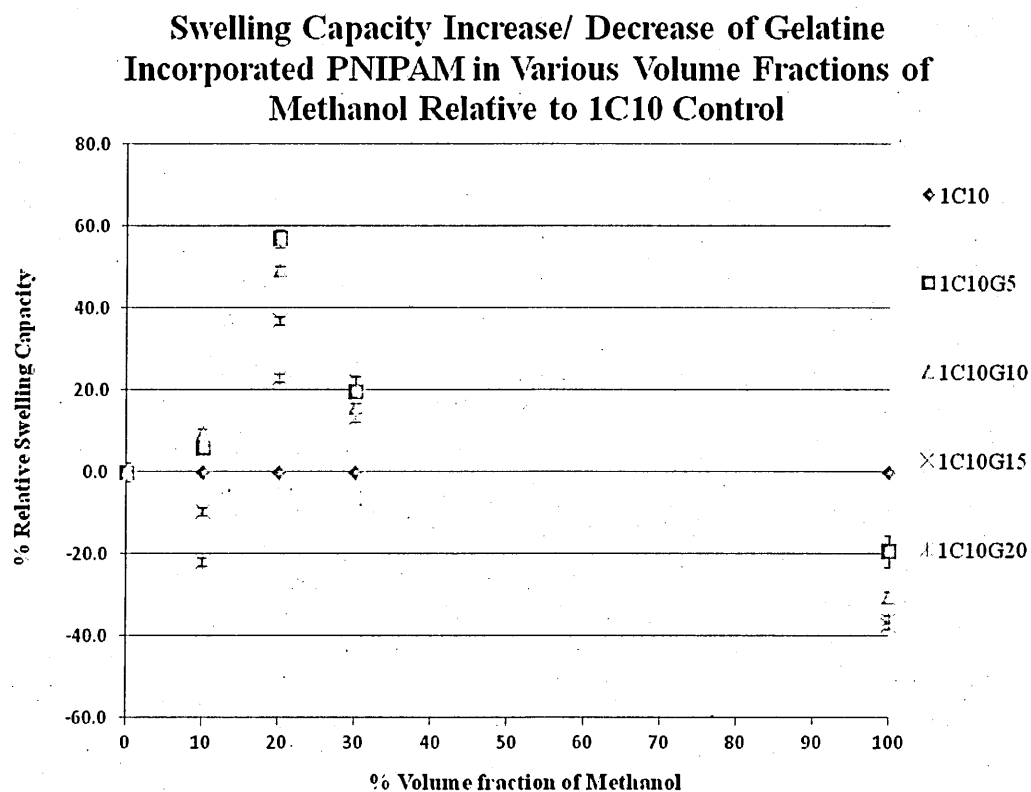
Figure 6.26. A rearrangement of data shown in figure 2.24 to demonstrate the increase in swelling and deswelling capacity of gelatine-incorporated clay cross-linked PNIPAM hydrogels (1C10Gx), as compared to a gelatine- free (1C10) control in matrices of various methanol concentrations.

209

Unlike the deswelling hindrance posed by gelatine in thermally deswollen systems (section 6.5.3), the degree of reswelling hindrance in alcoholic solutions relies upon the concentration of gelatine within the system, therefore indicating that the cause of the hindrance in alcoholic systems is separate from that causing hindrance in thermal systems. The % swelling capacity of all gelatine- doped gels at various alcohol concentrations relative to the $1C_{10}$ control are shown in figures 6.26 and 6.27. Generally speaking, gels containing lower concentrations of gelatine have a much larger swelling capacity in 20% alcohol solutions than their gelatine-free counterparts. A further increase in gelatine content results in a trend of restriction in this swelling capacity. Also, gels containing higher concentrations of gelatine reswell to a lesser extent in the alcohol-rich region than those containing lower concentrations of gelatine. It is observed that the gelatine % and the difference in deswelling/ reswelling capacity differ dramatically. That is to say, for example, a gel containing 5% gelatine does not have it swelling/ deswelling capacity altered by 5%, but in some circumstances, as much as ~64% (figure 6.27).

Swelling Capacity Increase/ Decrease of Gelatine Incorporated PNIPAM in Various Volume Fractions of Ethanol Relative to 1C10 Control
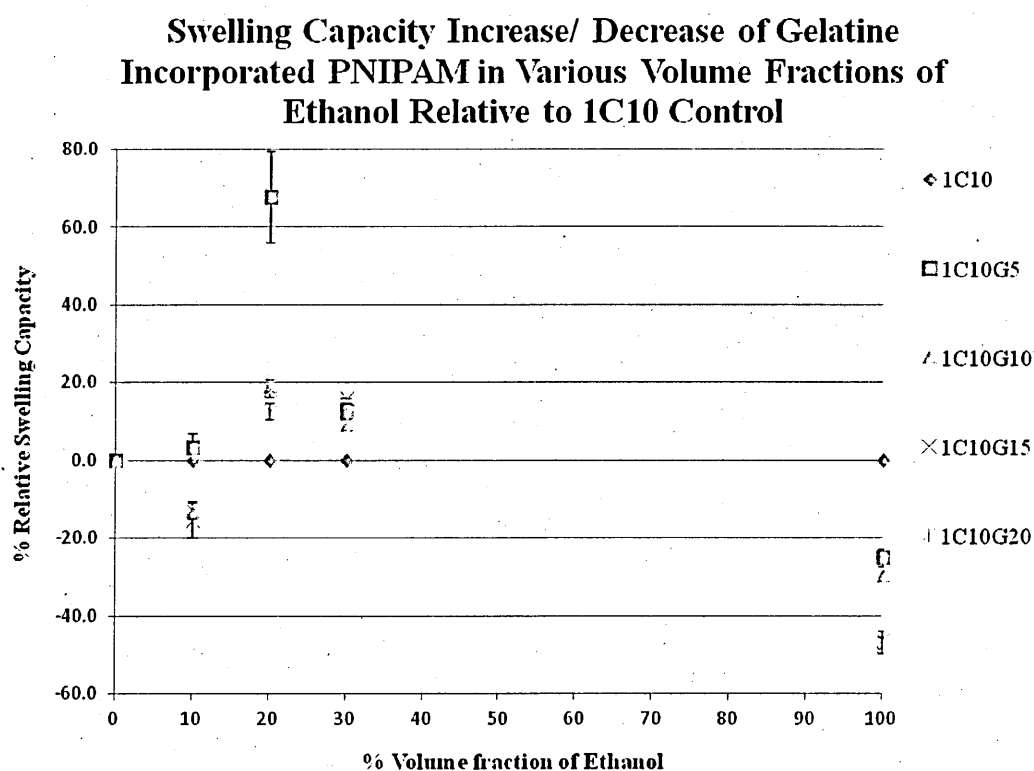
Figure 6.27. A rearrangement of data shown in figure 2.25 to demonstrate the increase in swelling and deswelling capacity of gelatine-incorporated clay cross-linked PNIPAM hydrogels (1C10Gx), as compared to a gelatine- free ($1C_{10}$) control in matrices of various ethanol concentrations.

210

It is thought that this observation is owed to the hydrophobic effect gelatine exerts at high alcohol volume fractions, and whilst PNIPAM chains freely interact with pure alcohol solutions, gelatine chains coacervate and coagulate, disrupting the thermodynamic balance and possibly preventing alcohol entering the interstitial spaces of the PNIPAM network. The degree of disruption to the thermodynamic process of reswelling of PNIPAM in alcoholic solutions (namely, the rupture of hydrogen bonds between gelatine and water molecules) directly correlates with the concentration of gelatine in the system.

6.5   Summary and Conclusions

The rate and magnitude of thermal deswelling in aqueous media is affected by the organic cross-linking agent BIS and clay cross-link density in all types of gel. The initiation method dramatically affects the deswelling behaviour of gels cross-linked with BIS. Upon very gradual warming, thermally initiated PNIPAM/ BIS gels have reached their full deswelling capacity at around 36°C, whilst UV initiated PNIPAM/ BIS gels sustain realtively steady deswelling rate up to at least 50°C.

Gels cross-linked with clay exhibit larger volume changes than those cross-linked with BIS, and the ratio of gel volume below LCST: above LCST increases with decreasing cross-linker content for both organically and clay cross-linked PNIPAM hydrogels. The deswelling behaviour of PNIPAM gels cross-linked with clay is sharper and more defined than those cross-linked with BIS. Gel flexibility varies between the two systems, as expected. All gels prepared using BIS were extremely brittle and could not withstand any significant degree of deformity. Contrarily, all gels prepared with clay as a cross-linking agent adopted rubber-like behaviour and can withstand high degrees of deformation regardless of clay loading and preparation method, unless they are diluted.

PNIPAM materials exhibit interesting optical properties. BIS/ PNIPAM gels exhibit consistently poor transparency regardless of temperature, which is thought to be due to the spatial cross-link inhomogeneity within the polymer network. Clay/ PNIPAM gels exhibit considerable transparency changes at LCST (excellent transparency below LCST and poor transparency above it) regardless of initiation method or clay concentration, suggesting uniform dispersion within the gel network regardless of cross-link density.

The incorporation of gelatine into the PNIPAM/ clay network severely hinders its ability to deswell upon an increase in temperature, and the degree of this hindrance is independent of the concentration of gelatine.

211

The incorporation of hyaluronic acid (HA) into the PNIPAM/ clay network severely hinders its ability to deswell upon an increase in temperature, and the degree of this hindrance is independent of the concentration of HA.

The dilution of PNIPAM/ clay precursor hydrogels (PCPHs) with water before solidification hinders the deswelling ability of the network as a function of temperature up to 38°C, and this degree of hindrance is independent of degree of dilution between 25 and 50%. Beyond 38°C, diluted PNIPAM/ clay gels undergo a large degree of collapse which brings their deswelling behaviours in line with that expected of non-diluted PNIPAM/ clay gels.

Although the deswelling capabilities of PNIPAM/ clay gels can be controlled somewhat by dilution with water, the mechanical stability of the gels is greatly affected, with weaker gels attributed to higher degrees of dilution.

The de/reswelling behaviour of PNIPAM/ clay gels and gelatine incorporated PNIPAM/ clay gels can be controlled by adjusting the alcohol volume fraction of the media, and although gels cross-linked with BIS exert restricted swelling/ deswelling behaviours compared to those cross-linked with clay, the cross-link density within systems does not have a significant impact on this de/reswelling behaviour.

6.7 References

1.   Hoffman, A.S., Hydrogels for biomedical applications. Advanced Drug Delivery Reviews, 2002. 54(1): p. 3-12.

2. .   Schexnailder, P., Schmidt, G., Nanocomposite polymer hydrogels. Colloid and Polymer Science, 2009. 287(1): p. 1-11.

3.   Freitag, R., Garret-Flaudy, F., Salt effects on the thermoprecipitation of poly-(N-isopropylacrylamide) oligomers from aqueous solution. Langmuir, 2002. 18(9): p. 3434-3440.

6.   Garcia, A., et al., Photo-, thermally, and pH-responsive microgels. Langmuir, 2007. 23(1): p. 224-229.

5.   Hirokawa, Y., Tanaka, T., Volume phase transition in a nonionic gel. Journal of Chemical Physics, 1986. 81(12): p. 6379-6380.

6.   Klaikherd, A., et al., Multi-Stimuli Sensitive Amphiphilic Block Copolymer Assemblies. Journal of the American Chemical Society, 2009. 131(13): p. 4830-4838.

7.   Liang, L., et al., Thermosensitive poly(N-isopropylacrylamide)-clay nanocomposites with enhanced temperature response. Langmuir, 2000. 16(25): p. 9895-9899.

8.   Lue, S.J., et al., Tuning of Lower Critical Solution Temperature (LCST) of Poly(N-Isopropylacrylamide-co-Acrylic acid) Hydrogels. Journal of Macromolecular Science Part B-Physics, 2011. 50(3): p. 563-579.

9.   Schmidt, D., et al., New advances in polymer/layered silicate nanocomposites. Current Opinion in Solid State & Materials Science, 2002. 6(3): p. 205-212.

10.   Tanaka, T., et al., phase transitions in ionic gels. Physical Review Letters, 1980. 45(20): p. 1636-1639.

11.   Wu, C., Zhou, S., Volume phase transition of swollen gels: Discontinuous or continuous? Macromolecules, 1997. 30(3): p. 574-576.

12.   Petrillo, C., et al., Hydration structure of ethanol water solution at low alcohol concentration. Molecular Physics, 1989. 67(3): p. 697-705.

13.   Zhu, P.W., Napper, D., Coil-to-globule type transitions and swelling of poly(N-isopropylacrylamide) and poly(acrylamide) at latex interfaces in alcohol-water mixtures. Journal of Colloid and Interface Science, 1996. 177(2): p. 343-352.

16.   Schild, H.G., et al., Cononsolvency in mixed aqueous solution of poly(N-isopropylacrylamide). Macromolecules, 1991. 24(4): p. 948-952.

15.   Haraguchi, K., Takehisa, T., Nanocomposite hydrogels: A unique organic-inorganic network structure with extraordinary mechanical, optical, and swelling/de-swelling properties. Advanced Materials, 2002. 14(16): p. 1120-1126.

16.   Gomez-Alejandre, S., et al., Partial specific volume of hyaluronic acid in different media and conditions. International Journal of Biological Macromolecules, 2000. 27(4): p. 287-290.

17.   Schmidt, D.J., et al., Electrochemically Controlled Swelling and Mechanical Properties of a Polymer Nanocomposite. Acs Nano, 2009. 3(8): p. 2207-2216.

18.   Ahn, S., E.C. et al., Ion and pH Effect on the Lower Critical Solution Temperature Phase Behavior in Neutral and Acidic Poly(organophosphazene) Counterparts. Langmuir, 2009. 25(4): p. 2407-2418.

19.   Zhu, P.W., Napper, D., Volume phase transitions of poly(N-isopropylacrylamide) latex particles in mixed water-N,N-dimethylformamide solutions. Chemical Physics Letters, 1996. 256(1-2): p. 51-56.

20.   Etsuo, K., Functional immobilized biocatalysts. Progress in Polymer Science, 1992. 17(4): p. 647-697.

21.   Peters, H.J.W., et al., Effect of gelatin properties in complex coacervation processes. Drug Development and Industrial Pharmacy, 1992. 18(1): p. 123-136.

22.   Mohanty, B., Bohidar, H., Systematic of alcohol-induced simple coacervation in aqueous gelatin solutions. Biomacromolecules, 2003. 4(4): p. 1080-1086.

23.   Mohanty, B., Bohidar, H., Microscopic structure of gelatin coacervates. International Journal of Biological Macromolecules, 2005. 36(1–2): p. 39-46.

7

PCPH as an Injectable, Functional Therapy for Degenerative Disc Disease

Chapter 7. PCPH as an injectable, functional therapy for degenerative disc disease.

7.1   Introduction

Synthetic biomaterials have been gaining an ever growing interest in the replacement, regeneration and restoration of lost and diseased/ dysfunctional biological tissue in recent years. Polymeric hydrogels are of particular interest because of their ability to retain large amounts of water and their morphological and mechanical similarity to natural tissue [1-2]. Their interactions with aqueous matrices induce thermodynamically driven equilibrium swelling/shrinking phenomena which result in utilisable properties in biochemical delivery systems [2].

Therapeutic hydrogel formulations which are capable of administration by injection are particularly attractive not only because of their ease of administration, but their minimally invasive delivery, reduced risk of infection, reduced healing time and minimal scarring when compared with surgically implanted devices [3]. Injectable formulations also prove to be of particular use when the size and shape of the final device is defined by the dimensions of space or void to be filled, even moreso when the cavity is complex and/or contains very narrow fissures [4].

Cross-linking of polymer materials *in situ* is usually achieved through enzymatic processes where injectable precursors are administered separately and react within the body, or photo irradiation following the injection of a photo-reactive hydrogel precursor. Both of these techniques harbour some significant drawbacks. For example, the toxicity risk of side reactions to nearby biological tissue, the risk of some leachable chemical species remaining unreacted within the cavity (cross-linking agents and monomers, for example) and the requirement for the reaction to take place in biologically compatible conditions [5-7]. The material must possess low enough viscosity to allow injection yet form a mechanically stable gel quickly enough to prevent burst release. For enzymatic processes, kinetics of the cross-linking dictates a very precise injection time and constituent quantity. Hydrogels can also be pre-formed into micro or nano-sized particles, thus rendering them injectable. However, these particulate systems are injectable by virtue of their small size and offer limited mechanical support *in situ*.

7.1.1 Degenerative disc disease and low back pain

Intervertebral discs (IVDs) provide spinal structural support by anchoring adjacent vertebral bodies to one another, as well as act as shock absorbing "sponges" capable of withstanding stress created by normal human movement. Their very high water content and subsequent high elasticity are integral in allowing this [8].
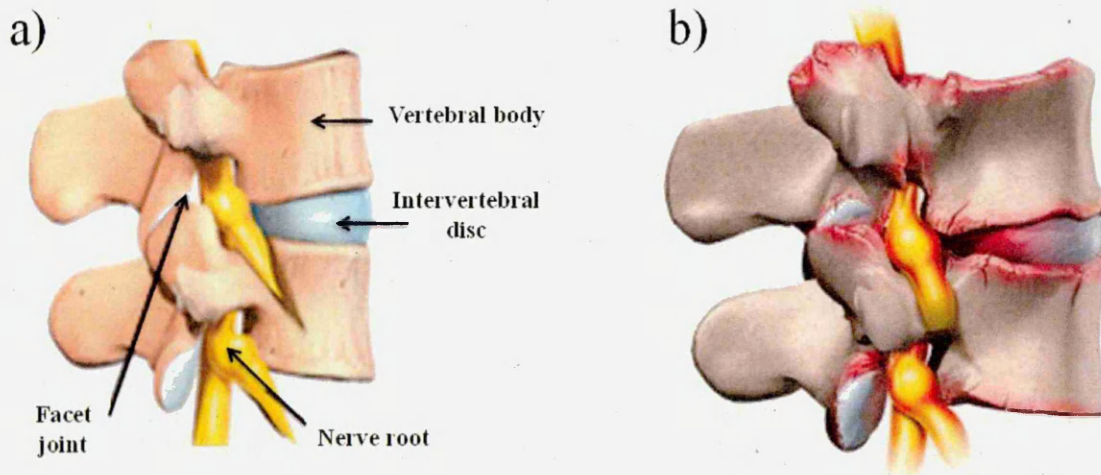
Figure 7.1. Schematic showing human spinal anatomy and the difference between a) a healthy spine and b) a spine affected by degenerative disc disease [9].

IVDs are located within very close proximity to the nerve root of the spine (figure 7.1), and a decrease in disc height with age and disease not only alters and restricts the mechanical movement of the spine, but also inflicts pressure on the spinal nerve and can be the cause of significant pain. Approximately 40% of low back pain cases are associated with the degradation and disease of intervertebral disc tissue.

In the centre of the disc is a jelly-like material called the nucleus pulposus (NP) which in a healthy individual, consists of 80-90% water. The NP is constrained around the peripherals of the spinal disc by a very tough structure called the annulus fibrosus, which consists of concentric rings of collagen. Figure 7.2a demonstrates the appearance of healthy IVD tissue. Figure 7.2b shows an IVD which exhibits a number of features consistent with degenerative disc disease. These include the formation of fissures or slits within the IVD, damage to the end plates. It is via the endplates that the majority of nutrients enter and waste products such as lactic acid exit the IVD via the circulatory network within the vertebral body. When this area is damaged, cells within the disc begin to exhibit abnormal morphologies and a

subsequent loop of cell death and end plate damage ensues. Loss of vertebral height and the physical bulging out of the NP from the disc is also clearly identifiable.
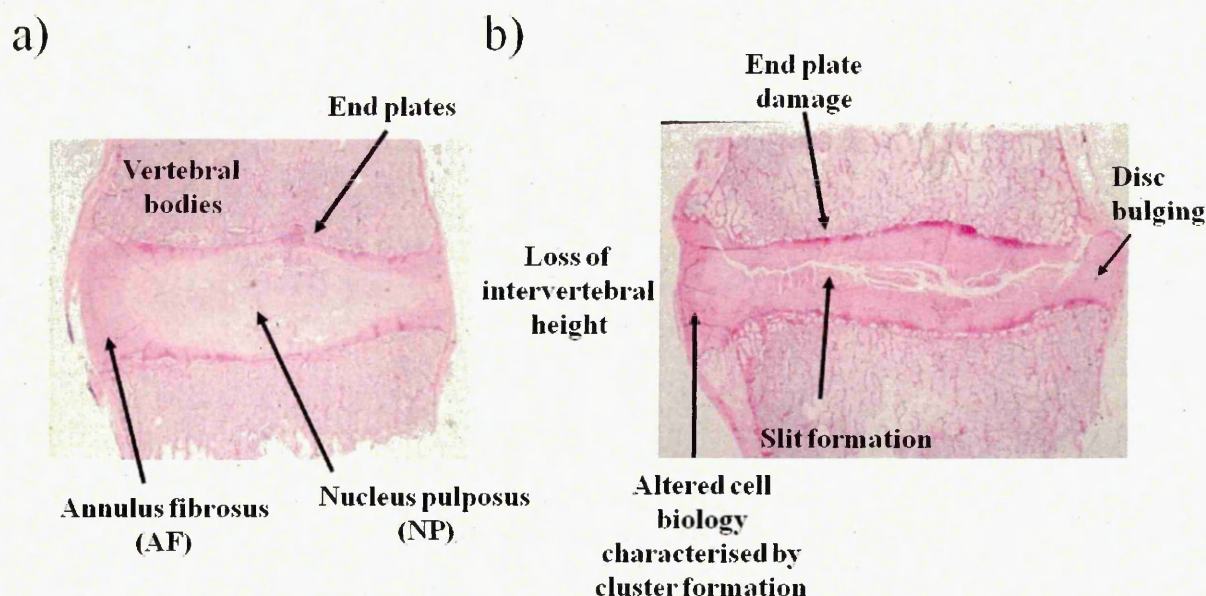
**Figure 7.2. Structure of the human IVD showing annulus fibrosus, nucleus pulposus and position of end plates and vertebral bodies in a) a healthy spinal disc and b) a disc subject to degenerative disc disease [10].**

Although not a life threatening condition, low back pain sufferers experience a severe decrease in quality of life. At present, treatments for the condition are generally unsuccessful from a long-term viewpoint and do not directly target the cause. Several previous treatments such as spinal fusion [11] and disc prostheses [12] have been abandoned in recent years by many spinal surgeons as the subsequent side-effects, such as adjacent segment degeneration [13] and movement restriction, do not outweigh the benefits of such procedures, and indeed many cause accelerated degeneration in adjacent spinal discs.

The IVD consists of 3 morphologically separate regions, as indicated in figure 7.2. These are the nucleus pulposus (NP), which is a hydrogel-like material located at the centre of the IVD. The annulus fibrosus (AF), is a fibro-cartilaginous region comprised of ~ 15 –25 concentric lamellae of type I collagen, adapted to dissipate mechanical impact and tensile loading during normal movement [14]. It encapsulates the NP and holds it in place. Cartilage endplates (CEP) is a ~0.6 -1mm thick layer of tissue which resembles articular cartilage [14]. It is located at the interface between the vertebral body and the adjoining IVD and is sufficiently permeable to allow the diffusion of nutrients and waste products to and from the avascular IVD, whilst limiting the escape of osmotically active proteoglycan [15].

218

The biochemical composition of spinal disc tissue reflects the specialist functions of each tissue type. In addition to their high water content (typically 70-90%), their biochemical constituents include proteoglycans, (figure 7.3a), collagen type II (figure 7.3b), and other non-collagenous proteins, which are differentially distributed throughout the different tissue types. The number and distribution of proteoglycans is a determining factor in the tissue swelling behaviour and compressive mechanical properties [16-18].

a)   b)   c)
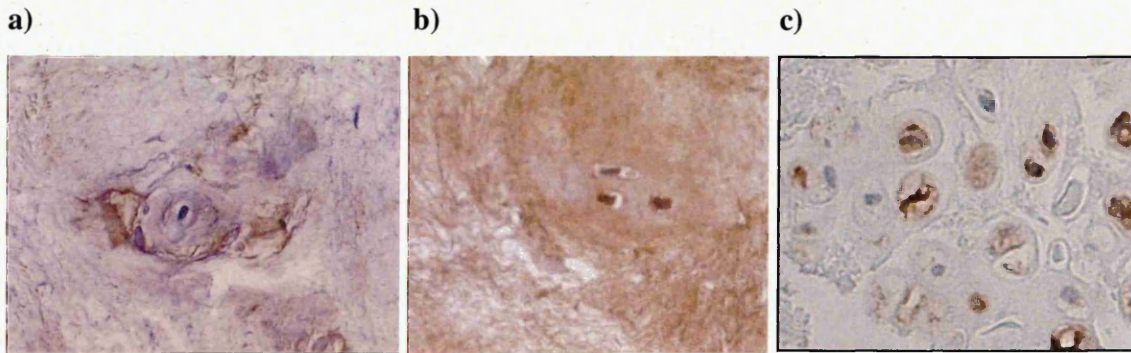
Figure 7.3. Light microscopy images showing the distribution of of a) proteoglycans (stained purple), collagen type II (stained brown), and c) the effect of destructive enzymes on healthy living NP cells [10].

Collagen type II is a constituent of the loose hydrogel-like NP network and forms a scaffold to which the proteoglycans attach [19]. A clear indication of IVD degeneration is a reduction in production of collagen II, and therefore proteoglycans, in the central NP [20-21]. Instead, there is an increased production of a number of enzymes which chemically break down the collagen and proteoglycan matrix (figure 7.3c), and a degenerative cycle ensues. In addition to this, a reduction in collagen II stimulates an increase in production of collagen I within the NP, making the soft, jelly-like substance tougher and more fibrous.

Ideally, new therapies would involve the development of a hydrogel-like material which would replace and help regenerate NP material, relieve pain and provide support to the healing disc without the need for surgical removal of existing tissue. Except in the case of herniation, for which keyhole surgery can be applied in the removal of the prolapsed material which can subsequently be replaced.

7.1.2   Potential regenerative options/ maintenance of tissue architecture

A number of strategies are currently in place to reduce low back pain in patients with degenerative disc disease. These include surgical intervention with complete IVD removal and arthodesis (the artificial induction of fusion between the two vertebral bodies), and more conservative measures such as annuloplasty [22] (a heated wire is inserted into the IVD, sealing disc ruptures and burning nerve endings), percutaneous disc decompression [23-24] (the removal of herniated disc tissue using rotary action through a needle, which creates a vacuum within the disc and pulls the bulge or herniation backward) and percutaneous discectomy [25] (the surgical removal of bulging or herniated IVD tissue that exerts pressure on a nerve root or the spinal cord). Further to this, the use of analgesia, corticosteroids, and muscle relaxants are commonplace [26]. As treatments are aimed toward the reduction of pain, their results are often palliative and do not prevent degeneration of adjacent tissues caused by alterations in disc height, intradiscal pressure, poor load distribution, and consequently, unnatural motion [27]. New treatments would involve the regeneration of the spinal disc involving restoration of disc height as well as biomechanical function.

7.1.2.1   Human mesenchymal stem cell (MSC) therapy

Cell-based IVD therapy used in conjunction with the dynamic restoration of the spinal segment as a future treatment concept looks promising [28].

MSCs are multipotent stromal cells that have robust clonal self-renewal and multilineage differentiation potential, capable of differentiation to chondrocytes (cartilage cells), intervertebral disc cells (IVDs) osteoblasts (bone cells), and adipocytes (fat cells). The MSCs used in this study are harvested from adult human bone marrow, and as part of spinal disc regeneration therapy are injected directly into the degenerated spinal disc where they are proposed to produce the correct type of matrix.

Presented in this chapter is a novel, injectable hydrogel delivery system which may assist in the restoration of mechanical function and disc height, inhibit the spinal degeneration cycle and deliver human mesenchymal stem cells (MSCs) as well as growth factors which can trigger the IVD tissue regeneration process.

7.1.3   An injectable hydrogel carrier system.

When designed into an injectable format, invasiveness of the insertion of hydrogel materials into the body is greatly reduced, the risk of infection is diminished, healing time is minimised, and surgical costs are lowered.

The overall goal of the next line of enquiry was to combine MSCs with PCPH in order to create a double-approach therapy to IVD disease. The system would allow the MSCs to be delivered to the IVD via injection, whilst the hydrogel scaffold formed *in situ* on order to provide some of the mechanical properties that may have been lost during disk degenaration.
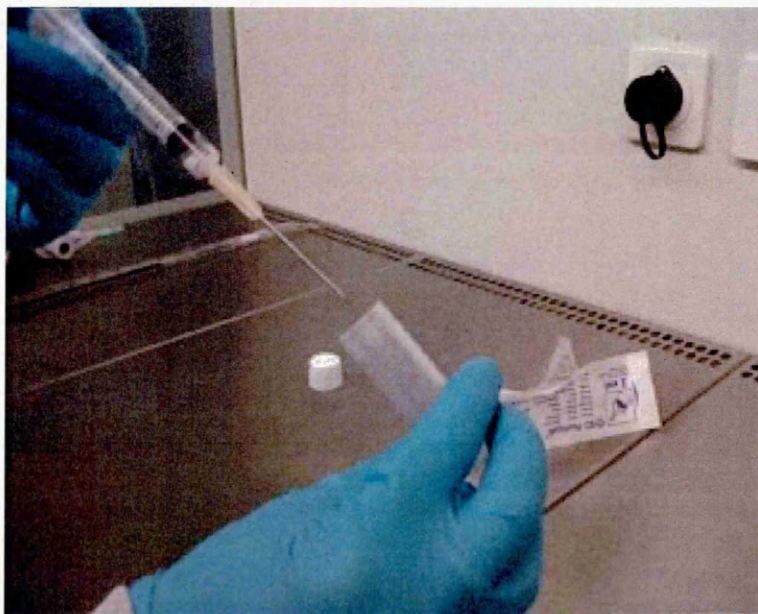
Figure 7.4. Dr. Christine Le Maitre passing a warm $1C_{10}$ PCPH formulation through a 21 gauge needle with ease.

A vital consideration in the design of injectable hydrogels is the requirement for the precursor to be injectable through a very fine bore needle, as the insertation of a wide needle into the IVD may cause further degeneration issues. Figure 7.4 shows Dr. Christine Le Maitre at the Biomedical Research Institute at Sheffield Hallam University passing a warm $1C_{10}$ PCPH formulation through a 21 guage needle and into a sample vial with ease. Immediately following this, the PCPH which had collected in the sample vial cooled and underwent PTTNAG, forming a rubbery $1C_{10}$ polymer/ clay nanocomposite hydrogel.

7.2. Human cell viability studies in the presence of various hydrogel formulations

Although the NIPAM in its monomeric form is toxic to living cells [29] cytocompatibility of purified, fully-reacted PNIPAM has been demonstrated [30-37]. The methodology used in PCPH synthesis requires that in contrast to previous work involving PNIPAM and live tissues, no purification steps may be performed between initiation and injection. This potentially allows for cytotoxic monomers and oligomers to remain in the "fully reacted"

PCPH solutions. A series of cytocompatibility tests were designed and carried out by Dr. Christine Le Maitre and Mrs. Becky Barthrop at the Biomedical Research Institute, Sheffield Hallam University.

7.2.1 Cells used in this study

The cells used for the work carried out in this chapter were human adult mesenchymal stem cells (MSCs) derived from bone marrow tissue (Lonza).

7.2.2 MSC cell viability study in the presence of PNIPAM/ clay nanocomposite hydrogels

A 5mm^2 piece of cast 1C$_{10}$ prepared as described in Section 2.2.1.2,was suspended via cell culture inset (Nunc), as illustrated in figure 7.5, in cell culture media containing human MSCs at a concentration of 100,000 cells/ ml. Cells were maintained at 37°C, 5% CO$_2$ for 14 days.
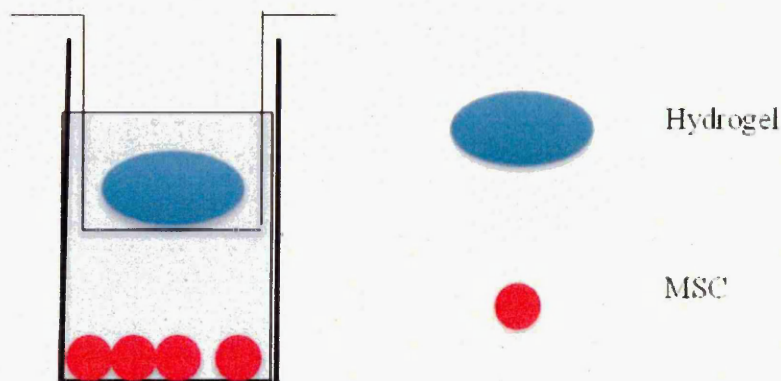
Figure 7.7. Schematic of the apparatus used to determine the cell viability of human MSCs in the presence of unpurified PNIPAM/ clay nanocomposite hydrogels.

The experiment was conducted to establish whether any toxic elements were being leeched by the hydrogel which would affect the cell viability. A cell viability assay using Hoechst /propidium iodide staining and live/ dead cell counts was performed and compared to that of controls inoculated from the same cell cultures without the presence of hydrogel. Hydrogel formulations tested included .5C$_{10}$ and 1C$_{10}$.
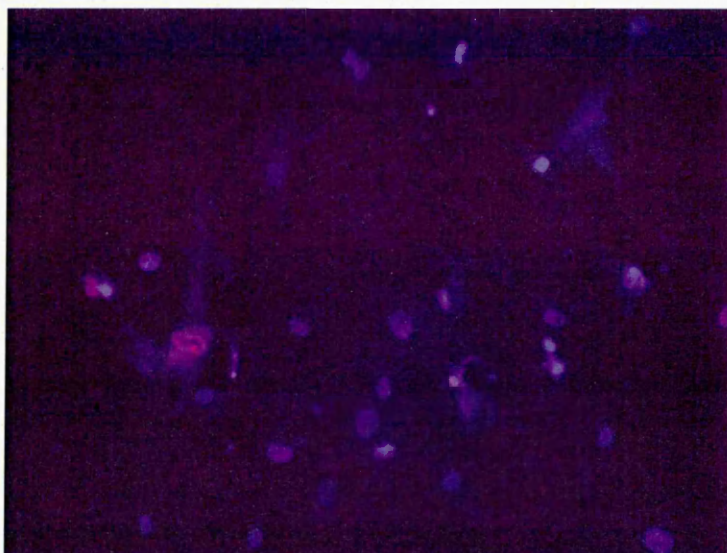
Figure 7.6. A light micrograph of human MSCs cultured for 2 weeks in the presence of a 1C10 PNIPAM/ clay nanocomposite hydrogel and suject to a live/ dead assay. Live cells appear blue/ purple and dead cells appear red.

A light micrograph of the assay derived from the $1C_{10}$ formulation is shown in figure 7.6. This assay highlights live cells with normal morphologies which appear as bright blue/ purple dots on the micrograph, and dead cells/ those with abnormal nuclear morphologies which appear red. The single dead cell locatable in the 200 cells counted is shown to the middle left of the micrograph.

Figure 7.7 shows the viability graph for cells which are in a control environment (without the presence of hydrogel), in the presence of a $1C_{10}$ hydrogel, and in the presence of a $.5C_{10}$ hydrogel, respectively. It was concluded that culture media containing gel sheets of any clay concentration did not affect viable cell numbers, conclusively showing that the hydrogels did not leech any toxic substances into the culture media which was cytotoxic to the human MSCs.
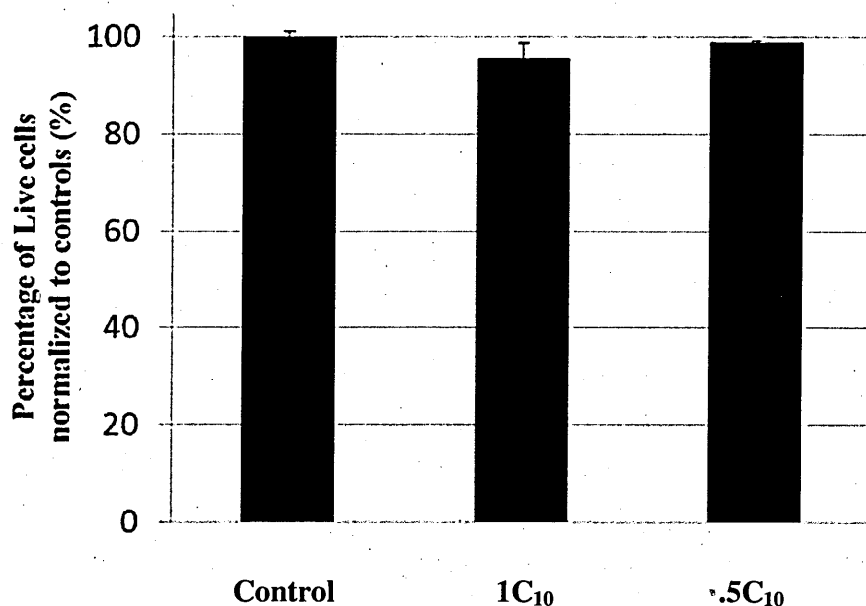
Figure 7.7 Live/ dead assay cell viability graphs for MSCs cultured alone in cell culture media and in the presence of PNIPAM/ clay nanocomposite hydrogels of 2 clay concentrations (see table 2.1) for 2 weeks.

7.2.3   MSC cell viability study in contact with PNIPAM/ clay nanocomposite hydrogels

To examine interaction behaviour between MSCs and the PNIPAM/ clay nanocomposite hydrogel, gelated $5mm^2$ sheets of $1C_{10}$ hydrogel of ~2mm thickness, prepared as described in Section 2.2.1.2, were placed on the bottom of *in vitro* cell culture plates filled with cell culture media. ~ 100,000 MSCs were labelled with a green fluorescent membrane dye (Sigma) and inoculated onto the sheet surface. The plates were then incubated at 37°C, 5% CO_2 for 2 weeks.

Figure 7.8a shows the light micrograph of the bottom of the cell culture plate after 24 hours. Clearly visible are live cells, which appear as bright green spots, adhered to the plate. To establish whether cell/ hydrogel interactions were occurring elsewhere in the system, the microscope was focussed onto the surface of the hydrogel (figure 7.8b). The micrograph revealed live cells adhered to the hydrogel upper surface, positively rendering the hydrogel a viable environment for MSC attachment after 1 day.
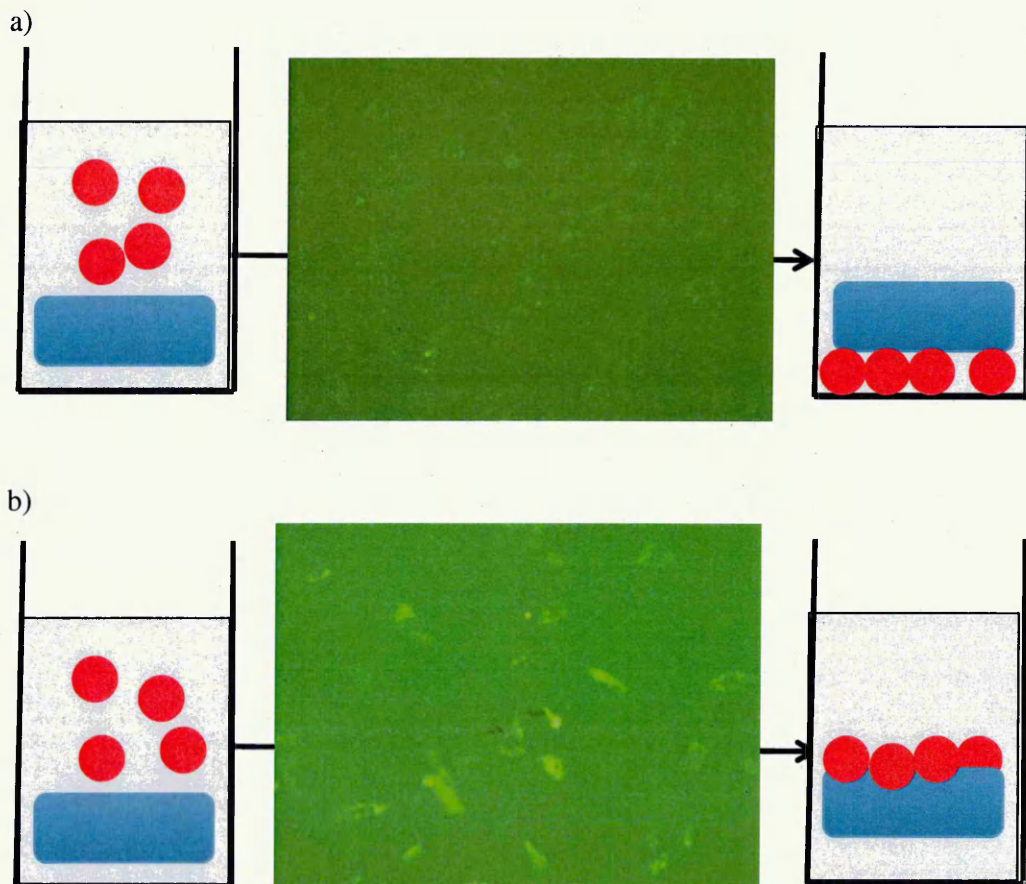
Figure 7.8. Live MSCs, visible as bright green dots, were applied to the surface of a block of assembled 1C$_{10}$ hydrogel. The micrographs show a) cells adhered to the bottom of a cell culture plate and b) cells adhered to the upper surface of the hydrogel after 24h culture.

Figure 7.9. Live MSCs, visible as bright green dots, were applied to the surface of a block of assembled 1C$_{10}$ hydrogel. The micrographs show a) cells adhered to the bottom of a hydrogel-free control cell culture plate, b) cells adhered to the bottom of the cell culture plate containing 1C$_{10}$ and c) cells adhered to the upper surface of the 1C$_{10}$ hydrogel after 2 weeks culture.
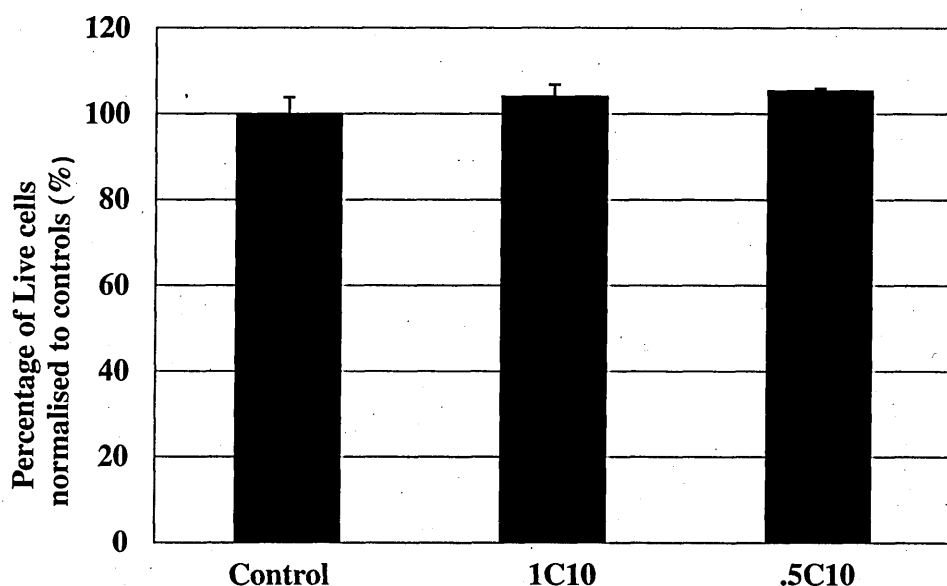
Figure 7.10. Live/ dead assay cell viability graphs for MSCs cultured alone and adhered to PNIPAM/ clay nanocomposite hydrogels of 2 clay concentrations (see table 2.1) for 2 weeks.

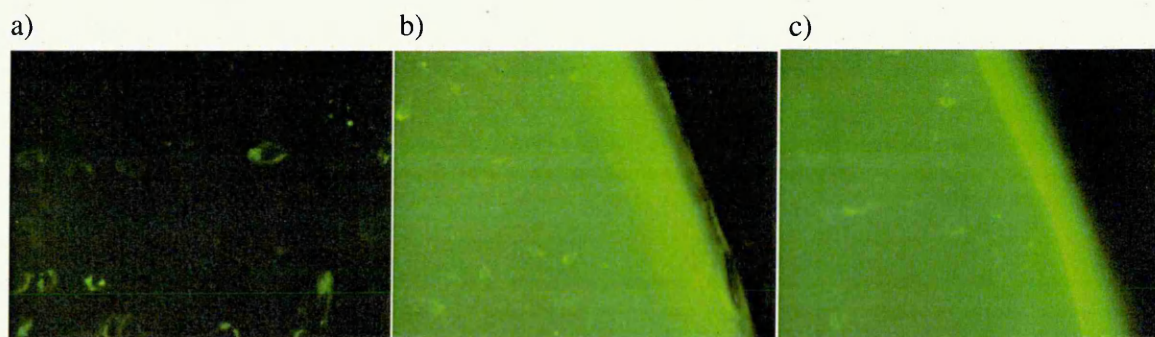Figure 7.9 shows the optical micrographs taken of the fluorescent dyed cells after 2 weeks' culture. 7.9a shows the control system, cells kept in identical conditions proliferating on the bottom of a culture well plate without the presence of hydrogel for comparison purposes.

7.9b shows n optical a micrograph taken when focussed onto the bottom of a well plate which contained $1C_{10}$ hydrogel. Many live, proliferating cells are clearly seen. 7.9c shows an optical micrograph taken when focussed onto the upper surface of the $1C_{10}$ hydrogel where many live, proliferating cells are also clearly observable.

The live/ dead assay cell viability graph shown in figure 7.10 shows that regardless of clay · content, direct cell/polymer interactions do not have an effect on MSC cell viability during after 2 weeks.

For the purposes of IVD tissue regeneration in the presence of a tissue scaffold, it is important that the cells do not preferentially adhere to the outer surfaces of the hydrogel but migrate through it, repopulating the disc. To clearly determine whether cell migration is a feasible occurrence in an assembled PNIPAM/ clay system, the experiment was repeated using a 5mm diameter x 15mm length cylinder of $1C_{10}$ hydrogel. ~100,000 cells were applied to the surface of the hydrogel and incubated at 37°C, 5% CO_2 for 14 days, following which time Hoescht stain was applied to visualise cell nuclei. The cells were then visualised inder

a)

Hydrogel

MSC

b) c)

d) e)

Figure 7.11. Live MSCs, visible as small blue dots, were applied to the surface of a block of assembled 1C$_{10}$ hydrogel. The cell migration process, shown schematically in a), was visualised microscopically and imaged at various depths of the gel from the surface to the culture plate bottom and micrographs are shown in figures b-e respectively.

an inverted florescent microscope. Figure 7.11 shows a schematic of the migration process (7.11a) as well as series of micrographs taken at regular sectioned intervals through the gel of 2.5mm (7.11b showing the upper gel surface, 7.11e showing the culture plate bottom). The cells appear in the micrographs as small blue dots. Each section clearly showed new, viable

227

cells. This conclusively demonstrates the cytocompatibility of the unpurified PNIPAM/ clay hydrogels, also that they allow for MSC cell proliferation and migration through interstitial hydrogel spaces.
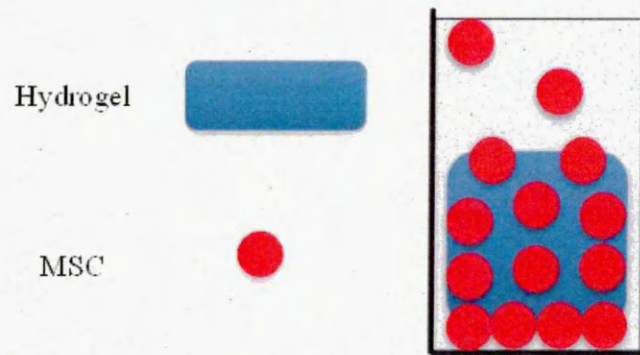
7.9b shows n optical a micrograph taken when focussed onto the bottom of a well plate which contained $1C_{10}$ hydrogel. Many live, proliferating cells are clearly seen. 7.9c shows an optical micrograph taken when focussed onto the upper surface of the $1C_{10}$ hydrogel where many live, proliferating cells are also clearly observable.

The live/ dead assay cell viability graph shown in figure 7.10 shows that regardless of clay content, direct cell/polymer interactions do not have an effect on MSC cell viability during after 2 weeks.

For the purposes of IVD tissue regeneration in the presence of a tissue scaffold, it is important that the cells do not preferentially adhere to the outer surfaces of the hydrogel but migrate through it, repopulating the disc. To clearly determine whether cell migration is a feasible occurrence in an assembled PNIPAM/ clay system, the experiment was repeated using a 5mm diameter x 15mm length cylinder of $1C_{10}$ hydrogel. ~100,000 cells were applied to the surface of the hydrogel and incubated at 37°C, 5% CO_2 for 14 days, following which time Hoescht stain was applied to visualise ce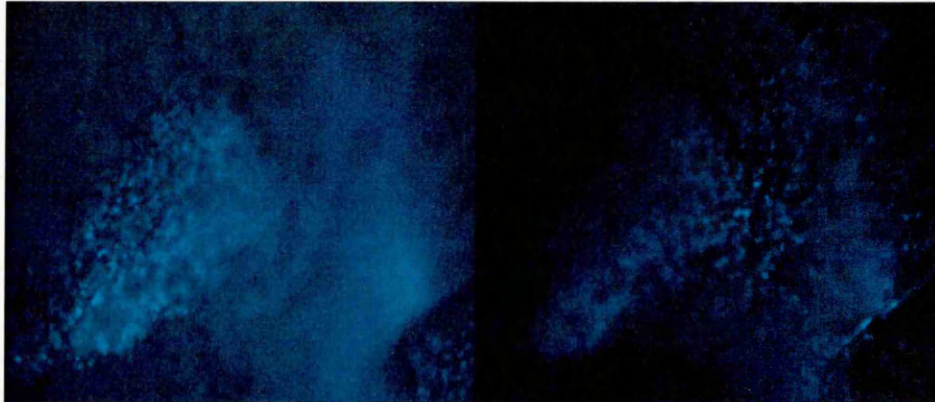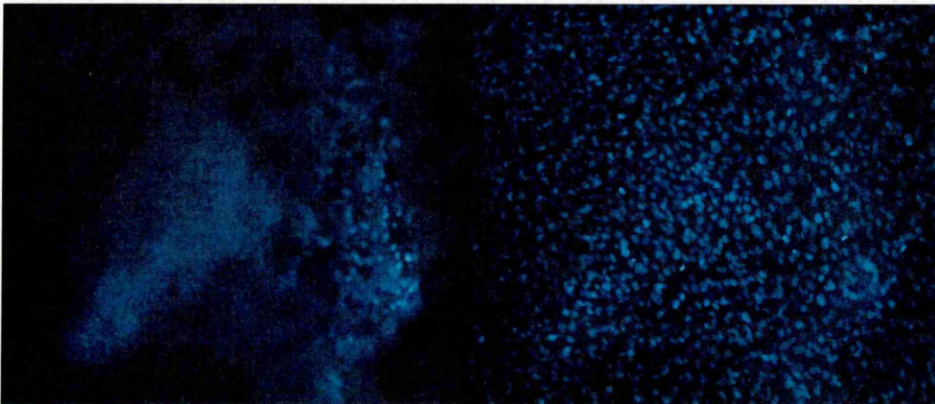ll nuclei. The cells were then visualised inder an inverted florescent microscope. Figure 7.13 shows a schematic of the migration process (7.11a) as well as series of micrographs taken at regular sectioned intervals through the gel of 2.5mm (7.11b showing the upper gel surface, 7.11e showing the culture plate bottom). The cells appear in the micrographs as small blue dots. Each section clearly showed new, viable cells. This conclusively demonstrates the cytocompatibility of the unpurified PNIPAM/ clay hydrogels, also that they allow for MSC cell proliferation and migration through interstitial hydrogel spaces.

7.2.4.   The viability of human MSCs when incorporated into the PCPH prior to PTTNAG.

In a clinical setting, it is anticipated that the cells would be mixed with the liquid PCPH and injected above the polymer PTTNAG temperature in order to form a PNIPAM/ clay nanocomposite hydrogel doped with live MSC cells at a desired location *in vivo*. The next line of enquiry involved the determination of cell viability during a simulation of this process.

For these experiments, a $1C_{10}$PCPH formulation, prepared as described in Section 2.2.1.2, was cooled to 38°C, remaining as a low viscosity liquid. One million fluorescently labelled

MSCs were added to 1ml of the PCPH, of which 0.05ml was pipetted into a well plate which was briefly cooled to 35°C to facilitate gel PTTNAG. 0.2ml growth media was added to the gel and the system was allowed to incubate at 37°C, 5% CO_2. After 24h incubation, a micrograph (figure 7.12a) showed an abundance of live MSCs through the centre of the gel. After 28 days incubation, MSCs were still visible throughout the gel (figure 7.12b), demonstrating very good viability. Encouragingly, it appeared as though cells were creating "lacunae" within the gel matrix. In simple terms, these are small spaces the cells generate in order to produce its own specific functional environment.

a)   b)
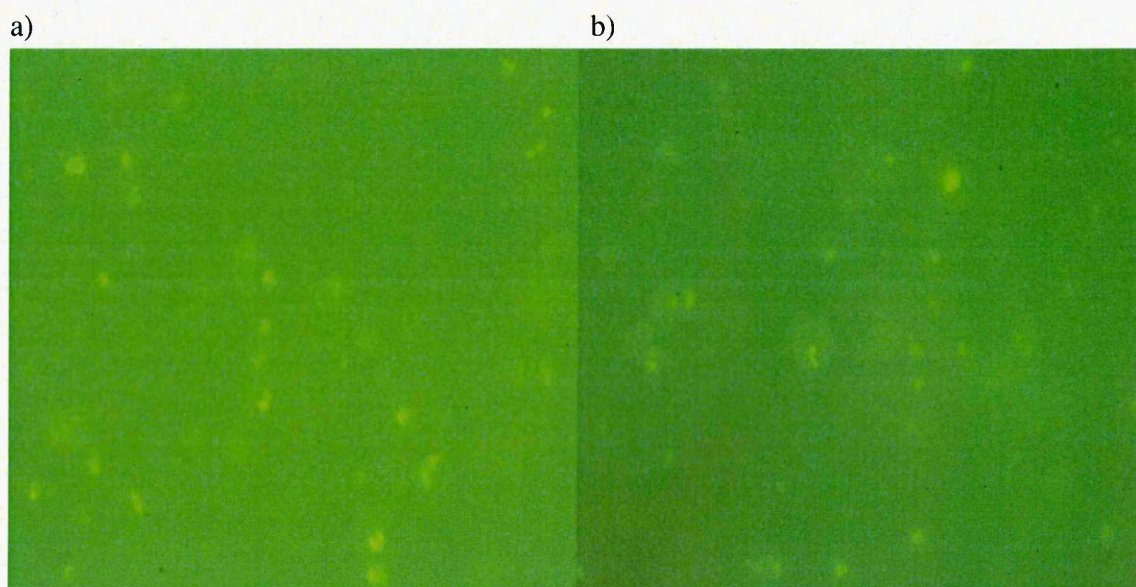
Figure 7.12. A micrograph of live MSC cells which had been combined with liquid phase PCPH prior to immediate polymer PTTNAG a) 24h after incubation, and b) 28 days incubation.

7.2.4.1   The production of cell matrix in the presence of PNIPAM/ clay nanocomposite hydrogels

In figure7.13, specific histological stains performed after 28 days incubation provided evidence of the production of proteoglycan (a) with alcran blue stain and collagen (b) with masson trichrome stain (which appear blue/purple following staining) within the gel by the proliferating cells, seen as small dark spots (arrowed) within white circles (pericellular matrix). This is natural behaviour demonstrated by healthy, naturally occurring cells within the human spinal disc integral for several natural biological processes.
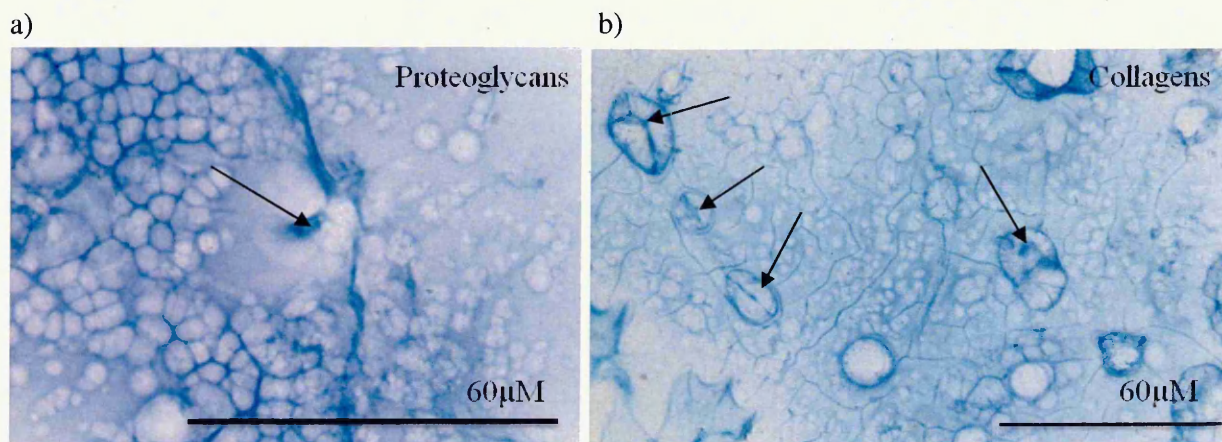
Figure 7.13. White light micrographs showing conclusively that MSC cells begin to produce natural proteoglycans and collagens within the matrix of the PNIPAM/ clay hydrogels within 28 days incubation. Matrix production is a natural process performed by healthy cells in their native environment.

7.3 The feasibility of PCPHs as cell delivery vehicles and structural support mechanisms for degenerative disc disease therapy

7.3.1 Visualisation of the injection of a PCPH into diseased spinal disc tissue

Nucleus pulposus (NP) tissue damage and cavity generation closely resembling degenerative disc disease was induced in bovine disc tissue via injection of 0.1ml 1mg/ml collagenase type II, which effectively digests all collagens types within the IVD. The collagenase was allowed to degrade the disc tissues for 24hrs whilst being incubated at 37°C. The resulting tissue contains holes and fissures that are visible under white light microscopy (figure 7.14a).A $1C_{10}PCPH$ was prepared as described in Section 2.2.1.2 and held in the liquid phase at 40°C.

0.1-0.2ml of the PCPH containing a very small amount of alcran blue dye was injected through the annulus fibrosus (outer intervertebral disc) into the NP cavity using a 21 gauge needle. Tissues were allowed to cool to 35°C for 10 minutes to facilitate PTTNAG of the PCPH inside the disc, and then immediately placed inside an incubator set to 37°C. After 24h, the NP regions of the disc was excised from the spinal tissue, embedded in paraffin wax and sliced into 4µm sections. Polarised light microscopy (under which highly organise collagen fibers appear white and the hydrogel appears blue-green due to the inclusion of the dye), it was observed that the gel not only filled the cavities in the disc created by the collagenase treatment including the very narrow fissures, but appeared to be well adhered to

230

the internal cavity surfaces (figure 7.14b). The gel was also observed to have filled the injection channel formed through the healthy tissues (shown in figure 7.15).

a)
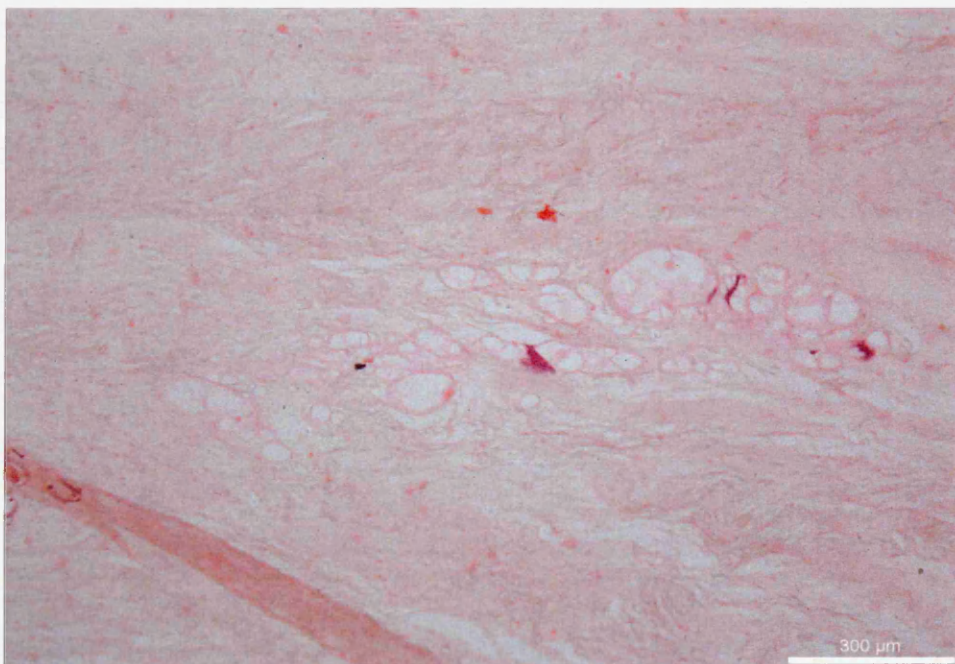
b)
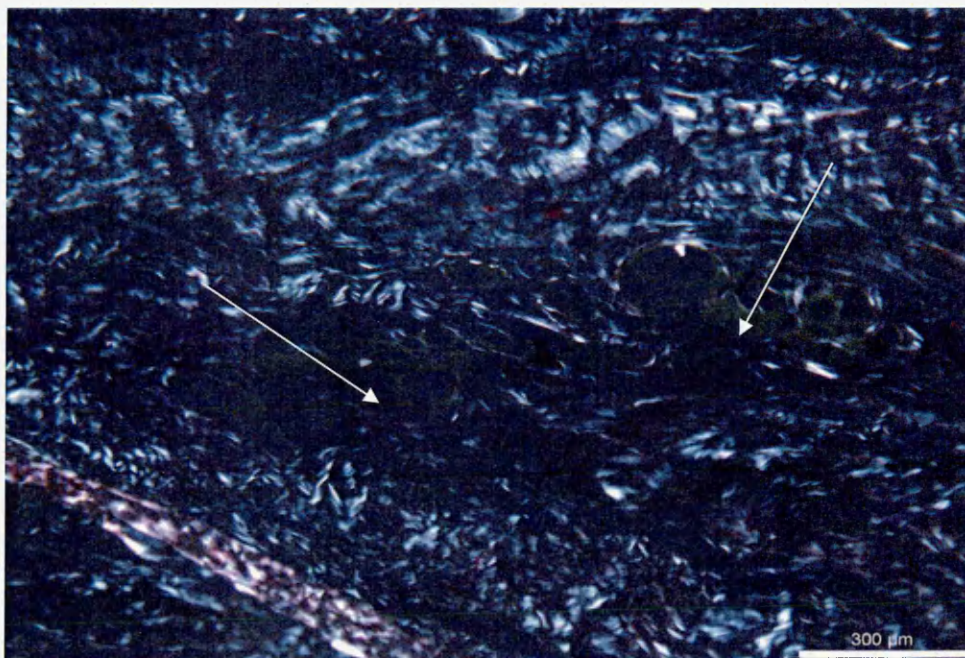
Figure 7.14. Fine fissures in the IVD were completely filled by the PCPH. a) shows a white light micrograph of the finely sliced tissue following PCPH injection and b) shows a polarised light micrograph of the same sample area, were the hydrogel appears green/ blue (arrowed).

Figure 7.17. a) shows a white light micrograph of the injection channel through which the PCPH was injected into the IVD, and b) shows a polarised light micrograph of the same sample area, were the hydrogel appears green/ blue. The hydrogel completely filled the injection channel.
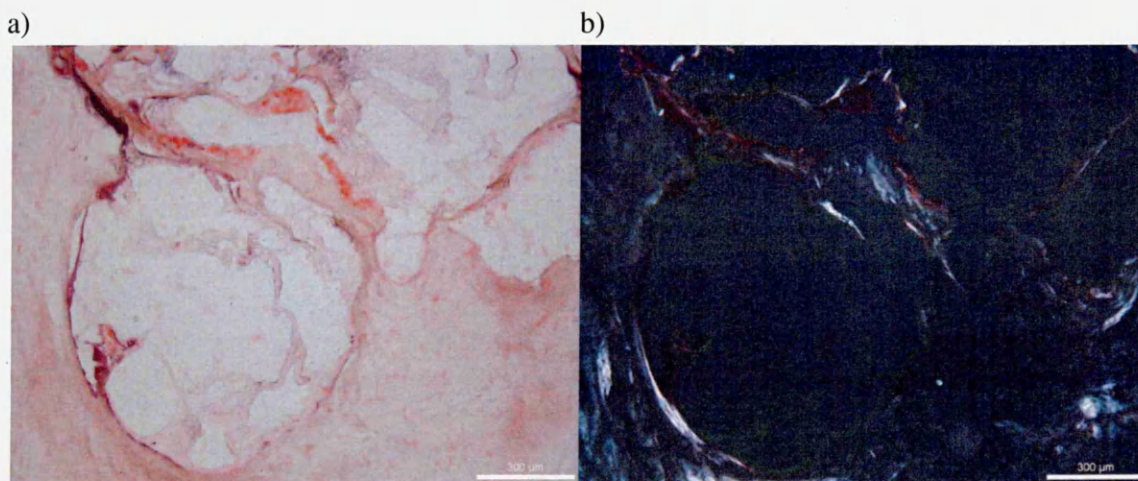
The micrographs confirm that the assembled hydrogels successfully and completely fill the holes (large and small) and microscopic fissures generated by the collagenase digestion.

7.4 Combinations of monomer and their effect on PTTNAG temperature, mechanical properties and cell viability.

An important requirement for *in situ* PTTNAG of the injectable hydrogel precursor is that PTTNAG is capable of occurring in biological conditions. Since the "usual" PNIPAM/ clay-based PCPH formulations undergo PTTNAG at temperatures at the LCST of PNIPAM, their injection into a region which is maintained at 37°C (the normal core body temperature of a healthy, resting adult human) would result in the PCPH remaining in the liquid phase, failing to cool sufficiently to undergo PTTNAG. In addition, any attempt to force a drop in temperature of the PCPH in situ could result in acute shock and necrosis of the MSC cells as well as the surrounding tissues.

The temperature at which the PCPH system undergoes PTTNAG can be increased with the addition of a relatively hydrophilic monomer and reduced with the addition of a relatively hydrophobic monomer to the monomer/ clay suspension prior to polymerisation. The addition of comonomers to PNIPAM systems for the purpose of altering the LCST has been explored in literature [38-47]. As discussed in Chapter 1, the principals involved in a thermoreversible coil to globule transition involve interactions between the polymer and solvent which result in negative values for the changes in entropy (ΔS_m) and enthalpy (ΔH_m) of mixing. If thermally-induced phase separation is to occur in aqueous solutions, the relative magnitudes

of ΔS_m and ΔH_m must be sufficient as to result in reversal in the sign of the free energy change, ΔG_m, at temperatures below 100 °C [46, 48]. It has been reasoned that the LCST behaviour of an aqueous polymer will depend entirely on its hydrophilic - hydrophobic equilibrium [49]. In addition, it is proposed that the LCST of a matrix of polymers containing a common thermoresponsive monomer can be continuously increased by the incorporation of increasingly hydrophilic component through copolymerisation, and decreased by incorporation of increasingly hydrophobic species. This has been proven by the LCST evaluation of a range of comonomers [48-50] .

Cloud point measurements and fluorescence techniques have been employed to examine hydrophilic/hydrophobic balance alterations in NIPAM/N,N-dimethylacrylamide (DMAc) statistical copolymers in aqueous media [45-46], and it was found that an increase in LCST of the resulting polymer was directly proportional to DMAc content. It was noted by Barker [45], however, that the use of such a hydrophilic modifier reduces the magnitude of the coil-to-globule thermal collapse and consequently is of value only in applications not requiring significant thermally- switchable carrier/release properties. For the purposes of cell delivery and structural support, a hydrogel polymer which undergoes phase change at a temperature very close to that of the human body is useful to the point of PTTNAG *in situ*, after which it is favourable for the material to remain in a swollen, hydrophilic state indefinitely. This renders the aforementioned "limitation" for PNIPAM-co-DMAc hydrogel systems an advantage for the purposes discussed in this research. PNIPAM-co-DMAc - based films have been previously shown to be cytocompatible materials for medical devices and drug delivery products, therefore DMAc was chosen as the candidate comonomer to be incorporated into the PCPH system for the purposes of raising the PTTNAG temperature to a more biologically utilisable range.

In this section, a series of NIPAM-based PCPH formulations were synthesised, within which the LCST (via hydrophilic/hydrophobic balance) and hence PTTNAG temperature, has been increased through copolymerisation with varying concentrations of DMAc, and in order to demonstrate versatility, has been decreased with the copolymerisation with glycedyl methacrylate (GMAc). It was shown, in agreement with the aforementioned previous work [45-46], that an increase in LCST of a NIPAM/DMAC copolymer is observable upon increasing the DMAc concentration present in the system. It was also demonstrated that a decrease in LCST is observable in a pseudo linear fashion upon increasing fractions of GMAc in the system.

Mechanical properties of assembled hydrogel systems were affected by DMAc incorporation. These gels were examined using dynamic mechanical analysis and the data was compared to DMAc-free systems. Also included are cell viability data for DMAc-incorporated gels which showed excellent system cytocompatibility comparable to that of PNIPAM/ clay systems.

7.4.1 The synthesis and preparation of a PNIPAM/ clay/ DMAc PCPH

Please refer to section 2.2.5.2

7.4.2 The synthesis and preparation of PNIPAM/GMAc/clay copolymer nanocomposite precursor liquid

Please refer to section 2.2.5.3.

7.4.3 Effect of co-monomers on PTTNAG temperature

To measure the PTTNAG temperature of the PCPH formulations, a thermocouple setup was used as shown in figure 7.17. The end of the thermocouple probe was positioned to reside in the centre of a stabilised glass sample vial (7.17a). 3ml of a given PCPH suspension of a starting temperature of ~80°C was carefully pipetted into the vial and the apparatus was allowed to cool slowly at room temperature. Figure 7.17b shows the appearance of a$1C_{10}D20$ PCPH suspension above its PTTNAG temperature. The liquid is completely turbid and the probe is not visible. When the PCPH undergoes PTTNAG, it spontaneously loses its turbidity and transforms to an optically transparent gel. Initial formulations of $1C_{10}$ (as a control), $1C_{10}D10$, $1C_{10}D20$, $1C_{10}D30$, $1C_{10}G20$, $1C_{10}G50$ and $1C_{10}G80$ were examined this way.

Natural temperature gradients across the sample vial during cooling result in the very centre cooling and gelating last, appearing as a "ball" of opaque PCPH which gradually shrinks and eventually disappears, elegantly demonstrating the sharpness of the thermal transition process. When the probe became just visible through the centre of the gel, as shown in figure 7.17c, the temperature was recorded and plotted as a function of DMAc concentration, a plot of which is shown in figure 7.18.

a)   b)   c)
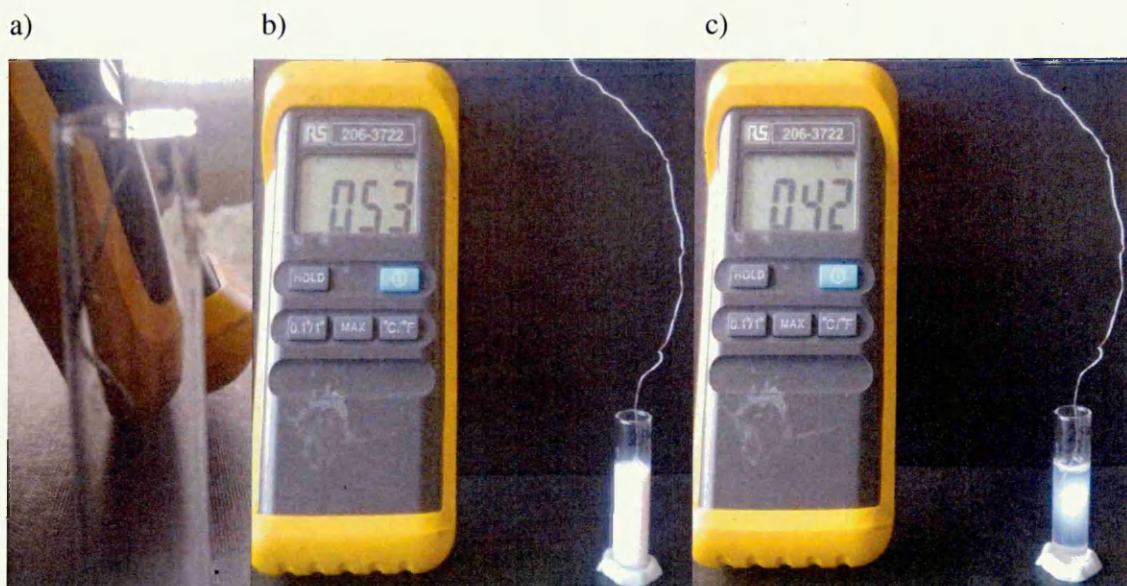
Figure 7.17. The thermocouple setup used to find approximate PTTNAG temperatures of PCPH formulations examined in this chapter. The temperature was recorded when the thermocouple probe became visible through the centre of the gel.
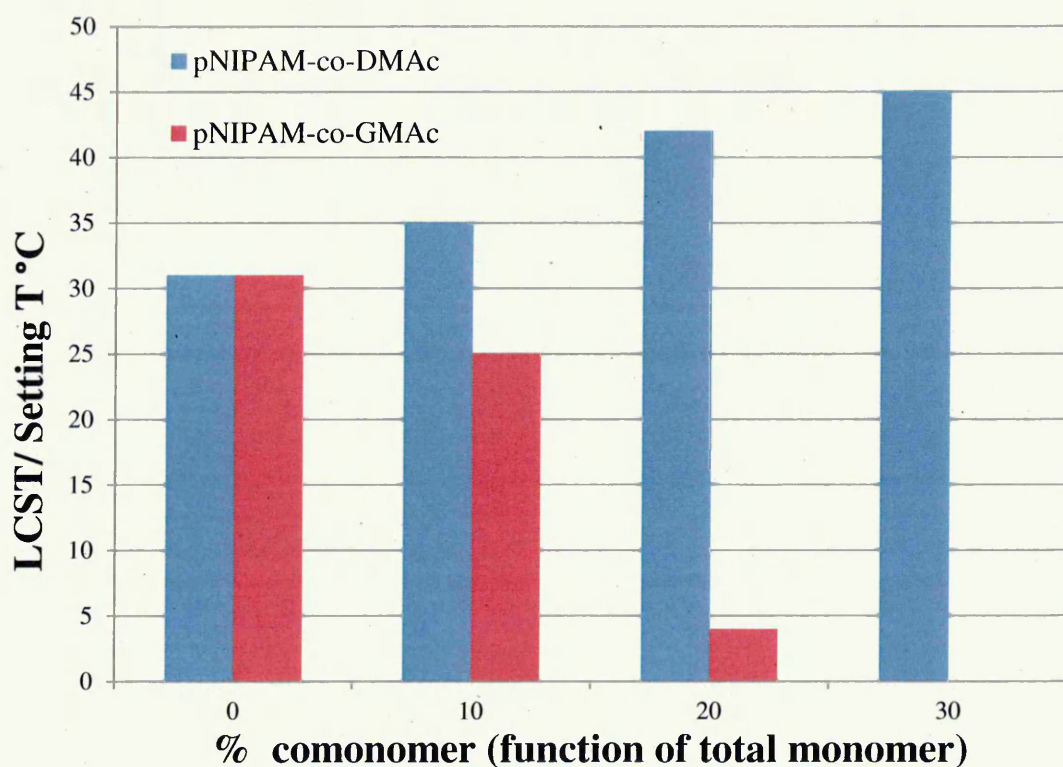
Figure 7.18. The effect of DMAc and GMAc fraction on the measured PTTNAG temperature of a range of PNIPAM/DMAc and PNIPAM/GMAc PCPH formulations. From this data it was deduced that a $1C_{10}D13$ PCPH formulation will undergo PTTNAG at the human core temperature of 37°C.

235

The PTTNAG temperatures of PCPH formulations with high GMA volume fraction were extremely low and difficult to characterise. In the case of 1C$_{10}$G50, the PCPH remained in liquid form at room temperature and began to exert loss of opacity characteristic of PTTNAG only when chilled in a refrigerator with a measured temperature of 4°C. At GMA volume fractions above this, the gels appeared to possess PTTNAG temperatures below freezing temperature of water. Predictably, the incorporation of hydrophilic DMA as a co-monomer in the PCPH formulations leads to an increase in the PTTNAG temperature and the incorporation of hydrophobic GMA leads to a decrease in the PTTNAG temperature. The magnitude of this change is fully controllable by the adjustment of the relative composition of either comonomer.

7.4.4 Effect of DMAc incorporation on gel mechanical properties

Figures 7.19 and 7.20 show the results of the dynamic mechanical analysis of gelated 1C$_{10}$ and co-monomer (DMAc)-incorporated 1C$_{10}$DMA13 formulations (section 2.2.5.2), with natural bovine NP of the same dimensions for comparison. The experimental parameters used for this data series are detailed in section 2.1.9.1 of this thesis.
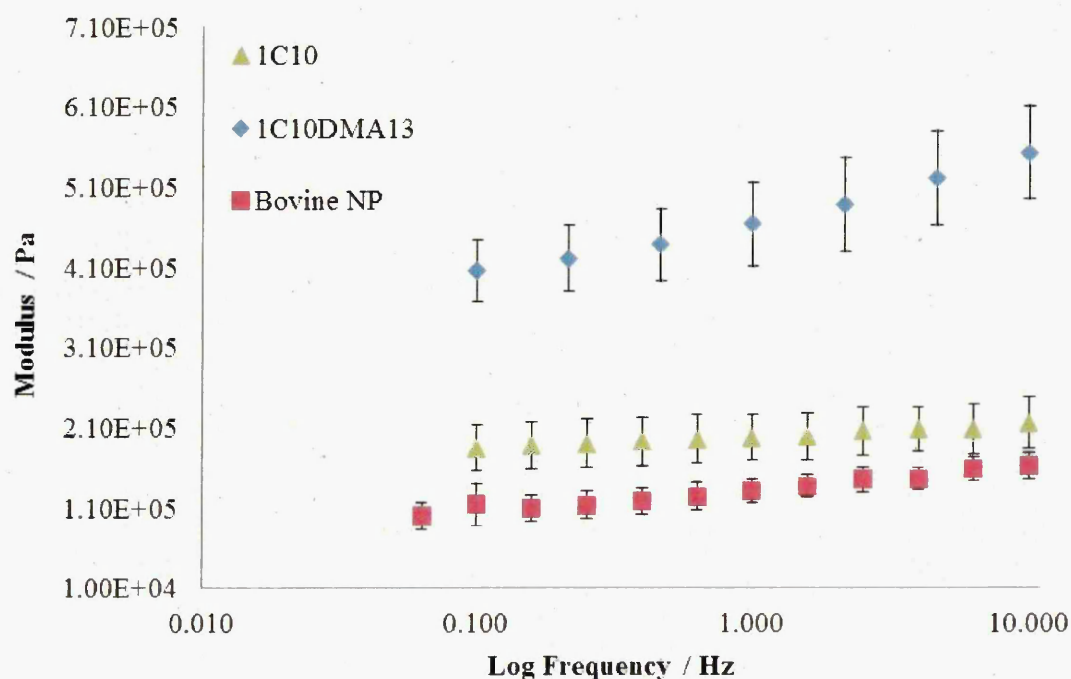
Figure 7.19. Frequency sweep data obtained using DMA for the PNIPAM/ clay hydrogel and a co-monomer (DMAc)-incorporated variant, showing their relative

236

storage moduli (Pa) in comparison to bovine NP. The experiments were performed at room temperature. n=3.
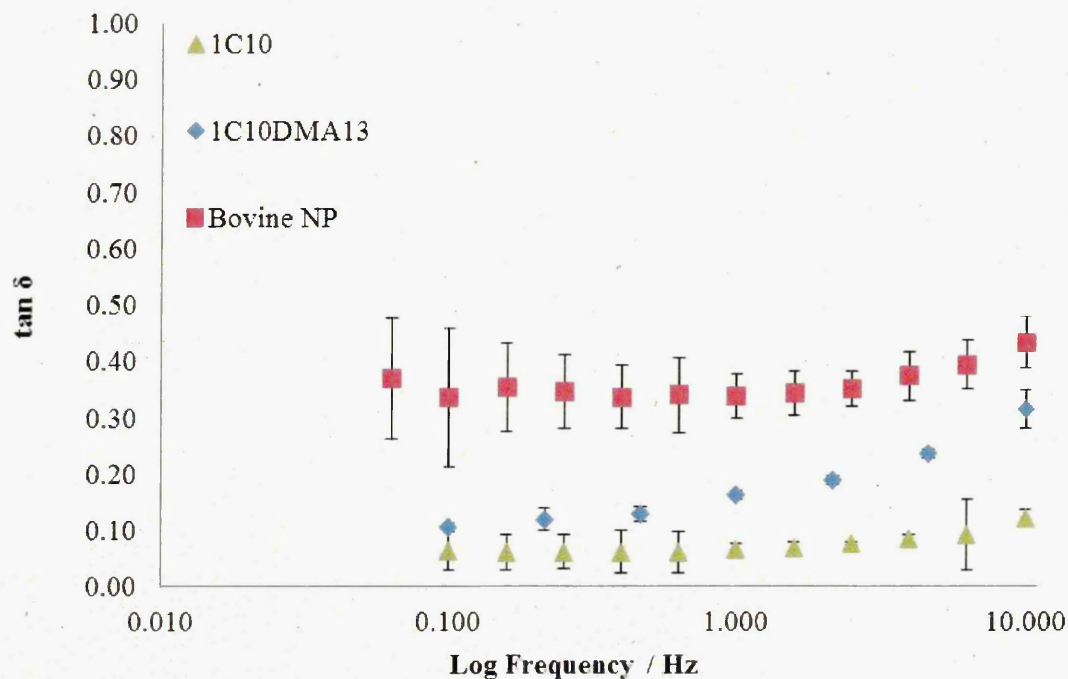
Figure 7.20. Frequency sweep data obtained using DMA for the PNIPAM/ clay hydrogel and a co-monomer (DMAc)-incorporated variant, showing their relative tan δ values. The experiments were performed at room temperature. n=3.

The pseudo-linear increase in storage modulus as a function of frequency is indicative of visco-elasticity. In other words, the material becomes marginally less elastic and "tougher" at higher oscillatory frequencies. From this data it is clear that the incorporation of DMAc as a comonomer into the PCPH has a significantly greater impact upon the resulting hydrogel mechanical properties than the incorporation of biologically active dopants, the data for which are presented in section 5.9. Consequently, it is evident that mechanical behaviour can be tailored by careful selection of dopant and comonomer.

7.4.5   Effect of incorporation of DMAc on cell viability

For this experiment, a $1C_{10}D13$ PCPH formulation was prepared as described in section 2.2.5.2. The PCPH was cooled to 38°C, remaining as a low viscosity liquid. One million fluorescently labelled MSCs were added to 1ml of PCPH, and 0.05ml of this suspension was pipetted into a well plate which was subsequently cooled to 37°C to facilitate gel PTTNAG. 0.2ml growth media was added to the gel and the system was allowed to incubate at 37°C, 5% CO_2, for 7 days.

237
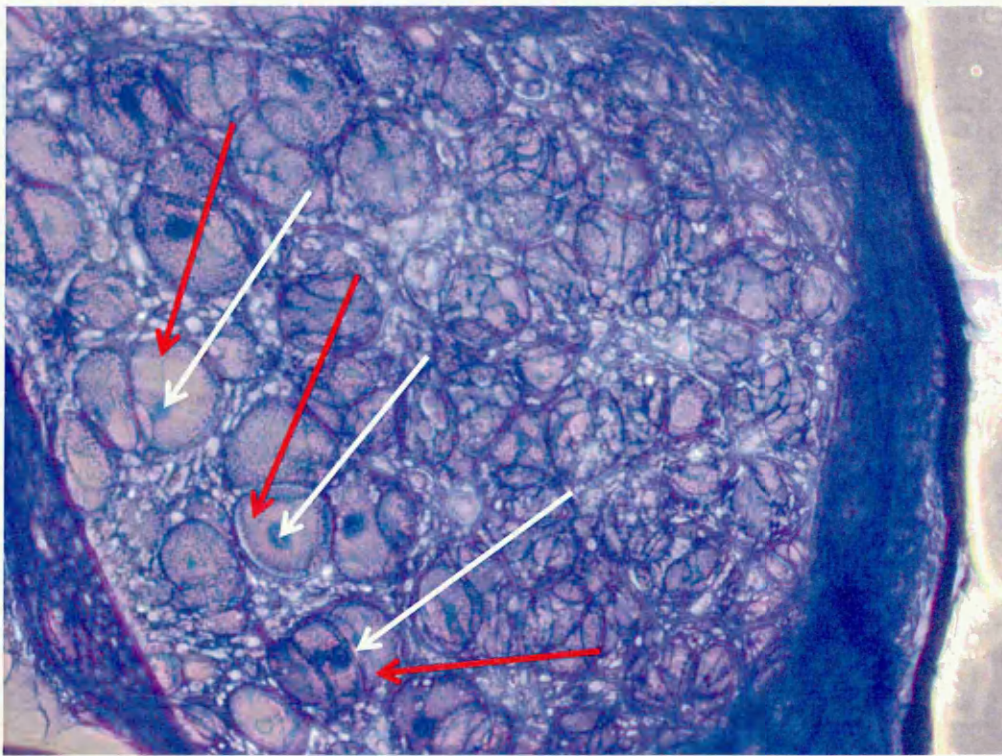
Figure 7.21. A white light micrograph of live human MSCs within a $1C_{10}D13$ hydrogel matrix after 7 days incubation. Histological staining shows the MSC cells produce natural proteoglycans and collagens within the matrix of the hydrogel.
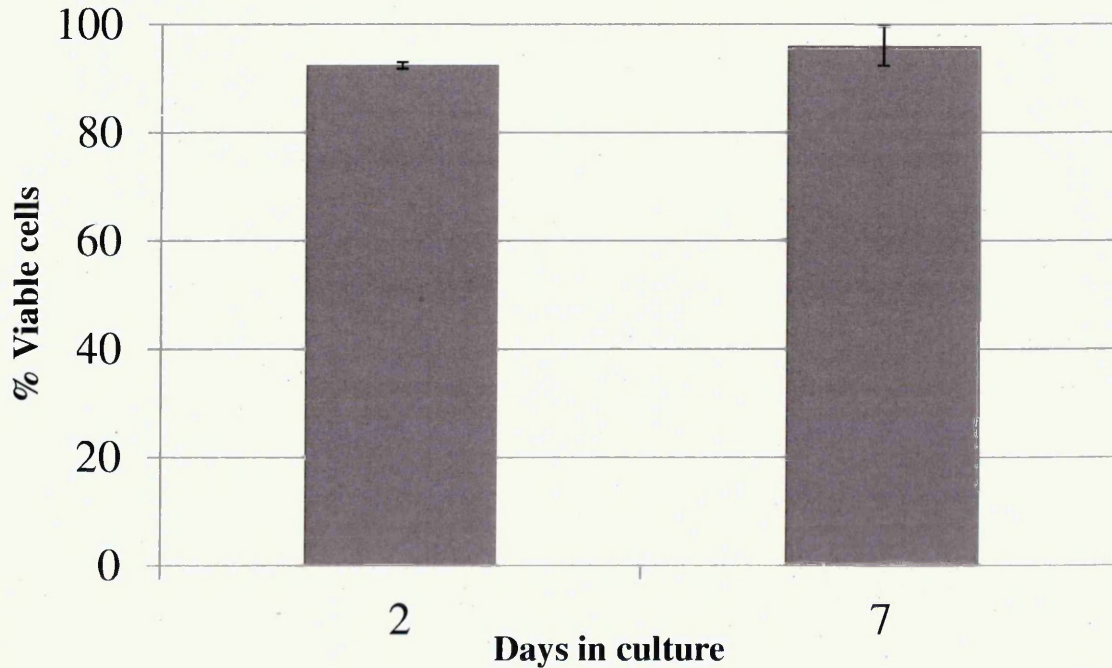
Figure 7.22. Human MSC viability in $1C_{10}D13$ when the cells are added to the PCPH prior to PTTNAG.

Alcran blue and masson trichrome histological stains performed after 7 days incubation provided evidence of the production of both proteoglycans and collagen (which appear purple/ blue in the micrograph shown in figure 7.21) within the gel by proliferating cells (arrowed white). It appeared as though cells were also creating lacunae within the gel matrix (arrowed red), which strongly indicate native cellular behaviour and importantly, that $1C_{10}D13$ formulations are entirely suitable for the inhabitation of live human MSCs. This evidence is supported by cell viability tests (figure 7.22), which indicate that the presence of $1C_{10}D13$ causes no adverse effect on the survival a proliferation of the cells.

7.4.6 Mechanical properties of the assembled hydrogel following administration into the IVD.

As discussed in the introductory paragraphs, the function of the spinal disc is to act shock absorbing sponges, capable of withstanding stress and load generated by movement. A preliminary experiment was designed to test whether the hydrogel materials, once injected and PTTNAG has occurred, will remain in place inside the IVD once reasonable stress is applied.

The following experiment was carried out by Dr David Asquith of Mechanical Engineering at Sheffield Hallam University and Mrs. Debra Booth of the Biomedical Research Institute at Sheffield Hallam University. An IVD within a bovine spinal column was subject to collagenase type II digestion treatment and incubation (2mg/ ml for 30 minutes. A $1C_{10}DMA13$ PCPH was prepared as described in Section 2.2.1.2 and 0.1-0.2ml was injected into the subsequent IVD cavities. The spine was inserted into a loading system (figure 7.23a), in which 1.5K Newtons of pressure was applied longitudinally to the spine (1.5K Newtons is force in excess of that applied to the spine during daily activities [51]) and during the experiment, the spine deformed excessively.

Following loading the spine was dissected and the IVD containing the hydrogel was examined closely. Just visible in figure 7.23b is the hydrogel located firmly in place within the NP at the disc centre, still fully occupying the cavities and voids created by the collagenase treatment.
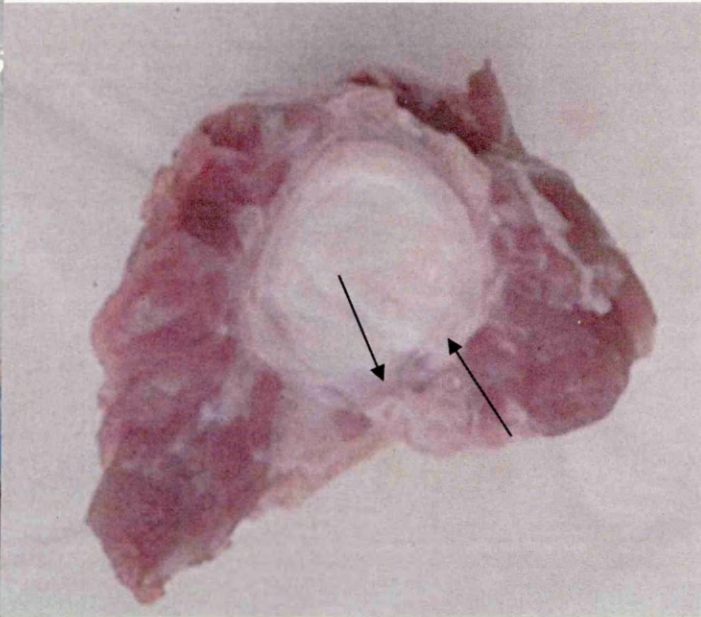
Figure 7.23 a) shows the loading system setup into which the spine was inserted. The photograph was taken toward the end of the experiment and the deformation in the spine is clearly observable, b) shows the hydrogel (arrowed) still in place within the NP after the experiment.

7.5   Summary

This chapter presented a method which incorporates living human cells into a biocompatible hydrogel which is injectable via a narrow bore needle as a low- viscosity liquid which solidifies to form a live cell-containing cell scaffold *in situ*.

In addition to those mentioned above, the material exerts a basic set of properties that are advantageous for the purpose of cell delivery and cell scaffold, such as;

- Easily injectable, even through very narrow-gauge needles.
- Fast PTTNAG which prevents the extrusion of the gel under pressure.
- High water content and excellent biocompatibility, demonstrated by the proliferation of MSCs and their production of extracellular matrix.
- Ability to fill even very narrow fissures and holes ($<100\mu m$), and solidify to exact dimensions of the cavity.

- Simple, effective cell-loading.
- No purification steps required.
- Ability to tune both mechanical properties and PTTNAG temperature with the addition of a hydrophilic comonomer, which itself does not have any adverse effect on cell viability.

7.6 References

1.   Van Vlierberghe, et al., Biopolymer-Based Hydrogels As Scaffolds for Tissue Engineering Applications: A Review. Biomacromolecules, 2011. 12(5): p. 1387-1408.

2.   Peppas, N.A., et al., Hydrogels in pharmaceutical formulations. European Journal of Pharmaceutics and Biopharmaceutics, 2000. 50(1): p. 27-46.

3.   Hou, Q., P.A., et al., Injectable scaffolds for tissue regeneration. Journal of Materials Chemistry, 2004. 14(13): p. 1915-1923.

4.   Du, H., et al., Injectable in situ Physically and Chemically Crosslinkable Gellan Hydrogel. Macromolecular Bioscience, 2012. 12(7): p. 952-961.

5.   Malonne, H., et al., Preparation of poly (N-isopropylacrylamide) copolymers and preliminary assessment of their acute and subacute toxicity in mice. European Journal of Pharmaceutics and Biopharmaceutics, 2005. 61(3): p. 188-194.

6.   McCollister, D.D., et al., Toxicologic investigations of polyacrylamides. Toxicology and Applied Pharmacology, 1965. 7(5): p. 639-651.

7.   Shipp, A., et al., Acrylamide: Review of toxicity data and dose-response analyses for cancer and noncancer effects. Critical Reviews in Toxicology, 2006. 36(6-7): p. 481-608.

8.   Raj, P.P., Intervertebral disc: anatomy-physiology-pathophysiology-treatment. Pain practice : the official journal of World Institute of Pain, 2008. 8(1): p. 18-44.

9.   Freemont, A.J., et al., Current understanding of cellular and molecular events in intervertebral disc degeneration: implications for therapy. Journal of Pathology, 2002. 196(4): p. 374-379.

10.   LeMaitre, C.L., Pathogenesis of disc degeneration: IL-1 as a therapeutic target. 2004, University of Manchester.

11.   Ray, C.D., Spinal interbody fusions: A review, featuring new generation techniques. Neurosurgery Quarterly, 1997. 7(2): p. 135-156.

12.   Guyer, R.D. and D.D. Ohnmeiss, Intervertebral disc prostheses. Spine, 2003. 28(15): p. S15-S23.

13.   Videbaek, T.S., et al., Adjacent Segment Degeneration After Lumbar Spinal Fusion: The Impact of Anterior Column Support A Randomized Clinical Trial With an Eight- to Thirteen-Year Magnetic Resonance Imaging Follow-up. Spine, 2010. 35(22): p. 1955-1964.

14.   Humzah, M.D., Soames, R., Human intervertebral disk structure and function. Anatomical Record, 1988. 220(4): p. 337-356.

15. Holm, S., et al., Nutrition of the intervertebral disk - solute transport and metabolism. Connective Tissue Research, 1981. 8(2): p. 101-119.

16. Urban, J.P.G., McMullin, F., Swelling pressure of the lumbar intervertebral disk - influence of age, spinal level, composition and degeneration. Spine, 1988. 13(2): p. 179-187.

17. Iatridis, J.C., et al., Influence of fixed charge density magnitude and distribution on the intervertebral disc: Applications of a poroelastic and chemical electric (PEACE) model. Journal of Biomechanical Engineering-Transactions of the Asme, 2003. 125(1): p. 12-24.

18. Perie, D.S., et al., Correlating material properties with tissue composition in enzymatically digested bovine annulus fibrosus and nucleus pulposus tissue. Annals of Biomedical Engineering, 2006. 34(5): p. 769-777.

19. Jahnke, M.R., McDevitt, C., Proteoglycans of the human intervertebral disk - electrophoretic heterogeneity of the aggregating proteoglycans of the nuleus pulposus. Biochemical Journal, 1988. 251(2): p. 347-356.

20. Adams, P., et al., Biochemical aspects of development and aging og human lumbar intervertebral disk. Rheumatology and Rehabilitation, 1977. 16(1): p. 22-29.

21. Antoniou, J., et al., The human lumbar intervertebral disc - Evidence for changes in the biosynthesis and denaturation of the extracellular matrix with growth, maturation, ageing, and degeneration. Journal of Clinical Investigation, 1996. 98(4): p. 996-1003.

22. Karasek, M. Bogduk, N., Twelve-month follow-up of a controlled trial of intradiscal thermal anuloplasty for back pain due to internal disc disruption. Spine, 2000. 25(20): p. 2601-2607.

23. Singh, V., Derby, R., Percutaneous lumbar disc decompression. Pain Physician, 2006. 9(2): p. 139-46.

24. Singh, V., et al., Percutaneous Lumbar Laser Disc Decompression: A Systematic Review of Current Evidence. Pain Physician, 2009. 12(3): p. 573-588.

25. Hirsch, J.A., et al., Automated Percutaneous Lumbar Discectomy for the Contained Herniated Lumbar Disc: A Systematic Assessment of Evidence. Pain Physician, 2009. 12(3): p. 601-620.

26. Wenger, M., Markwalder, T., A novel surgical treatment of lumbar disc herniation in patients with long-standing degenerative disc disease. Journal of Neurosurgery-Spine, 2005. 2(5): p. 515-520.

27. da Silva, M.R., et al., New perspectives on degenerative disc disease treatment. Acta Reumatologica Portuguesa, 2009. 34(2B): p. 327-335.

28. Schnake, K.J., et al., Mechanical concepts for disc regeneration. European Spine Journal, 2006. 15: p. S354-S360.

29.   Tanii, H., Hashimoto, K., Invitro neurotoxicity study with dorsal root ganglia for acrylamide and its derivatives. Toxicology Letters, 1991. 58(2): p. 209-213.

30.   Henderson, E., et al., In vivo evaluation of injectable thermosensitive polymer with time-dependent LCST. Journal of Biomedical Materials Research Part A, 2009. 90A(4): p. 1186-1197.

31.   Liu, D., et al., Intelligent Cell Detachment Materials Based on Poly (N-Isopropylacrylamide). Progress in Chemistry, 2011. 23(11): p. 2353-2359.

32.   Matsuda, T., et al., Cell sorting technique based on thermoresponsive differential cell adhesiveness. Biomacromolecules, 2007. 8(8): p. 2345-2349.

33.   Naito, H., et al., Three-dimensional cardiac tissue engineering using a thermoresponsive artificial extracellular matrix. Asaio Journal, 2004. 50(4): p. 344-348.

34.   Ohya, S., Matsuda, T., Poly(N-isopropylacrylamide) (PNIPAM)-grafted gelatin as thermoresponsive three-dimensional artificial extracellular matrix: molecular and formulation parameters vs. cell proliferation potential. Journal of Biomaterials Science-Polymer Edition, 2005. 16(7): p. 809-827.

35.   Ohya, S., et al., In vivo evaluation of poly(N-isopropylacrylamide) (PNIPAM)-grafted gelatin as an in situ-formable scaffold. Journal of artificial organs : the official journal of the Japanese Society for Artificial Organs, 2004. 7(4): p. 181-6.

36.   Reed, J.A., et al., The effects of cell culture parameters on cell release kinetics from thermoresponsive surfaces. Journal of Applied Biomaterials & Biomechanics, 2008. 6(2): p. 81-88.

37.   Wang, T., et al., Rapid cell sheet detachment from alginate semi-interpenetrating nanocomposite hydrogels of PNIPAm and hectorite clay. Reactive & Functional Polymers, 2011. 71(4): p. 447-454.

38.   Picos-Corrales, L.A., et al., Well-defined N-Isopropylacrylamide Dual-Sensitive Copolymers with LCST similar to 38 degrees C in Different Architectures: Linear, Block and Star Polymers. Macromolecular Chemistry and Physics, 2012. 213(3): p. 301-314.

39.   Yusa, S., et al., Thermo-responsive diblock copolymers of Poly(N-isopropylacrylamide) and Poly(N-vinyl-2-pyrroridone) synthesized via organotellurium-mediated controlled radical polymerization (TERP). Macromolecules, 2007. 40(16): p. 5907-5915.

40.   Zhao, C., et al., Syhthesis and self-assembly of poly(N-isopropylacrylamide)-b-poly (epsilon-Benzyloxycarbonyl-L-lysine)-b-poly(ethylene glycol). Acta Polymerica Sinica, 2008(11): p. 1096-1101.

41.   Zhou, Y., et al., Thermo-induced formation of unimolecular and multimolecular micelles from novel double hydrophilic multiblock copolymers of N,N-dimethylacrylamide and N-isopropylacrylamide. Langmuir, 2007. 23(26): p. 13076-13084.

42.   Li, G.Y., et al., Synthesis and self-assembly of temperature- and pH-sensitive diblock copolymer of poly(acrylic acid)-b-poly(N-isopropylacrylamide). Chemical Journal of Chinese Universities-Chinese, 2006. 27(5): p. 956-960.

43.   Roth, P.J., et al., Comparison between the LCST and UCST Transitions of Double Thermoresponsive Diblock Copolymers: Insights into the Behavior of POEGMA in Alcohols. Macromolecules, 2012. 45(7): p. 3221-3230.

44.   Wintgens, V., et al., Triggering the thermosensitive properties of hydrophobically modified poly(N-isopropylacrylamide) by complexation with cyclodextrin polymers. Macromolecular Chemistry and Physics, 2005. 206(18): p. 1853-1861.

45.   Barker, I.C., et al., Studies of the "smart" thermoresponsive behavior of copolymers of N-isopropylacrylamide and N,N-dimethylacrylamide in dilute aqueous solution. Macromolecules, 2003. 36(20): p. 7765-7770.

46.   Shibayama, M., Mizutani, S., Nomura, S., Thermal Properties of Copolymer Gels Containing N-Isopropylacrylamide. Macromolecules, 1996. 29(6): p. 2019-2024.

47.   Chee, C.K., et al., Manipulating the Thermoresponsive Behavior of Poly(N-isopropylacrylamide). 1. On the Conformational Behavior of a Series of N-Isopropylacrylamide–Styrene Statistical Copolymers. Macromolecules, 2001. 34(21): p. 7544-7549.

48.   Feil, H., et al., Effect of comonomer hydrophilicity and ionization on the lower critical solution temperature of N-isopropylacrylamide copolymers. Macromolecules, 1993. 26(10): p. 2496-2500.

49.   Schild, H.G., Poly(N-isopropylacrylamide): experiment, theory and application. Progress in Polymer Science, 1992. 17(2): p. 163-249.

50.   Taylor, L.D., Cerankowski, L., Preparation of films exhibiting a balanced temperature dependence to permeation by aqueous solutions—a study of lower consolute behavior. Journal of Polymer Science: Polymer Chemistry Edition, 1975. 13(11): p. 2551-2570.

51.   Kettler, A., et al., In vitro dislocation tendency, stabilizing effect, and subsidence tendency of different lumbar interbody fusion cages. Orthopade, 2002. 31(5): p. 481-487.

8

Conclusions and Further Work

Chapter 8 - Conclusions and Further Work.

The principal aim of this thesis was to explore new avenues for the utilisation of stimuli-responsive PNIPAM/ clay nanocomposite materials. More specifically, to devise methods by which the phase- transitional behaviour of these materials can exploited in the medical and biological fields. Their physical and chemical properties had already made them attractive materials in these scientific disciplines; they showed excellent potential as cell scaffolds and biological delivery vehicles. The principal difficulty arose in the processing of such cross-linked materials, and researchers have looked at *in situ* polymerisation or stimuli responsive gelation to overcome this. These approaches have significant drawbacks, mainly stemming from the cytotoxicity of unreacted chemical species and absence of cross-links, making them unsuited to clinical applications or those which require short term or long term mechanical stability.

Chapter 3 details a new synthetic method which allows the fully-reacted PNIPAM/ clay system to remain liquid until it is cooled to a predetermined temperature. Below this temperature, it spontaneously undergoes PTTNAG to a hydrogel that does not re-liquefy upon re-heating, but exhibits the highly utilisable stimuli-responsive properties reported by Haraguchi in 2002 [1].

This process opened a wealth of processing possibilities. The successful facile incorporation of biologically active components in the liquid phase, which were shown to become homogenously distributed throughout the system, as well as casting, extruding, injecting and electrospinning effectively demonstrates the high processability of these nanocomposite materials.

The morphology of well defined, uniform electrospun fibres with diameters ~300nm was examined using SEM in chapter 4. The data represent the first time electrospun cross-linked PNIPAM hydrogel mats have successfully been produced. This chapter also highlights the novel and straightforward production of continuous, uniform flat PNIPAM/ clay films of 300µm -1000µm thickness achieved using an industrial film extrusion line at Smith & Nephew Extruded Films, Gilberdyke.

Characterisation of various PNIPAM/ clay-based hydrogel formulations post- PTTNAG is presented in chapter 5. The absence of clay diffraction patterns in XRD data proved the exfoliation or near-exfoliation of clay in the nanocomposite system. DMA investigations

247

revealed that the viscoelasticity of the gels can be tailored by varying the nature and quantity of dopant materials, and those containing a HA solution closely resemble the mechanical properties bovine NP tissue.

Attempts to remove the clay from the polymeric system post- PTTNAG in order to establish M_w, and M_n were unsuccessful. GPC analysis, of the linear, uncross-linked polymers was met with very limited success. This was attributed to the nature and behavior of the polymer during and following the precipitation polymerisation process. A protocol to address these issues is presented in section 8.1. The electrostatic interactions/ hydrogen bonding present in 3 separate formulations were examined by monitoring the drying of these formulations with ATR-FTIR. The diffusion coefficient D (in this instance, the diffusion of water *out* of the polymer matrix) was calculated for each of the formulations. It was observed that although D was indistinguishable between formulations, the intercept value *y* was altered significantly.

The swelling and deswelling behaviour of the composite gels are integral to their utilisable potential. In chapter 6, the magnitude and rate of swelling of the clay nanocomposite materials was compared to those synthesised in the presence of the chemical cross-linking agent BIS. A matrix of PNIPAM based gels were synthesised which enabled the direct comparison of deswelling behaviours of gels containing various cross-link densities of both cross-link types. In addition, 2 distinct methods of free-radical initiation (thermal dissociation of the free-radical initiator AIBN and UV irradiation dissociation of diethoxyacetophenone) were added to the matrix for comparison. In summary, gels cross-linked with clay exhibit larger volume changes than those cross-linked with BIS, and the magnitide of deswelling increases markedly with decreasing cross-linker content for gels of both cross-link types, as expected. Gels synthesised in the presence of clay adopted rubber-like physical characteristics and could withstand high degrees of deformation irrespective of clay loading and preparation method. Conversely, gels prepared using BIS were extremely brittle and could not withstand any significant degree of deformation. Thermal deswelling is markedly hindered in dopant-incorporated networks. This is thought to be due to the formation of separate polymer/ dopant domains upon PNIPAM collapse above the system LCST. The aqueous dilution of the nanocomposite in the liquid phase yields hydrogels which undergo similar magnitudes of deswelling as their undiluted counterparts.

The phenomenon of cononsolvency-induced swelling/ deswelling of PNIPAM in alcoholic solutions are also presented in chapter 6. The de/reswelling behaviour of PNIPAM- clay as

well as gelatine-doped formulations can be controlled by adjusting the alcohol volume fraction of the media. BIS cross-linked gels exhibit restricted swelling/ deswelling behaviours compared to those cross-linked with clay, as expected. The cross-link density within systems does not have a significant impact on this de/reswelling cononsolvency behaviour, although the incorporation of gelatine imposes some restriction on it, relative to gelatine concentration.

The excellent biocompatibility of the composites in both liquid and solid phases was proven by extensive cell viability studies, detailed in chapter 7. The temperature at which the liquid material undergoes PTTNAG can be tailored by i) the aqueous dilution of the PCPH in the liquid phase ii) adjusting the clay-loading of the material, and iii) incorporating comonomers of carefully selected polarity into the system. It has also been shown that not only do none of these approaches have an adverse effect on cell viability, but they alter the mechanical properties of the resulting hydrogel. This therefore also allows the resulting mechanical properties to easily be tailored to the intended purpose.

Human MSC cells proliferate, migrate and produce extracellular matrix in the presence of the hydrogel whether they have been combined in the liquid phase or the gel had undergone PTTNAG prior to cell-loading, despite no purification steps of the hydrogel being taken in either case. The hydrogel, after injection through a narrow (21 gauge) needle into an artificially degenerated bovine IVD, integrates with the digested tissue, easily filling narrow fissures and large voids alike. The hydrogel is then retained in place even during excessive stress loading of the vertebrae.

These initial studies demonstrate the potential for the development of a minimally invasive degenerative disc disease treatment. Other potential medical applications for this material include:

- Cartilage applications/ replacement.
- Injectable fixation of synthetic joints.
- Skin regeneration/ wound management.
- Drug delivery vehicles - as an injectable subcutaneous substrate.
- Bone fracture treatment by filling micro cracks, and treatment for osteoporotic patients.

8.1. Further Work

The work in this thesis could be expanded on in several ways:

- A $1C_{10}$ PCPH suspension has been observed to remain in a liquid phase for periods of time exceeding 2 weeks at 80°C post- initiation, and this same PCPH was still capable of assembling to a solid gel upon cooling. A clearer understanding of the limitations posed on PCPH retention at elevated temperatures for extended periods of time would be achieved by the examination of physical and chemical properties of the gel after extended timeframes have elapsed.

- The method of measuring optical clarity, and therefore phase-transition, upon cooling may be significantly improved through the use of a turbidimeter equipped with thermocoupled warming device.

- DLS measurements would be repeated in triplicate in order to establish standard error of results.

- More data are needed to make mechanistic inferences on the M_w of PNIPAM in the presented system. Possible future approaches could include;

    1) Inducing phase transition of the aq. PNIPAM solution at 50°C before filtering the precipitant and exchanging the solvent with THF to help reduce chain aggregation.

    2) Use a viscosity technique such as online viscometery, whereby the sample is injected into a triple detection GPC device without the use of a separation column, equipped with a differential refractometer/viscometer. The precise polymer concentration is calculated from the refractometry signal, which is used to calculate the intrinsic viscosity using the specific viscosity (given by the viscometer). One important limitation with this technique is that it does not give reasonable values for low M_w polymers [2].

    3) Membrane osmometry is a technique employed to directly measure the osmotic pressure of a polymer solution separated from pure solvent by a semi-permeable membrane. It can be used to very accurately measure the M_w of colloidal suspensions without a limit on sample concentration, although it requires a time- consuming calibration process and large sample volumes. Also, due to membrane porosity, it may not be suitable for very small polymer molecules.

- Expansion and completion of the full range of gelatine and hyaluronic acid-doped gel swelling/ deswelling experiments in response to cononsolvency phenomena in the presence of alcohols of increasing chain length.

- Determination of the survival and differentiation of MSCs in the presence of the hydrogel under natural vertebral loading patterns would be a requirement prior to any foreseeable clinical trials of the material.

- Rheological data to be generated for PNIPAM/ clay-based hydrogels of several formulations, including those of various solids: water ratios, diluted formulations and those containing dopants.

- A larger selection of comonomers will be incorporated into the PNIPAM/ clay system, and these systems will be examined for cell viability, swelling/ deswelling capacities and mechanical properties. Hydrophilic (PNIPAM LCST- raising) comonomers could include; hydroxyl ethyl vinyl ether (HEVE), N-vinyl-2-pyrrolidone (NVP) and 2-hydroxyethylacrylate (HEA). Hydrophobic (PNIPAM LCST- reducing) comonomers could include hydroxyethyl methacrylate (HEMA), vinyl phenyl ether (VPE). and vinyl butyl ether (VBE).

- Different clay species could be incorporated in place of laponite. It is anticipated that clay platelets with larger surface areas/ aspect ratios may enhance gel mechanical stability, whilst possibly compromising optical clarity and/ or efficient platelet separation (swellability) in water. An optimisation of clay type and concentration to various eventual hydrogel applications would be desirable.

9

Associated Work

Chapter 9 - Associated Work

9.1   Awards and presentations

1.   1st Prize Winner for "The Best Poster Presentation" at MERI Research Student Day, Sheffield Hallam University-UK, 26th May 2009.

2.   Victoria Boyes, C. Le Maitre, B. Barthrop, C. Sammon, C. Breen, J. Foulkes "NOVEL, EASILY PROCESSIBLE POLY(N-ISOPROPYLACRYLAMIDE NANOCOMPOSITE HYDROGELS FOR BIOMEDICAL APPLICATIONS", Poster Presentation at MacroGroup UK international Conference on Polymer Synthesis, Warwick University, July 9th 2012.

3.   Victoria Boyes, C Sammon "FTIR STUDY OF HOW THE INTERACTION WITH WATER AND ALCOHOL INFLUENCES THE SWELLING / DESWELLING CAPABILITIES OF CLAY-CROSSLINKED PNIPAM HYDROGELS", Poster Presentation at EUROCLAY 2011 Conference, Antalya, Turkey, 26th June - 1st July 2011.

4.   Victoria Boyes, C. Sammon, C. Breen, S. Sabnis, J. Foulkes "THE EFFECT OF CROSS-LINK TYPE, CROSS-LINK CONCENTRATION AND INITIATION METHOD ON THE SWELLING/ DESWELLING CAPABILITIES OF PNIPAM HYDROGELS IN AQUEOUS AND ALCOHOLIC SOLUTIONS", Poster Presentation at Trilateral Meetings on Clays, Seville, Spain, 8 - 11th June, 2010.

5.   Victoria Boyes, C. Sammon, C. Breen, S. Sabnis, J. Foulkes "THE EFFECT OF CLAY LOADING ON THE STIMULI RESPOSIVE PROPERTIES OF PNIPAM/ CLAY NANOCOMPOSITE HYDROGELS", Poster Presentation at Macro Group Young Research Meeting 2010, Nottingham, UK, 29 - 30th April 2010.

6.   Victoria Boyes, C. Sammon, C. Breen, S. Sabnis, J. Foulkes "THE EFFECT OF INITIATION METHOD AND CROSS-LINK TYPE ON THE PROPERTIES OF PNIPAM/ CLAY NANOCOMPOSITE HYDROGELS", Oral Presentation at MERI Research Student Day, Sheffield Hallam University-UK, 26th May 2010.

7.   Victoria Boyes, C. Sammon, C. Breen, S. Sabnis, J. Foulkes " THE EFFECT OF INITIATION METHOD AND CROSS-LINK TYPE ON THE PROPERTIES OF PNIPAM/ CLAY NANOCOMPOSITE HYDROGELS", Poster Presentation at MERI Research Student Day, Sheffield Hallam University-UK, 20th May 2009.

9.2　Conferences attended

1. MacroGroup UK international Conference on Polymer Synthesis, Warwick University, July 9th 2012.

2. The 197th Infra-Red and Raman Discussion Group Christmas Meeting, London, UK, 20th December 2011.

3. EUROCLAY 2011 Conference, Antalya, Turkey, 26th June - 1st July 2011.

4. MERI Research Student Day, Sheffield Hallam University, UK, 25th May 2011.

5. The 194th Infra-Red and Raman Discussion Group Christmas Meeting, London, UK, 16th December 2010.

6. The TMC "Trilateral Meeting on Clays": General Meeting and Symposium in Seville, Spain, 8 - 11th June 2010.

7. MERI Research Student Day, Sheffield Hallam University, UK, 26th May 2010.

8. Macro Group Young Research Meeting 2010, Nottingham, UK, 29 - 30th April 2010.

9. The Futuroclays Meeting, Newcastle, UK, 14 - 16th December, 2009.

10. The XIV International Clay Conference, Iterly, 14 - 20th June 2009.

11. MERI Research Student Day, Sheffield Hallam University, UK, 20th May 2009.

9.3   Publications

- Patent filed - (UK Patent Application No. GB1114446.6) - Composite Hydrogel, in the name of Sheffield Hallam University.

  Abstract: A nanocomposite hydrogel formed from free radical dissociation of an initiator and polymerisation of a water soluble monomer. The resulting hydrogel finds particular application within the medical field for both soft and hard tissue repair in human and animals. The hydrogel is particularly advantageous for spinal disc repair.

- Paper in preparation - "The synthesis and characterisation of a novel and cytocompatible PNIPAM/clay precursor liquid synthesised by free-radical polymerisation".

- Paper in preparation - "The preparation and characterisation of a novel cytocompatible PNIPAM/Clay/Gelatine precursor liquid, and PNIPAM/clay/hyaluronic acid precursor liquid, and their applications".

- Paper in preparation - "The cell viability of Human mesenchymal stem cells suspended in PNIPAM/Clay precursor liquid, PNIPAM/clay/gelatine precursor liquid, and PNIPAM/clay/hyaluronic acid precursor liquid prior to and after phase transition triggered nanoparticle anchored gelation ".

- Paper in preparation - "FTIR study of the diffusion behaviour of ethanol/water mixtures into novel PNIPAM/Clay/Gelatine hydrogel formulations".